

# Sheffield Hallam University

*Mantle conditions and kimberlite geochemical criteria controlling diamond survival in Kimberlites*

YAMBISSA, Mubuabua Tshivangulula

Available from the Sheffield Hallam University Research Archive (SHURA) at:

<http://shura.shu.ac.uk/16553/>

## A Sheffield Hallam University thesis

This thesis is protected by copyright which belongs to the author.

The content must not be changed in any way or sold commercially in any format or medium without the formal permission of the author.

When referring to this work, full bibliographic details including the author, title, awarding institution and date of the thesis must be given.

Please visit <http://shura.shu.ac.uk/16553/> and <http://shura.shu.ac.uk/information.html> for further details about copyright and re-use permissions.

**Mantle Conditions and Kimberlite Geochemical Criteria  
Controlling Diamond Survival in Kimberlites**

A thesis submitted in partial fulfilment of the requirements of  
Sheffield Hallam University  
for the degree of Doctor of Philosophy (PhD)

By

Mubuabua Tshivangulula Yambissa

February 2017

Materials and Engineering Research Institute, Faculty of Arts, Computing, Engineering and  
Sciences, Sheffield Hallam University, UK

## Abstract

Diamonds are formed at high pressure, temperature and low oxygen fugacity conditions in the Earth's deep mantle. However, during their residence in the mantle and transport to the surface by kimberlite magma, they may be exposed to deformation or oxidising conditions outside of their stability field, causing diamond corrosion and resorption processes. The infiltration of silicate-rich melts and hydrothermal fluids are key processes that cause this corrosion (oxidation). Understanding the processes involved in diamond transport and preservation is important for diamond exploration and to assess the potential diamond grade for economic geology of kimberlite deposits. However, a thorough understanding of variations in diamond grade and survival or preservation conditions in the Lunda province (LP) has not yet been developed. Here a diamond preservation index model has been developed. Chemical analyses and petrography both support the view that the observed variations in diamond grade or abundance within Lunda Province (NE Angola) are associated with oxygen fugacity ( $fO_2$ ), oxidation state, viscosity of kimberlite magma, speed of kimberlite emplacement. Variations in temperature and pressure can impose conditions that are sufficiently oxidising for diamond resorption or to form  $CO_2$ . Several kimberlite pipes were sampled and it is known that they transported different amounts of diamond to the Earth's surface. In this study, both mantle xenoliths and kimberlite rocks from five kimberlite pipes (Catoca, Camatxia, Camagico, Caixepa and Camutue) from the Lucapa graben (NE Angola) were investigated, with the highest diamond concentrations occurring in LP

Alteration characteristics of kimberlite indicator minerals (KIMs) from the sampled deposits were investigated by optical microscopy, SEM, electron probe microanalysis (EMPA), XRF, XRD and  $^{57}Fe$  Mössbauer spectroscopy. The results of petrography and geochemical studies of peridotite, eclogite and kimberlite rocks during this project have revealed that the sampled kimberlite diamond deposits have experienced several alteration processes and the analysed diamond indicator minerals (olivine, garnet, spinel, ilmenite and pyroxene) reflect these alteration / redox reactions. The hydrothermal-metasomatic processes are associated with factors that controlled kimberlite emplacement. Mössbauer spectroscopy and EMPA results reveal that in the diamondiferous pipes of Camatxia, Caixepa and Camutue, iron redox ratios in ilmenites are considerably lower, indicating lower  $fO_2$  and consequently better diamond preservation conditions than for Catoca diamonds. The observed low diamond quality from Catoca pipe and the higher measured  $Fe^{3+}/\sum Fe$  ratio of Catoca indicator minerals agrees with a model which supports the use of ilmenite redox ratios to measure diamond and estimate the resorption on diamond. Results from Mössbauer and EMPA suggest that even with higher  $Fe^{3+}/\sum Fe$ , and a lack of the original Mg-rich ilmenite and complex ilmenite formation, the presence or mineralization of diamond within Lucapa graben kimberlites cannot be ruled out.

**KEYWORDS:** NE Angola, tectonics, metasomatoses, geochemistry, petrography, diamond indicator minerals, diamond preservation, kimberlite, mantle xenoliths (P-type and E-type), viscosity, iron redox ratio, oxygen fugacity ( $fO_2$ ), Mössbauer spectroscopy, XRD, and EMPA.

## Acknowledgements

Firstly I would like to acknowledge my special key two supervisors who have lasted the entire journey with me, Dr Paul Bingham and Dr Sue Forder of the Sheffield Hallam University. Their contribution to the project cannot be underestimated. Their expertise in materials science and Mössbauer spectroscopy always produced a number of interesting and intriguing discussions, whether through 3-5 pages long documents, emails or through intense weeks of meetings in offices or laboratories, training programmes, seminar at Sheffield Hallam University and organising/preparing the conditions for sending me to attend and to present my project at 30<sup>th</sup> International Conference on “Ore Potential of Alkaline, Kimberlite and Carbonatite Magmatism” on 29 September - 02 October 2014 Antalya - Turkey. In addition, their assistance for me to attend an International Conference on the Applications of the Mössbauer Effect (ICAME 2015), on 13 – 18 June 2015 in Hamburg, Germany, was crucial and well appreciated. I have great respect and admiration to my supervisors, especially Dr Paul Bingham of his enthusiasm in science, critical thinking and hard work, for helping me to publish scientific papers.

Thanks to Mr Colin Cunningham (University of Leicester) for producing polished thin sections and blocks for analysis and petrographic work. Also special thanks to Mr Rob (University of Leicester) and Dr Richard (University of Leeds), both for helping me with analytical works for this research.

I would also like to thank all staffs from MERI department at Sheffield Hallam University for their dedication and support provided to this project. Special thanks go to Mr Robert Burton and Tony who have contributed to my dissertation by producing XRD and XRF works. I would like to express my gratitude to my fellow group research students for their friendship and support, including Ben, Alex, Shuchi and Khalid. Special thanks go to former General Director of Catoca mine Dr Ganga Junior for permitting the access to the diamond mine in order to obtain samples. I also would like to express my special thanks to Mr Francisco João the manager of the mineralogy and petrography laboratory at Catoca Diamond mine, and Dr Pervov (geologist at Catoca mine) and Engineer Carlos Viegas, the operational manager of the geological department/exploration at Luo diamond mine for their professional commitment, in providing the special support by taking me to the different diamond exploration fields to collect the suitable samples (both mantle xenoliths and kimberlites rocks) for this study. My deepest gratitude goes to my family Huguette Kiala, my kids, brothers, sisters, Nkoswe family and my friend Paulo Valdemar. Their love and support are critically important for me to accomplish this project.

Finally, I would like to pay my respects and dedicate part of this work to my second supervisor Dr Sue Forder who passed away last year (2016). Sue's contribution to my research was extremely important.

## **Declaration**

Hereby, I declare that the work in this thesis was carried out in accordance with the regulations of the Sheffield Hallam University. All the material described herein is the original work of the author, except where otherwise referenced/acknowledged. This work has not been submitted for any other academic award. However, any views expressed in the thesis are those of the author.

## Glossary of Abbreviations

Ilm → Ilmenite ( $\text{FeTiO}_3$ )

Amp → Amphibole

Hem → Hematite ( $\text{Fe}_2\text{O}_3$ )

Rut → Rutile ( $\text{TiO}_2$ )

Grt/Gnt → Garnet. Possible group of minerals use:

- ✓ Almandine →  $\text{Fe}_3\text{Al}_2(\text{SiO}_4)_3$
- ✓ Pyrope →  $\text{Mg}_3\text{Al}_2(\text{SiO}_4)_3$
- ✓ Spessartine →  $\text{Mn}_3\text{Al}_2(\text{SiO}_4)_3$

Px → Pyroxene. Possible group of minerals used:

- ✓ Opx → Orthopyroxene (e.g. Enstatite, →  $\text{Mg}_2\text{Si}_2\text{O}_6$  and Ferrosilite →  $\text{Fe}_2\text{Si}_2\text{O}_6$ )
- ✓ Cpx → Clinopyroxene (e.g. diopside  $\text{CaMgSi}_2\text{O}_6$  and when diopside is rich in Cr it becomes Chrome diopside ( $\text{CaMg}(\text{Fe,Cr})\text{Si}_2\text{O}_6$ )]

Olv → Olivine group members (forsterite ( $\text{Mg}_2\text{SiO}_4$ ) and fayalite ( $\text{Fe}_2\text{SiO}_4$ )]

Spl → Spinel (group members mostly used)

- ✓ Mag → Magnetite ( $\text{Fe}_3\text{O}_4$ )
- ✓ Chr → Chromite ( $\text{FeCr}_2\text{O}_4$ )
- ✓ Mg and Al can substitute for Fe as they form solid solutions leading to other series such as magnesium chromite ( $\text{MgCr}_2\text{O}_4$ ) and hercynite ( $\text{FeAl}_2\text{O}_4$ )

Pht → Phlogopite

Cab → Carbonate

Sep → Serpentine

Kpht → Kelyphite

# TABLE OF CONTENTS

---

Abstract.....	i
Acknowledgements.....	ii
Declaration.....	iii
Glossary of Abbreviations .....	iv
List of Figures.....	viii
List of Tables .....	xvii
Chapter One . Introduction, aims, objectives and research problems.....	1
<b>1. 1. Geographical area of interest</b> .....	1
<b>1. 2. Aims and objectives of the research</b> .....	4
<b>1. 3. Research problems</b> .....	5
<b>1. 4. Research questions</b> .....	5
<b>1. 5. Methodologies</b> .....	6
<b>1. 6. Why has this research focussed on mantle xenoliths and kimberlite host rocks samples?</b> 7	
<b>1. 7. Outline of thesis.</b> This thesis consists of six chapters, as follows.....	8
Chapter Two . Background and literature review: regional setting, geochemistry of kimberlites, indicator minerals and application of advanced techniques in diamond research .....	9
<b>2. 1. The geodynamic setting and geochemistry of the Lunda kimberlite pipes</b> .....	9
<b>2. 1. 2. Geological setting of Lunda province</b> .....	10
<b>2. 2. Kimberlites: a review and discovery history</b> .....	15
<b>2. 2. 1. Classification of kimberlites</b> .....	16
<b>2. 2. 2. The Origin of kimberlite magma and diamond in the Earth.</b> .....	17
<b>2. 2. 3. The natural processes of kimberlite magma eruptions</b> .....	22
<b>2. 3. Carbon diamond formation</b> .....	23
<b>2. 4. Critical evaluation and discussion</b> .....	28
<b>2. 5. Indicator minerals and application of advanced spectroscopic techniques in diamond research</b> .....	34
2. 5. 1. Indicator minerals: a review.....	34
<b>2.6. Application of advanced methods to the study of kimberlite indicator minerals (KIMs)</b> ..	37
2. 6. 1. Electron microprobe analysis (EMPA) for compositional analysis of kimberlites.....	37
Chapter Three . Field work, experimental procedures and petrographic study of mantle xenoliths and kimberlite rocks .....	54

<b>3. 1. Field work</b> .....	54
3. 1. 3. Catoca kimberlite pipe .....	57
3. 1. 3. Caixepa and Camutue kimberlite pipes.....	60
3. 1. 4. Camatxia and Camagico kimberlite pipes.....	63
3. 1. 5. Heavy concentrate (kimberlite indicator minerals) from sampled kimberlites .....	64
<b>3. 2. Experimental procedures, sample collection and preparation overview</b> .....	66
3. 2. 1. Petrographic analysis .....	67
<b>3. 2. 2. Mössbauer spectroscopy: theory, sample preparation and analysis methodology</b> .....	69
3. 2. 2. 8. Some advantages of Mossbauer spectroscopy .....	80
<b>3. 3. X-ray diffraction, theory, sample preparation and analysis</b> .....	81
3. 3. 1. Principles of X-ray diffractometry .....	81
<b>3. 4. X-ray fluorescence (XRF) spectrometry</b> .....	83
3. 4. 1. XRF, sample preparation for major and minor elements analysis .....	87
<b>3. 5. Electron Probe Microanalysis (EMPA)</b> .....	88
Chapter Four . Results.....	91
<b>4. 1. Petrographic analysis</b> .....	91
4. 1. 1. CAT-18 from Catoca kimberlite pipe. ....	92
4. 1. 2. CAT - 22 Mantle xenoliths (eclogite) included in the kimberlite rock .....	93
4. 1. 3. CMT – 05 Mantle xenoliths (eclogite) from Camatxia pipe.....	94
4. 1. 4. CMT - 01 Mantle xenoliths (eclogite) from Camatxia pipe.....	96
4. 1. 5. CMT - 02 mantle xenoliths (peridotite) from Camatxia kimberlite.....	97
4. 1. 6. CM 003 mantle xenoliths (peridotite) from Camutue kimberlite, .....	99
4. 1. 7. CMG 002 Mantle xenoliths (peridotite) from Camagico kimberlite .....	100
4. 1. 8. CAT- 61 Catoca kimberlite (pyroclastic kimberlite- PK).....	101
4. 1. 9. CAT 59. Kimberlite rock. Tuffisitic kimberlite breccia (TKB), Catoca pipe .....	103
4. 1. 10. CM-CW 045 (7) pyroclastic kimberlite (PK), with inclusion of mantle xenoliths (from Camutue pipe).....	104
4. 1. 11. CAT 58 Coherent kimberlite (CK) from Catoca pipe.....	106
<b>4. 2. Megacrysts origins</b> .....	109
<b>4. 3. Mössbauer spectroscopy</b> .....	113
4. 3. 1. Ilmenite indicator minerals .....	113
4. 3. 2. Garnet and pyroxene and indicator minerals .....	118
<b>4. 4. X-ray diffractometry (XRD) results</b> .....	130
<b>4. 6. EMPA (Electron micro probe -analysis)</b> .....	136

<b>4. 7. Diamond heterogeneous mantle model .....</b>	<b>149</b>
<b>4. 8. Diamond preservation model for sampled kimberlites .....</b>	<b>150</b>
4. 8.1. Classification of Angolan kimberlites based on ilmenite criterion .....	152
<b>4. 9. Viscosity model for sampled kimberlite rocks.....</b>	<b>153</b>
<b>4. 10. Results from studied crystals of diamond from Catoca kimberlite.....</b>	<b>159</b>
Chapter Five . Discussion .....	160
<b>5. 1. Discussion - petrography of the sampled diamondiferous kimberlites. ....</b>	<b>160</b>
<b>5. 2. Discussion - Mössbauer spectroscopy .....</b>	<b>166</b>
<b>5. 3. X-ray diffractometry (XRD) .....</b>	<b>176</b>
<b>5. 5. Discussion of studied diamond heterogeneous mantle.....</b>	<b>180</b>
<b>5. 6. Discussion of diamond preservation model for sampled kimberlites.....</b>	<b>181</b>
<b>5. 7. Viscosity model for sampled kimberlite magmatic rocks and its implication on diamond survival within Lunda province.....</b>	<b>182</b>
5.7.1. Overview and discussion .....	182
<b>5. 8. Resorption features of studied crystals of Angolan diamond (Catoca kimberlite) .....</b>	<b>186</b>
<b>5. 9. Comparison of Lunda pipes and geochemistry with other kimberlite pipes.....</b>	<b>188</b>
Chapter Six . Conclusions and suggestions for future work .....	193
Chapter Seven: References. ....	214

## List of Figures

Figure 1.1. Main cratonic blocks in Southern Africa. Basement fractures: 1 - Damba structure; 2 - Cuanza-Kassai structure; 3 - Mwembeshi structure (Pereira <i>et al.</i> , 2003).....	2
Figure 1.2. Illustration of minerals included in diamond: a) P-type diamond showing the cubo-octahedral morphology of harzburgitic garnet inclusions (Taylor <i>et al.</i> , 2003); b) a purple peridotitic garnet; and c) colourless olivine inclusions in a diamond from Damtshaa, Botswana (Stachel and Harris, 2007). .....	7
Figure 2.1. Geological setting of Angola, showing the distribution of carbonatites and kimberlites. In general, the high-grade deposits of diamonds are in the north-east of the belt, decreasing towards the south-west. Modified and reproduced after Torro <i>et al.</i> (2012) with the permission of the Mineralogical Society of Great Britain & Ireland.....	11
Figure 2.2. Diagram of the possible relationships between basement faults, basin structures and kimberlites in a graben. The same relationship will hold for lamproites. This shows that as the depth of sediment infill increases, the basement faults or shears become less distinct and more dispersed and consequently the kimberlite clusters also become wider and more dispersed (White <i>et al.</i> , 1995).....	14
Figure 2.3. Global distribution of cratons, age provinces (Archons, 2.5 Ga; Protons, 2.5 to 1.6 Ga; and Tectons, 1.6 to 0.8 Ga), and major diamond deposits (red colour is diamonds) (Haggerty 1999).	15
Figure 2.4. Model for genesis of kimberlite magma: a rising convection current from the lower mantle. Garnetite (metamorphic rock consisting >70% garnet) (Ringwood <i>et al.</i> , 1992). .....	18
Figure 2.5. Diamond source in the Earth's upper mantle, transition zone, and lower mantle. Modified after Stachel (2003) and Stachel <i>et al.</i> (2005).....	19
Figure 2.6. Pressure-temperature diagram showing the melting of mantle peridotite containing volatiles and carbonate (black) and mantle peridotite that is dry and free of volatiles and carbon (red), from Shirey and Shigley (2013).....	20
Figure 2.7. Illustration of the ages of continental keels and their relationships with tectonic processes, diamond-hosting magmas, and different diamond types. Note the antiquity of mantle keels and lithospheric diamonds greater than 1 billion years and the youth of most kimberlite eruptions (less than 550 million years). Solid vertical bars represent the duration of ongoing processes, magmas, or diamond-forming events, whereas solid dots show single known occurrences. Dashed lines demonstrate the possible ages of occurrence of these events. From Shirey and Shigley (2013).....	21
Figure 2.8. Model of six stages of explosive eruption of kimberlite pipes (Cas <i>et al.</i> , 2008) .....	23
Figure 2.9. Schematic diagrams illustrating possible mantle conditions (e.g., depth, oxygen fugacity) and geodynamic settings in which lithospheric and sub-lithospheric diamonds and their mineral inclusions are formed. The relative roles of mantle and subducted lithospheric, crystallization from partial fluids, mantle redox, and mantle flow, are all connected with studies of diamonds and their inclusions (Shirey and Shigley, 2013). Nomenclature: G → graphite, D → diamond, LAB → lithosphere/ asthenosphere boundary. ....	25

Figure 2.10. Illustration of a simple relationship between a continental craton, its lithospheric mantle keel and diamond stable regions in the keel, and the convecting mantle. (Shirey and Shigley, 2013). 26

Figure 2.11. Pressure-temperature-depth diagram outlining the boundary between the stability fields of diamond and graphite, shown as a dotted line. Possible geothermal gradients (geotherms) for cratonic, continental and oceanic lithospheres are shaded grey. Diamonds are only stable in cratonic settings at pressures greater than > 40 kbars, which corresponds to depths of more than > 140 km. Modified after Tappert and Tappert (2011). ..... 27

Figure 2.12. Illustration of Gondwana supercontinent and its orogenic episodes at the end of the Neoproterozoic period (approximately 540 Ma), also demonstrating the general arrangement of Pan-African belts, from Kusky *et al.* (2003). AS- Arabian Shield; BR- Brasiliano; DA -Darnara; DM- Dom Feliciano; DR-Denman Darling; EW- Eilsworth Whitmore Mountains; GP- Gariep; KB- Kaoko; MA-Mauretanides; MB-Mozambique Belt; NS- Nubian Shield; PM -Peterman Ranges; PB- Pryolz Bay; PR-Parnpean Ranges; PS- Paterson; QM- Queen Maud Land; RB- Rokelides; SD- Saldania; SG- Southern Granulite Terrane; TS- Trans Sahara Belt; WB-West Congo; ZB- Zambezi..... 29

Figure 2.13. Demonstration of diamond exploration activity at Camutue kimberlite, (NE Angola, Photo taken during field work in 2012). ..... 31

Figure 2.14. Geological sketch displaying the location of the main Cratonic blocs in Africa and Fold belts Source Ministry of Mines and Mineral Development Zambia (2014). ..... 32

Figure 2.15. Model for the lithosphere beneath southern Africa based on geothermobarometry for xenolith suites. Ratio of depth scale to horizontal scale is 4:1 below sea level. Vertical bars represent xenolith suites, and the maximum depths shown are for dusters of xenoliths of deepest origin in each suite. A-A' represents points of inflection in xenolith geotherms and are interpreted as points for high- and low-temperature xenoliths (boundary of the lithosphere). (Boundary of the lithosphere). The xenolith suites are: L → Lauwrencia; F → Finsch; FS → Frank Smith; K → Kimberley; P → Premier; NL → Northern Lesotho; and EG→ East Griqualand. From Boyd and Gurney (1986)..... 33

Figure 2.16. Schematic of inclusions of peridotitic and eclogitic suites within diamonds (Stachel, 2003). ..... 35

Figure 2.17. Schematic vertical section through the Earth’s crust and part of the upper mantle. The upper mantle is separated into two mineralogical layers, spinel facies and garnet facies. Small volume melt fractions in the asthenosphere are indicated as red dots. With the exception of subducting oceanic slabs, the sublithospheric upper mantle appears to be void of macro-diamonds (Stachel and Harris, 2008). ..... 36

Figure 2.18. Plot of Cr<sub>2</sub>O<sub>3</sub> vs. CaO contents for peridotitic diamond inclusion garnets from worldwide localities. The diagonal line distinguishes sub-calcic ‘G10’ garnets from calcium-saturated ‘G9’ garnets. The horizontal line drawn at 2 wt% Cr<sub>2</sub>O<sub>3</sub> is used as an arbitrary division between eclogitic garnets (< 2 wt% Cr<sub>2</sub>O<sub>3</sub>) and peridotitic (> 2 wt% Cr<sub>2</sub>O<sub>3</sub>). From Gurney and Moore (1993). ). Harzburgite (G10) P-type and lherzolite (G9) ..... 38

Figure 2.19. Plot of TiO<sub>2</sub> versus Na<sub>2</sub>O content for eclogitic diamond inclusions in garnet from worldwide kimberlite localities. From Gurney *et al.* (1993). ..... 39

Figure 2.20. Plot of MgO versus Cr <sub>2</sub> O <sub>3</sub> content for chromite diamond inclusions from worldwide localities, from Gurney <i>et al.</i> (1993).....	40
Figure 2.21. Plot of MgO vs. Fe <sub>2</sub> O <sub>3</sub> content of kimberlite ilmenites. Modified after Nowicki <i>et al.</i> (2007), originally from Gurney and Zweistra (1995). .....	41
Figure 2.22. Thin section sample images showing several alteration processes: a) Camatxia pipe; b) Camutue pipe; and c) Catoca pipe. ....	45
Figure 2.23. Plot of temperature vs. log ( <i>f</i> O <sub>2</sub> ) for Oman chromites and harzburgites. The buffer curves shown are magnetite-haematite (M–H), quartz-fayalite-magnetite (QFM) and iron-wustite (I-W). Rollinson <i>et al.</i> (2012). ....	46
Figure 2.24. Room temperature Mössbauer spectra of chromites inclusion, spectra for the low Fe <sup>3+</sup> /ΣFe group (04-02 and 04-26) and the high Fe <sup>3+</sup> /ΣFe group (03-11 and 04-11). From Rollinson <i>et al.</i> (2012).....	46
Figure 2.25. Speciation of carbon in a rapid, uncontrolled upwelling mantle. Mid-Ocean-Ridge Basalt (MORB). Modified after Stagno <i>et al.</i> (2013). ....	48
Figure 2.26. Room temperature Mössbauer spectra of garnet inclusions from George Creek diamonds. Data were fitted using one Fe <sup>2+</sup> and one Fe <sup>3+</sup> doublet; the latter is shaded black. The arrow indicates the region where Fe <sup>3+</sup> absorption is observed in spectra of mantle-derived garnets (McCammon <i>et al.</i> , 1998). ....	49
Figure 2.27. Room temperature Mössbauer spectra of clinopyroxene inclusions from George Creek diamonds. The data were fitted with two Fe <sup>2+</sup> doublets and one Fe <sup>3+</sup> doublet; the latter is shaded black. The arrow indicates the region where the high velocity component of Fe <sup>3+</sup> absorption is observed in spectra from mantle-derived clinopyroxenes (McCammon <i>et al.</i> , 1998). ....	50
Figure 2.28. <sup>57</sup> Fe Mössbauer spectra of an untreated FeTiO <sub>3</sub> sample at room temperature plotted on a restricted velocity scale. Solid curves are theoretical fits to the experimental data. Modified after Seda and Hearne (2004).....	51
Figure 2.29. Room temperature Mössbauer spectra of ilmenite inclusions in ophiolite rock. Doublets represent Fe <sup>2+</sup> and Fe <sup>3+</sup> in ilmenite (thick lines) and Fe <sup>2+</sup> in amphibole. The sextet represents hematite at both samples. In the case of AZM 13HM two additional sextets with lower magnetic splitting, due to magnetite, are also present. Modified after Waerenborgh <i>et al.</i> (2002). ....	53
Figure 3.1. The classic South African model of a kimberlite pipe with old nomenclature (left side of figure) and a revised nomenclature system (right side of figure) to describe rocks from kimberlite magmatic systems as recently suggested by Sparks <i>et al.</i> (2006); Scott Smith <i>et al.</i> (2008); and Cas <i>et al.</i> (2008). Figure from Kjarsgaard (2007). ....	54
Figure 3.2. Photographs of Caixepa kimberlite samples, showing inequigranular texture with large inclusion of mantle xenolith (P-type).....	56
Figure 3.3. Photographs illustrating how the samples were catalogued and stored in the petrography laboratory of the Catoca diamond mine. ....	56

Figure 3.4. Illustration of a complex geological cross section of the Catoca kimberlite pipe, modified after Pervov <i>et al.</i> (2011). .....	58
Figure 3.5. Different Catoca mantle rock types from LP. a) Bimineralic eclogite, composed mainly of garnet (red-brown) and clinopyroxene (green), b) Peridotite inclusion in kimberlite rock, and c) Coherent kimberlite .....	59
Figure 3.6. Diamond-bearing kimberlite rock, pyroclastic kimberlite (PK) from diatreme facies, at Catoca mine (Diamonds are not visible).....	59
Figure 3.7. Surface diamond exploration activity at Caixepa kimberlite mine. Inset - common equigranular texture of kimberlite mantle xenolith included in diamond-bearing kimberlite rock, from Caixepa mine. ....	60
Figure 3.8. Photograph of a diamond-bearing kimberlite rock, from Caixepa mine (diamonds are not visible). This is a pyroclastic kimberlite core (Caixepa mine).....	61
Figure 3.9. Photographs of sampling activity by drilling core method at Camutue mine.....	62
Figure 3.10. Photographs of sampling activity through hammer at Camatxia diamond exploration mine. P-type are inclusions of mantle peridotite.....	63
Figure 3.11. Photograph of an inclusion of mantle xenolith (P-type) in kimberlite rock (Camatxia kimberlite).....	63
Figure 3.12. Photographs of diamond indicator minerals separated from Camatxia kimberlite rock ..	64
Figure 3.13. Illustration of relationship between the eluvial and alluvial diamondiferous deposits of NE Angola and the post-pliocene morphogenesis (Modified after Pereira <i>et al.</i> , 2013). ....	65
Figure 3.14. Flow-chart showing key aspects of the sample preparation process .....	67
Figure 3.15. Petrographic microscopy equipment: a) Leica TCS SP5 and b) Olympus FV1000.....	68
Figure 3.16. Schematic of a Mössbauer spectrometer (b) and an example of the resulting spectrum (Seda, 2003). .....	70
Figure 3.17. Representation of nuclear emission and absorption processes between the excited and ground nuclear states where $E_\gamma$ is transition gamma ray energy, $E_e$ is excited state energy and $E_g$ is ground state energy .....	72
Figure 3.18. Illustration of $^{57}\text{Fe}$ nuclear energy levels and resulting Mössbauer spectra due to (a) electric monopole interactions; (b), quadrupole interactions in the source and absorber and (c) Zeeman splitting for the excited ( $I = 3/2$ ) and ground ( $I = 1/2$ ) nuclear levels and transitions between these levels,. Modified after Seda (2003).....	74
Figure 3.19. Room temperature IS vs. QS for rock-forming minerals. Purple symbols (3.5a) represent oxide phases; orange symbols represent sulphides, sulphates and phosphates; and silicate minerals are	

green. Figure (3.5b) shows that distinctive IS and QS ranges occur for each valence state and site occupancy of Fe. From Dyar <i>et al.</i> (2006).....	75
Figure 3.20. Illustration of nuclear decay scheme for $^{57}\text{Co} \rightarrow ^{57}\text{Fe}$ and various backscattering processes for $^{57}\text{Fe}$ that can follow resonant absorption of an incident gamma photon with different energy level (Dyar <i>et al.</i> , 2006).....	76
Figure 3.21. Apparatus for Mössbauer sample preparation: scales (1). The finely ground rock powder, (3) mixed in some cases with a small amount of graphite powder (6), mixed in the agate mortar and pestle (9 and 10) and then it is compressed into the disc (4) and sealed with (5) for sealing the disc. The mixture is spatulas (2) into a specific cap of sample weight (7).....	79
Figure 3.22. Mössbauer spectrometer used in this study .....	80
Figure 3.23. Illustration of parallel X-ray beams travelling over different distances (Adapted from Bragg diffraction.svg, 2015) .....	82
Figure 3.24. Schematic of an X-ray powder diffractometer .....	82
Figure 3.25. X-ray diffractometer used in this study .....	83
Figure 3.26. Schematic diagram of XRF instrumentation (MagiXPRO), used in this study .....	84
Figure 3.27. XRF (MagiXPRO) analytical instrument used in this study. ....	84
Figure 3.28. Schematic representation of X-ray fluorescence using a generic atom and generic energy levels. Illustration process of moving electrons to shells and the replacement process, (Horiba, 2016) .....	85
Figure 3.29. Illustration of wavelength dispersive (WD) in red and energy dispersive (ED). X-ray spectroscopy.....	86
Figure 3.30. Apparatus for preparation of pressed powder pellets for XRF: (a). Rock powder and binder were mixed using the agate mortar and pestle and then the powder sample was compressed into the die (c). The die consists of a cylindrical and base, two polished steel pellets and a plunger.....	87
Figure 3.31. Polished thin sections 28 $\mu\text{m}$ thick on glass slides (50mm $\times$ 28mm) for used for EMPA, SEM, reflected light and transmitted light microscopy. ....	89
Figure 3.32. JEOL JXA-8230 electron microprobe analysis (EMPA) instrument used in this study...	89
Figure 4.1. Transmitted-light optical microscopy images of thin sections of E-type rock mantle xenoliths with mineral assemblages from Catoca kimberlite sample Cat-18. Indicator row 1 shows serpentinisation texture between the host and guest clinopyroxenes (Cpx) and Indicator row 2 shows Cpx, exhibiting mechanical deformation (shear). ....	93
Figure 4.2. Mineral assemblages in thin section samples from petrographic and geochemical analyses of mantle xenolith P-types (CAT-22, from Catoca pipe.).....	94

Figure 4.3. Transmitted-light optical microscopy and mineral assemblages in thin section from petrographic and geochemical analyses of mantle xenolith P-types (Cmt-05).....	95
Figure 4.4. Transmitted-light optical microscope images of thin section analysis. Mineral assemblages in thin section from petrographic and geochemical analyses of the mantle xenolith P-types (CMT 01), photographs illustrating textures of CMT - 01.....	97
Figure 4.5. Transmitted-light optical microscopy images of thin section mineral assemblages from petrographic and geochemical analyses of mantle xenolith eclogite (CMT-02), illustrating textures of kimberlite rock.....	98
Figure 4.6. Transmitted-light optical microscope images of thin sections analysis. Mineral assemblages in thin section from petrography and geochemistry analyses of P-type (Cm-003), photographs illustrating textures of kimberlite rock. ....	100
Figure 4.7. Transmitted-light optical microscopy images of thin sections of mantle xenolith with mineral assemblages from Camagico kimberlite sample Cmg-002; Sep = serpentine, Sp = spinel, Kpht = kelyphite, Gnt = garnet, Ol = olivine, Ilm = ilmenite, Cab = Carbonates. ....	101
Figure 4.8. Transmitted-light optical microscopy images of thin sections of Lunda province mantle xenolith with mineral assemblages from Catoca kimberlite, garnet exhibiting mechanical deformation. ....	102
Figure 4.9. Transmitted-light optical microscope images of thin section analysis. Mineral assemblages in thin section from petrography and geochemistry analyses. Tuffisitic kimberlite breccia (TKB), CAT 59, photographs illustrating textures of kimberlite rock. ....	104
Figure 4.10. Transmitted-light optical microscopy images of thin section analysis of pyroclastic kimberlite rock (CW045-7, Camutue), with minerals assemblages from Camutue kimberlite sample Cm/Cw 45; Sep = serpentine, Sp = spinel, Kpht = kelyphite, Gnt = garnet, Ol = olivine, Ilm = ilmenite, Cab = Carbonates.....	105
Figure 4.11. Diamond-bearing kimberlite rock from Catoca mine (diamonds are not visible). Also illustrates the porphyritic texture on Catoca kimberlite rock.....	106
Figure 4.12. Fitted room temperature Mössbauer spectra of ilmenite inclusion samples from diamondiferous pipes Catoca (CAT-5, CAT 62a) and Camatxia (CMT 60). Data were fitted with Fe <sup>2+</sup> and Fe <sup>3+</sup> doublets as shown.....	114
Figure 4.13. Fitted room temperature Mössbauer spectra of ilmenite inclusion samples from two diamondiferous pipes of Caixepa (CX1) and Camutue (CW045b CW 63). Data were fitted with Fe <sup>2+</sup> and Fe <sup>3+</sup> doublets as shown.....	115
Figure 4.14. Room temperature Mössbauer spectra of ilmenite and amphibole mineral inclusions from diamondiferous pipe Catoca (samples CAT 67NMM and CAT59HM1).....	117
Figure 4.15. Fitted room temperature Mössbauer spectra of garnet inclusion samples from diamondiferous pipes Catoca (Garnet - CAT- 67 Grt) and Camatxia pipe (Garnet - CMT 05 Grt, CMT01 and pyroxene - CMT01). Data were fitted with Fe <sup>2+</sup> and Fe <sup>3+</sup> doublets as shown.....	119

Figure 4.16. Room temperature Mössbauer spectra of complex mineral inclusions of magnetite and pyroxene, samples from diamondiferous pipes of Camatxia (CMT 58) and Catoca (CAT 67M).....	121
Figure 4.17. Room temperature Mössbauer spectra of amphibole and magnetite inclusions from diamondiferous pipe (CAT 59d) and (CAT=MY001C), with possible presence of Ilmenite in the sample. ....	123
Figure 4.18. Room temperature fitted Mössbauer spectra of amphibole, ilmenite and magnetite inclusions from diamondiferous pipe of Camatxia (CMT 25, poorly magnetic phase) and hematite inclusion from Caixepa pipe (CX 12N). Possible presence of ilmenite in the sample. ....	124
Figure 4.19. Room temperature fitted Mössbauer spectra of hematite (Hem) sample (CX 022) and magnetite (Mag), sample CX 027) inclusions from diamondiferous pipe of Caixepa.....	126
Figure 4.20. Room temperature fitted Mössbauer spectra of hematite (Hm) and ilmenite in sample (CW 0045D) from Camutue and magnetite (Mt) and hematite (Hm), sample (CX 03) from Caixepa diamondiferous pipes. ....	127
Figure 4.21. X-ray diffraction patterns of crystalline materials present in and studied kimberlite samples from Catoca pipe, samples CAT5 (order 10) and CAT62 (order 1) and Camatxia pipe sample CMT60 (order 32). ....	130
Figure 4.22. X-ray diffraction patterns of crystalline materials present and studied kimberlite samples from Camutue pipe, samples CW0045D (order 24), CW045b (order 23) and Caixepa pipe, sample CX 1 (order 20).....	131
Figure 4.23. X-ray diffraction patterns of complex crystalline materials present in studied kimberlite samples from Caixepa pipe, samples CX027 (order 25), CX027 (order 18) and Catoca pipe, samples CAT 50 (order 6); CAT 59 ilm (order 6). ....	132
Figure 4.24. X-ray diffraction patterns of crystalline materials present in studied kimberlite samples from Catoca pipe, samples CAT 67HMa (order 5); 50HM2 (order 6), 59HM1 and 59D. This ilmenite contains minor inclusion of amphibole and an unidentified complex phase. ....	133
Figure 4.25. Application process and sample preparation method for XRF analysis. Kimberlite rock (a), powdered rock (b), high temperature furnace instrument (c), melted powder rock ready (d) - for XRF analysis.....	134
Figure 4.26. Electron Probe Micro-Analysis (EPMA), backscattered electron images (sample CAT 5) showing the mineral assemblage and metasomatic alterations processes in mantle-derived ilmenite, spinel and garnet/pyroxene. Replacements of ilmenite (a, b) and Garnet (c) and equilibrium contact between Grt and Cpx (d). Strongly anisotropic ilmenite and spinel. ....	137
Figure 4.27. Electron Micro Probe -Analysis (EMPA), backscattered electron images (sample CAT 62) showing the mineral assemblage and metasomatic alterations processes in mantle-derived ilmenite and spinel (NE Angola). Replacements of ilmenite (a, b, c) and equilibrium contact between Ilm and Spl is at samples (a). Zoning features on Ilm are indicated in rectangle, square signs in sample (a) and Carbonate in circle sign at sample (b). Mechanical and chemical deformation at sample (d).....	138

Figure 4.28. Backscattered electron images Analysis of kimberlite rock from Caixepa pipe (sample CX 030), showing the mineral assemblage and metasomatic alteration processes in mantle-derived ilmenite, spinel and garnet/pyroxene with replacement of ilmenite (a, b); garnet (c); and equilibrium contact between garnet and clinopyroxene (d). Images show strongly anisotropic ilmenite and spinel. Grt = garnet; Olv = olivine; Pyn = pyroxene; Spl = spinel; Pht = phlogopite; Ilm = ilmenite; Cab = carbonate; Sep = serpentine .....	139
Figure 4.29. Plot of Cr <sub>2</sub> O <sub>3</sub> versus CaO content for diamond inclusion garnets from locality of Catoca. The horizontal line drawn at 2 wt. % Cr <sub>2</sub> O <sub>3</sub> is only used as an arbitrary division between eclogitic (< 2 wt % Cr <sub>2</sub> O <sub>3</sub> ) and peridotitic (>2 wt.% Cr <sub>2</sub> O <sub>3</sub> ) garnets. ....	145
Figure 4.30. Plot of TiO <sub>2</sub> versus FeO content for diamond inclusion garnets of eclogite (sample CAT18) from Catoca kimberlite. ....	146
Figure 4.31. Plot of Cr <sub>2</sub> O <sub>3</sub> content against Fe <sup>3+</sup> /ΣFe (iron redox ratio) of ilmenite diamond indicator minerals.....	147
Figure 4.32. Plot of TiO <sub>2</sub> content against Fe <sup>3+</sup> /ΣFe (iron redox ratio) of ilmenite diamond indicator minerals.....	148
Figure 4.33. Plot of MgO content against Fe <sup>3+</sup> /ΣFe (iron redox ratio) of ilmenite diamond indicator minerals.....	148
Figure 4.34. Developed heterogeneous model for diamondiferous kimberlites, Western Africa (NE Angola) showing relative locations of 5 principal pipes investigated in this study. ....	149
Figure 4.35. Preservation of diamond index model and illustration the composition of ilmenite Fe <sub>2</sub> O <sub>3</sub> vs MgO in wt % (Catoca and Camatxia kimberlite pipes).....	151
Figure 4.36. Ternary diagram showing the field of kimberlite ilmenite composition from Western Africa (NE Angola, samples Cat 5, Cat 62 in red colour and CMT 60 in back colour), plotted as function of hematite, ilmenite and geikeilite.....	152
Figure 4.37. Ternary diagram showing the contour lines field of kimberlite ilmenite composition from Western Africa (NE Angola) plotted as function of hematite, ilmenite and geikeilite. ....	153
Figure 4.38. Calculated viscosities for typical kimberlite magmatic melts. The plotted points correspond to viscosities calculated at 50°C intervals according to the Table 2. ....	157
Figure 4.39. Diamond surface textures resulting from late stage etching process, poor quality. Photographs taken on optical microscope.....	159
Figure 5.1. Redox ratio vs carats/100 tonnes of kimberlite rock .....	181
Figure 5.2. Plots showing the relationship between melt viscosity (η), and H <sub>2</sub> O content at 1000°C from a basaltic andesite sill from MtTheron, Antarctica (Petford, 2009). ....	184
Figure 5.3. Dynamics of viscosity of kimberlite and basaltic magmas during their ascent from mantle to the Earth surface crust (Persikov and Bukhtiyarov, 2013). ....	185

Figure 5.4. Temperature dependence of the viscosity, a) Persikov and Bukhtiyarov (1999) ,and b) Bottinga and Weill (1972) ..... 186

Figure 5.5. Illustration of kimberlite pipe and its terminology (Field and Scott Smith, 1998)..... 190

Figure 5.6. Demonstration model of class 1crater formation (Skinner, 2008)..... 191

## List of Tables

Table 1.1. Sampled studied kimberlite deposits, with their latitude and longitude co-ordinates.....	3
Table 2.1. Timeline of main Angolan orogenic episodes. ....	12
Table 2.2. Episodes of kimberlite and lamproites volcanism (Nixon, 1995). *Diamondiferous, (Other volcanic rocks with reported diamond are shown in brackets). ....	14
Table 2.3. Room temperature fitted Mössbauer hyperfine parameters of mineral inclusions (CS - centre shift; QS- quadrupole splitting, W- full width at half maximum). Numbers in parentheses show the standard deviation of the last digit; parameter values in italics were fixed during the fitting process (McCammon <i>et al.</i> , 1998). ....	51
Table 2.4. Abundance of each component of ilmenite sample spectra derived from absorption areas at room temperature. Modified after Seda and Hearne (2004). ....	52
Table 2.5. Room temperature fitted Mössbauer hyperfine parameters of mineral inclusions (ilmenite, magnetite, hematite and amphibole), (CS - centre shift; QS- quadrupole splitting, W- full width at half maximum). Modified after Waerenborgh <i>et al.</i> (2002). ....	53
Table 3.1. Periodic table of Mössbauer active elements (Gütlich, 2005). ....	77
Table 4.1. Summary of kimberlite petrography of LP and its terminology. ....	107
Table 4.2. Summary of selected samples. All are the same age. ....	108
Table 4.3. Room temperature fitted Mössbauer hyperfine parameters of ilmenite and amphibole inclusions. ....	115
Table 4.4. Room temperature hyperfine parameters of mineral inclusions (ilmenite) from Caixepa (CX1) and Camutue (CW045b) determined from Mössbauer spectroscopy, (CS→ centre shift; QS→ quadrupole splitting, W→ half width, half maximum line width. ....	116
Table 4.5. Room temperature hyperfine parameters of mineral inclusion (ilmenite amphibole) from samples (CAT CAT 67NMM) (CAT 59 HM1) multiphase minerals, determined from Mössbauer spectroscopy, (CS→ centre shift; QS→ quadrupole splitting, W→ half width at half maximum). ....	117
Table 4.6. Summary of redox ratio for pyroxene and garnet diamond indicator mineral inclusions..	118
Table 4.7. Room temperature hyperfine parameters of mineral inclusions (garnet, and clinopyroxene) determined from Mössbauer spectroscopy, (CS→ centre shift; QS→ quadrupole splitting; W→ half width, half maximum line width. Samples (CMT 05 Cpx and CMT 05 Grt) are from Camatxia pipe whereas CAT 67 Grt is from Catoca pipe. ....	120
Table 4.8. Room temperature fitted hyperfine parameters of mineral inclusions (ilmenite, amphibole and magnetite) for samples CAT 67M and CMT 58, with isomer shift (CS), quadrupole splitting (QS) line width of the high velocity peak (w+), low and high velocity line widths (w-/w+) = 1 to keep	

equal, line width of the most intense sextet peak (w3), effective hyperfine field (H) and relative site intensities area.....	122
Table 4.9. Room temperature fitted Mössbauer hyperfine parameters of mineral inclusions (ilmenite, amphibole, magnetite) from samples CAT 59 d and CAT=MY001C. Values with * were fixed during the fitting process.....	123
Table 4.10. Room temperature hyperfine parameters of mineral inclusions (ilmenite, amphibole and magnetite) for Camatxia (CAT 253) and Caixepa (CX 12N) samples. Isomer shift (CS), quadrupole splitting (QS) line width of the high velocity peak (w+), low and high velocity line widths (w-/w+) = 1 to keep equal, line width of the most intense sextet peak (w3), effective hyperfine field (H) and relative site intensities area. ....	125
Table 4.11. Room temperature Mössbauer spectra of hematite (Hm) sample (CX 022) and magnetite (Mt), sample CX 027) inclusions from diamondiferous pipe of Caixepa. Data were fitted to two doublets Fe <sup>2+</sup> and Fe <sup>3+</sup> for ilmenite sample at CX 022 and sextets for Hematite and Magnetite.....	126
Table 4.12. Room temperature hyperfine parameters of mineral inclusions (hematite, magnetite, amphibole and ilmenite) Room temperature hyperfine parameters of mineral inclusion from Camutue (CW0045D) and Caixepa (CX 03) pipes determined from Mössbauer spectroscopy (CS→ centre shift; QS→ quadrupole splitting; W→ half width at half maximum). The parameters with asterisks were fixed during the fitting process. ....	128
Table 4.13. Summary of samples studied using advanced spectroscopic techniques.....	129
Table 4.14. Semi- quantitative XRF analysis results (Fused bead) of kimberlite samples.....	135
Table 4.15. Quantitative analyses ( Fused Bead) and Loss on Ignition ( LOI) measurement. Note that the Total 1 was obtained through the XRF before the calculation of Loss On Ignition (LOI) and Total 2 was obtained after the LOI.....	136
Table 4.16. Summary of Electron Probe Micro-Analysis (EPMA) of major chemical elements of ilmenite crystals from diamondiferous pipes. Catoca samples (Cat 62 and Cat 5) are in normal text and the Camatxia sample (CMT 60) is in italic text. ....	143
Table 4.17. EPMA analysis of garnet (wt %) sample reference: CAT 18.....	145
Table 4.18. Grade variations of diamonds from a single pipe. Shows diamond carats per hundred tonne of rock that each pipe produces, and possible percentages of diamond brought to surface by kimberlite. Source of information: local geologists in NE Angola.....	149
Table 4.19. Composition of representative kimberlite magma types used in sample viscosity calculation. Data from XRF analyses. CAT 67, CAT60→Catoca pipe; CX027→Caixepa pipe; CMG171→Camagico pipe; CM=CW45→Camutue pipe and CMT006, CMT02→Camatxia pipe. .	155
Table 4.20. Calculated viscosities for studied kimberlite magmas samples using model from Bottinga and Weill (1972). ....	157

Table 4.21. Validation of viscosity model. Temperature depending viscosity data used for validation of viscosity model by comparing the calculated viscosity with those published viscosity data (graphic data). .....	158
Table 5.1. Comparison of redox ratios obtained for Lunda ilmenite mineral inclusions with literature values for ilmenites obtained from Portugal and South Africa.....	169
Table 5.2. Comparison of redox ratios obtained for Lunda garnet mineral inclusions with literature values for garnet obtained from South Africa kimberlites.....	174

# Chapter One . Introduction, aims, objectives and research problems

## 1. 1. Geographical area of interest

The area of study is Lunda province (Figure 1.1), located in NE Angola; it falls within the Archaean Congo Kassai craton (Stachel and Harris 2007) which houses substantial quantities of mineral resources including primary (kimberlite) and secondary (alluvial) diamond deposits. This project only focuses on kimberlite deposits. Kimberlites are CO<sub>2</sub>-rich ultramafic potassic igneous rocks (Sparks *et al.*, 2006; Scott Smith *et al.*, 2008; and Kjarsgaard, 2007) dominated by multiple complex mineral phases or assemblage of olivine, magnesia, chromium, garnet (almandine-pyrope), chromium diopside, phlogopite, pyroxene, ilmenite spinel and rutile as well as carbonate minerals (Skinner, 2008; and Mitchell, 1991). Kimberlites exhibit a distinctive inequigranular texture (Cas *et al.*, 2008) caused by macrocrystic (large grains) materials set in a fine to medium grained groundmass of serpentine, carbonate and altered olivine (Mayer *et al.*, 1994). In addition, the kimberlite bodies are products of multiple intrusive and extrusive magmatic events and these events are recognised as distinctive kimberlites facies (Patterson *et al.*, 2009 and Pervov *et al.*, 2011).

The petrogenesis of kimberlites is, however, controversial, with disagreements over the nature and depth of its source region (Mitchell and Giardini, 1977 and Keshav *et al.*, 2005), whether they are primary in origin, and the cause of melting, with some suggesting that they derived at the core and mantle boundary or mantle transition zone (Stachel, 2003; Stachel. *et al.*, 2009 and Heaman *et al.*, 2003). As demonstrated in Figure 1.2, the new discoveries of diamondiferous kimberlites, diamond xenocrysts containing syngenetic inclusions of garnet are indicative of a deeper and transition zone origin for kimberlites (Ringwood *et al.*, 1992, see Chapter two for more details) and consequently kimberlites are considered be transporter agents of diamond from deep source to the surface (Stachel, 2003; Ringwood *et al.*, 1992; and Cas *et al.*, 2008).

All diamondiferous kimberlites sampled and used in this project are from Lunda province. This is the region of highest diamond concentration in Angola. The Lunda craton lithosphere underwent partial melting in the late Archean era, which produced crustal rocks that were successively tectonically reworked over several geological Proterozoic eras (Paleoproterozoic, Mesoproterozoic and Neoproterozoic) (Batumike *et al.*, 2009). These events caused a system of deep faults - Lucapa graben - an extensional tectonic structure which crosses the country from north-east to south-west (Boyd and Danchin, 1980) and finally resulting in the emplacement of Angolan kimberlites during breaking up of Gondwanaland and the opening of the Atlantic (Pereira *et al.*, 2003). This tectonic belt is associated with magmatic activity related to rifting at the West African continental margin (Helmstaedt and Gurney, 1997) during the opening of the Atlantic Ocean in the early Cretaceous era (Pervov *et al.*, 2011).

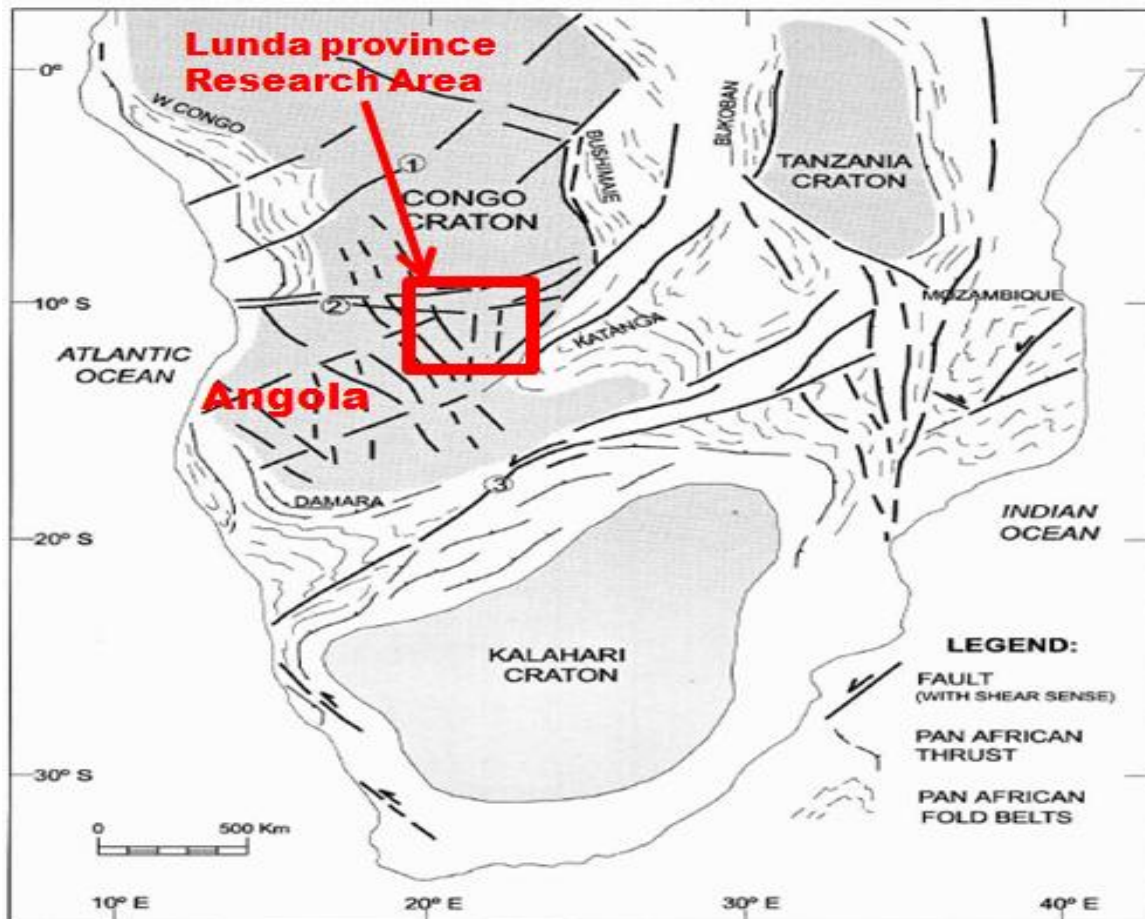


Figure 1.1. Main cratonic blocks in Southern Africa. Basement fractures: 1 - Damba structure; 2 - Cuanza-Kassai structure; 3 - Mwembeshi structure (Pereira *et al.*, 2003).

The kimberlite bodies from Lunda province are products of multiple intrusive and extrusive magmatic events and these events are recognised in distinctive kimberlites facies. (Skinner, 2008 and Cas *et al.*, 2008). For example, different rock textures, geochemistry, mineralogy, diamond grades, quality and distribution are important data that characterise individual kimberlite facies such as crater, diatreme and hypabyssal (Kjarsgaard, 2007; Boyd and Danchin, 1980). See Chapter Two. The examined samples for this research were collected from different mantle xenoliths (P- types and E-type) and five kimberlite pipes (Table 1.1) from different diamond mining explorations in Lunda province. These include samples from the Catoca, Camagico, Camatxia, Camutue and Caixepa diamondiferous kimberlite pipes.

<b>Sampled kimberlite pipes</b>	<b>Latitude</b>	<b>Longitude</b>
Camatxia	8°56'03"S	20°28'05"E
Camagico	8°58'05"S	20°29'00"E
Caixepa	8°30'09"S	21°41'09"E
Catoca	9°24'24"S	20°17'57"E
Camutue	8°78'00" S	21°59'00"E

Table 1.1. Sampled studied kimberlite deposits, with their latitude and longitude co-ordinates

Although kimberlites have attracted interest mainly by a) being derived from depths greater than any other igneous rock (Stachel, 2003) and b) by transporting diamonds, garnet peridotite and eclogite mantle xenoliths to the Earth's surface, nevertheless the geology of kimberlite remains poorly understood (Keshav *et al.*, 2005; Field *et al.*, 2008; Dasgupta, 2013). This problem is probably due to several factors associated with its nature and forming processes such as different chemical composition observed throughout the pipe, mantle source, emplacement model facies and processes of contamination by crustal and mantle xenoliths (Mayer *et al.*, 1994).

Despite having suffered several tectonic episodes during the opening of Atlantic Ocean, the Angolan lithosphere and in particular the geology of Lunda province (NE Angola) provides better conditions for the existence of the diamond compared to the neighbouring country Namibia. The presence of diamond is indicative that the Angolan cratonic block is refractive and relatively cool, with low density peridotitic roots about 3.31 g/cm<sup>3</sup>, that protected against reheating and excessive tectonic reworking and remained attached to the cratons during subsequent plate motions (Pereira *et al.*, 2003). The presence of diamondiferous kimberlites in Lunda province is validated by Clifford's Rule which states that diamondiferous kimberlites are found within the older Archean cratonic regions (Hatton, 2009; Creighton *et al.*, 2011). The amount of diamond present in Angolan kimberlites, in particular Lunda province, will depend on the following criteria or factors.

- The quantity of diamond peridotite and eclogite mantle that have sampled.
- Distribution or average diamond grade within the peridotite and eclogite mantle.
- The degree of preservation of diamonds during transportation to the surface.
- Speed of kimberlite emplacement and the efficiency with which the diamonds were transported to the Earth's surface. Rapid transport of diamond to the surface is always better for preservation (Wilson and Head, 2007).

Note that the amount of diamond peridotite or diamond eclogite that has been sampled should be reflected in the quantity of disaggregated mineral grains or xenoliths in the kimberlite. The major problem, however is how to identify or forecast whether diamonds could be present or not, and the amount present in kimberlites. That is why this research considers the use and a comprehensive study of diamond indicator minerals such as ilmenite, chromites, garnets, and pyroxenes as important tools for diamond indication.

## **1. 2. Aims and objectives of the research**

Most of our academic and scientific knowledge on the chemical evolution and mineralogy of the Earth`s mantle is derived from a number of different sources such as geophysical data, mantle xenoliths, primary melts, and high pressure experiments (Griffin and Ryan, 1995; Powell and Powell, 1977; Fedortchouk *et al.*, 2007; and Creighton *et al.*, 2007). The most direct information, however, comes from mantle xenoliths which originate in the lithospheric mantle at depths of approximately 200 km (Stachel, 2003) or even much deeper 400–650 km than any other igneous rock (Ringwood *et al.*, 1992). In this case, a comprehensive understanding of the mantle petrography, geochemistry of indicator minerals (peridotite, eclogite and kimberlite rock) and the deposit source is fundamental for success in diamond exploration environments across of the world, in particular the entire region of Lunda provinces.

Even though the five sampled kimberlite pipes in Lunda provinces are all grouped together along a loose line of less than 160 km end to end they vary dramatically in diamond grade and quality. The principal aims of this research are to investigate the mantle conditions and geochemistry of these five diamondiferous kimberlites (Figure 1.1) and to understand their diamond grade variation and preservation conditions. This research is important because a clear understanding of diamond survival and preservation conditions in NE Angola has not yet been formed.

### 1. 3. Research problems

Diamondiferous kimberlites and the geology of Lunda province (NE Angola) have been studied by several workers including Pereira *et al.* (2003); Eugenio and Fernando (2006); Castillo-Oliver (2011), Ganga *et al.* (2003); Nixon (1995); Pervov *et al.* (2011); Robles-Cruz *et al.* (2008 & 2009) and White *et al.* (1995). Despite this prior research, there is no clear understanding of diamond survival or preservation conditions within the Lucapa graben. For example, the recent work of Robles-Cruz *et al.* (2009) has placed Catoca kimberlite within a no-diamond-preservation zone, which implies that the Catoca pipe should not contain diamond, in agreement with Gurney and Zweistra (1995) and Nowicki *et al.* (2007). In reality the Catoca pipe contains the highest level (volume) of diamond in NE Angola and it ranks as the world's fourth largest diamond mine (Ganga *et al.*, 2003). In addition highly variable grades of diamond quality are observed in NE Angola kimberlite deposits. For the above reasons, this research concerned a new study of diamond indicator minerals (from peridotite, eclogite and kimberlite host rocks), which was needed in order to provide new information on preservation conditions and diamond grade variations (or diamond content/volume) within primary kimberlite deposits from Lunda province, using advanced analytical methods in diamond research.

### 1. 4. Research questions

**This investigation has developed the following questions:**

- ✓ Is the diamond grade controlled primarily by variation in diamond survival during kimberlite ascent, in particular the  $fO_2$  conditions in the kimberlite magma?
- ✓ Were diamonds absorbed in the mantle before kimberlite emplacement?
- ✓ Were there any variations in mantle conditions and petrology within Lucapa Graben which led to variations in diamond abundance and grade at different mantle depths and locations?
- ✓ Based on my prior experience as a mineralogist at Catoca Diamond Company, 60% of all Catoca diamonds have poor quality and are used as industrial diamonds. The question is: why does the Catoca pipe contain such a high percentage of industrial diamonds and large diamond crystals, compared with other kimberlites located in the same tectonic structure?
- ✓ Was the lithosphere mantle beneath the Lunda kimberlite province homogeneous or heterogeneous, and did this have consequences for diamond distribution?
- ✓ How rich was the mantle in this region, in terms of diamond content?

Heat flow calculations (Castillo-Oliver *et al.*, 2011 and Stachel *et al.*, 2003) for the lithospheric mantle beneath the Lunda kimberlite province support diamond formation. What other methods or interpretations can be carried out to further understand diamond preservation conditions within Lunda province?

## 1. 5. Methodologies

**In order to achieve the goals and test the hypotheses outlined in Chapter 1.4, the project involved the following approaches:**

1. Literature survey of Angolan geology and its primary diamond deposits.
2. Detailed literature review of kimberlitic diamond deposits.
1. Field work and sampling activities in diamond mining / exploration companies, Western Africa (NE Angola).
2. Preparation of samples and laboratory work.
3. A systematic petrographic study of samples (mantle xenoliths, P-E-types and kimberlite rocks) using hand and microscopic techniques.
4. Comprehensive characterisation of samples through a multi-technique approach.
5. Scanning electron microscopy (SEM)
6. Electron microprobe analysis (EMPA) of major and trace element geochemistry of kimberlite indicator minerals such as garnets, chromite, ilmenite, pyroxene & olivine (from peridotite, eclogite and kimberlite rocks) and to assess detailed compositions - particularly  $\text{Cr}_2\text{O}_3/\text{CaO}$ ,  $\text{Cr}_2\text{O}_3/\text{MgO}$ ,  $\text{Fe}_2\text{O}_3/\text{MgO}$ ,  $\text{TiO}_2/\text{Na}_2\text{O}$  ratios. In addition, the compositions of ilmenite will be used to give some measure of redox conditions in the mantle and magma ( $f\text{O}_2$ ). Note that variations in the oxygen fugacity may affect the extent of absorption in the diamonds.
7.  $^{57}\text{Fe}$  Mössbauer spectroscopy to measure or determine the ratio of  $\text{Fe}^{3+}/\sum\text{Fe}$  from kimberlite indicator minerals (garnet, ilmenite, pyroxene) and amphibole.
8. Determination of oxygen fugacity ( $f\text{O}_2$ ) and Fe oxidation states for sampled kimberlite pipes.
9. X-ray fluorescence (XRF) spectroscopy, for chemical analyses of major and trace elements of sampled peridotite, eclogite and kimberlite host rocks.
10. X-ray diffraction (XRD), this analytical technique was deployed to identify the phases present in crystalline material or minerals.
11. Modelling of high temperature viscosity of sampled kimberlite rocks. Note that a rapid transport of diamond to the surface is always better for preservation.

## 1. 6. Why has this research focussed on mantle xenoliths and kimberlite host rocks samples?

The geochemistry of indicator minerals (garnet, spinels, pyroxene, ilmenite and olivine) from both mantle xenoliths and kimberlites host rock have been used for many years in exploration to locate deposits that may contain diamonds through assessment of their composition (Grutter *et al.*, 2004). Their detailed compositions can be used to assess mantle conditions, through which kimberlites passed and sampled both diamonds and the associated megacrystic mineral suite which helps us to understand how these relate to diamond stability fields. The occurrence of high numbers of G10 garnets (see section 2.6) from the stability field is validated by the presence of diamonds in Lunda province (Correia and Laiginas, 2006)

Apart from providing an indication of potential diamond sources, some of the observed inclusions in diamond (Figure 1.2) are also of interest because they crystallized in the upper mantle and formed at the same time as diamonds (Taylor *et al.*, 2003). For this reason, this project was based on the study of diamonds, their mineral inclusions (Figures 1.2 and 3.12) and their kimberlites host rocks, to provide new information on the mineralogy and how the metasomatose processes affected Lunda lithosphere mantle, where diamonds were formed and the changes in mineralogy, geochemistry and the diamond preservation conditions and the geological processes, which took place within it.

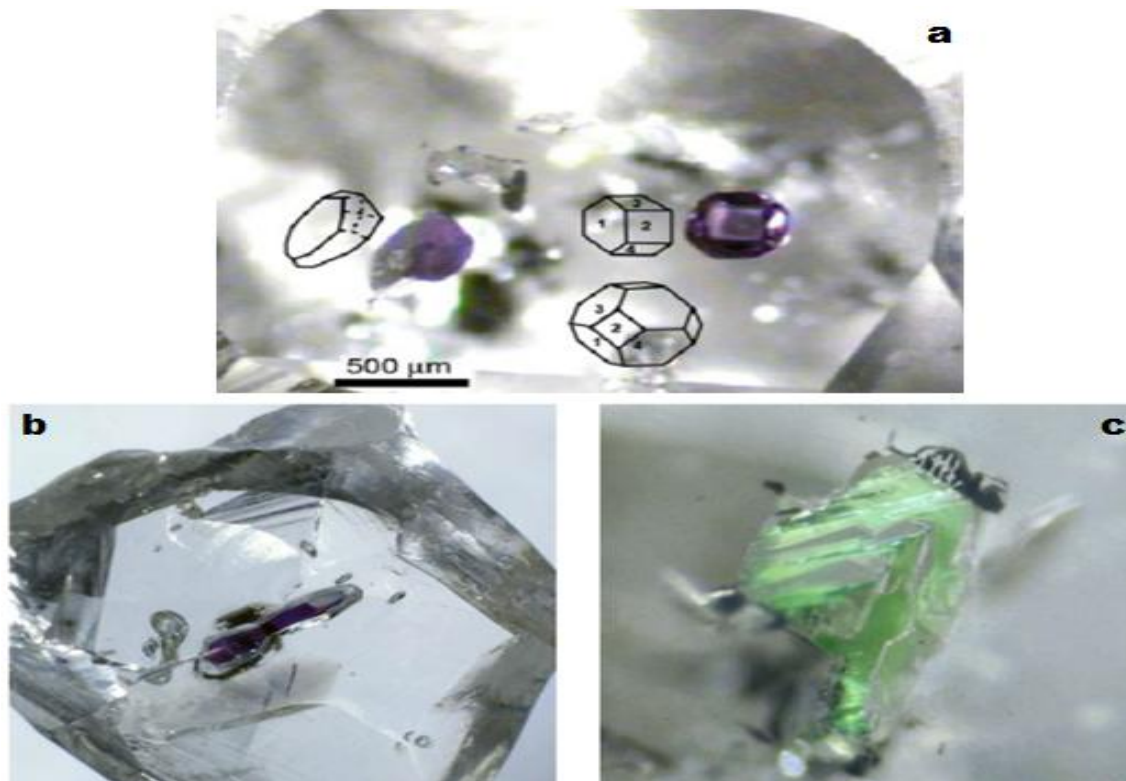


Figure 1.2. Illustration of minerals included in diamond: a) P-type diamond showing the cubo-octahedral morphology of harzburgitic garnet inclusions (Taylor *et al.*, 2003); b) a purple peridotitic garnet; and c) colourless olivine inclusions in a diamond from Damtshaa, Botswana (Stachel and Harris, 2007).

This project considers and further develops an ilmenite compositional model, to give a measure of oxygen fugacity ( $fO_2$ ) and hence redox conditions which influenced diamond absorption, quality and shape characteristics in kimberlitic magma, and where available diamond size distribution data. In addition the analysis of morphology and shape (e.g. deformation) of indicator minerals such as garnet and ilmenite can provide information about the metasomatic processes that occurred in the Lunda kimberlites. The results of chemical analyses of eclogite garnet from this project (see Chapter Four) show low Ti content and an increased Ca content is observed (Table 4.17). The higher Ca content may have been derived from carbonate activity in Lunda mantle. The carbonate activities in the mantle are linked with oxygen fugacity in mantle (McCammon *et al.*, 2001) and oxygen fugacity is diamond destroyer (Fedortchouk *et al.* 2007; Robinson *et al.* 1989; Arima and Kozai, 2008). Therefore the elevated Ca content in samples could be indicative of resorption process of diamond in the host magma before kimberlite emplacement (Griffin and Ryan, 1995). This result is also consistent with the work of (Nowicki *et al.*, 2007) who explained that when mantle xenolith (peridotite/eclogite) was subjected to significant metasomatism, it normally increases the Ca content and reduces the proportion of G10 peridotite garnet. Such compositions of peridotitic garnet in certain instances appear to be associated with significant increases in oxygen fugacity, increasing the potential for diamond resorption (McCammon *et al.*, 2001).

**1. 7. Outline of thesis.** This thesis consists of six chapters, as follows.

**Chapter One** provides the introduction, background theories and methodology; aims, objectives and research problem. **Chapter Two** provides the literature review, the regional setting of Lunda province, origin of tectonic structures and how they are related to diamondiferous kimberlites in Angola, and how this information can assist geologists and mineralogists to identify and interpret different types of primary economical diamond deposits in Africa and globally.

**Chapter Three** Field work and advanced analytical techniques in diamond research for a comprehensive study and characterisation of mantle xenolith and kimberlite rocks and how these methods can assist the geologists and mineralogist to analyse and better understand the effects of changes in the sampled mantle / kimberlites rock during and after cooling.

**Chapter Four** presents the new findings / results linked to the geological problem associated with preservation conditions of diamond, diamond grade variation, quality, and size distributions observed among kimberlite pipes studied and how this information can be used to support future diamond exploration. **Chapter Five** contains discussion of the project results and their critical evaluation for greater understanding of mantle and kimberlite emplacement conditions and their implications for diamond preservation and quality.

**Chapter Six** the overall conclusion of the thesis, and suggestions and recommendation for further research. **Chapter Seven** contains the reference list.

## **Chapter Two . Background and literature review: regional setting, geochemistry of kimberlites, indicator minerals and application of advanced techniques in diamond research**

### **2. 1. The geodynamic setting and geochemistry of the Lunda kimberlite pipes**

This Chapter describes the fundamental aspects of Angola's geological setting and their implications for economical diamond exploration, focussing principally on Lunda province (LP) within the Congo craton. The study of this Cratonic lithosphere mantle is crucial, since it assists us in understanding the physical behaviour of old continents and Angolan minerals deposits (kimberlites and alluvial). Kimberlites contain diamondiferous xenoliths (P-type - peridotitic and E-type Eclogite) which are representative of various mantle levels (Stachel *et al.*, 2003) and provide important information about mantle petrology and conditions of diamond formation (Spetsius *et al.*, 2008; and Stachel *et al.*, 2003).

Angola has a complex geological history resulting from a complex series of past tectonic events (Guiraud *et al.*, 2005; and Batumike *et al.*, 2009). The most prominent geological feature in Angola is a structural zone of weakness (corridor faults, see Figure 2.1) that crosses the entire country, from Lunda province in the NE to the SW (Robles-Cruz *et al.*, 2008, Pervov *et al.*, 2011). Several hundred kimberlites are known in Angola and most of them are aligned along the zone of weakness. These kimberlites are a result of the breakup of Gondwanaland (Helmstaedt and Gurney, 1997) during the Jurassic to Cretaceous period approximately 60 -190 Ma ago (Jelsma *et al.*, 2004).

The tectonic events that occurred in the region of Lunda province have been described by Pereira *et al.* (2003) as an important diastrophism (deformation of the Earth's crust), with several fractures that created the Lucapa Graben. This tectonic structure is understood to be an important tectonic indicator in the search for the kimberlites in Angola (Ganga *et al.*, 2003). Deep-reaching fracture zones in the crystalline basement of the Congo craton played a crucial role in controlling the mineralization process in Angola (de Boorder, 1982). These deformation events were also accompanied by metasomatic processes within the Angolan lithosphere mantle.

#### **2. 1. 1. Objective**

The main objective of this Chapter is to elucidate and understand how tectonic events emplaced and controlled diamondiferous kimberlites in Angola, in particular Lunda province, and also how these episodes affected part of the Congo craton. In addition, this Chapter has the objective of providing an understanding of how the Gondwana episodes are related to the genesis of the Angolan kimberlite pipes and the consequences of the opening of the Atlantic Ocean to the Congo craton.

### **2. 1. 2. Geological setting of Lunda province**

The area under study lies in NE Angola and underwent several orogenies or complex series of tectonic events which have contributed to the geology of Lunda province having a complex formation history (Boyd and Danchin 1980; Guiraud *et al.*, 2005; and Batumike *et al.*, 2009). These orogeny events, significantly affected the Angolan shield, leading to the formation of the Lucapa graben and emplacement of diamondiferous kimberlites (Roberts *et al.*, 2004).

Figure 2.1 shows a map of Angola and the research area, Lunda province (LP), which is located in the northeast of the country. It is located within the old lithosphere (Congo Kassai craton) with several mineral resources including diamond deposits. Lunda province is the region of the highest diamond concentration in Angola and is consequently heavily mined.

The Appendix 6 shows the ages of African crustal basement whereas Table 2.1 summarises the main orogenic episodes that took place in Angola. The same events occurred in other parts of Africa (Dirks *et al.*, 2003), which have been grouped in several series (Kröner and Stern 2004; Roberts *et al.*, 2004; Pereira *et al.*, 2003; Guiraud *et al.* 2005; and Batumike *et al.*, 2009). The Eburnean orogeny is the one that most affected the Archean of the Angolan block including several locations in Lunda province (Dirks *et al.*, 2003; Roble-Cruz *et al.*, 2009). This is depicted in Figure 2.1. During field work and sampling activities by the author in Lunda province, it was observed that Lunda province shields are composed of different crystalline rocks including granulite, granite gabbro, norite and charnockitic complexes (quartzites, gneisses, amphibolites and meta-gabbro's) (Pereira *et al.*, 2003). The charnockitic complex rocks from the Archean time have been shown by Batumike *et al.* (2009) and Dirks *et al.* (2003), to constitute the Precambrian crystalline basement of Angola.

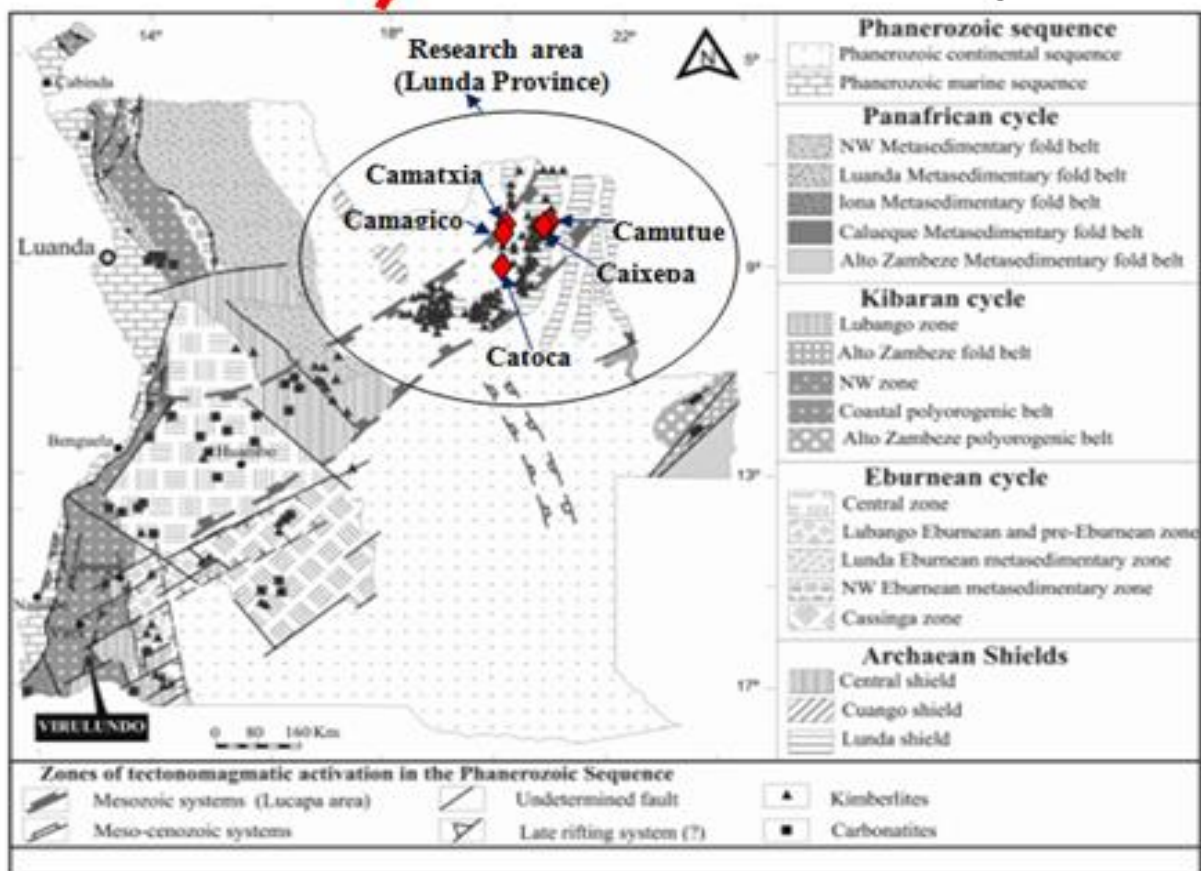
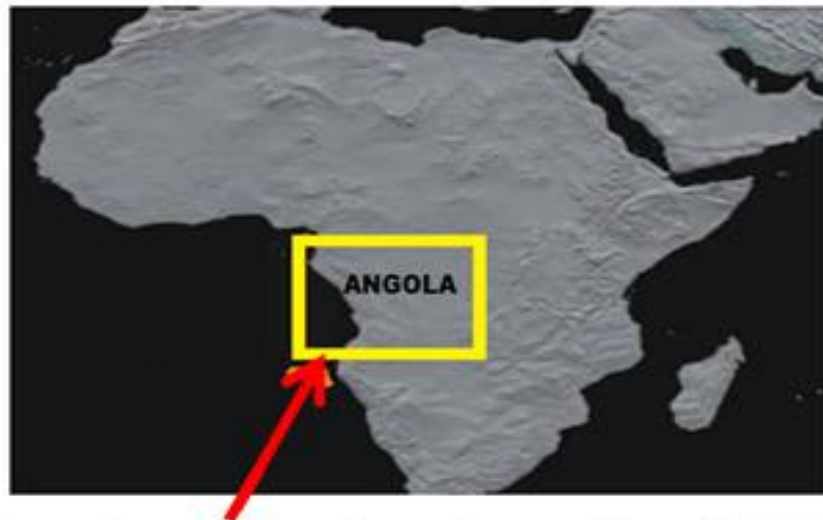


Figure 2.1. Geological setting of Angola, showing the distribution of carbonatites and kimberlites. In general, the high-grade deposits of diamonds are in the north-east of the belt, decreasing towards the south-west. Modified and reproduced after Torro *et al.* (2012) with the permission of the Mineralogical Society of Great Britain & Ireland.

The presence of charnockitic rocks in Angola are clear evidence of the occurrence of intensive metamorphic events. This is because charnockitic rocks form extensive orthogneiss plutons in many granulite terranes. Pereira *et al.* (2003) used isotopic data (Rb/Sr and U/Pb) that indicates an age between 2.9 - 2.85 Ga for the charnockitisation of the mafic complex such as norite (a coarse-grained intrusive igneous rock similar to gabbro); tonalites (a plutonic igneous rock composed mainly by Quartz, and Na-plagioclase) and amphibolites (a metamorphic rock composed mainly of amphiboles, plagioclase and minor quartz) in Angola. The implications of these metamorphic episodes on diamond exploration is that they may have affected the primary mantle forming minerals by causing alterations, as it observed on several thin sections investigated (see Chapter Four).

<b>Geological scale time Era</b>	<b>Orogeny types</b>	<b>Ages</b>	<b>Main outcome</b>
<b>Palaeoproterozoic (The oldest era (age) of Proterozoic Eon)</b>	Eburnean	2.2-1.8 Ga	<p>1- Extensive deformation of foundation of Africa (cratonic nuclei) including Congo-Kasai craton. Volcano-sedimentary, magmatic (e.g. granites), metamorphic (e.g. gneiss) and metasediment across Western Africa and Chela Group rocks in SW Angola.</p> <p>2- Angola block is more complicated than previously known (Dirks <i>et al.</i>, 2003), due to post events (high grade of metamorphism).</p> <p>3- The syn- and post-Eburnean crustal evolution and recycling processes have generated economic resources in SW Angola (Pereira <i>et al.</i>, 2011). 4- The Archean orogeny /belt with a high grade tectono-metamorphic event, accompanied by gabbro, gneiss, norite granulite and charnockite complex, associations are recognized in central and NE Angola (Lunda province)</p>
<b>Mesoproterozoic (The second era of Proterozoic)</b>	Kibaran	1.4-0.85 Ga	<p>1- Very long extensional / belt tectono-metamorphic trending NE over 1300 km across the Central African Congo craton, from Angola- Zambia-D.R.Congo through Rwanda, Burundi, Uganda and NW-NE Tanzania (Tack <i>et al.</i>, 2010)</p> <p>2- The extensional Kibaran event occurred on border of the Congo craton, and caused the formation of sequenced stratigraphy of clastic-carbonate in SW Angola.</p> <p>3- Merging of the Southern Africa and Central cratons as part of Rodinia supercontinent (Earth's landmass)</p>
<b>Neoproterozoic (The last era of Proterozoic)</b>	Pan-African	0.85-0.5 Ga	<p>1- Multi- orogenic cycles, resulting in the opening and closing of large oceanic area. Metamorphic series and accretion and final suturing of continental fragments to form the supercontinent Gondwana</p> <p>2- Deep fractures, faults and formation of Lucapa graben and emplacement of diamondiferous kimberlites in NE Angola. 3- Separation between Brazilian and African cratons</p>

Table 2.1. Timeline of main Angolan orogenic episodes.

The breakup of Gondwanaland and the opening of the Atlantic caused several fractures in the African continent (Helmstaedt and Gurney, 1997), including Angola. The geological episodes that took place in Angola are related to the opening of the Atlantic episodes (Pereira *et al.*, 2003). According to several researchers (Kröner and Stern, 2004; Batumike *et al.*, 2009; and Dirks *et al.*, 2003), the Atlantic opening processes may have induced intensive tensile forces that caused the division of major Archean Cratonic nuclei that form the foundation of Africa such as Congo, Kaapvaal, Zimbabwe and Tanzania (see section 2.4).

During the Cretaceous period, prior to and after the separation of South America from Africa, between 132 and 125 Ma, (White *et al.*, 2012), the southern African continent underwent extensive uplift and erosion. The oceanic rifting event may have important tectonic consequences in the African plate, reactivating structures from previous orogenic cycles (Pereira *et al.*, 2003). The major implications for this tectonic structure is that they have exerted a key control on kimberlite emplacement and mineralization (de Boorder, 1982), particularly in the region of Lunda, during the Cretaceous time (Castillo-Oliver *et al.*, 2011; Pervov *et al.*, 2011; and Robles-Cruz *et al.*, 2008). In Angola, the most famous tectonic structure generated by the oceanic rift event is the Lucapa graben.

Figure 2.2 shows similar tectonic structures that control the kimberlites in Angola, in particular those from Lunda province (NE Angola). The basement structures are the results of connection between regional structures (major mobile zones or faults, fracture corridors) and local structures (linear graben, rift valleys, internal fractures and deep faults within the Lucapa corridor) have produced deep structures that cut through the crust into the upper mantle and have consequently controlled kimberlite emplacement in NE Angola (White *et al.*, 1995; and Jelsma *et al.*, 2009). Similar tectonic structures have been described by Vearncombe and Vearncombe (2002) to be the key controlling the emplacement of kimberlites located in the Kaapvaal Craton such as Orapa and Jwaneng kimberlites from Botswana and Premier, Kimberley, Jagersfontein, Koffiefontein and Finsch kimberlites from South Africa and some kimberlites from Lesotho.

The ideal model of tectonic structures that control kimberlites from Lunda province (NE Angola) is illustrated in Figure 2.2, this is because many researchers (Helmstaedt and Gurney, 1997; Vearncombe and Vearncombe, 2002; Jelsma *et al.*, 2009; Pereira, *et al.* 2003; White *et al.*, 1995) have proven that diamondiferous kimberlites occur in environments where there is an association with deep faults in the old Archean crust within thick lithospheres, (Stachel, 2003; Nixon, 1995; and Janney *et al.*, 2010).

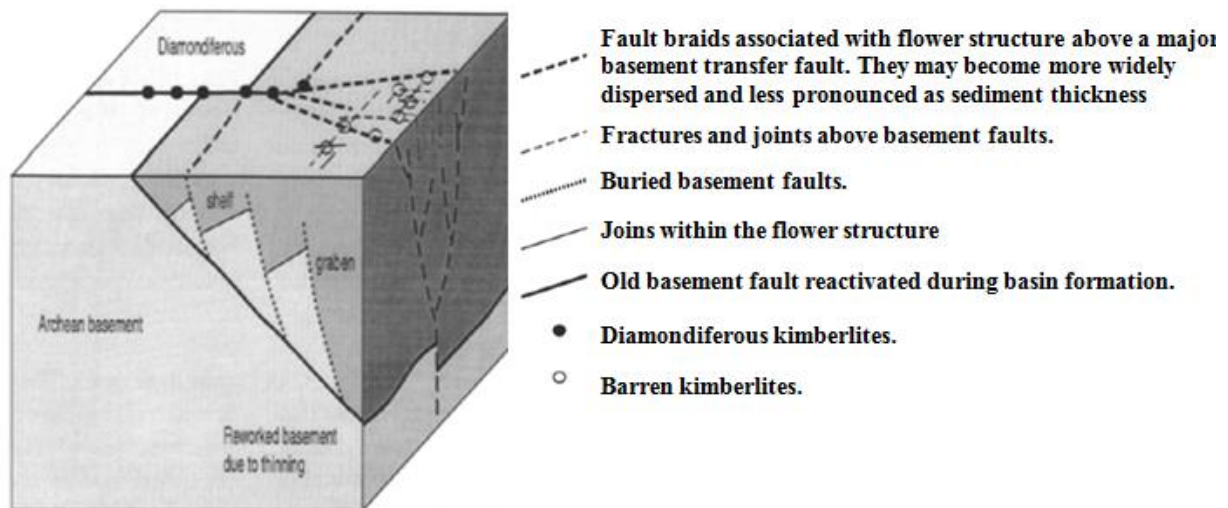


Figure 2.2. Diagram of the possible relationships between basement faults, basin structures and kimberlites in a graben. The same relationship will hold for lamproites. This shows that as the depth of sediment infill increases, the basement faults or shears become less distinct and more dispersed and consequently the kimberlite clusters also become wider and more dispersed (White *et al.*, 1995).

The ages of known kimberlites vary from early Proterozoic to early tertiary (Sparks *et al.*, 2006), but the Angolan kimberlites, including the pipes from Lunda province, have been confirmed to be from the earlier Cretaceous age (Nixon, 1995, see also Table 2.2). Angolan kimberlites are from the Mesozoic Era, and are frequently associated with continental structures that gave rise to the transformation of the Mid-Oceanic ridge (White *et al.*, 1995).

Time	Ma	Kimberlite volcanism	Lamproite
Quaternary		Igwisi, Tanzania	Gaussberg; Leucite Hills; (SW Uganda); (Sulawesi)
Miocene	5–25		SE Spain; Algeria; Tunisia; Ellendale *, W Australia; Francis, Utah; (Moroto, Uganda) Smoky Butte, Montana; (Copeton, NSW)
Oligocene	26–38		
Eocene	45–53	Tanzania	
Eocene–Paleocene	50–64	Namibia; Tanzania; NWT, Canada	Yellow Water Butte, Montana
U. Cretaceous	65–79	SW Cape; Namibia; Mbuji–Mayi, Zaire	
M. Cretaceous	80–114	Kimberley; Kundelungu, Zaire; Lesotho; Orapa; Brazil; Sask, Canada; Huangjiacun, China; Sierra Leone–Guinea–Mali	Hills Pond, Kansas; Prairie Creek *, Arkansas; Coromandel *, Brazil
L. Cretaceous	115–144	S. Africa Gp II; Angola; Kuoika, Siberia; Liberia	Murun, Irkutia
U. Jurassic	145–174	New York; Swartuggens, S. Africa; Pri–Lena, L.Olenek, Yakutia; SE Lesotho; E. Griqualand; SE Australia	Swartuggens, S. Africa; (Wandagee, Western Australia)
L. Jurassic	175–204	Pennsylvania; Jwaneng; E. Griqualand; Dokolwayo, Swaziland	
Triassic	205–239	Kimberlites, W. Greenland	Kapamba *, Zambia
Permian	240–290	Kentucky; Cross, Canada	
Pennsylvanian	305		(Bulljah Pool, Western Australia)
Devonian	340–409	Alakit–Daldyn, Malo Botuobinsk, Yakutia; Colorado–Wyoming Somerset Island, Canada	
Silurian–Ordovician	410–499	Muna, Yakutia; Shandong and Liaoning, China; Arkhangelsk, Russian Platform	Mt. Bayliss, Antarctica
Cambrian	500–600	Zimbabwe; Venetia, S. Africa; West Greenland	
U. Proterozoic	800–1250	North Western Australia; India; Premier, S. Africa; Bubiki, Tanzania	Holsteinsborg, W. Greenland; Majhgawan *, India; Argyle *, W Aust; (Ngualla, Tanzania)
M. Proterozoic	1300–1500	Gabon; Liberia	Bobi *, Ivory Coast; Chelima, India
L. Proterozoic	1600–1800	Kuruman, S. Africa; Venezuela	Disko Bugt, W. Greenland
L. Proterozoic	ca. 2000	(Burkina Faso)	

Table 2.2. Episodes of kimberlite and lamproites volcanism (Nixon, 1995). \*Diamondiferous, (Other volcanic rocks with reported diamond are shown in brackets).

The presence of diamondiferous kimberlites in Lunda province is validated by Clifford's Rule (Hatton, 2009) which states that diamondiferous kimberlites are almost exclusively encountered in the Archaean Cratonic regions (continental crust older than 2.5 billion years, Mitchell, 1991) or 3.5 to 3.2 billion years (Helmstaedt *et al.*, 2010; Creighton *et al.* 2011; Helmstaedt and Gurney, 1997).

Boyd and Gurney (1986) studied diamonds of the African lithosphere and concluded that, in Southern Africa, kimberlites with diamonds are only those erupted within the boundaries of the craton that contain significant quantities of diamonds (Figures 1.1 and 2.3), this includes the pipes from NE Angola (Lunda Province).

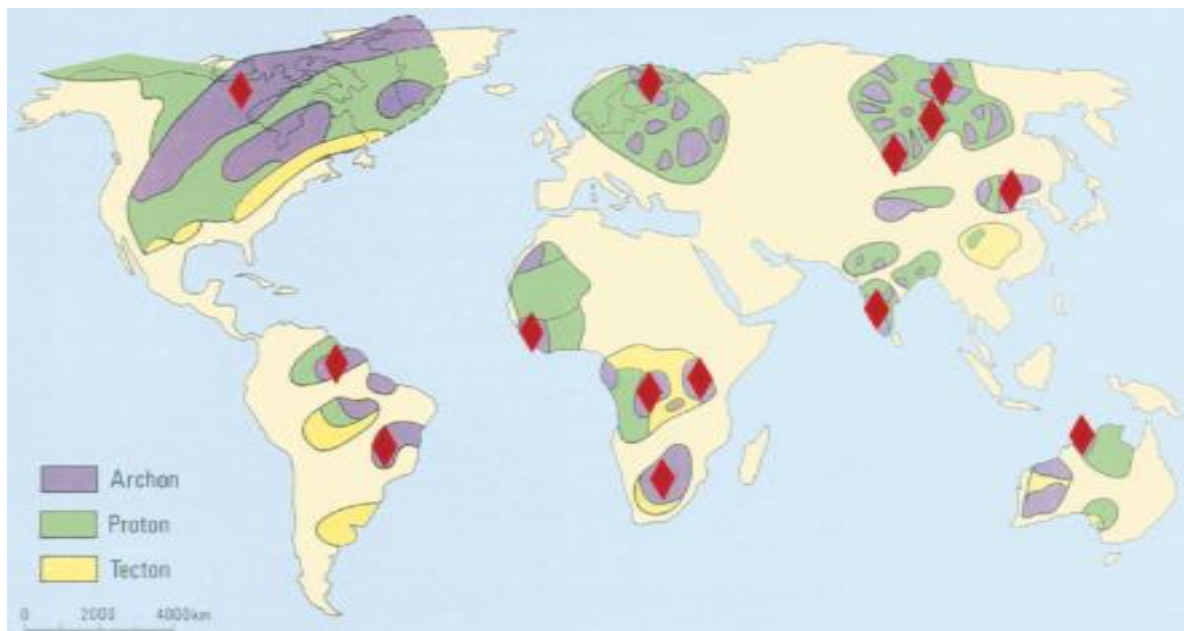


Figure 2.3. Global distribution of cratons, age provinces (Archons, >2.5 Ga; Protons, 2.5 to 1.6 Ga; and Tectons, 1.6 to 0.8 Ga), and major diamond deposits (red colour is diamonds) (Haggerty 1999).

## 2. 2. Kimberlites: a review and discovery history

Prior to 1720, when the world did not know the existence and exploration of kimberlite, all diamonds known they were from alluvial deposits in the Krishna River of Madhya Pradesh in India, where had been mined since ancient times (Field *et al.*, 2008). Following the development of scientific research and exploration of the New World, diamonds were discovered elsewhere, and the first of these new discoveries was still diamonds of alluvial origin, in 1725-1726, in rivers in the Minas Gerais district near the town of Tijuco, in Brazil (Field *et al.*, 2008; Harlow and Levinson, 2008).

The name of kimberlite only came after the first diamonds discovered in southern Africa between 1866 and 1867 (Harlow and Levinson, 2008) by a 15-year old boy named Erasmus Jacobs who discovered a transparent stone (21.25 carat diamond) on his father's farm, on the south bank of the Orange river. These discoveries ignited a major rush of European and American geologists to prospect for diamonds in South Africa. The term kimberlite was originally proposed in 1887 by Professor, Henry Carvill Lewis (American geologist and mineralogist), in Manchester, UK (Field *et al.*, 2008), who described the rock as a volcanic breccia and porphyritic. It was named after the town of Kimberley in South Africa followed the nomenclatures rules during its discovered period. The largest-ever diamond was discovered in Premier kimberlite in South Africa in 1905. It was a rough and unpolished original that weighed 3,106.75 carats (621.350 g), this diamond was named as Cullinan diamond. In addition, the largest ever octahedral (Kimberley Octahedron) diamond, weighed 616 carats, was recovered in 1974 within Kaapvaal Craton, at Dutoitspan mines (Field *et al.*, 2008).

Skinner and Clement (1979) defined kimberlite as a volatile-rich, potassic ultrabasic igneous rock which occurs as small volcanic structures such as pipes, dykes and sills, that exhibit distinctive inequigranular texture. This texture results from the presence of macrocrysts or megacrysts set in a fine grained matrix (Mitchell, 1995). The macrocryst (0.4-12mm) or megacryst assemblages consist of rounded anhedral, mantle-derived, ferromagnesian minerals which include olivine, phlogopite, picroilmenite, chromian spinel, magnesian garnet, clinopyroxene, and orthopyroxene (commonly enstatite). This matrix wherein megacrysts are placed, are groundmass (Francis and Petterson, 2009) composed by altered olivine, phlogopite, carbonate (commonly calcite), serpentine, clinopyroxene (commonly diopside), monticellites (are silicate minerals of the olivine group, with chemical composition  $\text{CaMgSiO}_4$  and gray in colour), apatite and minor grained oxides (perovskite, ilmenite and spinels), Masun and Scott Smith, (2006).

### **2. 2. 1. Classification of kimberlites**

Different classification schemes for the host- kimberlite magma have been proposed over time. For example, the first classification of group 1 and 2 of kimberlite rocks was proposed by Wagner (1914) who recognize that there were at least two varieties of diamond-bearing kimberlites in South Africa, which he referred to as “basaltic” and “lamprophyric” kimberlites (Field *et al.*, 2008). Later on, this major difference classification was recognised and quantified geochemically by Smith (1983). Based on an isotope geochemistry study Smith, (1983) proposed that Group-1 kimberlites have a smaller amount of radiogenic Sr-Nd signatures relative to present day bulk earth whereas Group-2 are significantly enriched with radiogenic Sr-Nd relative to bulk earth (Donnelly *et al.*, 2010). Another key difference is that the Group-1 contains radiogenic Pb isotopic signatures, whereas Group 2 has

non-radiogenic Pb isotopic signatures. Later, this classification has been supported by Field *et al.* (2008) who demonstrated that Group-1 kimberlites are basaltic.

In addition the geochemistries of the two groups (1 & 2) are also distinct (Skinner, 1989; Skinner and Marsh, 2004). For example Group 1 are composed of diverse minerals of olivine, monticellite, calcite, phlogopite, spinel, perovskite, apatite and ilmenite whereas Group 2 are micaceous or lamprophyric (Francis and Pettersson, 2009; Mitchell, 1991) and contain minerals such as rounded olivine, diopside, spinel, perovskite, apatite and lesser amounts of melilite due to alteration processes, but phlogopite is a dominant groundmass mineral (Field *et al.*, 2008). In terms of geographical distribution and age, there is also a difference. For example, Group 2 kimberlites have been found only in South Africa (Helmstaedt and Gurney, 1997; Donnelly, 2010) where they form in older regions with ages ranging from 114 -200 Ma (Smith *et al.*, 1985) whereas group1 kimberlite rocks with ages less than 100 Ma occur throughout the world (Mitchell, 1995). The kimberlites from Lunda provinces and South Africa are classified as Group I kimberlites (Ganga *et al.*, 2003; Skinner, 2008; and Mitchell, 1991).

### **2. 2. 2. The Origin of kimberlite magma and diamond in the Earth.**

As explained in Chapter Two, Angolan kimberlites are related to the breakup of Gondwanaland and the opening of the Atlantic Ocean (Jelsma *et al.*, 2004). The petrogenesis of worldwide kimberlites is, however, controversial with disagreements over the nature and depth of the source region (Keshav *et al.*, 2005), whether they are primary in origin, and the cause of melting (Shantanu *et al.*, 2005), with some suggesting that they derived at the core and mantle boundary or mantle transition zone (Heaman *et al.*, 2003).

But the most plausible finding from many researchers (Ringwood *et al.*, 1992 and Sparks *et al.*, 2006) is that kimberlites magma are formed by small degrees of partial melting of a carbonated garnet lherzolitic minerals assemblage under hydrous conditions at depth 150- 300 km, but in contrast to the new discoveries, based on diamond xenocrysts containing syngenetic inclusions of garnet, are crucial indicators of a deeper and transitional zonal origin for kimberlites (Ringwood *et al.*, 1992).

Figure 2.4 shows a model for the genesis of kimberlite magma. This involves a rising convection current process from the lower mantle with a dynamic uplift of the garnetite layer forming a structural dome at the 650 km discontinuity. High temperatures arising from convection currents caused partial melting of the earlier harzburgite boundary layer (Ringwood *et al.*, 1992) and this produced kimberlites (Keshav *et al.*, 2005).

The hypothesis of derivation of kimberlites from depths of 400-650 km (Figure 2.4), deeper than any other igneous rock (Ringwood *et al.*, 1992) makes it important to understand kimberlite petrogenesis and constraint of the melting processes and composition of the mantle near the cratonic lithosphere

and asthenospheric boundary. Also another key aspect from kimberlite magma is linked to low contents of silicon oxide ( $\text{SiO}_2$ ) and high volatile and trace element contents (Field and Scott Smith, 1998). These factors helped diamond to be transported at higher speeds from deep sources to the surface due to the lower viscosities of the liquids present, which will have aided transportation, according to the Figures 2.4 and 2.5.

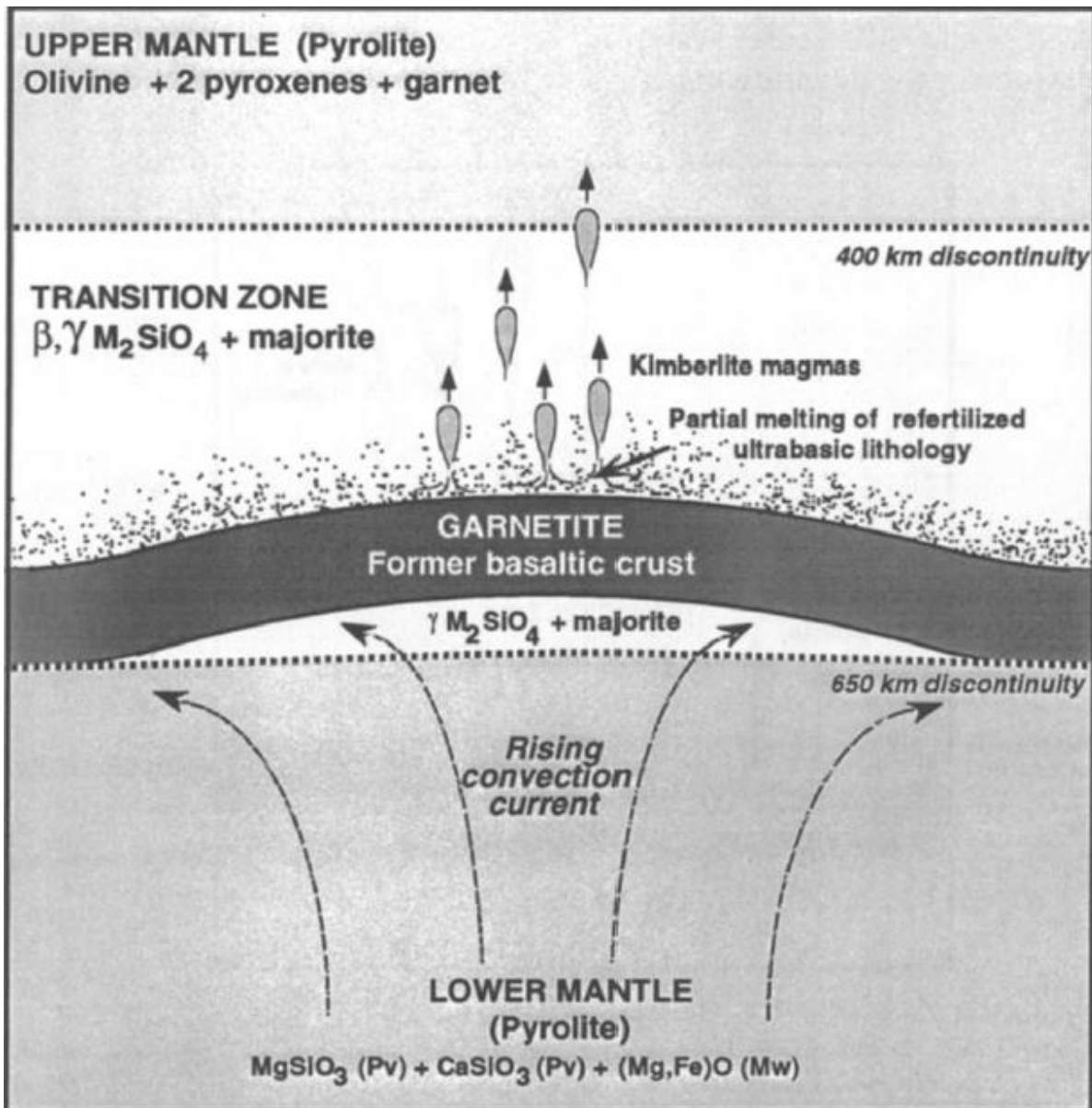


Figure 2.4. Model for genesis of kimberlite magma: a rising convection current from the lower mantle. Garnetite (metamorphic rock consisting >70% garnet) (Ringwood *et al.*, 1992).

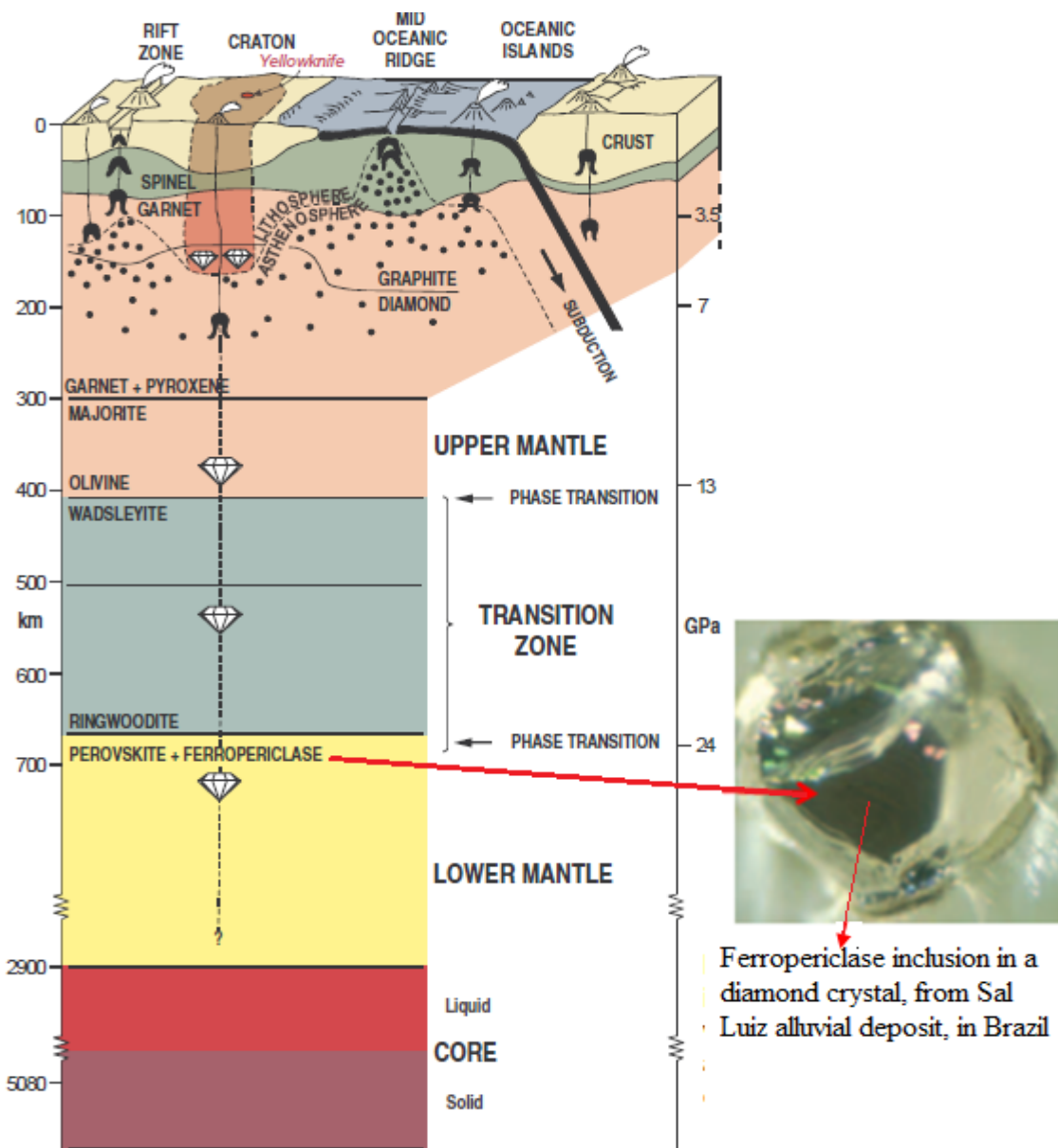


Figure 2.5. Diamond source in the Earth's upper mantle, transition zone, and lower mantle. Modified after Stachel (2003) and Stachel *et al.* (2005).

As shown in Figure 2.5, the origin of diamond is a complex process. For instance an origin of diamonds from the lower mantle (with depths of more than 660 km see Figure 2.5) is usually recognized by the observation of inclusions of ferropericlase coexisting with phases of CaSi-perovskite, MgSi-perovskite, and stishovite ( $\text{SiO}_2$ ) (Stachel *et al.*, 2009). Based on chemical, mineralogical, and petrological studies, Mitchell and Giardini, (1977) concluded that all natural diamonds are formed at depths below 100 to 200 km under diamond-stable conditions (graphite-diamond equilibrium boundary of the carbon system). In contrast, Stachel (2003) concluded that diamonds have different sources in the Earth, including the upper mantle, transition zone, and lower mantle, which implies that they are arise from much greater than depths (see Figure 2.6). Another

crucial piece of evidence for the origin of kimberlite and diamonds comes from the work of Persikov and Bukhtiyarov (2013) who explained that kimberlite melts could be generated in the mantle with small degrees of partial melting (0.1-0.7 vol. %) of carbonated peridotite at depths ranging from 250-340 km and pressures of 8-10 GPa (80 – 100 kbar), temperature approximately 1700 °C. Under these conditions the volume content of crystals would be approximately 10 % and the viscosity of this melt would tend to be high (approximately 5000 Poise or 500 Pa·s) whereas at near – surface during kimberlite formation, the viscosity of kimberlite melts would be lower (approximately 250 Poise or 25 Pa·s), with temperatures of approximately 1150 °C and pressures of 50 –100 MPa (Persikov and Bukhtiyarov 2013). According to Dasgupta (2013) the upwelling ambient mantle at the present day falls within the green band (the zone with > 240km of depth, that increase with pressure and temperature, which goes through upper to low mantle where the eruptions of kimberlite magma starts). As seen from Figure 2.6, at depths shallower than 300 km the carbonated mantle melting temperature drops below 1400°C where the melting process take place (below the base of the continental lithosphere) and consequently, starts to generate the carbonatitic liquids that will consequently evolve to kimberlite magma.

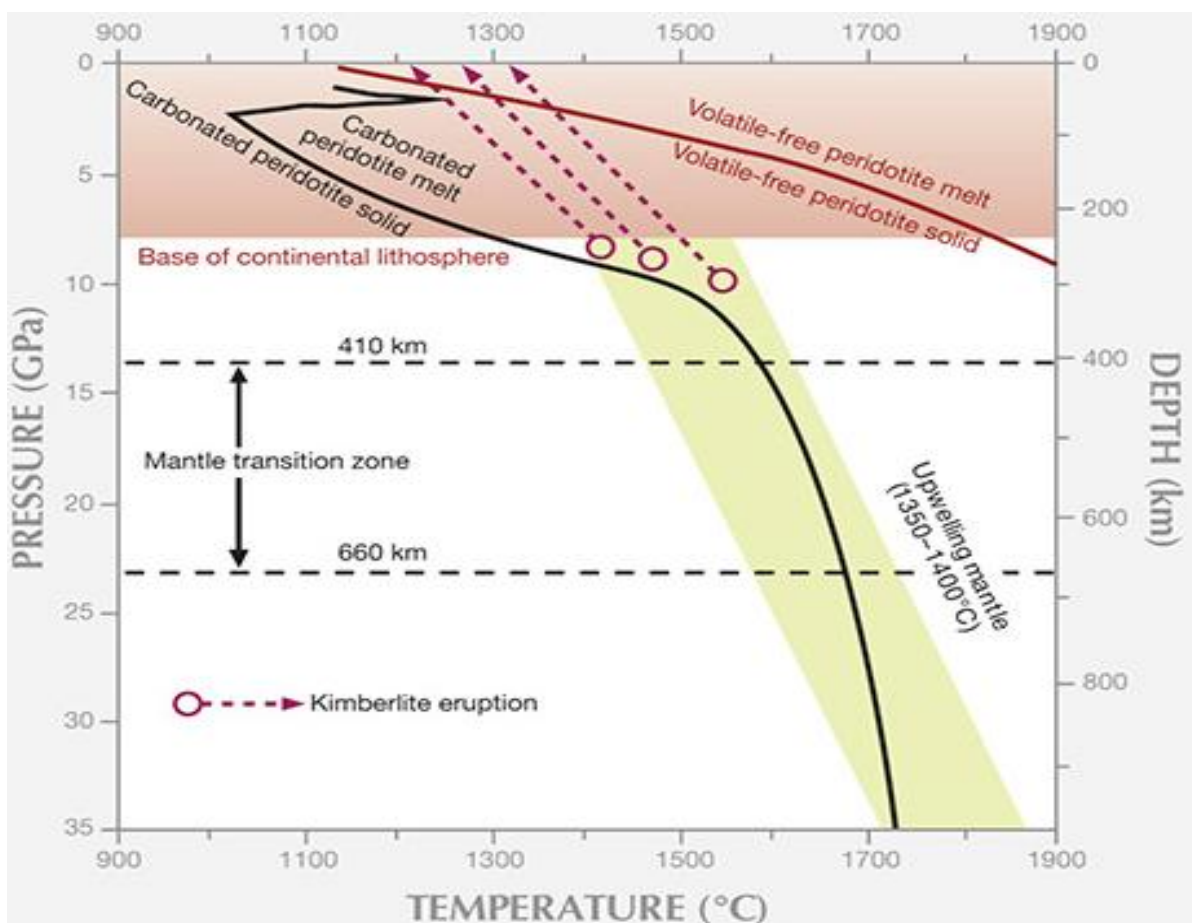


Figure 2.6. Pressure-temperature diagram showing the melting of mantle peridotite containing volatiles and carbonate (black) and mantle peridotite that is dry and free of volatiles and carbon (red), from Shirey and Shigley (2013).

As illustrated in Figure 2.7, the host kimberlite magma that carried diamonds is shown to be younger than the diamonds and the ancient continental cratons they intrude (Haggerty 1999; 1995), with only a few exceptions Argyle, and Wawa kimberlites pipes (Gurney *et al.*, 2010). For example Premier pipe with  $1750 \pm 100$  Ma (Allsopp *et al.*, 1967), and  $1126 \pm 9$  Ma for Argyle pipe (Skinner *et al.*, 1985),  $1097 \pm 7$  Ma for Wawa kimberlites pipes (Kaminsky *et al.*, 2002), but all known diamond-bearing kimberlites are less than about 550 Ma in age (Shirey and Shigley, 2013; Nixon, 1995) and most of them less than 300 Ma, with abundant episodes of kimberlite eruption at less than 120 Ma in southern Africa and less than 80 Ma in North America (Gurney *et al.*, 2010).

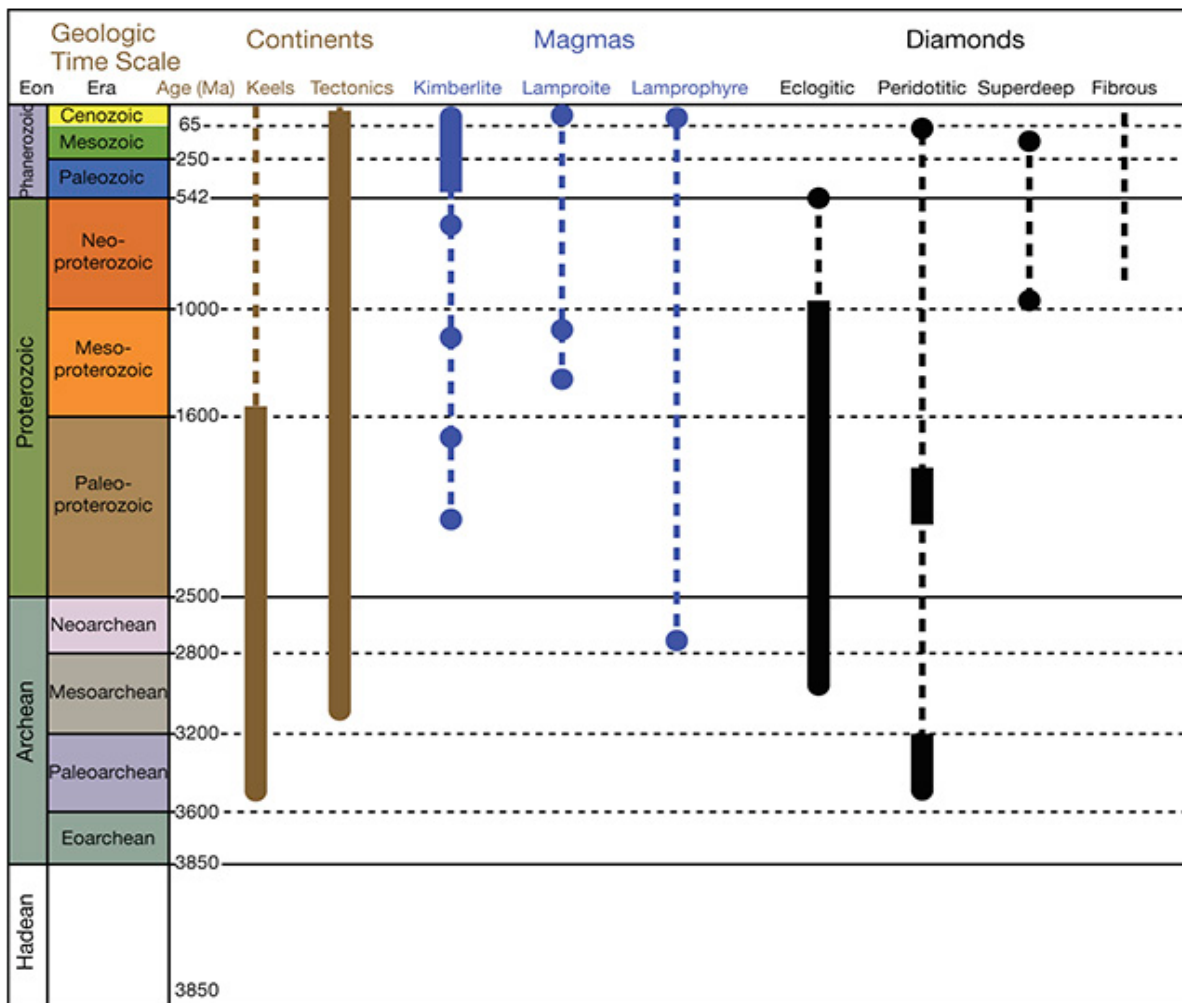


Figure 2.7. Illustration of the ages of continental keels and their relationships with tectonic processes, diamond-hosting magmas, and different diamond types. Note the antiquity of mantle keels and lithospheric diamonds greater than 1 billion years and the youth of most kimberlite eruptions (less than 550 million years). Solid vertical bars represent the duration of ongoing processes, magmas, or diamond-forming events, whereas solid dots show single known occurrences. Dashed lines demonstrate the possible ages of occurrence of these events. From Shirey and Shigley (2013).

### 2. 2. 3. The natural processes of kimberlite magma eruptions

The process of kimberlite magma eruption is a complex event. For example Webb *et al.* (2004) and Kamenetsky *et al.* (2006) pointed out that the eruption takes place in a violent manner, due to the high-energy mechanism from the deep mantle and the emplacement of kimberlite magma. Normally, these emplacements occur through explosive kimberlite magma eruptions and are generated by the rising column of kimberlite magma and gases such as CO<sub>2</sub> and H<sub>2</sub>O (Gurney *et al.*, 1993) which are believed to be powerful enough to fracture their way to the surface (Figure 2.8). The fluid can move through the crust in fractures only if the total fluid force or pressure exceeds the tensile strength and minimum principal stress component of the lithostatic pressure (Cas *et al.*, 2008). The SiO<sub>2</sub> content of 50-70% (Philpotts and Ague, 2006) and presence of gases (CO<sub>2</sub> and H<sub>2</sub>O) are crucial factors which combine to give magma viscosities of 0.1-1 Pa s at 1200-1400°C and 2-2.5 GPa. These are conditions under which the kimberlite magma is thought to be generated (Philpotts and Ague, 2006).

In relation to diamond, kimberlite magmas (Figure 2.8) are considered to be transporting agents that sample the deep mantle xenolith rock. Occasionally they may contain diamond-bearing mantle material and they rapidly carried it to the Earth's surface (Haggerty, 1999; and Stachel, 2003). The major implication during transport is that diamond passed outside its stability field. By doing so, providing the kinetics of the reaction is sufficiently rapid, diamond may be converted to graphite or more frequently to CO<sub>2</sub> (Gurney *et al.*, 1993). Under these conditions the conversion of diamond to CO<sub>2</sub> can be highly accelerated with higher oxygen activity in the magma, and consequently the effect of this resorption on the diamond content of an intrusion can be high. Therefore, in order for diamond to survive transportation to the Earth's surface, kimberlite magmas should have low viscosities and high buoyancies that enable fast transport (> 4 m/s) from the source region (Wilson and Head, 2007; and Kamenetsky *et al.*, 2001).

As shown in Figure 2.8, the fragmentation of magma in current magmatic explosive settings takes place through gas driven exsolution, vesiculation and explosive growth, and bursting of gas bubbles. Under these conditions and due to the violent emplacement mechanism explained by Webb *et al.* (2004) and Kamenetsky *et al.*, (2006), kimberlite magmas are categorized as chaotic mixtures (Patterson *et al.* 2009) of xenoliths of crustal rocks and mantle, minerals released from the xenolith disintegration during eruption, phenocryst minerals, alteration of previous minerals phases, and pieces of pre-existing kimberlite (Cas *et al.* 2008). In addition, contamination of materials from kimberlite magma has been supported by Kamenetsky *et al.*, (2006) who stated that in most cases kimberlites are modified by syn- and post magmatic changes that have altered the original alkali and volatile element contents.

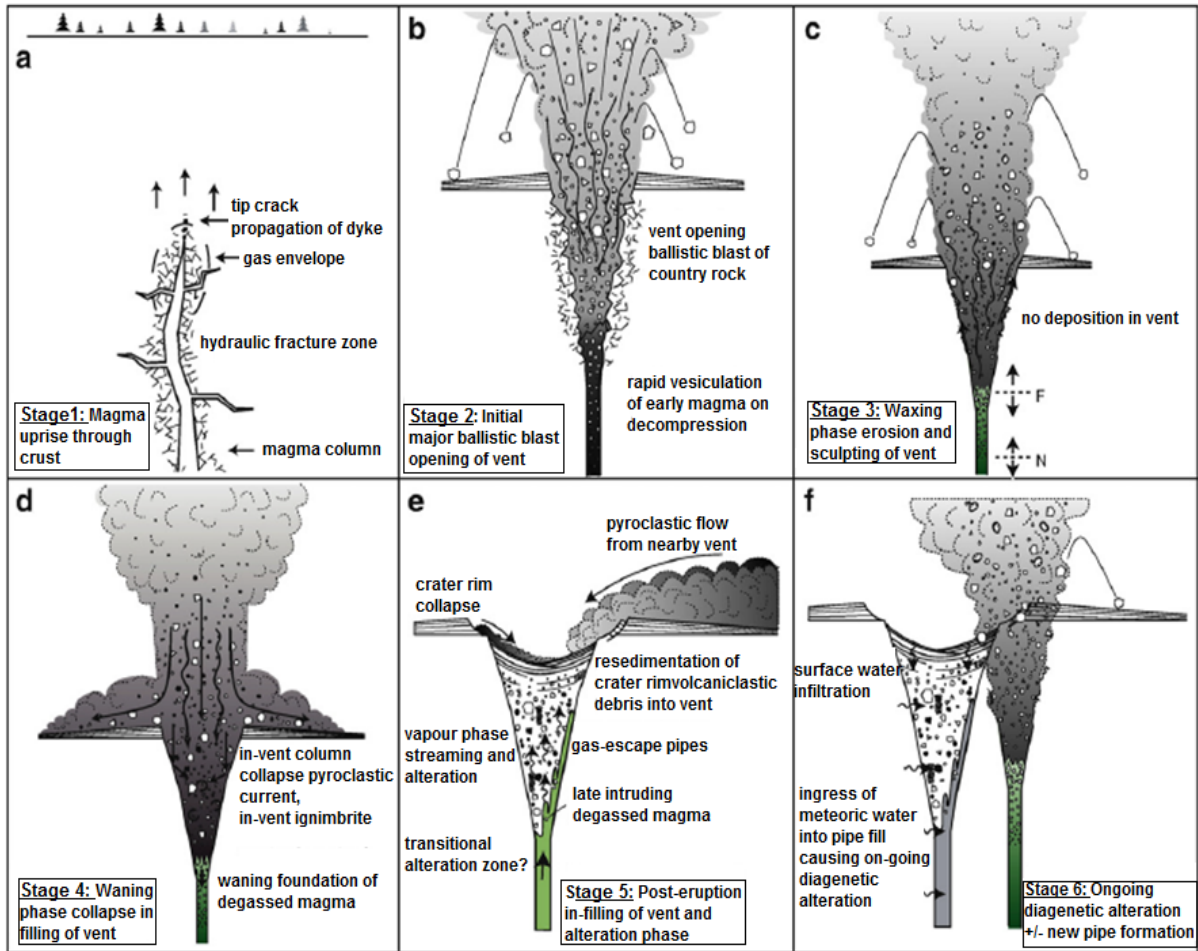


Figure 2.8. Model of six stages of explosive eruption of kimberlite pipes (Cas *et al.*, 2008)

### 2. 3. Carbon diamond formation

On Earth, carbon is widely dissolved in the Earth's silicate minerals at part-per-million levels (measures of concentration rather than total amounts) and lower. It has been pointed out by Shirey *et al.* (2013) that whenever carbon occurs as a free species, this leads to the potential for diamond formation. It has been understood that carbon in the Earth can occur in oxidized forms, such as when bound with oxygen in CO<sub>2</sub>, in reduced forms such as diamond, or graphite, or bound with hydrogen in methane and other organic molecules (Shirey *et al.*, 2013).

With respect to diamond-forming carbon, however, there are a number of fundamental questions remaining unresolved (Stachel *et al.*, 2009; Maruoka *et al.*, 2004; and Dobosi and Kurat, 2009), which can be grouped as follows:

1. Does diamond precipitate from a fluid or melt, or are solid state reactions or phase transitions involved?

2. What is the direction of diamond forming redox reactions (oxidation of methane or reduction of carbonate)?
3. What is the ultimate source of diamond forming carbon (mantle-derived or subducted)?

Diamond has been studied over the last 40 years and these studies provide information about the interior of the lithosphere (Shirey *et al.*, 2013). For example, the study of diamond inclusions such as perovskites and ferropericlase (magnesium/iron oxide) [(Mg, Fe) O] high-pressure phase, that are recognized as the only material sampling the very deep mantle to depths up to 800 km (Harte, 2010). Diamond geochemistry usually infers their formation to be strongly connected to crystallization from a methane-bearing metasomatic fluid (Thomassot *et al.*, 2007; Stachel *et al.*, 2009; Stachel and Harris, 2007). Similar conclusions have been reached by Dobosi and Kurat (2009), who suggested that diamonds crystallized from fluids of mantle origin under high pressures ranging from 45 to 60 kbar (4.5 to 6 GPa) and temperatures of 900 - 1200 °C (Boyd and Gurney, 1986) at depths of 140 km or more (Tappert and Tappert, 2011).

According to Shirey *et al.* (2013), the source and evolution of these fluids, is in diamondites (mantle xenoliths where diamond is intergrown with garnet and minor clinopyroxene). The derivation of carbonatitic fluid that produces crystallisation of diamonds has been described to originate from the asthenosphere mantle, and consequently this fluid would migrate upwards, percolating and penetrating the subcontinental lithospheric mantle where it reacted with the more oxidized peridotite wall rocks (Thomassot *et al.*, 2007).

Several debates have occurred over diamond formation. The crucial point from these studies is that a metasomatic process in the mantle is seen as the genesis of diamond formation (Haggerty, 1999). For example Gurney *et al.* (2010) and Stachel *et al.* (2005) explained that agents of metasomatism (e.g. supercritical fluids or melts), will infiltrate through mantle and then react with the mantle rocks, and diamond crystallizes as a consequence of the reduction of carbon via redox reactions (1 and 2 below), and both oxidized CO<sub>2</sub> or carbonate-bearing and reduced (degassing) methane-rich fluids (Figure 2.9) have been suggested as origins for diamond crystallization. This statement is also supported by Dobosi and Kurat (2009) who pointed out that CH<sub>4</sub>-H<sub>2</sub>O rich fluid phases are considered to be the primary source of carbon. This was confirmed by Shirey *et al.* (2013), with the process of crystallization taking place throughout the mantle below about 150 km and can occur metastably (state of stable/equilibrium) in the crust (diamond crystallization, Figures 2.9 and 2.10). Maruoka *et al.* (2004) found that the fluid inclusions in diamonds and trace element abundances in coexisting silicates support the presence of CO<sub>2</sub> during diamond formation according to reactions (1) and (2) below:



Based on the model of Maruoka *et al.* (2004), methane in the fluid will be oxidized to form elemental C and CO<sub>2</sub> from CO which will decompose according to 2CO = C + CO<sub>2</sub>. The elemental carbon (C) produced through this reaction can easily be dissolved in carbonatitic fluids or melts and consequently crystallise in the form of diamond in a very short time (Dobosi and Kurat, 2009) under the conditions described above. The elemental carbon (C) produced through this reaction and the formation of diamond will be intimately associated with the oxidation state of mantle rocks, which may be partially controlled, and which can be estimated, by the content of Fe<sup>0</sup>, Fe<sup>2+</sup> and Fe<sup>3+</sup> (Shirey *et al.*, 2013).

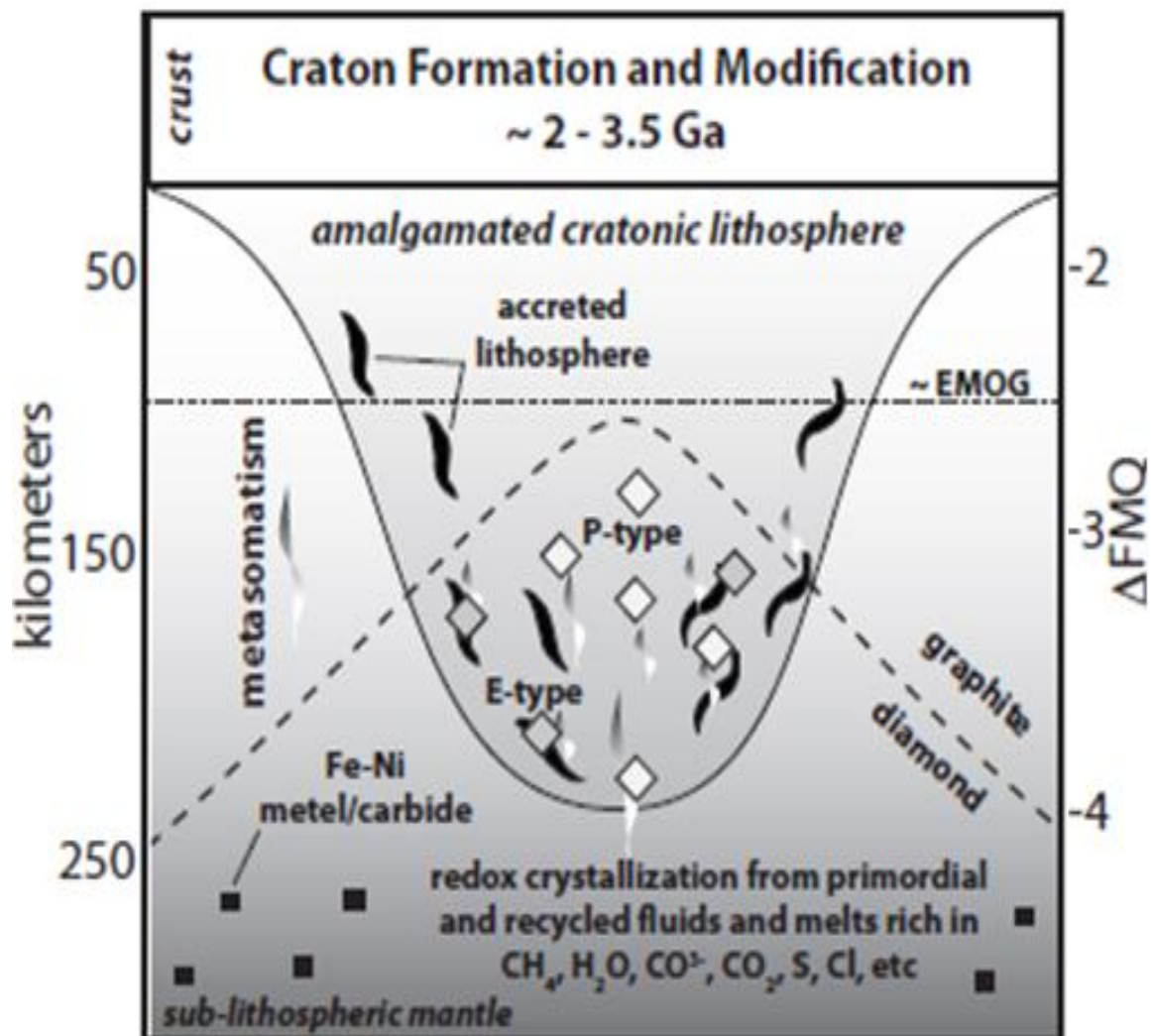


Figure 2.9. Schematic diagrams illustrating possible mantle conditions (e.g., depth, oxygen fugacity) and geodynamic settings in which lithospheric and sub-lithospheric diamonds and their mineral inclusions are formed. The relative roles of mantle and subducted lithospheric, crystallization from partial fluids, mantle redox,

and mantle flow, are all connected with studies of diamonds and their inclusions (Shirey and Shigley, 2013). Nomenclature: G → graphite, D → diamond, LAB → lithosphere/ asthenosphere boundary.

The interpretation from Figure 2.10 shows that under given oxygen fugacity ( $fO_2$ ), diamonds can form in the convecting mantle, the subducting slab and the mantle keel. Peridotitic or ultramafic inclusions are shown on the left side and eclogitic or basaltic inclusions are on the right side (see also Shirey *et al.*, 2013).

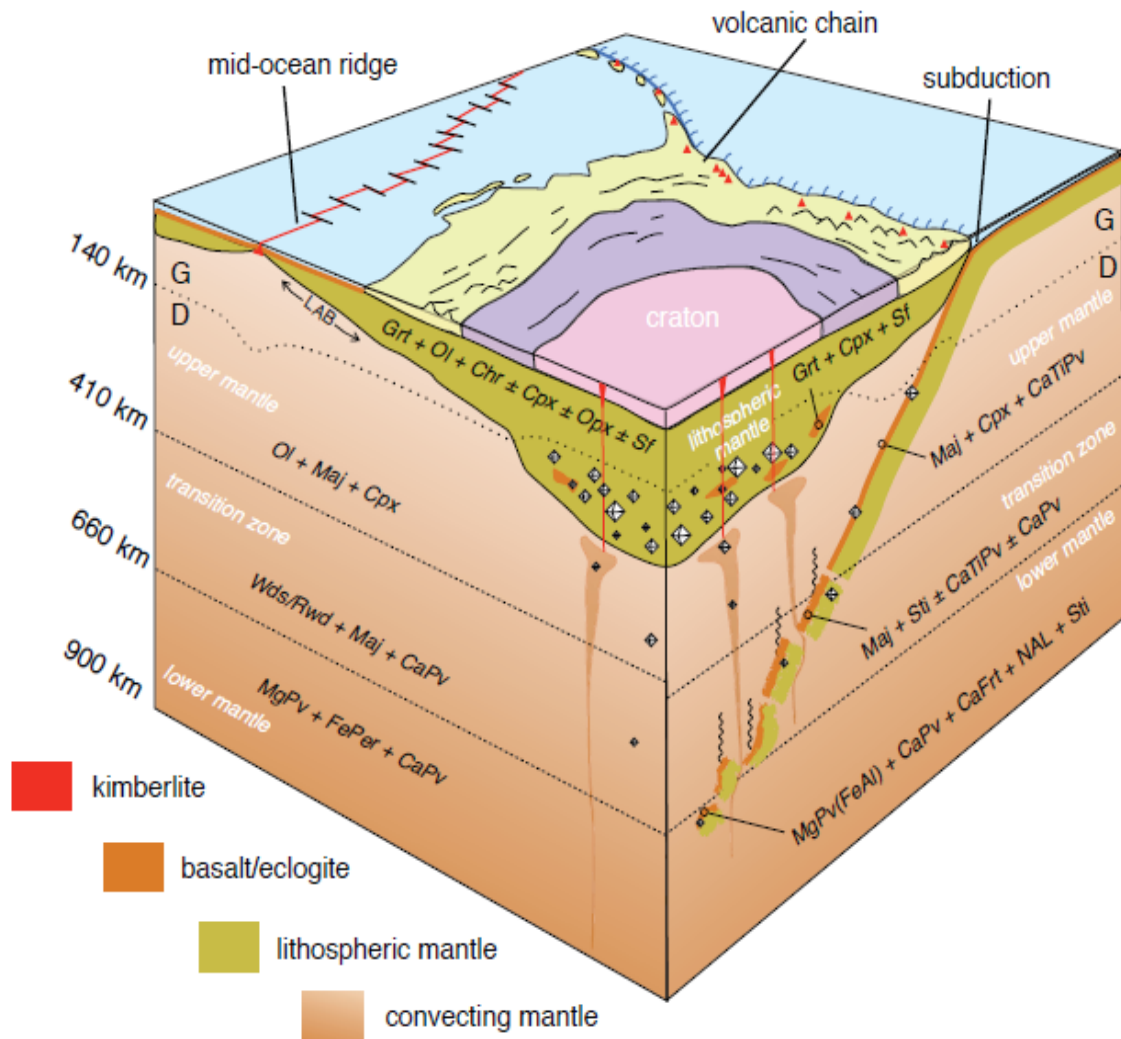


Figure 2.10. Illustration of a simple relationship between a continental craton, its lithospheric mantle keel and diamond stable regions in the keel, and the convecting mantle. (Shirey and Shigley, 2013).

As shown in Figure 2.10, the lithospheric mantle roots beneath cratons can extend to depths of more than 250 km, and due to their relatively low temperatures and extreme thicknesses, these cratons are the main locations of diamond formation in the Earth's mantle. These regions with relatively low temperature (geothermal gradients) and high pressures, geologically are called old parts of continents, which are referred to as cratons (Figure 2.10) composed of crustal basement rocks, such as granites and gneisses that are more than ~1.5 billion years old (Tappert and Tappert, 2011). The geothermal

gradient (geotherm) is the rate of increasing internal temperature of the earth with respect to increasing depth in the Earth's interior (Press and Siever, 1986). The average geothermal gradient near the surface is about 25°C for every kilometre of depth. Different tectonic provinces or some regions (e.g. mid-oceanic spreading ridges) are characterized by more rapid increases of temperature with depth (higher heat flows) because of active tectonic forces, deep fault zones, rifting and magmatic intrusions (Tracy and Blatt, 1995). Under these conditions, the geothermal gradient can make conditions in deep underground mines hot enough to explode rocks or bend steel support, if is not strong enough.

As illustrated in Figure 2.11, the shaded red-grey coloured region shows the potential extent of the diamond window for geotherms exceeding 35mW/m<sup>2</sup> (Griffin and Ryan, 1995) and assuming a temperature at the base of the lithosphere is approximately 1370°C. According to Nowicki *et al.* (2007), the geotherm of 44mW/m<sup>2</sup> may not intersect the diamond stability field at all, because diamonds cannot be formed and/or preserved in the lithosphere in this case, because it is much hotter.

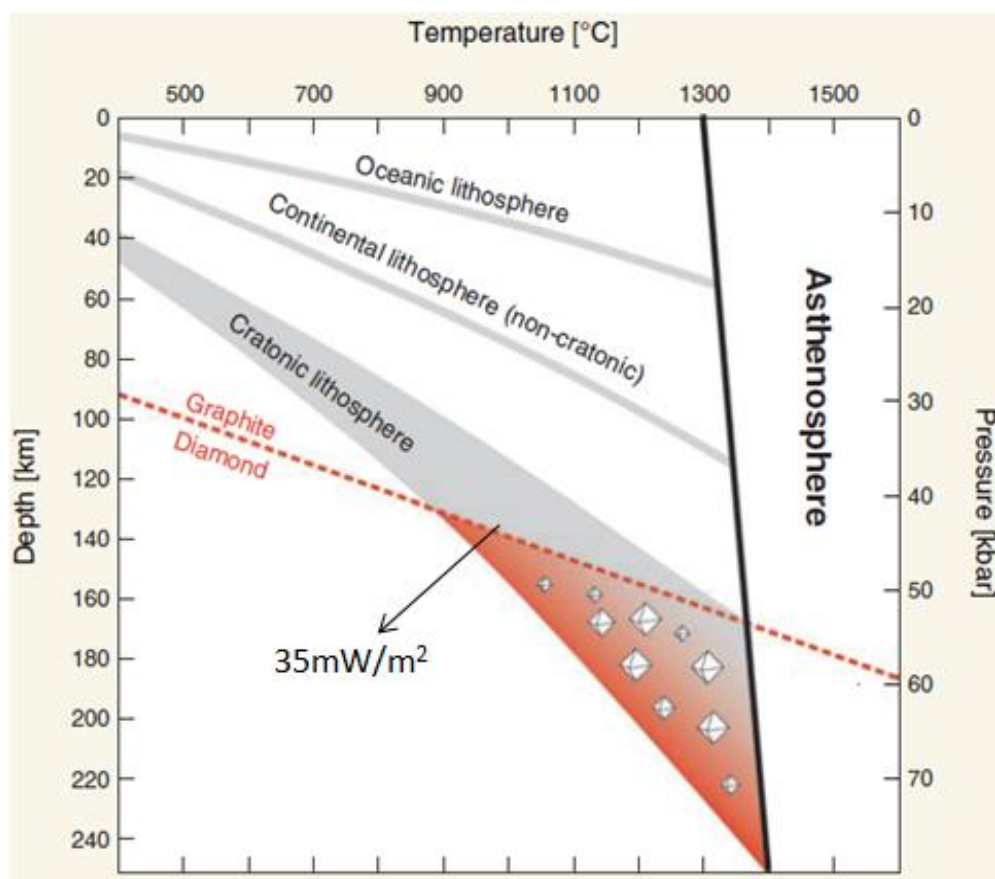


Figure 2.11. Pressure-temperature-depth diagram outlining the boundary between the stability fields of diamond and graphite, shown as a dotted line. Possible geothermal gradients (geotherms) for cratonic, continental and oceanic lithospheres are shaded grey. Diamonds are only stable in cratonic settings at pressures greater than > 40 kbars, which corresponds to depths of more than > 140 km. Modified after Tappert and Tappert (2011).

## 2. 4. Critical evaluation and discussion

This section provides some critical discussion, evaluation and interpretation of Angola's geological setting, principally on the Lunda province kimberlites. In addition, this section provides the information about the geodynamic relationship events between Lunda pipes and other pipes from around the world.

This research focuses on the locations of highest diamond concentration in NE Angola, in particular Lunda province. The critical evaluation is that even knowing that the sampled kimberlite pipes in Lunda zone are only a few metres apart, they vary dramatically in diamond grade and quality. The main arising questions from this project are: what are the factors that controlled and caused the diamond grade variation among NE Angola kimberlites? How was diamond distributed within the Angolan lithospheric mantle? The answers for these questions are provided in Chapter Four. As mentioned above, Lunda province is controlled by a system of deep faults called the Lucapa graben, an extensional tectonic structure (corridor) which crosses the entire country from north-east to south-west (Figure 2.1). According to Boyd and Danchin (1980), who studied the geology of Angola, the fault zones have been described by Ganga *et al.* (2003) and Pervov *et al.* (2011) to be approximately 55 - 85 km wide and 1200 km long, crossing the Angolan territory and it has extended into the Democratic Republic of Congo. This tectonic belt is associated with magmatic activity related to rifting at the West African continental margin during the opening of the Atlantic Ocean in the early Cretaceous (Pervov *et al.*, 2011), consequently it dramatically modified the primary mantle petrology and minerals (see thin section results in Chapter Four) and as a result it has contributed significant complexity to diamond exploration in Angola (Dirks *et al.*, 2003).

Some authors (Kusky *et al.*, 2003) have discussed in detail the major tectonic events affecting Angola, which are associated with those powerful events that also affected the African continent. The African continent has suffered several orogenic episodes and this conserves important information on crust forming events dating back 3.8 Ga (Dirks *et al.*, 2003). In addition, these events represent the cycles of continental break up and growth, which are recognised worldwide and can be largely explained in a plate tectonic context (Kusky *et al.*, 2003). When Stern (2007) examined and explained the splitting of the Pangaeon supercontinent at the beginning of the Mesozoic era and after the rifting process, he explained that the southern part of Pangaea formed as the Gondwana supercontinent ~ 0.55 Ga (Dirks *et al.*, 2003) and from the late Jurassic period Gondwanaland rifted, resulting in the African plate (Figure 2.12). This led to tectonic activity controlled by extension and hot spot activity (Stern, 2007) and these hotspots have also have been found in NE Angola and are related to genesis of diamondiferous kimberlite deposits (Jelsma *et al.*, 2004; and Fereira *et al.*, 2003). The Gondwana

episodes are linked to the genesis of many kimberlites in the world (Kusky *et al.*, 2003) including those from NE Angola. According to Haeman *et al.* (2003), the increases of Mesozoic kimberlite activity or kimberlite magmatism, recorded in many continental environments, are associated with the breakup of Gondwanaland (Helmstaedt and Gurney, 1997; see also Figure 2.12)

The illustration (Figure 2.12) illustrates how powerful tectonic forces were responsible for triggering mantle melting that produced kimberlite magma. Kimberlite magmatism has been described by Kröner and Stern (2004) to be linked with subduction of the oceanic lithosphere, rifting of continents or impact of the mantle plume, that generated faults and mafic dyke intersections which are classed as a final structural control of kimberlite emplacement within individual regions (Haeman *et al.*, 2003).

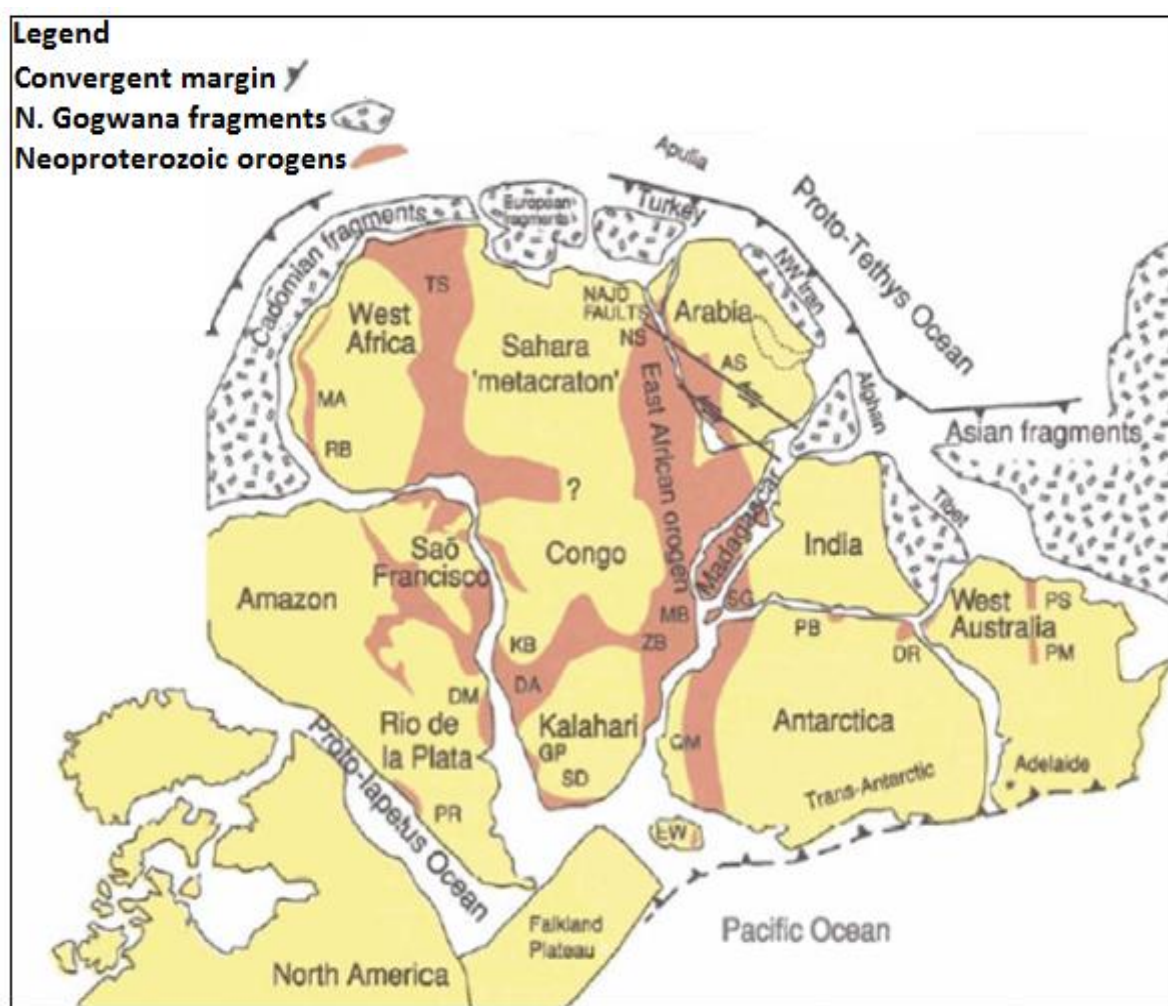


Figure 2.12. Illustration of Gondwana supercontinent and its orogenic episodes at the end of the Neoproterozoic period (approximately 540 Ma), also demonstrating the general arrangement of Pan-African belts, from Kusky *et al.* (2003). AS- Arabian Shield; BR- Brasiliano; DA -Darnara; DM- Dom Feliciano; DR-Denman Darling; EW- Eilsworth Whitmore Mountains; GP- Gariiep; KB- Kaoko; MA-Mauretaniides; MB-Mozambique Belt; NS- Nubian Shield; PM -Peterman Ranges; PB- Pryoloz Bay; PR-Parnpean Ranges; PS- Paterson; QM- Queen Maud Land; RB- Rokelides; SD- Saldania; SG- Southern Granulite Terrane; TS- Trans Sahara Belt; WB-West Congo; ZB- Zambezi.

In relation to the Congo craton, and in the specific case of Angola, as it seen in Figure 2.12 the orientations of the main weakness zones are related to the opening of the Atlantic Ocean, including the WSWENE, NW-SE and NNE-SSW rifts (Pereira *et al.*, 2003). The Archean of the Angolan block was largely reworked during the Eburnean orogeny (Dirks *et al.*, 2003), this is depicted in Figure 2.1, in several locations of Lunda province (Central shield, Cuango shield and Lunda shield). The Archean gneiss was heavily metamorphosed at approximately 2.8 Ga and subsequent magmatic activity, the Achaean system was intruded by crystalline granite at between 2.83-2.62 Ga (Dirks *et al.*, 2003). The Angolan kimberlites, including the pipes of Lunda province, have been confirmed to be from the Cretaceous age (Ganga *et al.*, 2003), and also similarly-aged kimberlites have been found in other parts of the world by Nixon (1995, see table 2.2). The Mesozoic kimberlites, however, have been described by White *et al.* (1995) and are frequently associated with continental structures that gave rise to the transformation of the Mid-Oceanic ridge.

In the Mesozoic Era, particularly the Cretaceous period prior to and after the separation of South America from Africa between 132 to 125 Ma (White *et al.*, 2012), the southern African continent underwent extensive uplift and erosion. This led to the interpretation that the oceanic rifting events produced important tectonic consequences in the African plate, reactivating structures from previous orogenic cycles (Pereira *et al.*, 2003). Following these events, the major implications from these tectonic structures is that they exerted a key control on the structure of kimberlite emplacement in Angola, particularly in the region of Lunda, during the Cretaceous period (Jelsma *et al.*, 2009; Castillo-Oliver *et al.*, 2011; Pervov *et al.*, 2011; and Robles-Cruz *et al.*, 2008). In Angola, the most important tectonic structure generated by the oceanic rift event is the Lucapa graben.

Due to the several past tectonic events, Congo craton has been summarized (Figure 2.1) as one of relative complexity during the Proterozoic era (Dirks *et al.*, 2003; and Batumike *et al.*, 2009) and Angola has a complex geological history due to a series of tectonic events (Table 2.1). These geological events have dramatically modified the primary mantle petrology (see Chapters Three and Four, thin section and rock investigations), and have contributed significant complexity to diamond exploration in Angola during the Pan-African period. Also it has been confirmed by Pereira *et al.* (2003) that during the period of Archaean-Proterozoic transition, the Angolan lithosphere suffered extensive deformation and consequently intrusion of mafic-ultramafic masses resulting in the formation of the gabbro-anorthositic complex in Angola (Robles-Cruz *et al.*, 2008).

Another implication that can be taken from the Mesoproterozoic, Palaeoproterozoic and Neoproterozoic tectonic episodes is that the mantle masses may have induced partial fusion of the Archaean crust and consequently formed the granitoids and granodioritic porphyries occurring in the western part of Angola, (Pereira *et al.*, 2003) whereas in Lunda province (NE Angola), the main tectonic direction WSW-ENE fragmented the lithosphere and subsequently produced important subsiding zones (for example the Lucapa graben), where sedimentary sequences accumulated. These are now found on the surface as medium to high-grade metamorphic rocks arising during the Ebumean-Ubendian orogeny events (Kröner and Stern, 2004; and Dirks *et al.*, 2003). The tectonic structures described above (Figure 2.1) that controlled the emplacement of diamondiferous kimberlites in Lunda province have also occurred in other parts of the world including South Africa, Zimbabwe, Canada, USA, Australia and Russia (Helmstaedt and Gurney, 1997) and Greece (White *et al.*, 1995).

Jelsma *et al.* (2009) showed that during the Atlantic opening episodes or Pan African events, intrusive magmatic kimberlites were preferentially associated with deep basement structures that extended into the upper mantle. According to White *et al.* (1995), kimberlite intrusions are favoured by extensional tectonic activity caused during times of major oceanic or continental rifting. Concerning Lunda province (the study region), however, the basement structures are the results of connection between regional structures (major mobile zones or faults, fracture corridors) and local structures (linear graben, rift valleys, internal fractures and deep faults within the Lucapa corridor (Pereira *et al.*, 2003), and consequently these structures enabled kimberlite magma to reach the earth's surface (Helmstaedt and Gurney 1997) and to cool to form the kimberlite deposit which incorporates the diamond reservoir and facilitates its economical exploration at Camutue mine (Figure 2.13).



Figure 2.13. Demonstration of diamond exploration activity at Camutue kimberlite, (NE Angola, Photo taken during field work in 2012).

According to Basseka *et al.* (2011) the Pan-African orogeny strongly affected the African continent, which resulted in the Tanzania and Congo cratonic blocks being separated from the Kalahari craton by the Mwembeshi transform fault (Pereira *et al.*, 2003), with this last resulting in formation of the Damara belt and the Lufilian Arc structures and Zambezi belts (Figure 2.14) along the margins of the shield (Roberts *et al.*, 2005). The mobile belt, or Damaran structure described by Batumike *et al.* (2009) and Kröner and Stern (2004), is situated in the south of Angola (Figure 2.14). It can be evaluated that the tectonic episodes which produced the Damaran belt (Namibia) may have significantly decreased or affected diamond grade in kimberlite pipes in south Angola. This is because diamond grade in Angola decreases in a southern direction (see Figure 2.1, Robles-Cruz *et al.*, 2009) whereas the Namibian kimberlite pipes Hanaus and Lauwrensia (see Figure 2.15) are classed as barren (Mitchell, 1991), but diamondiferous Venetia kimberlites in the Limpopo mobile belt area are located between the Archean Kaapvaal and Zimbabwe cratons and have been considered as an exception as they produce diamonds (White *et al.*, 1995). The lineament which separates the Cratons and the mobile belt (Figure 2.14) is believed to have been created by a major crustal faulting during the Pan-African orogeny (Basseka *et al.*, 2011) and correspond to deep-seated basement structures.

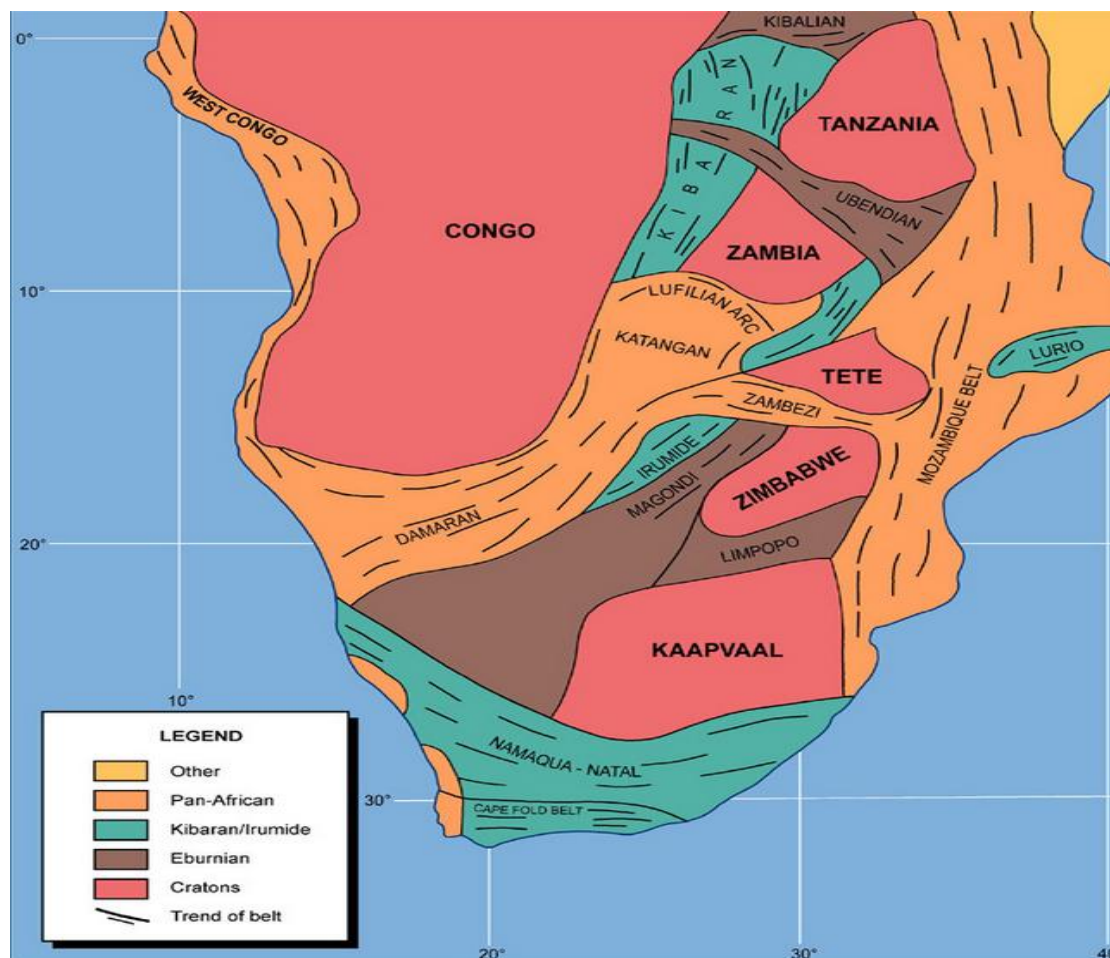


Figure 2.14. Geological sketch displaying the location of the main Cratonic blocs in Africa and Fold belts  
Source Ministry of Mines and Mineral Development Zambia (2014).

The work of Boyd and Gurney (1986, Figure 2.15), provides a clear explanation of why some kimberlite pipes in other parts of the world do not contain diamond, in particular the Namibian pipes. This was recognised by Mitchell (1991) who also confirmed and classified Namibian kimberlites as being barren in diamond. Metasomatic processes linked to high thermal heat from tectonic events associated with opening of Atlantic Ocean may have affected the Namibian pipes. This view is supported by Kröner and Stern (2004), Boyd and Gurney (1986) and Mitchell (1991), who explained that the mantle upwelling related to break-up of the Mesozoic supercontinent and Karoo flood basalt magmatism appears to have caused thermal erosion that affected the off-craton lithosphere, thinning it by approximately 30 km (Janney *et al.*, 2010) relative to the cratonic lithosphere (Figure 2.15), leading to modification of the primary mantle composition (e.g. peridotite garnet), and consequently under these conditions diamond may not have survived in the Namibian kimberlite pipes.

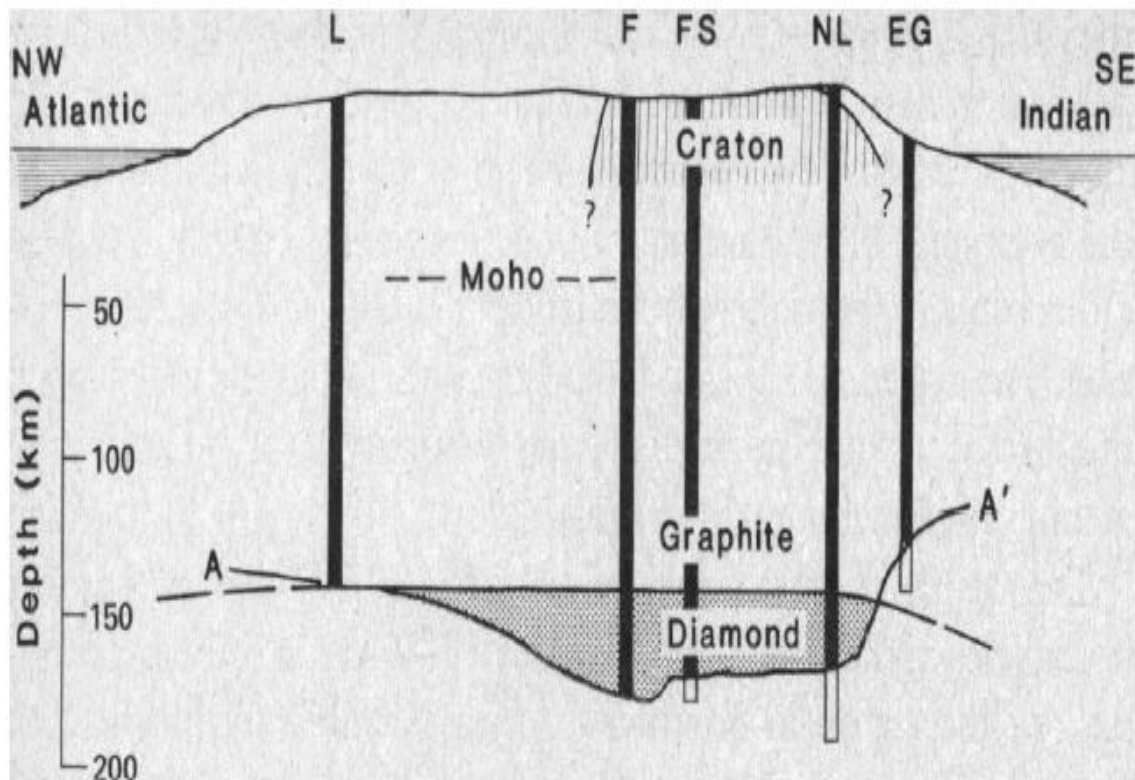


Figure 2.15. Model for the lithosphere beneath southern Africa based on geothermobarometry for xenolith suites. Ratio of depth scale to horizontal scale is 4:1 below sea level. Vertical bars represent xenolith suites, and the maximum depths shown are for clusters of xenoliths of deepest origin in each suite. A-A' represents points of inflection in xenolith geotherms and are interpreted as points for high- and low-temperature xenoliths (boundary of the lithosphere). The xenolith suites are: L → Lauwencia; F → Finsch; FS → Frank Smith; K → Kimberley; P → Premier; NL → Northern Lesotho; and EG → East Griqualand. From Boyd and Gurney (1986).

Even though kimberlites such as Hanaus and Lauwrensia (Namibian pipes) contain garnet harzburgites, these pipes still contain no diamonds. According to Mitchell (1991), the garnets from these pipes present deformation features (recrystallization, rounded to irregular fractures) with mosaic porphyroclastic texture. These deformations are the result of metasomatic events (Boyd and Gurney 1986), but similar garnet deformations have been noticed in diamondiferous kimberlites from Lunda province (Figure 2.1). The difference between the pipes from these two countries is that the Namibian pipes are barren off-cratonic kimberlites within the graphite stability field and are located within mobile belts (Batumike *et al.*, 2009; see also Figure 14) and are younger in age (see Nixon 1995, Table 2.2) than the Angolan pipes located in the cratonic continental crust, older in age (>2.5 billion years) (Dirks *et al.*, 2003).

## **2. 5. Indicator minerals and application of advanced spectroscopic techniques in diamond research**

### **2. 5. 1. Indicator minerals: a review**

Indicator minerals are minerals and transported as grains in clastic sediments which indicate the presence in bedrock of a specific type of mineralization (e.g P-type and E-type, etc), hydrothermal alteration or lithology (McClenaghan, 2005). Kimberlite indicator minerals or ‘KIMs from sediment samples have been used as indicators to discover kimberlite (Griffin *et al.*, 1997; Nowicki *et al.*, 2007; Sobolev, 1977 McClenaghan, 2005).

However, the recent study of mantle-derived indicator mineral compositions by Cookenboo and Grütter (2010), the abundance of KIMs proved to be DIMs or diamond indicator minerals, therefore both terminologies (KIMs and DIMs) are used in this project.

The disaggregation of mantle rocks sampled by kimberlite during eruption, yields relatively large quantities of other mantle minerals, commonly referred to as KIMs or kimberlitic indicator minerals (Nowicki *et al.*, 2007; McCandless, 1990; Mitchell and Giardini, 1977). These are used to target kimberlite and consequently the exploration and prospecting of diamond. From this point of view, the most important indicator minerals are garnet, chromite, ilmenite, Cr-diopside and olivine (Griffin *et al.*, 1997; Stachel, 2003; Robles Cruz *et al.*, 2008, 2009; and Griffin and Ryan, 1995). The more chemically resistant kimberlite indicator minerals are garnet, ilmenite and chromite, and these are particularly useful due to their greater ability to survive weathering in the surface environment (Moore and Gurney, 1989; Cookenboo and Grütter, 2010; and Gurney and Moore, 1993). Kimberlite indicator minerals have been successfully used in diamond exploration for more than 50 years worldwide (Mitchell and Giardini, 1977). These minerals display and diagnose visual and compositional characteristics, making them ideal pathfinders for economical kimberlite exploration and identification (Stachel and Harris, 2007; Moore and Gurney, 1989).

Indicator minerals have long been the strongest tool in the exploration of diamond bearing kimberlite host rocks. For example, DeBeers group is the world's leading diamond company; a key aspect of their business is to discover economical kimberlite deposits. However, the geologists of the DeBeers Company have been able to discover several diamondiferous kimberlites in different places in the world only through the studies of kimberlite indicator minerals (Scott Smith *et al.*, 2008; Nowicki *et al.*, 2008; Gurney and Moore, 1993; and Cookenboo and Grütter, 2010). For example the discovery of the Orapa kimberlites (Botswana) and the Udachnaya kimberlites (Siberia) since 1967, was made on basis of the chemistry of garnet inclusions and the calcium-chromium relationship of kimberlitic garnets (Mayer *et al.*, 1994). A detailed study of kimberlitic indicator minerals and tracing these back to their source is thus a key component of most diamond exploration programs. Studies of diamond inclusions and diamond-bearing xenoliths permit geochemical characterisation of diamond source materials (Nowicki *et al.*, 2007) and have led to major advances in the understanding of the relationship between diamond and its host rock in the mantle (Griffin and Ryan, 1995). Many diamond researchers have shown that the majority of mineral inclusions in diamonds belong to two mantle assemblages: peridotitic (P-type, ultramafic rock) and eclogitic (E-type) (see Figure 2.16). According to Stachel and Harris (2008); Gurney *et al.* (2010) and Nowicki *et al.* (2007), E-type and P-type are the main types/source of indicator mineral inclusions in diamond. Sulfide mineral inclusions (pyrrhotite and pentlandite) can help to differentiate diamonds according to their mantle source (peridotite and eclogite). For example peridotite diamonds contain elevated Ni sulfides content whereas eclogite diamonds contain lower-Ni (and slightly higher-Cu) sulfides inclusion in diamond (Shirey and Shigley, 2013)

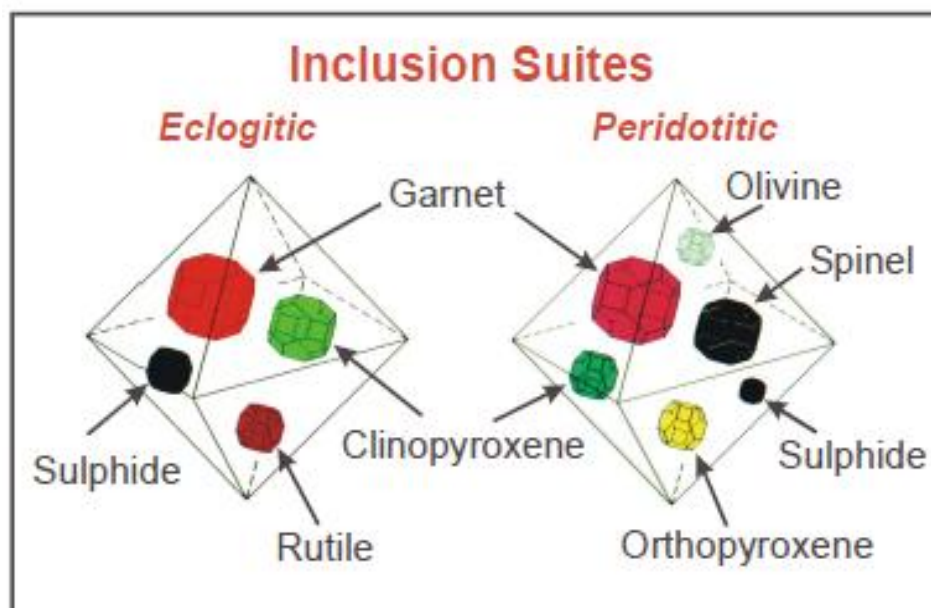


Figure 2.16. Schematic of inclusions of peridotitic and eclogitic suites within diamonds (Stachel, 2003).

In addition to providing indications for diamond prospecting, these DIMs or Diamond indicator minerals (Cookenboo and Grütter 2010) occur not only in the surrounding kimberlite rock, but also as inclusions in diamonds themselves (Figure 2.16). DIMs are therefore of even further interest because of the strong probability that they crystallized in the upper mantle; that they formed at the same time as diamond; and that they provide important information on the nucleation and growth of natural diamonds (Taylor *et al.*, 2003; and Nowicki *et al.*, 2007).

According to Moore and Gurney (1989) and Meyer (1968), the majority of natural diamonds probably crystallised in proximity to indicator minerals and consequently DIMs occurring as inclusions in diamonds are seen as samples of the mantle and they can be expected to provide direct information on the mineralogy and geochemistry of the Earth's mantle (Griffin and Ryan, 1995 and Nowicki *et al.*, 2007). One of the important factors in understanding the formation of natural diamond is afforded by detailed examination of the minerals included in diamond (Meyer 1985), this is because diamonds commonly contain syngenetic inclusions of silicates, oxides and sulphides (see Figure 2.16, Griffin and Ryan, 1995 and Stachel, 2003). These inclusions are interpreted as samples of the materials which co-existed with the diamond during its growth (Mitchell, 1991). Such studies provide strong evidence that the principal source of diamonds is the subcratonic lithospheric mantle (Stachel *et al.*, 2009; Stachel and Harris, 2007, see Figure 2.17).

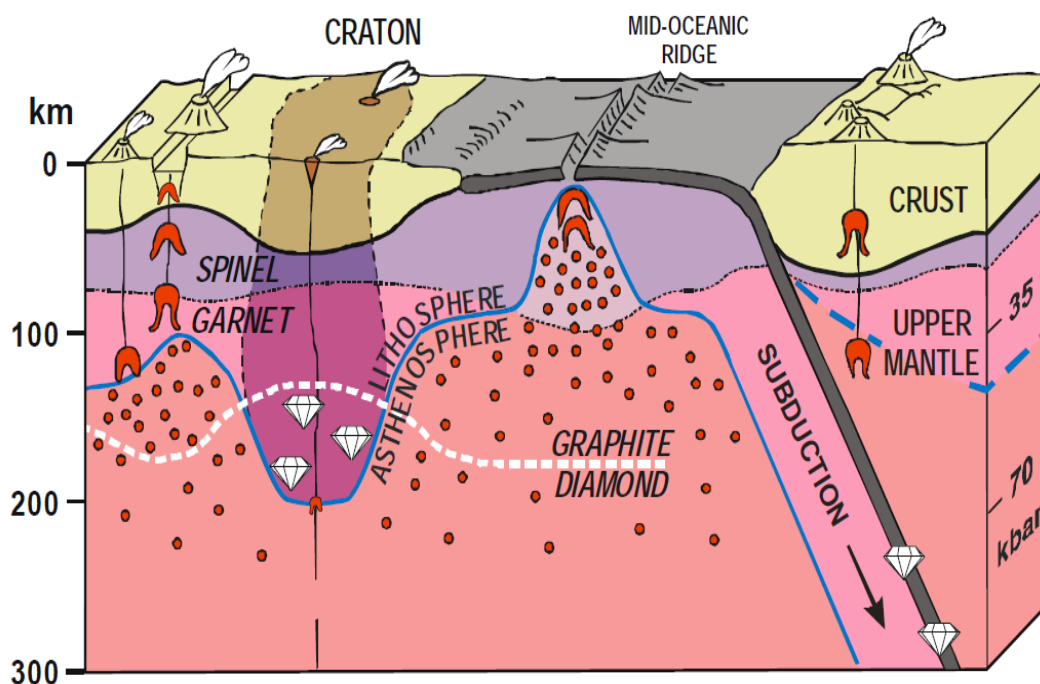


Figure 2.17. Schematic vertical section through the Earth's crust and part of the upper mantle. The upper mantle is separated into two mineralogical layers, spinel facies and garnet facies. Small volume melt fractions in the asthenosphere are indicated as red dots. With the exception of subducting oceanic slabs, the sublithospheric upper mantle appears to be void of macro-diamonds (Stachel and Harris, 2008).

## 2.6. Application of advanced methods to the study of kimberlite indicator minerals (KIMs)

### 2.6.1. Electron microprobe analysis (EMPA) for compositional analysis of kimberlites

The geologists of the DeBeers Company discovered several diamondiferous kimberlites in different places such as Orapa kimberlite (Botswana) and Udachnaya kimberlites (Siberia) in early 1967, on basis of chemistry of garnet (calcium and chromium relationship, Mayer *et al.*, 1994). A critical step in the study of KIMs involves chemical analysis and comparisons of major elements (Cookenboo and Gutter, 2010). Diamond researchers (Gurney *et al.*, 1993; Stachel and Harris, 2007) have used EMPA (McCammon *et al.*, 1998; Sobolev *et al.*, 1999; Canil and Bellis, 2007), in order to predict diamond sources by considering the oxides of certain elements (CaO and Cr<sub>2</sub>O<sub>3</sub>) from KIMs (pyrope garnet, Mg<sub>3</sub>Al<sub>2</sub>(SiO<sub>4</sub>)<sub>3</sub>) and plotted against each other. Their results have defined fields indicative of source from different mantle peridotite types such as Iherzolite (G9), harzburgite (G10, Figure 2.18) and websterite peridotite mantle (Gurney *et al.*, 1993). The harzburgite garnet (G10) is depleted in Ca relative to the Iherzolites (Gurney *et al.*, 1993) in three different ways, as follows:

- (1). Lack of a Ca saturated phase (diopside)
- (2). A low bulk Ca content
- (3). Low mineral content of Ca

Thus garnet is interpreted as the most informative of the diamond indicator minerals, probably due to the wide range of substitutions that can occur in the garnet configuration. Elements such as Ca, Cr, Fe and Mn occur in minor proportions in pyrope garnet (Cookenboo and Grütter, 2010). G10 are harzburgite (P-type) garnets derived from the diamond stability field, and the presence of G10 garnets is a clear indicator of the potential of finding diamond in the kimberlite as well as ore grade diamonds (Erlich and Hausel, 2003). This is in accordance with mantle-derived garnets classified under the scheme proposed by Grütter *et al.* (2004) who illustrated that peridotite (P-type) garnet inclusions in diamond have higher Cr<sub>2</sub>O<sub>3</sub> and lower CaO contents than garnet which crystallized in the graphite stability field. In addition, G10 garnets have MgO ≥ 14 wt% and Cr<sub>2</sub>O<sub>3</sub> >2 wt% and low calcium oxide CaO ≤4.5 wt% (Meyer *et al.*, 1994; Gurney *et al.*, 1993; and Griffin *et al.*, 1997). A small fraction of G9 garnets derived from the disaggregation of Iherzolite can also be formed within the diamond stability field (Nixon, 1987; Gurney *et al.*, 2010).

Harzburgite is a variety of peridotite which is an ultramafic igneous rock (Nixon, 1987) composed mostly of the two minerals olivine (forsterite -Mg<sub>2</sub>SiO<sub>4</sub>) and fayalite (Fe<sub>2</sub>SiO<sub>4</sub>) and enstatite (Mg<sub>2</sub>Si<sub>2</sub>O<sub>6</sub>, - pyroxene with low-calcium) with garnet and chromium-rich spinel accessory minerals.

Harzburgite forms by the extraction of partial melts from lherzolite (peridotite) which is an ultramafic igneous rock rich in two major minerals (olivine and orthopyroxene) with clinopyroxene as a minor component. The molten magma extracted from harzburgite peridotite erupted at the Earth's surface as basalt rock (Blatt and Tracy, 1995). If the process of partial melting of the harzburgite continues, it will form another ultramafic peridotite rock called dunite (poor in pyroxene and rich in olivine) if all of the pyroxenes are extracted from harzburgite then the magma rich in olivine (forsterite- $Mg_2SiO_4$ ) and fayalite ( $Fe_2SiO_4$ ) is formed. According to Erlich and Dan Hausel (2002), who used EMPA (McCammon *et al*, 1998) to analyse garnet, diamonds with inclusions of calcic-chrome pyrope are G9, derived from lherzolitic mantle peridotite; and subcalcic chrome pyrope are designated as G10 mantle peridotite which indication that the host intrusion originated in the diamond stability region of the upper mantle. Garnets from the G10 field are better described as a diamond field (Grütter *et al.*, 2004; Stachel and Harris, 2008; and Gurney *et al.*, 1993). However, one of the important limitations encountered by Erlich and Dan Hausel (2003) during their studies is that garnets do not provide information on diamond preservation, quality and grade size. Gurney *et al.* (1993) stated that it is possible that the G10 field may contain lherzolitic garnet but these will originate from high pressure regions of about 45 kbar, lherzolites which could be diamond bearing. Garnets in the G9 field may be harzburgitic, particularly if they occur close to the G9 / G10 boundary (Figure 2.18) but there will not be sufficiently high-pressure for them to be diamondiferous (Grütter *et al.*, 2004). In contrast, Cr-pyrope garnets with moderate Ca concentrations are located in the G9 field. They are associated with lherzolite and rarely occur as inclusions within diamond (Morris *et al.*, 1998).

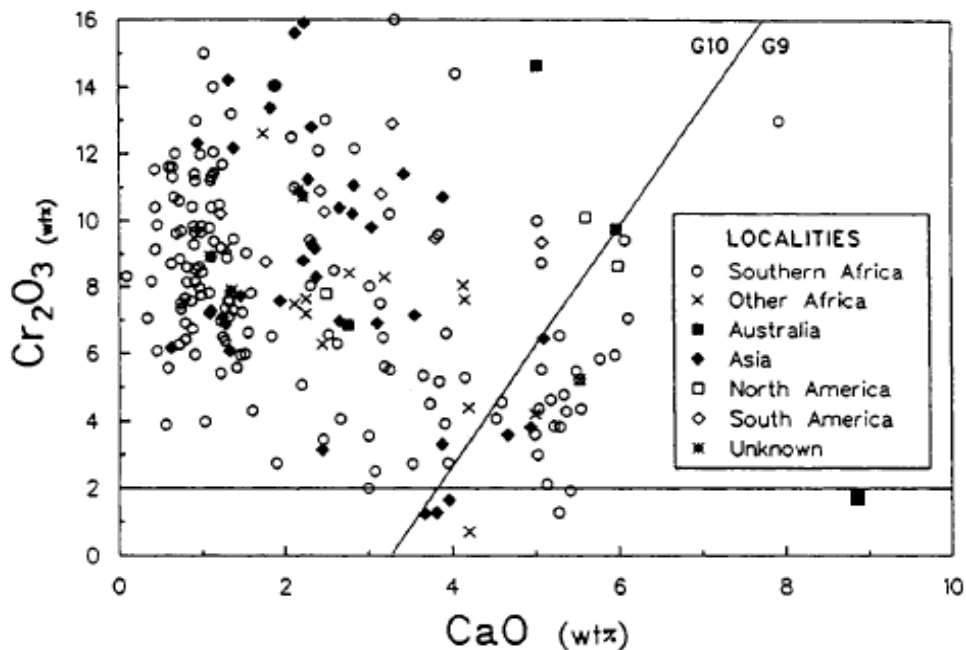


Figure 2.18. Plot of  $Cr_2O_3$  vs.  $CaO$  contents for peridotitic diamond inclusion garnets from worldwide localities. The diagonal line distinguishes sub-calcic ‘G10’ garnets from calcium-saturated ‘G9’ garnets. The horizontal line drawn at 2 wt%  $Cr_2O_3$  is used as an arbitrary division between eclogitic garnets (< 2 wt%  $Cr_2O_3$ ) and peridotitic (> 2 wt%  $Cr_2O_3$ ). From Gurney and Moore (1993). Harzburgite (G10) P-type and lherzolite (G9)

Based on their EMPA results, Gurney *et al.* (1993) discovered that for harzburgite diamonds, the garnets contain high levels of MgO and Cr<sub>2</sub>O<sub>3</sub> and low levels of CaO. Chromium pyrope diamond inclusions are consistently Mg-rich, Mn-poor, and usually lack TiO<sub>2</sub> (Cookenboo and Grütter, 2010). However, in some exceptional compositions, majoritic garnet (Mg<sub>3</sub>(MgSi)(SiO<sub>4</sub>)<sub>3</sub>) with excess SiO<sub>2</sub>, and Cr–Ca rich varieties from wehrlite (variety of peridotites, which is an ultramafic and ultrabasic rock composed mainly of olivine and clinopyroxene) also occurs occasionally as inclusions in diamond. The majoritic garnet is distinguished from other garnets (pyrope and almandine-Fe<sub>3</sub>Al<sub>2</sub>(SiO<sub>4</sub>)<sub>3</sub>) in having Si<sup>4+</sup> in octahedral as well as tetrahedral coordination and being from a lower transition zone in the uppermost lower mantle at depths of >550km (Mitchell and Giardini, 1977). Grutter *et al.* (2004) and Erlich and Dan Hausel (2003) concluded that high concentrations of both TiO<sub>2</sub> and Na<sub>2</sub>O is characteristic of eclogitic garnets associated with diamond. This conclusion is also supported by Dobosi and Kurat (2010) and (Gurney *et al.*, 1993) who noted that eclogite garnet inclusions in diamond contain elevated levels of TiO<sub>2</sub> and Na<sub>2</sub>O ≥ 0.07 wt% (see vertical dotted line Figure 2.19). Elevated levels of Na from the eclogite mantle reflect the high pressures appropriate for diamond formation (Morris *et al.*, 1998; Meyer, 1987; and Pearson *et al.*, 2003).

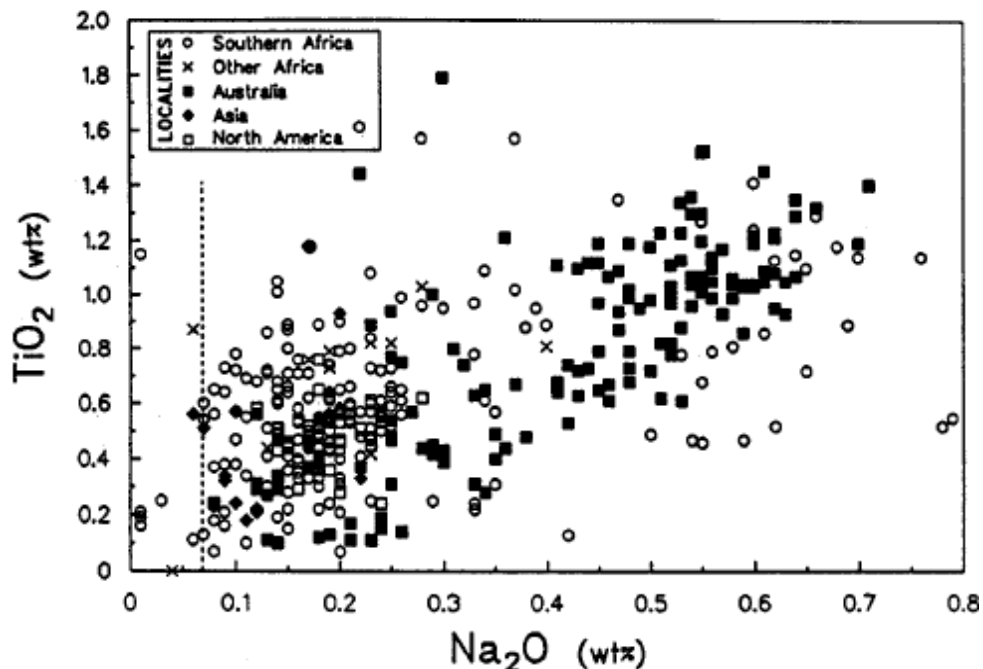


Figure 2.19. Plot of TiO<sub>2</sub> versus Na<sub>2</sub>O content for eclogitic diamond inclusions in garnet from worldwide kimberlite localities. From Gurney *et al.* (1993).

Cookenboo and Grütter (2010) have shown that several important diamond mines in world including Orapa, Jwaneng and Letlhakane in Botswana, Argyle in Australia, together with Jericho mine in Nunavut and Victor mine in Ontario (Canada), contain very low levels of sub-calcic G10 pyrope,

therefore the eclogitic mantle is the source for most of their diamond (Dobosi and Kurat, 2010). Gurney *et al.* (1993) used EMPA of major / minor elements such as Mg and Cr from spinel (chromite,  $\text{FeCr}_2\text{O}_4$ ) indicator minerals in order to determine their relative field (peridotite - harzburgite) and to assess mantle conditions and diamond distributions (Grutter *et al.*, 2004). Their results are presented in Figure 2.20. Chromites associated with diamonds have high concentrations of Cr ( $> 62.0$  wt%  $\text{Cr}_2\text{O}_3$ ) and Mg ( $> 11$  wt% MgO); and are poor in Al and Ti ( $< 0.50$  wt%  $\text{TiO}_2$  and  $\text{Al}_2\text{O}_3$  (Gurney *et al.*, 1993).

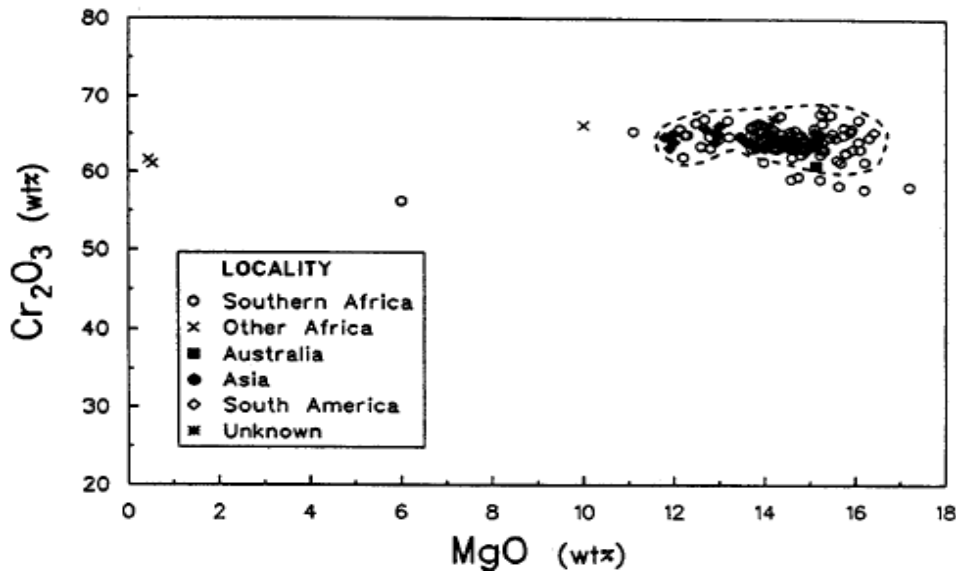


Figure 2.20. Plot of MgO versus  $\text{Cr}_2\text{O}_3$  content for chromite diamond inclusions from worldwide localities, from Gurney *et al.* (1993).

Whilst chemical analyses of garnet do not provide information on diamond preservation, quality and grade size (Erlich and Dan Hausel, 2003), ilmenite KIMs have been widely used to obtain the information on diamond preservation, quality and grade size (Grutter *et al.*, 2004; and Nowicki *et al.*, 2007). For example, Gurney and Zweistra (1995) used EMPA to calculate or analyse major oxides (MgO,  $\text{Fe}_2\text{O}_3$ ) in kimberlite ilmenites and plotted MgO vs.  $\text{Fe}_2\text{O}_3$  and obtained some measure of redox conditions (oxygen fugacity,  $f\text{O}_2$ ) in the mantle and magma and consequently to define the preservation conditions of diamond. Their results suggest that ilmenites with low  $\text{Fe}^{3+}/\text{Fe}^{2+}$  ratios are associated with higher diamond contents, and lower oxygen fugacity than ilmenites with higher  $\text{Fe}^{3+}/\text{Fe}^{2+}$  ratios which are indicative of higher  $f\text{O}_2$  (Nowicki *et al.*, 2007). In kimberlite pipes, ilmenites with high  $\text{Fe}^{3+}/\text{Fe}^{2+}$  ratios are associated with low MgO (Gurney *et al.*, 2010; 1993). According to Nowicki *et al.* (2007), the trend shown in Figure 2.21 corresponds to a gradual change in  $f\text{O}_2$  and is thus associated with changing diamond preservation potentials. When  $\text{Fe}_2\text{O}_3$  is calculated by assuming that is high in the mantle, the diamond content will be lower because the high  $f\text{O}_2$  will transform diamonds into  $\text{CO}_2$  (Robinson *et al.*, 1989; Gurney and Zweistra, 1995). Ilmenite is in fact

useful only in exploration for group I kimberlites, as it is rare in group II kimberlites (Gurney and Zweistra, 1995).

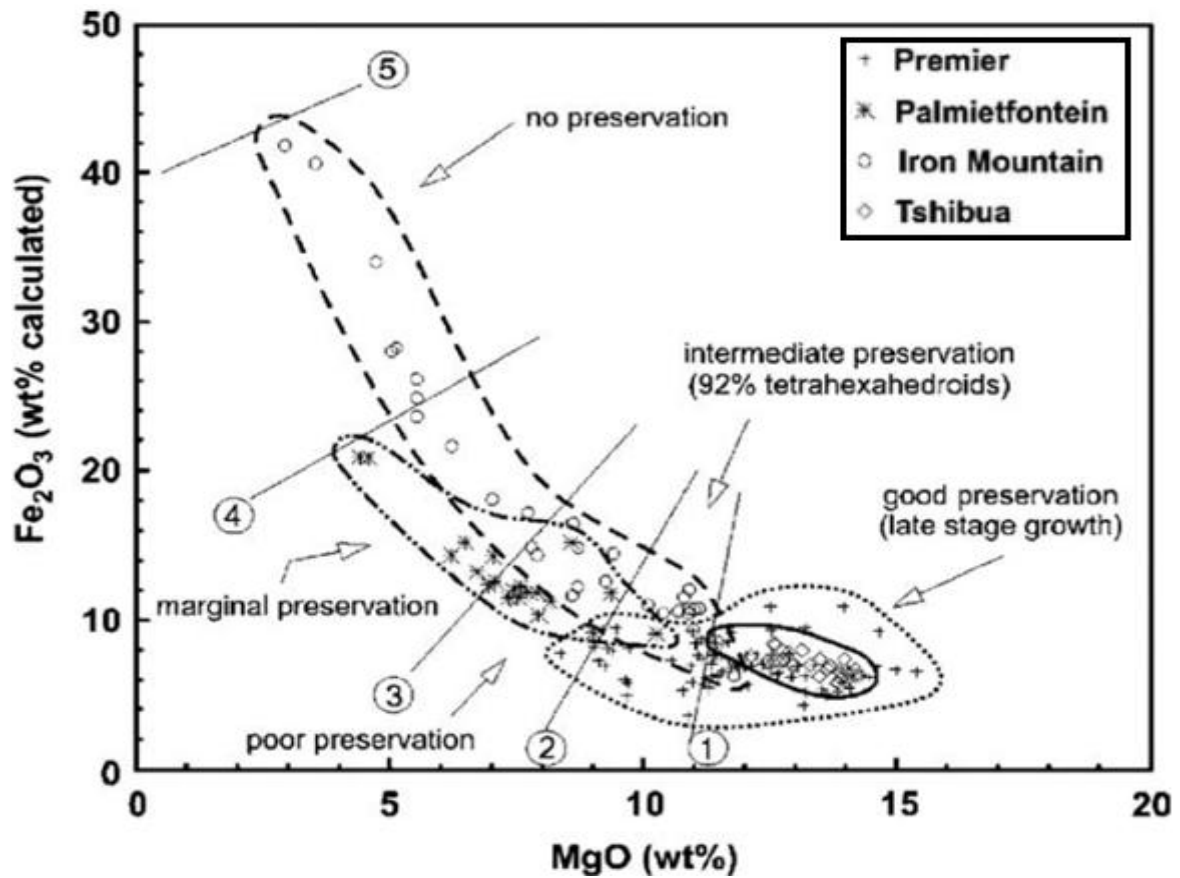


Figure 2.21. Plot of MgO vs. Fe<sub>2</sub>O<sub>3</sub> content of kimberlite ilmenites. Modified after Nowicki *et al.* (2007), originally from Gurney and Zweistra (1995).

After an extensive study of major elements from ilmenite using EMPA, Gurney and Zweistra (1995) found that diamond from Tshibua kimberlite (Democratic Republic of the Congo) shows good preservation conditions and kimberlites with high grade diamonds with late stages of growth. This implies reduced mantle conditions at the time of kimberlite emplacement, which means that Tshibua kimberlite has lower Fe<sub>2</sub>O<sub>3</sub>, while diamond from Premier kimberlite (South Africa) exhibits considerable resorption. The diamond resorption at Premier has been previously reported by Robinson *et al.* (1989), and the diamonds from Palmietfontein kimberlite (South Africa) are highly deformed (resorbed), while the Iron Mountain kimberlites (Wyoming, USA) are classed as nearly barren. According to Nowicki *et al.* (2007) who carried out chemical analysis of ilmenite diamond indicator minerals, young, fast-grown fibrous diamonds (Democratic Republic of the Congo and Sierra Leone) are associated with ilmenite of very high Mg, high Cr, and very low Fe<sup>3+</sup> contents, but these late stage fibrous coats on numerous diamonds were interpreted as originating from the latest events in the period of diamond growth.

### 2. 6. 1. 1. Redox and oxygen fugacity estimation using EMPA data and the Droop method

The so-called "Droop method" (Droop, 1987; Quintiliani, 2005; and Canil and O` Neil, 1996) is an empirical method widely used to calculate or estimate the  $\text{Fe}^{3+}$  content (and thereby estimate oxygen fugacities) of oxides and silicate minerals based on the results of electron microprobe analysis (EMPA). The Droop method is based on the assumptions that iron is the only element present with variable valence and that oxygen is the only anion. Droop's (1987) criteria for determination of  $\text{Fe}^{3+}$  are as follows:

- (i) The total cation charge. In order to maintain an electrostatically neutral mineral, this number (usually an integer in conventionally defined mineral formulae) is constrained to be exactly twice the number of oxygens in the formula unit if oxygen is the only anion present.
- (ii) The total number of cations. Again, this is usually an integer as the formula generally represents the atomic content of a whole unit cell or a simple fraction thereof.
- (iii) Any equation based on crystal chemical arguments linking the  $\text{Fe}^{3+}$  content to the concentrations of other elements.

The  $\text{Fe}^{3+}$  contents calculated using this method are extremely sensitive to errors in the concentrations of the most abundant elements present (Droop, 1987). Other factors such as statistical fluctuations in count rate, instrumental drift, poor analytical procedure, and poor choice of standards can influence the precision of this method (Rollinson *et al.*, 2012; and McCammon *et al.*, 1998). According to Droop (1987) his developed method is unlikely to yield accurate estimates unless the analyses are of superior quality. The vulnerability of this method in generating errors during the process of estimating  $\text{Fe}^{3+}$  has led to it being considered unsuitable for estimating trace quantities of  $\text{Fe}^{3+}$  in ferrous iron-rich minerals such as olivine (forsterite -  $\text{Mg}_2\text{SiO}_4$  and fayalite -  $\text{Fe}_2\text{SiO}_4$ ) and cordierite (magnesium iron aluminium silicate) (McCammon *et al.*, 1998). Hence this method is not suitable to estimate oxygen fugacity using chemical reactions that involve olivine, such as (garnet- orthopyroxene - olivine), (Olivine - orthopyroxene - chromite), (fayalite-magnetite-quartz (FMQ) buffer) (Canil and O` Neil, 1996). For example, Sobolev *et al.* (1999) explained that the use of crystal chemistry of silicate phases analyzed by EMPA to calculate the  $\text{Fe}^{3+}$  content of a mineral by using the method of Droop (1987) can result in gross imprecision in determinations of  $\text{Fe}^{3+}/\sum\text{Fe}$ , thus, large uncertainties in subsequent *P-T* estimations and oxygen fugacity (Canil and O`Neill, 1996; and Dollase and Newman, 1984), and consequently it could seriously affect petrologic interpretation (Quintiliani, 2005). Another limitation for this method is that inappropriate for minerals that contain two or more elements with variable valence (pyroxenes and spinels groups) (Droop, 1987).

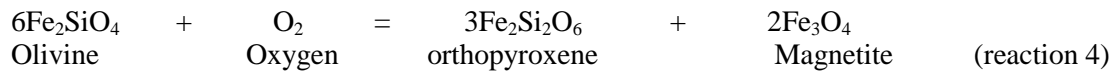
## 2. 6. 2. Mössbauer spectroscopy

Mössbauer spectroscopy (MS) has long been extensively used as one of the most reliable and accurate techniques for investigating the nature and relative contents of Fe-bearing phases and their oxidation state/s (McCammon *et al.*, 1998, 2000; Al-Rawas *et al.*, 2008; Frost *et al.*, 2004; Homonnay, 2004; see section 3.2.2). Several authors (see, for example, Canil and O'Neill, 1996; Rollinson *et al.*, 2012; and Sobolev *et al.*, 1999) have explained and illustrated that MS can provide precise determination of the iron redox ratio,  $Fe^{3+}/\sum Fe$ , and thereby enable estimates of oxygen fugacity, within geological mineral samples such as mantle minerals. These results are, in general, more accurate than those estimated from EMPA (McCammon *et al.*, 1998; Quintiliani, 2005; Rollinson *et al.*, 2012; Sobolev *et al.*, 1999). High oxygen fugacity is a destroyer of diamond (Fedortchouk and Zhang, 2011) within kimberlite during eruption. Precise information about the oxidation states of iron at the time of diamond formation by using kimberlite indicator minerals (KIMs) is important for understanding the mantle source region and the genesis of diamond (Stagno *et al.*, 2013).

As noted above, the iron redox ratio,  $Fe^{3+}/\sum Fe$ , can be accurately obtained using Mössbauer spectroscopy (Sobolev *et al.*, 1999). The redox information obtained from MS is known to be more accurate than redox ratios calculated from EMPA measurements using the method of Droop (1987) (see section 3.2.2). Kimberlite indicator minerals (ilmenite, spinel, garnet, and pyroxene) have been widely used for determination of both oxidation state of the mantle and accurate iron redox ratio ( $Fe^{3+}/\sum Fe$ ) (Stagno *et al.*, 2013; Sobolev *et al.*, 1999; McCammon and Kopylova, 2004). This aids determination of oxygen fugacity using oxygen geobarometers assuming that all phases are in equilibrium (McCammon *et al.*, 1998, 2000, 2001).

The term "equilibrium" refers to the stable coexistence of two or more mineral phases and is established relative to time (Nixon, 1987). The absence of any visible alteration and/ reaction rims between the minerals present that are physically in contact with each other, without any modification around them, suggest that the minerals were in equilibrium at the time of formation of the rock. In addition, when two or more minerals are in equilibrium, they have also crystallized at approximately the same pressure and temperature. Therefore these mineral phases can be used for thermobarometry based on EMPA data (McCammon *et al.*, 2001). If the mineral phases present in samples did not equilibrate with each other simultaneously, then any pressures and temperatures calculated using thermobarometry for the ideal reactions will be different to those actually experienced by the minerals or rocks under study. Therefore their chemical reactions cannot be used to estimate oxygen fugacity. Several chemical reactions for coexistent mineral phases in equilibrium, shown in (3-6) below, (for example, garnet- orthopyroxene - olivine; olivine - orthopyroxene -magnetite; fayalite-magnetite-quartz buffer and hematite- rutile – ilmenite) have been used to estimate the oxygen fugacity for

kimberlite rock (Luth *et al.*, 1990; McCammon and Kopylova, 2004; Stagno *et al.*, 2013; and Canil and O` Neil, 1996).



In contrast, the presence of visible rims and the products of a reaction between the mineral phase indicate that they not in equilibrium (Nixon, 1987). As is illustrated in Figure 2.22, the mineral phase from this project contains several alterations. The changing processes from original mineral structure / chemical composition to second any products, has caused the sampled mineral to be unsuitable for thermobarometry in this project. For example several spinel rims were observed around ilmenite (Figure 2.22 sample b). In addition, Figure 2.22, sample c, shows garnet indeed may have reacted with coexisting clinopyroxene to produce a kelyphite rim between them (Kerr *et al.*, 1997), revealing that these minerals were not always in equilibrium (Stagno *et al.*, 2013). It is thus believed that these minerals were formed under different thermobarometric conditions, and therefore they cannot be used in chemical reaction calculations to estimate oxygen fugacity (McCammon *et al.*, 2001).

Rollinson *et al.* (2012) used Mössbauer spectroscopy and EMPA to study spinel (chromite) samples (mantle harzburgites and dunites) from Oman (Wade Rajmi and Maqсад localities), to determine the oxidation state of the sub-oceanic mantle. They demonstrated that two groupings of chromite samples with different  $\text{Fe}^{3+}/\sum\text{Fe}$  ratios were present. The first group (Figure 2.24) showed low  $\text{Fe}^{3+}/\sum\text{Fe}$  values of 0.21-0.36, which arose from reducing environments and low oxygen fugacities between 1.9 and 2.7 log units above the quartz-fayalite-magnetite (QFM) buffer (Figure 2.23). The second group exhibited high  $\text{Fe}^{3+}/\sum\text{Fe}$  of 0.71-0.78, consistent with more oxidising environments with high oxygen fugacities between 3.2 and 3.4 log units above the QFM buffer (Figure 2.23). The oxidised samples were interpreted to be associated with a post-magmatic event which was heating related to melt flux, or interaction with a later oxidising melt. These two distinctive oxidation state groupings are evidence of two different source of magma within the Oman lithosphere. However, Rollinson *et al.* 2012, noted that their temperature estimates associated with calculations of oxygen fugacities (Figure 2.24) were unrealistically high (Rollinson *et al.*, 2012).

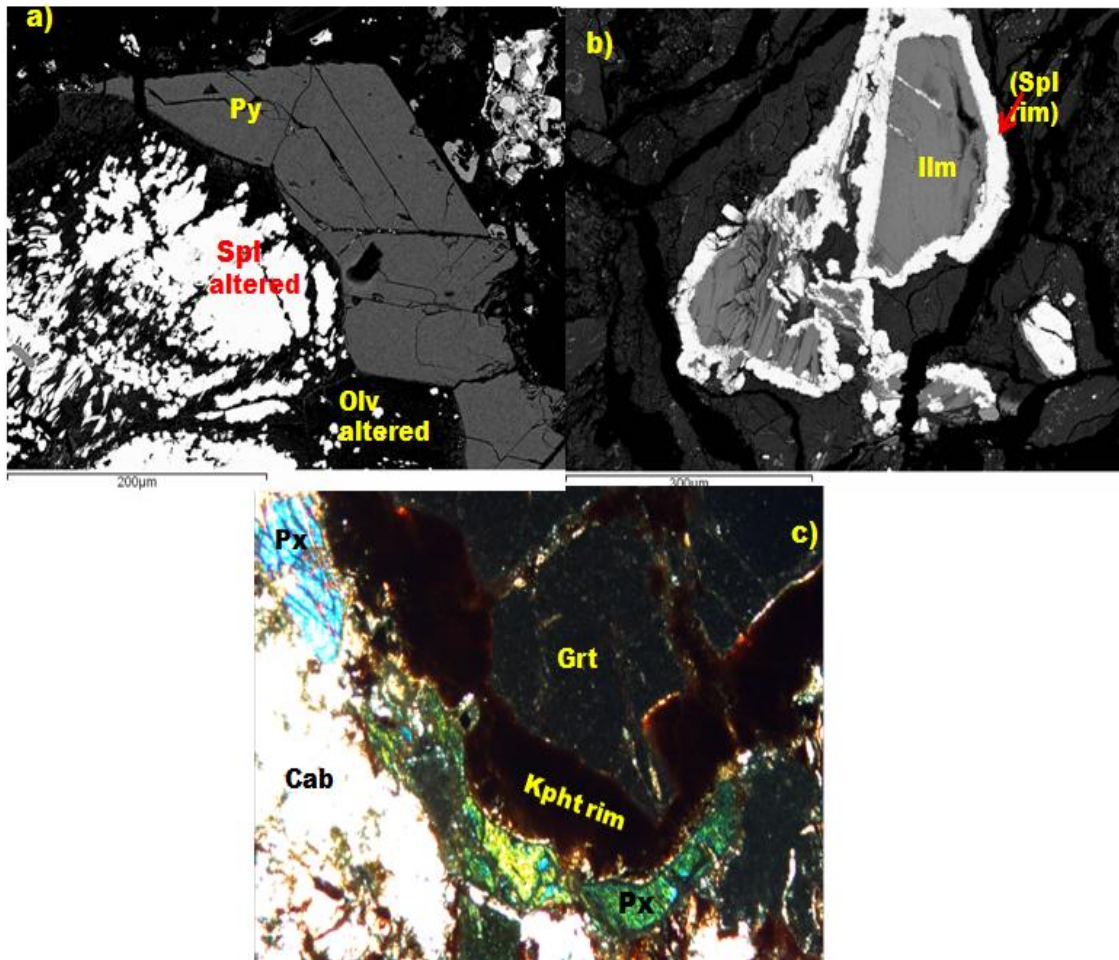


Figure 2.22. Thin section sample images showing several alteration processes: a) Camatxia pipe; b) Camutue pipe; and c) Catoca pipe.

Another Mössbauer study of chromites was carried out by Ruskov *et al.* (2010) who studied the chromite ores of the Luobasa ophiolite massif in Tibet. They discovered that high  $Fe^{3+}/\sum Fe = 0.42$  in chromite resulted from large mineral deposits believed to have been formed under, or were subsequently altered under, conditions of high oxygen fugacity in contrast with chromite with low  $Fe^{3+}/\sum Fe = 0.22$  arising from nodular and disseminated ores. This was because these nodules have crystallized from melts which have interacted with depleted mantle (Rollinson *et al.*, 2012).

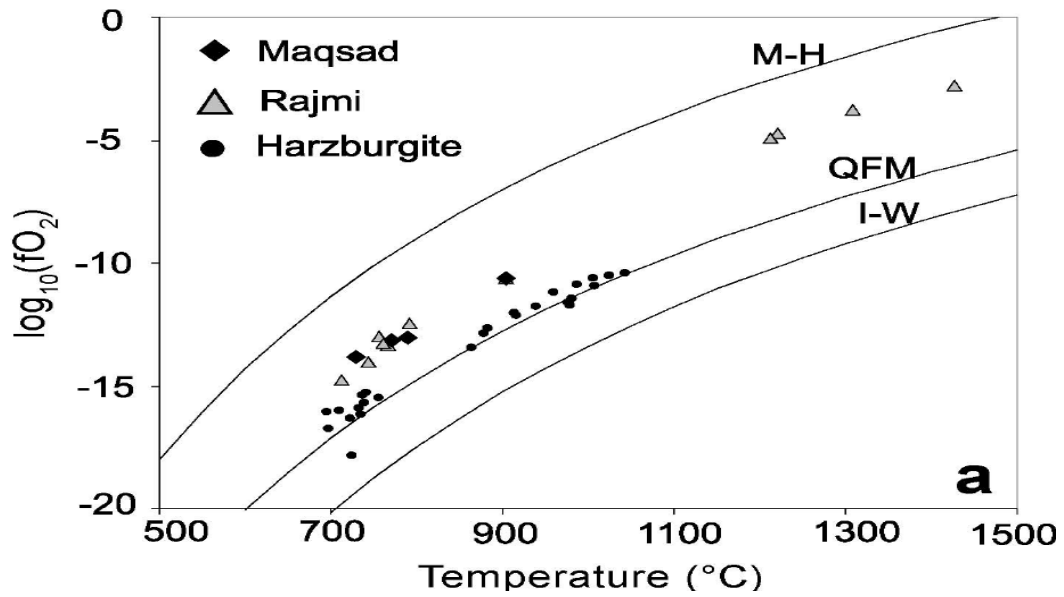


Figure 2.23. Plot of temperature vs.  $\log(fO_2)$  for Oman chromites and harzburgites. The buffer curves shown are magnetite-haematite (M-H), quartz-fayalite-magnetite (QFM) and iron-wustite (I-W). Rollinson *et al.* (2012).

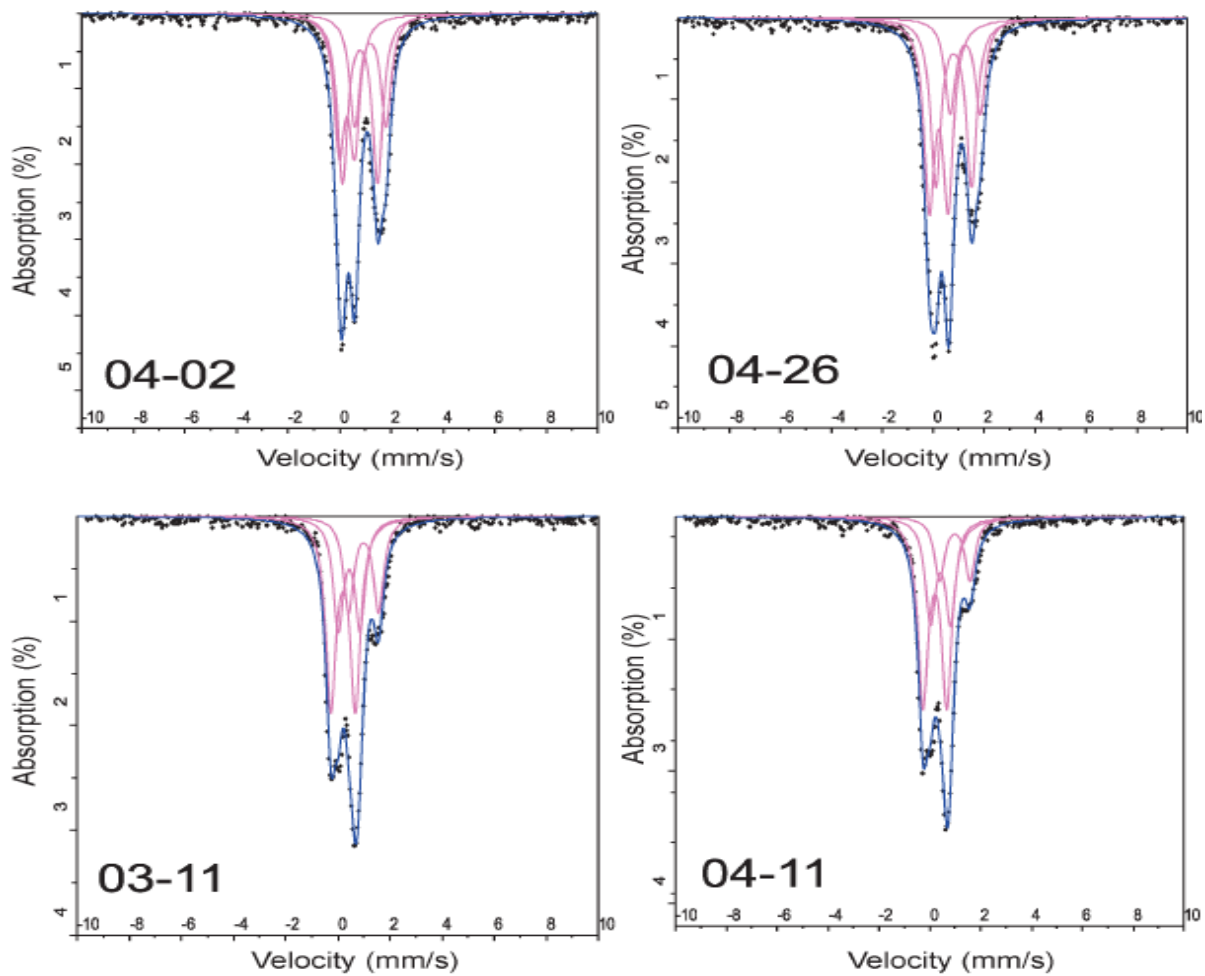


Figure 2.24. Room temperature Mössbauer spectra of chromites inclusion, spectra for the low  $Fe^{3+}/\Sigma Fe$  group (04-02 and 04-26) and the high  $Fe^{3+}/\Sigma Fe$  group (03-11 and 04-11). From Rollinson *et al.* (2012).

Pyroxene and garnet also have been widely used to determine the oxidation state of kimberlite rock samples. For example, Vieira and Knudsen (1983) who used Mössbauer spectroscopy to study pyroxene confirmed that terrestrial basalts and ocean floor basalts are more oxidized due to the high  $\text{Fe}^{3+}$  contents found in pyroxenes that are present within basalts. McCammon *et al.* (1998) investigated the ability of Mössbauer spectroscopy to determine  $\text{Fe}^{3+}/\sum\text{Fe}$  for garnet and clinopyroxene diamond inclusions, from a suite of mantle eclogites from George Creek, Colorado, USA. They discovered that clinopyroxenes had  $\text{Fe}^{3+}/\sum\text{Fe}$  ratios of 0.08 - 0.14 and garnet 0 - 0.07, which were interpreted to demonstrate low oxygen fugacities at the time of formation of these George Creek diamonds (Figures 2.26 and 2.27; and Table 2.3). Interpretation of oxygen fugacity depends critically on the accuracy of the  $\text{Fe}^{3+}/\sum\text{Fe}$  ratio, and accuracies determined by Mössbauer spectroscopy have been shown to be higher than those obtained from stoichiometric calculations based on EMPA data (McCammon *et al.*, 1999; and Canil and O'Neill, 1996).

Mössbauer spectroscopy of natural garnets has also been carried out by several authors (Stagno *et al.*, 2013; Dyar, 1984; Cerná *et al.*, 2000; Dachs *et al.*, 2012; and Luth *et al.*, 1990). Stagno *et al.* (2013) showed that oxygen fugacity of garnet-bearing rocks increases with decreasing depth during uncontrolled decompression, which means that carbon in the upper mantle at depths of approximately 80 - 200 km (asthenospheric mantle, Stachel, 2003), will be hosted as graphite (shallow depth about < 170 km) or diamond (at depths of > 170km with  $\text{Fe}^{3+}/\sum\text{Fe}$  of up to 0.04, as seen in Figure 2.25). Both the graphite and diamond will be oxidized to produce a carbonate melt at depths of  $150 \pm 50$  km through the reduction of  $\text{Fe}^{3+}$  in silicate minerals during upwelling (Figure 2.25 b). Luth *et al.* (1990) used Mössbauer spectroscopy to determine  $\text{Fe}^{3+}/\sum\text{Fe}$  for garnets from mantle-derived xenoliths from South Africa and Russia. They showed that garnet lherzolites from both countries, measured at low temperature of 77 K, gave  $\text{Fe}^{3+}/\sum\text{Fe}$  ratios < 0.07 and the samples were thus interpreted to be derived from a low oxidation region. In contrast, garnet lherzolites from the Kaapvaal craton (South Africa) measured at room temperature of 298 K, had  $\text{Fe}^{3+}/\sum\text{Fe} > 0.10$ , and consequently these garnets were interpreted as being sourced from a more oxidised region. In addition Luth *et al.* (1990), discovered that  $\text{Fe}^{3+}/\sum\text{Fe}$  ratio in garnet increases with increasing pressure and temperature of the host xenoliths.

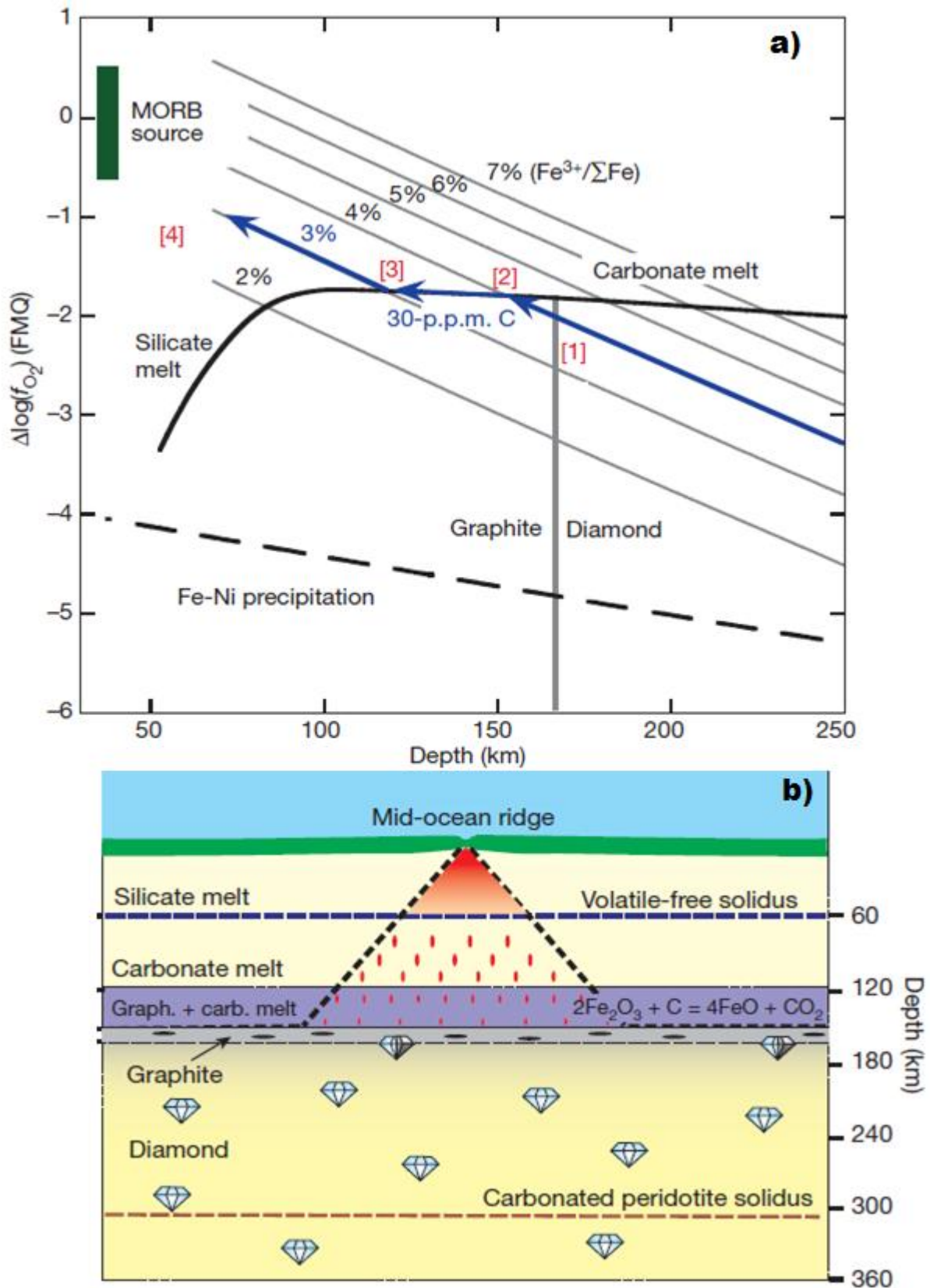


Figure 2.25. Speciation of carbon in a rapid, uncontrolled upwelling mantle. Mid-Ocean-Ridge Basalt (MORB). Modified after Stagno *et al.* (2013).

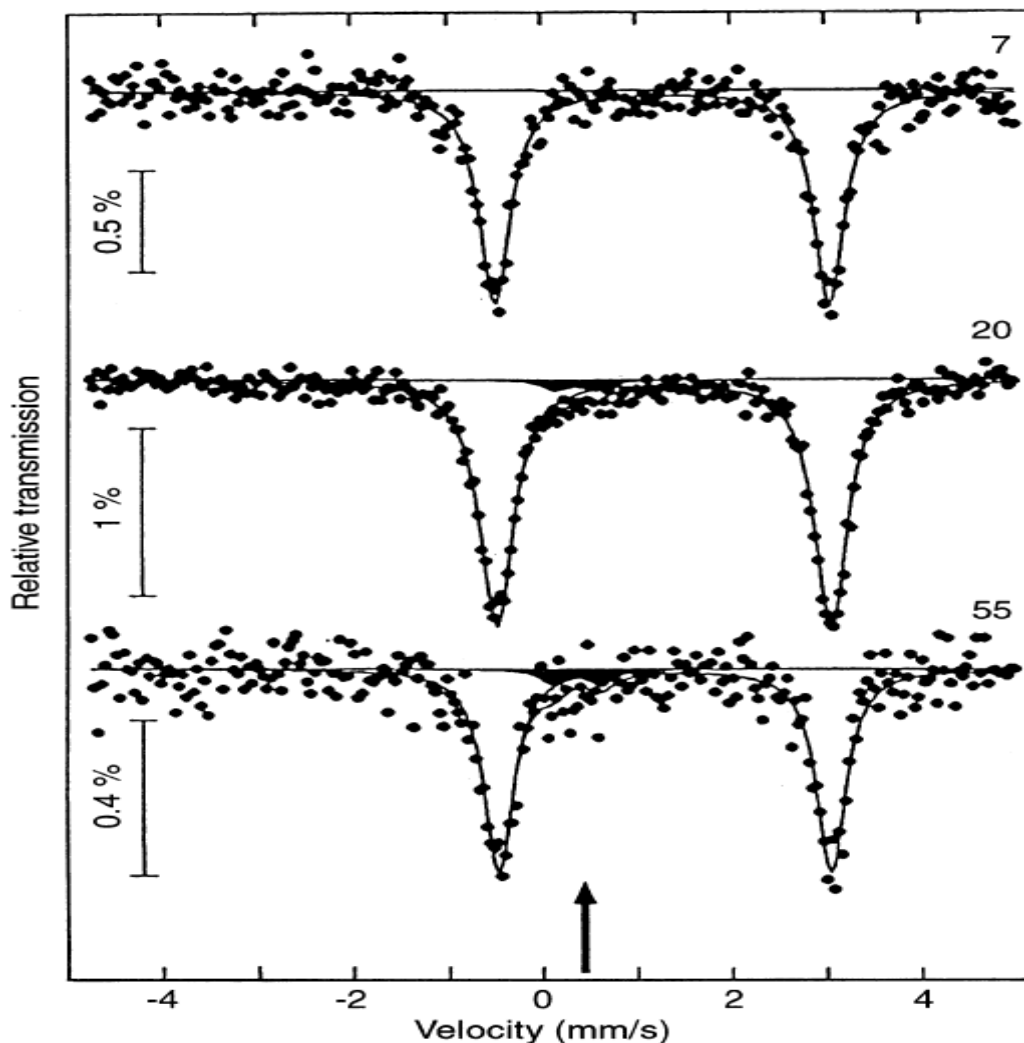


Figure 2.26. Room temperature Mössbauer spectra of garnet inclusions from George Creek diamonds. Data were fitted using one  $\text{Fe}^{2+}$  and one  $\text{Fe}^{3+}$  doublet; the latter is shaded black. The arrow indicates the region where  $\text{Fe}^{3+}$  absorption is observed in spectra of mantle-derived garnets (McCammon *et al.*, 1998).

Ilmenite is another important kimberlite indicator mineral which has been widely used to determine the oxidation state of the sample and the diamond preservation index condition. Naturally-occurring ilmenite,  $\text{FeTiO}_3$ , is an iron-bearing mineral with iron occurring in two oxidation states ( $\text{Fe}^{3+}$  and  $\text{Fe}^{2+}$ ), and is commonly found as rock inclusions in kimberlites and volcanic rocks (Press and Siever, 1986; and Blatt and Trace, 2001). Hence ilmenites are good candidates for studying the  $\text{Fe}^{3+}/\Sigma\text{Fe}$  ratio, in-situ under pressure. Determination of the ratio of the oxidation states of the two mineralogically important Fe cations ( $\text{Fe}^{3+}/\Sigma\text{Fe}$ ) has been useful in the study of iron bearing materials to obtain information concerning the weathering history of deposited minerals and including diagenesis of these materials after deposition (Waerenborgh *et al.*, 2002; and Canil and O'Neil, 1996). The oxidation states of ilmenite mineral inclusions have been explained by (Seda and Hearne, 2004, Figure 2.28 and Table 2.4) as a good indicator of the oxidation state of the host kimberlite assemblage, which in turn determines the origin and genesis of diamond.

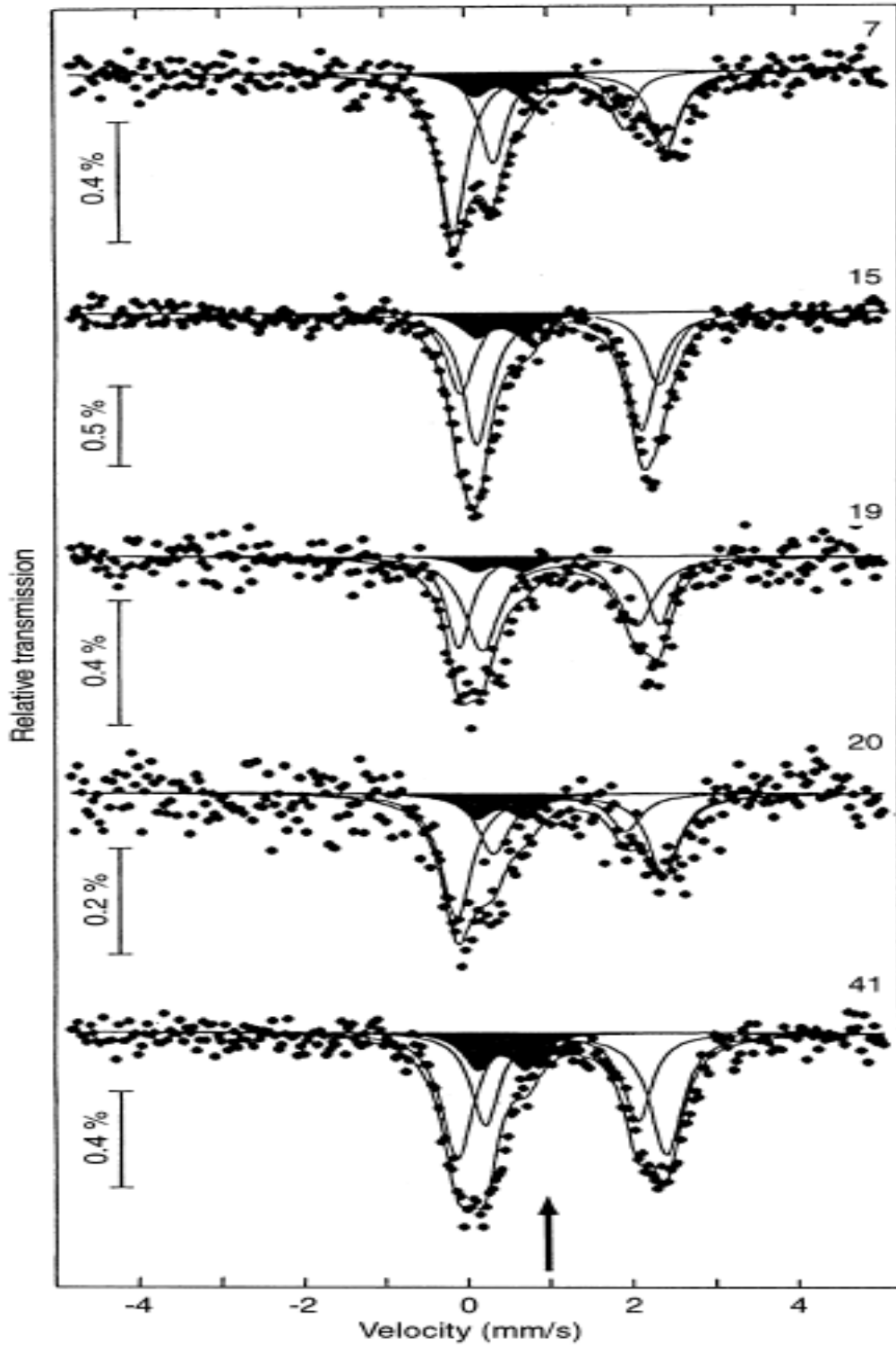


Figure 2.27. Room temperature Mössbauer spectra of clinopyroxene inclusions from George Creek diamonds. The data were fitted with two  $\text{Fe}^{2+}$  doublets and one  $\text{Fe}^{3+}$  doublet; the latter is shaded black. The arrow indicates the region where the high velocity component of  $\text{Fe}^{3+}$  absorption is observed in spectra from mantle-derived clinopyroxenes (McCammon *et al.*, 1998).

Diamond #	7	20	55	7	15	19	20	41
Phase	Gt	Gt	Gt	Cpx	Cpx	Cpx	Cpx	Cpx
<b>Fe<sup>2+</sup> (I):</b>								
CS (mm/s)	1.29 (1)	1.30 (1)	1.29 (1)	<i>1.13</i>	<i>1.13</i>	<i>1.13</i>	<i>1.13</i>	<i>1.13</i>
QS (mm/s)	3.54 (1)	3.55 (1)	3.52 (2)	1.59 (6)	2.00 (4)	1.87 (10)	1.61 (8)	1.85 (3)
W (mm/s)	0.40 (2)	0.42 (1)	0.37 (2)	0.37 (7)	0.40 (3)	0.52 (8)	0.45	0.41 (5)
<b>Fe<sup>2+</sup> (II):</b>								
CS (mm/s)				<i>1.13</i>	<i>1.13</i>	<i>1.13</i>	<i>1.13</i>	<i>1.13</i>
QS (mm/s)				2.57 (3)	2.41 (8)	2.44(6)	2.51 (4)	2.54 (3)
W (mm/s)				0.42 (3)	0.41 (6)	0.36(9)	0.45	0.46 (3)
<b>Fe<sup>3+</sup>:</b>								
CS (mm/s)	<i>0.37</i>	<i>0.37</i>	<i>0.37</i>	<i>0.41</i>	<i>0.41</i>	<i>0.41</i>	<i>0.41</i>	<i>0.41</i>
QS (mm/s)	<i>0.51</i>	<i>0.51</i>	<i>0.51</i>	<i>0.60</i>	<i>0.60</i>	<i>0.60</i>	<i>0.60</i>	<i>0.60</i>
W (mm/s)	<i>0.35</i>	<i>0.35</i>	<i>0.35</i>	<i>0.44</i>	<i>0.44</i>	<i>0.44</i>	<i>0.44</i>	<i>0.44</i>
Fe <sup>3+</sup> /ΣFe (%)	0 (3)	3 (2)	7 (3)	12 (6)	11 (5)	8 (6)	14 (8)	14 (7)

Table 2.3. Room temperature fitted Mössbauer hyperfine parameters of mineral inclusions (CS - centre shift; QS- quadrupole splitting, W- full width at half maximum). Numbers in parentheses show the standard deviation of the last digit; parameter values in italics were fixed during the fitting process (McCammon *et al.*, 1998).

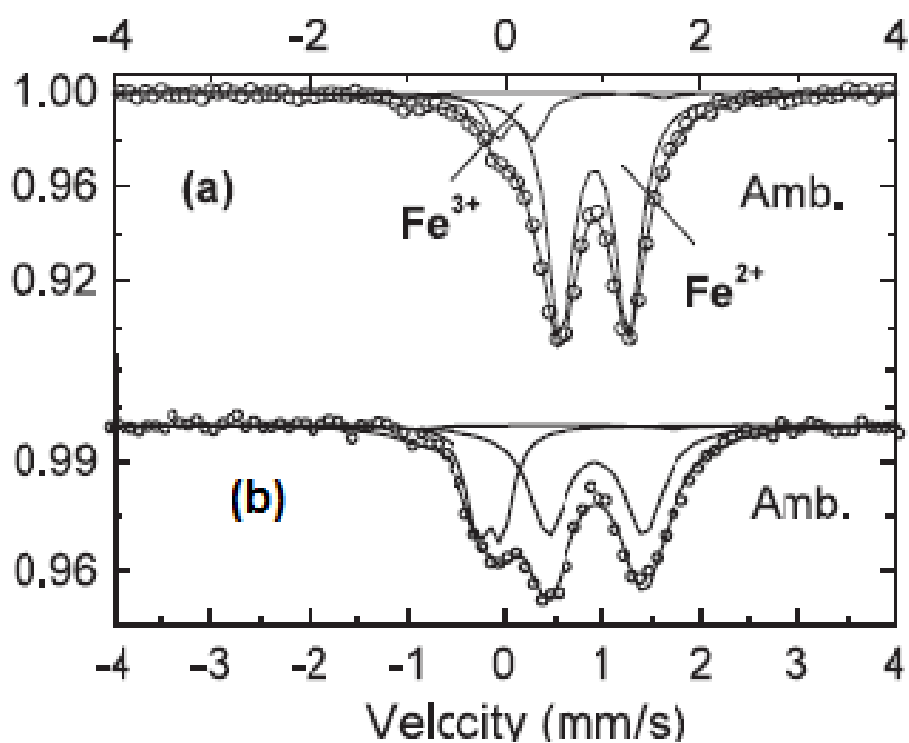


Figure 2.28. <sup>57</sup>Fe Mössbauer spectra of an untreated FeTiO<sub>3</sub> sample at room temperature plotted on a restricted velocity scale. Solid curves are theoretical fits to the experimental data. Modified after Seda and Hearne (2004).

(a)	Abundances (%)			$\delta$ (mm s <sup>-1</sup> )		$\Delta E_Q$ (mm s <sup>-1</sup> )		$\Gamma_A$ (Fe <sup>2+</sup> )
	Fe <sup>2+</sup>	Fe <sup>3+</sup>	Fe <sub>2</sub> O <sub>3</sub>	Fe <sup>2+</sup>	Fe <sup>3+</sup>	Fe <sup>2+</sup>	Fe <sup>3+</sup>	
Ambient	74.2	16.1	9.7	1.067(1)	0.272(8)	0.694(2)	0.32(2)	0.345(4)
(b)	Abundances (%)			$\delta$ (mm s <sup>-1</sup> )		$\Delta E_Q$ (mm s <sup>-1</sup> )		$\Gamma_A$ (Fe <sup>2+</sup> )
	Fe <sup>2+</sup>	Fe <sup>3+</sup>	Fe <sub>2</sub> O <sub>3</sub>	Fe <sup>2+</sup>	Fe <sup>3+</sup>	Fe <sup>2+</sup>	Fe <sup>3+</sup>	
Ambient	72.2	13.2	14.6	1.021(1)	0.21(1)	0.693(2)	0.39(2)	0.311(3)

Table 2.4. Abundance of each component of ilmenite sample spectra derived from absorption areas at room temperature. Modified after Seda and Hearne (2004).

Mössbauer studies of natural ilmenite from different diamond kimberlite deposits across the world, for example South Africa, Russia, Sierra Leone, have been extensively studied by Virgo *et al.*, (1998), who concluded that ilmenites from South African kimberlite pipes show two different oxidation conditions, one (ROM 264IL-41) is moderately oxidised with Fe<sup>3+</sup>/ΣFe ratios 0.27 and 0.26 and the second (ROM38) is reduced with Fe<sup>3+</sup>/ΣFe ratios of 0.09; 0.13 and 0.24. By comparison, ilmenites from Sierra Leone kimberlites (HAG 2) are more reduced with Fe<sup>3+</sup>/ΣFe ratios of 0.08 and 0.13, likewise ilmenites from Yakutia province (Russia) have Fe<sup>3+</sup>/ΣFe ratios ranging from 0.15-0.19.

An ilmenite from Portugal revealed a different scenario of oxidation conditions. According to Waerenborgh *et al.* (2002), highly oxidised ilmenite (Figure 2.29 and table 2.5) from southeast Portugal may be associated with post-emplacement evolution of the ophiolite (a segment of the Earth's oceanic crust and the underlying upper mantle that contains peridotite, layered gabbro, dikes, and volcanic sediments/rocks; Blatt and Trace, 2001) and the ophiolite sequence which contains different altered oceanic rocks (marine sediments and ocean crustal rocks which are part of the mantle; Press and Siever, 1986). Different minerals phases (magnetite, amphiboles, hematite and ilmenite, Table 2.5) present in the studied sample by Waerenborgh *et al.* (2002) have been identified using XRD.

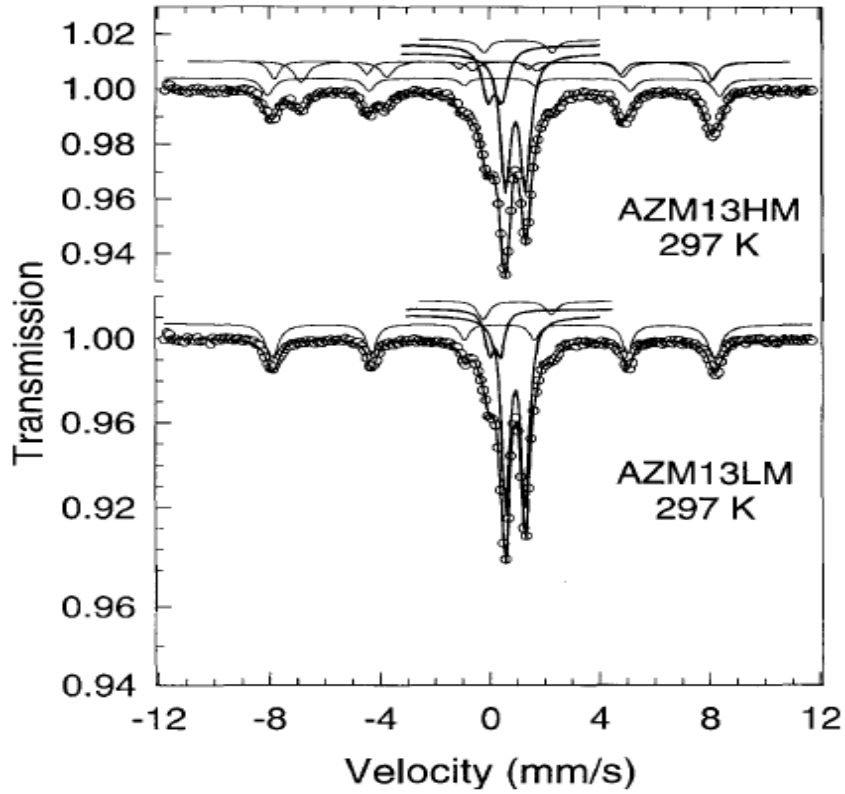


Figure 2.29. Room temperature Mössbauer spectra of ilmenite inclusions in ophiolite rock. Doublets represent  $\text{Fe}^{2+}$  and  $\text{Fe}^{3+}$  in ilmenite (thick lines) and  $\text{Fe}^{2+}$  in amphibole. The sextet represents hematite at both samples. In the case of AZM 13HM two additional sextets with lower magnetic splitting, due to magnetite, are also present. Modified after Waerenborgh *et al.* (2002).

AZM 13HM	Magnetite		Hematite $\text{Fe}^{3+}$	Ilmenite		Amphibole $\text{Fe}^{2+}$	
	$\text{Fe}^{3+}$	$\text{Fe}^{2.5-}$		$\text{Fe}^{2+}$	$\text{Fe}^{3+}$		
	$\delta$ (mm/s)	0.27	0.67	0.38	1.07	0.32	1.15
	$\Delta$ (mm/s)	-	-	-	0.73	0.52	2.49
	$\epsilon$ (mm/s)	0.00	0.00	-0.22	-	-	-
	$B_{\text{hf}}$ (T)	49.5	46.0	51.0	-	-	-
	$\Gamma$ (mm/s)	0.33	0.46	0.38	0.44	0.52	0.47
	$I$	11%	17%	12%	39%	17%	4%
AZM13LM		Hematite $\text{Fe}^{3+}$		Ilmenite $\text{Fe}^{2+}$ $\text{Fe}^{3+}$		Amphibole $\text{Fe}^{2+}$	
297 K	$\delta$ (mm/s)	0.38	1.06	0.32	1.14		
	$\Delta$ (mm/s)	-	0.71	0.40	2.49		
	$\epsilon$ (mm/s)	-0.22	-	-	-		
	$B_{\text{hf}}$ (T)	49.9	-	-	-		
	$\Gamma$ (mm/s)	0.38	0.36	0.38	0.47		
	$I$	29%	52%	12%	6%		

Table 2.5. Room temperature fitted Mössbauer hyperfine parameters of mineral inclusions (ilmenite, magnetite, hematite and amphibole), (CS - centre shift; QS- quadrupole splitting, W- full width at half maximum). Modified after Waerenborgh *et al.* (2002).

## Chapter Three . Field work, experimental procedures and petrographic study of mantle xenoliths and kimberlite rocks

### 3. 1. Field work

During field work in Lunda province (LP), rocks from crater, diatreme and hypabyssal facies were sampled. Figure 3.1 represents the ideal occurrence model and petrogenesis of kimberlites from South Africa. The kimberlites from NE Angola (Lunda provinces) and South Africa are similar and are both classified as Group I kimberlites (Skinner, 2008; Mitchell, 1991; and Field and Scott Smith, 1998). From studying the morphology and petrology of Lunda kimberlite magmas after emplacement and cooling, it has been shown (see Chapter 2) that Lunda kimberlites are products of multiple intrusive and extrusive magmatic events similar to those depicted for South African kimberlites in Figure 3.1

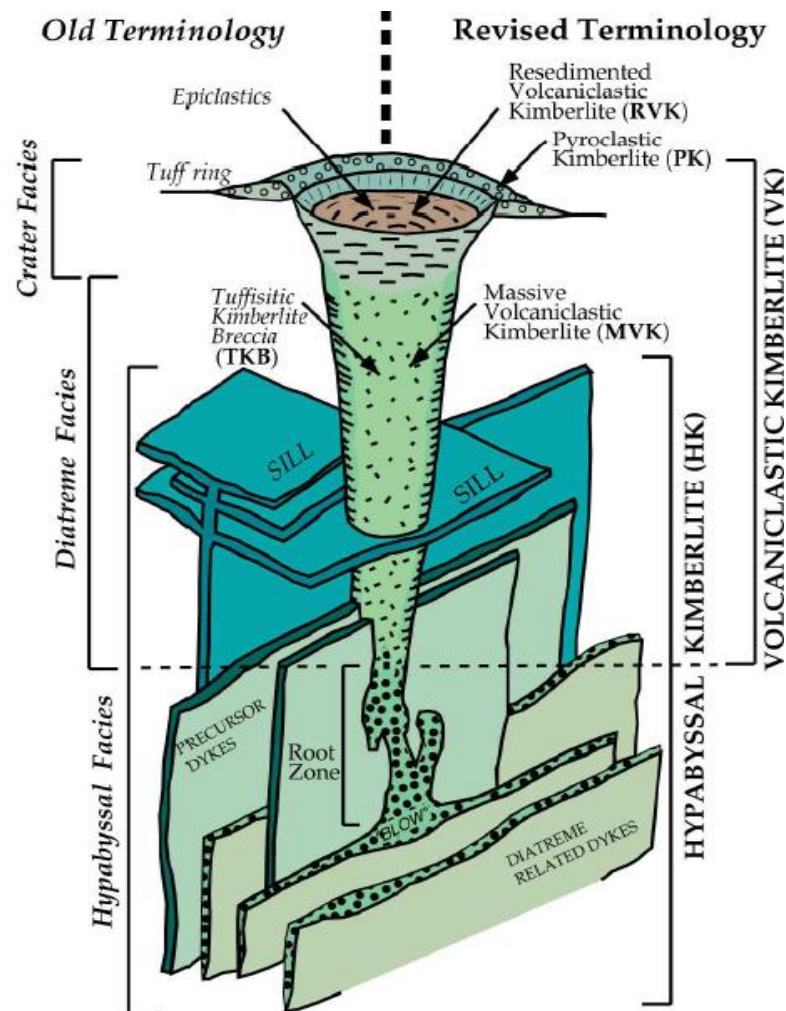


Figure 3.1. The classic South African model of a kimberlite pipe with old nomenclature (left side of figure) and a revised nomenclature system (right side of figure) to describe rocks from kimberlite magmatic systems as recently suggested by Sparks *et al.* (2006); Scott Smith *et al.* (2008); and Cas *et al.* (2008). Figure from Kjarsgaard (2007).

The field work described in this thesis was conducted across several active diamond exploration mines in the Lunda provinces region (see Figure 2.1). This investigation focuses on core samples of deep mantle facies rock recovered from exploration drill holes at five primary kimberlites diamond mines (Catoca, Camutue, Caixepa, Camatxia and Camagico). The core samples, with other samples from outcrop exposures, have helped to identify the architecture model of emplacement of Lunda kimberlite pipes (for example Figure 3.4) and have also provided some alluvial information for diamond indicator minerals (Figure 3.13).

Two different sampling methods were used during sampling activity:

1. Core drilling method (see figure 3.9)
2. Rock crushing using a geological hammer (see Figure 3.10)

Both of these methods were applied during sampling activity and diamond field work. Diverse mantle xenoliths, comprising lherzolite, harzburgite (Peridotite, Figures 3.2 and 3.5 sample b) and eclogite (Figure 3.5 sample a) are distributed throughout the north-east Angolan kimberlite and these materials were collected at different localities. Sampling of mantle xenoliths was primarily targeted toward garnet lherzolite and harzburgite assemblages (garnet, ilmenite olivine, pyroxene chromite) including bimineralic eclogite. Apart of mantle xenoliths, kimberlite rocks such as pyroclastic kimberlite (PK), resedimented volcanoclastic kimberlite (RVK), tuffisitic kimberlite (TK) and hypabyssal kimberlite (coherent or non-fragmental rocks) were mostly sampled rocks and the results of their petrographic analysis are provided below. These kimberlite rocks were sampled through several formation facies or zones: crater, diatreme and hypabyssal facies (see Chapter 4). Most of the samples exhibited an inequigranular texture (Figures 3.2; 3.5; 3.7 and 3.8 and also see further descriptions and classifications of samples in Appendix 2).

In order to avoid contamination, all samples were kept in sealed plastic bags and boxes (Figure 3.3) but throughout the sampling activities, it was observed that most olivine was serpentinised. Kimberlite indicator minerals were obtained from samples after they had been processed by the mining company to recover diamonds from the sampled kimberlites. All samples were attributed names according to their source (crater, diatreme and hypabyssal facies). The summary of representative samples, including their depth of drilled section from each pipe, is presented in Chapter 4.

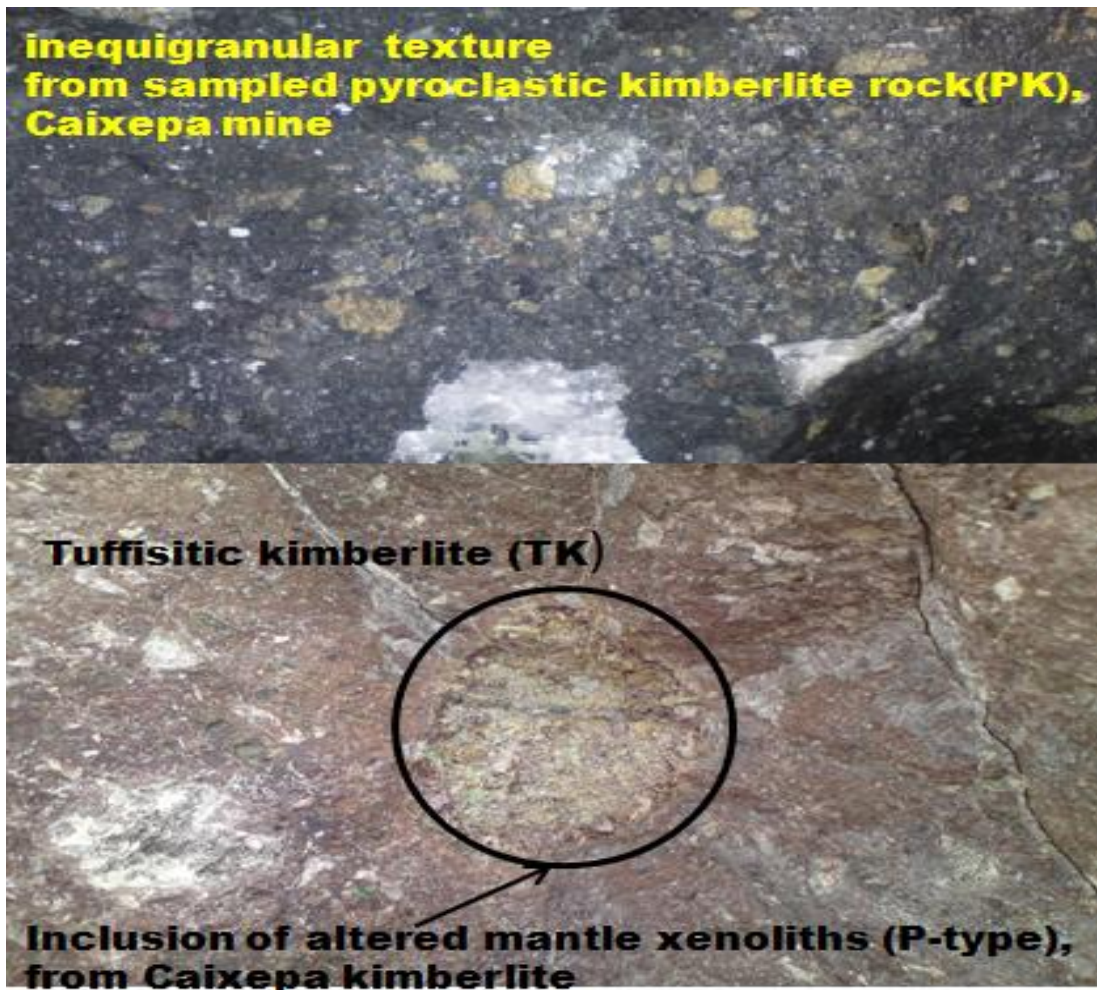


Figure 3.2. Photographs of Caixepa kimberlite samples, showing inequigranular texture with large inclusion of mantle xenolith (P-type).



Figure 3.3. Photographs illustrating how the samples were catalogued and stored in the petrography laboratory of the Catoca diamond mine.

### 3. 1. 3. Catoca kimberlite pipe

Several kimberlite rocks and mantle xenoliths were collected at different depths and localities at Catoca pipe. Sample locations are depicted in Figure 3.4 and Appendix 2. Figure 3.4 also demonstrates how samples would have been originally placed or fit in geological pipe (samples include: **A** (Cat-18); **B** (Cat-22); **C** (Cat-29); **D** (Cat-58); **E** (Cat-59); **F** (Cat-67).

As previously recognised by Ganga *et al.* (2003), Catoca chimney occupies 639,000 sqm (m<sup>2</sup>) and kimberlite bodies (900 x 900 m<sup>2</sup>) which resulting it to rank as the world's fourth biggest diamond mine in the world by reserve. The pipe contains a complex geological structure (Figure 3.4, and Appendix 3) whereas the Camafuca-Camazambo pipes are considered to be the biggest kimberlite bodies in the world (Ganga *et al.*, 2003) with surface area of 160 hectares. The reason for this may be associated with large volume magmatic events and their composite nature, which probably gives Camafuca-Camazambo the larger dimension. Apart from these kimberlites, other diamondiferous pipes along the Lucapa graben include Camutue, Caixepa and Camatxia-Camagico, which are also very large. Other important aspects related with the occurrence of diamond content within Angolan kimberlites, is that the diamond grade decreases a south-west orientation, and a series of alkaline and carbonatite complexes are located at southern extremity of the corridor structure, mentioned above (see Figure 2.1).

During field work and sampling activities, it was observed that most country rocks (host rocks) are composed of granite, gneisses and crystalline schists but they are covered by sediments of the Kalahari Formation and paleogene-neogene approximately 135m thick. The most important and complex aspect observed at Catoca pipe is the occurrence of its crater facies. This geological zone can be interpreted to be a complex formation event because its structure is associated with the kimberlitic pyroclastic suspension model (Pervov *et al.*, 2011) which has filled the central part of the pipe (Figure 3.4). The rock shows a wide variation in composition and inequigranular textural features. For example, the crater of Camatxia, Camutue and Caixepa and Catoca pipe is dominated by several rock types, including:

- ✓ Banded tuffisitic kimberlite.
- ✓ Sediments with little dilution by kimberlitic material.
- ✓ Volcanic sedimentary, tuffs argillaceous-sandstone and sediment-volcanic sequence.
- ✓ Kimberlitic tuffs breccia.

It was observed that most crater facies rocks are brownish-grey in colour, and some shale rocks exhibit layered textures and are poorly sorted.

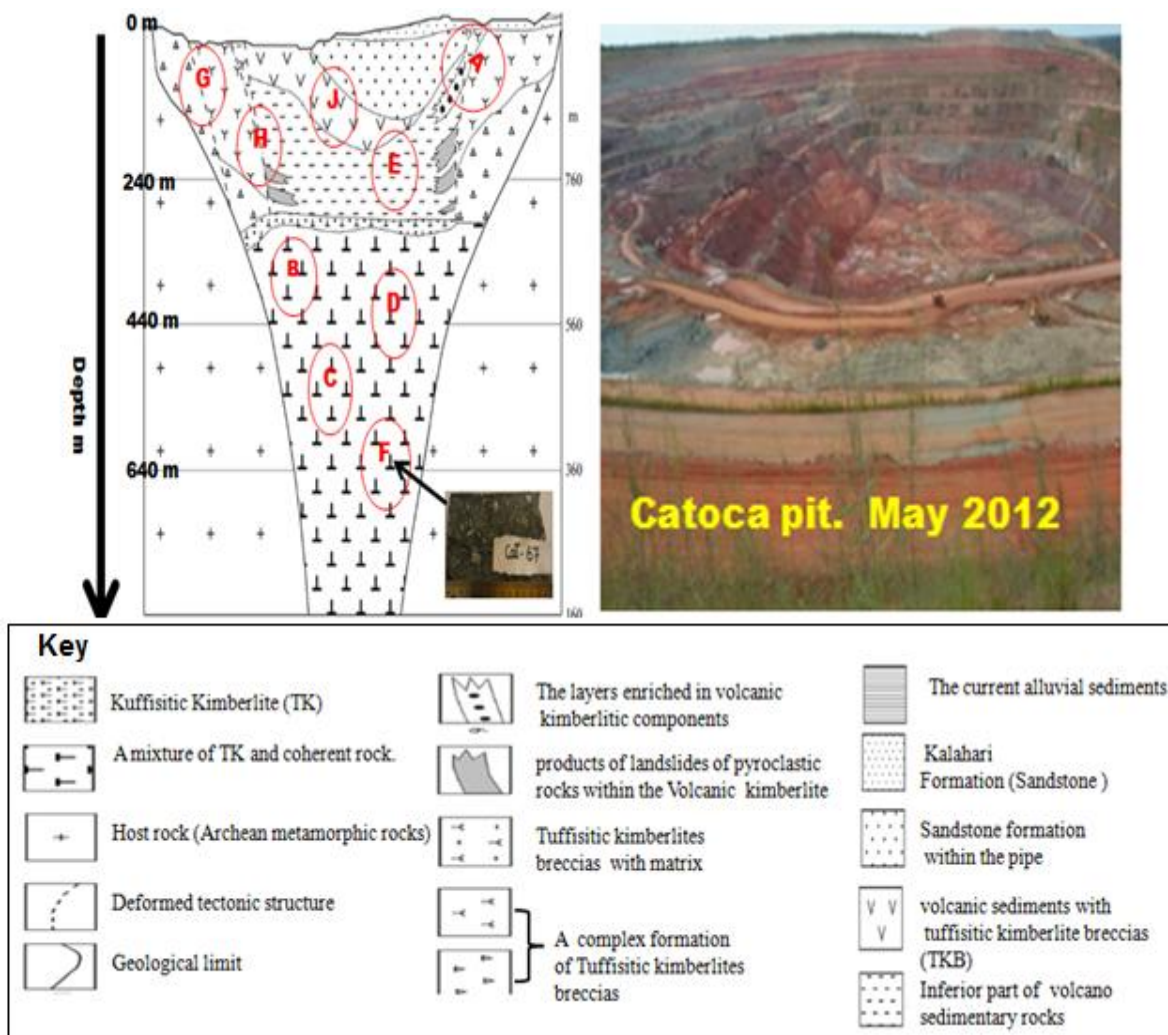


Figure 3.4. Illustration of a complex geological cross section of the Catoca kimberlite pipe, modified after Pervov *et al.* (2011).

Coherent magmatic kimberlite rocks (non-fragmented rocks, see Figure 3.20c) were only sampled at Catoca mine, probably due to its great depth (>600m). Most indicator minerals: ilmenite, Cr-diopside, garnets, chromites and pyroxenes are present in the facies, but most examined olivine is pseudomorphed by serpentine (Figure 3.20). As discussed in sections 2.2 and 2.2.1, kimberlites can be classified as Group I or Group II. The Lunda kimberlites are classified as Group I kimberlites (Skinner, 2008; and Mitchell, 1991). Kimberlites of Lunda province (Group I) exhibit a distinctive inequigranular texture (Figure 3.6). This is caused by macrocrystic and megacrystic materials incorporated in fine grain materials. The most abundant phenocrysts (macrocrysts) of olivine, garnet, spinel, pyroxene, ilmenite and phlogopite, are set in a fine to medium grained groundmass of serpentine, carbonate and altered olivine.

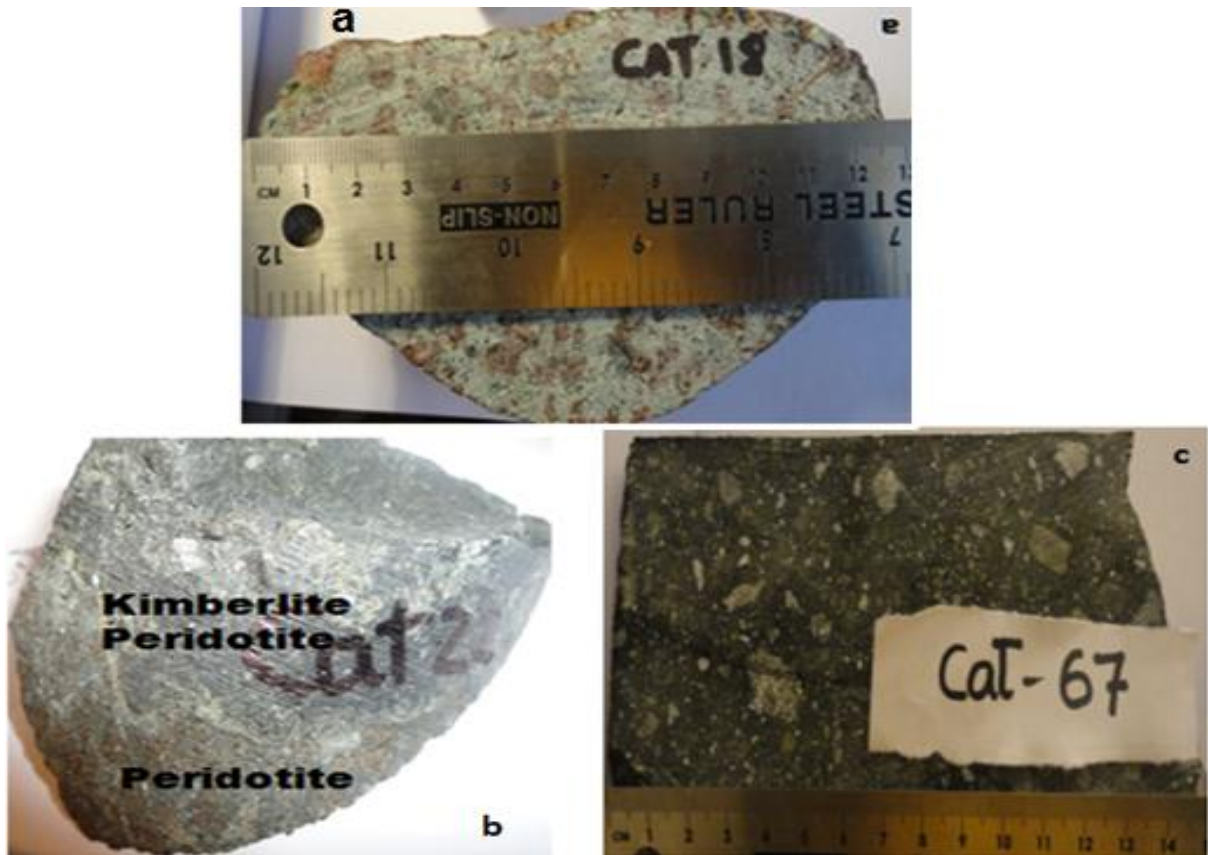


Figure 3.5. Different Catoca mantle rock types from LP. a) Bimineralic eclogite, composed mainly of garnet (red-brown) and clinopyroxene (green), b) Peridotite inclusion in kimberlite rock, and c) Coherent kimberlite

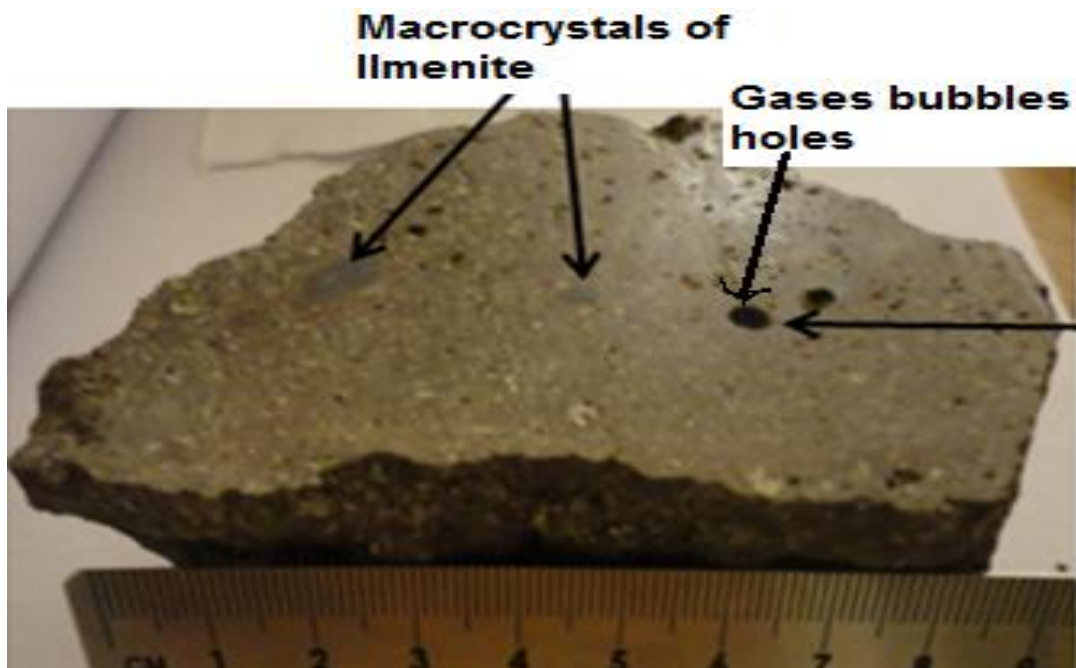


Figure 3.6. Diamond-bearing kimberlite rock, pyroclastic kimberlite (PK) from diatreme facies, at Catoca mine (Diamonds are not visible).

### 3. 1. 3. Caixepa and Camutue kimberlite pipes

Despite the fact that there may be some insignificant differences of kimberlite occurrence within the Lucapa Graben, the petrographic facies of Camutue, Caixepa (Figure 3.7), Camagico, Camatxia and Camagico are similar to those described for the Catoca pipe. For instance, one of the noticed differences among them is that the hypabyssal kimberlite facies were observed only at Catoca pipe, probably due to the geological factors associated with the occurrence of the pipe and that Catoca pipe is bigger and deeper than other sampled pipes.

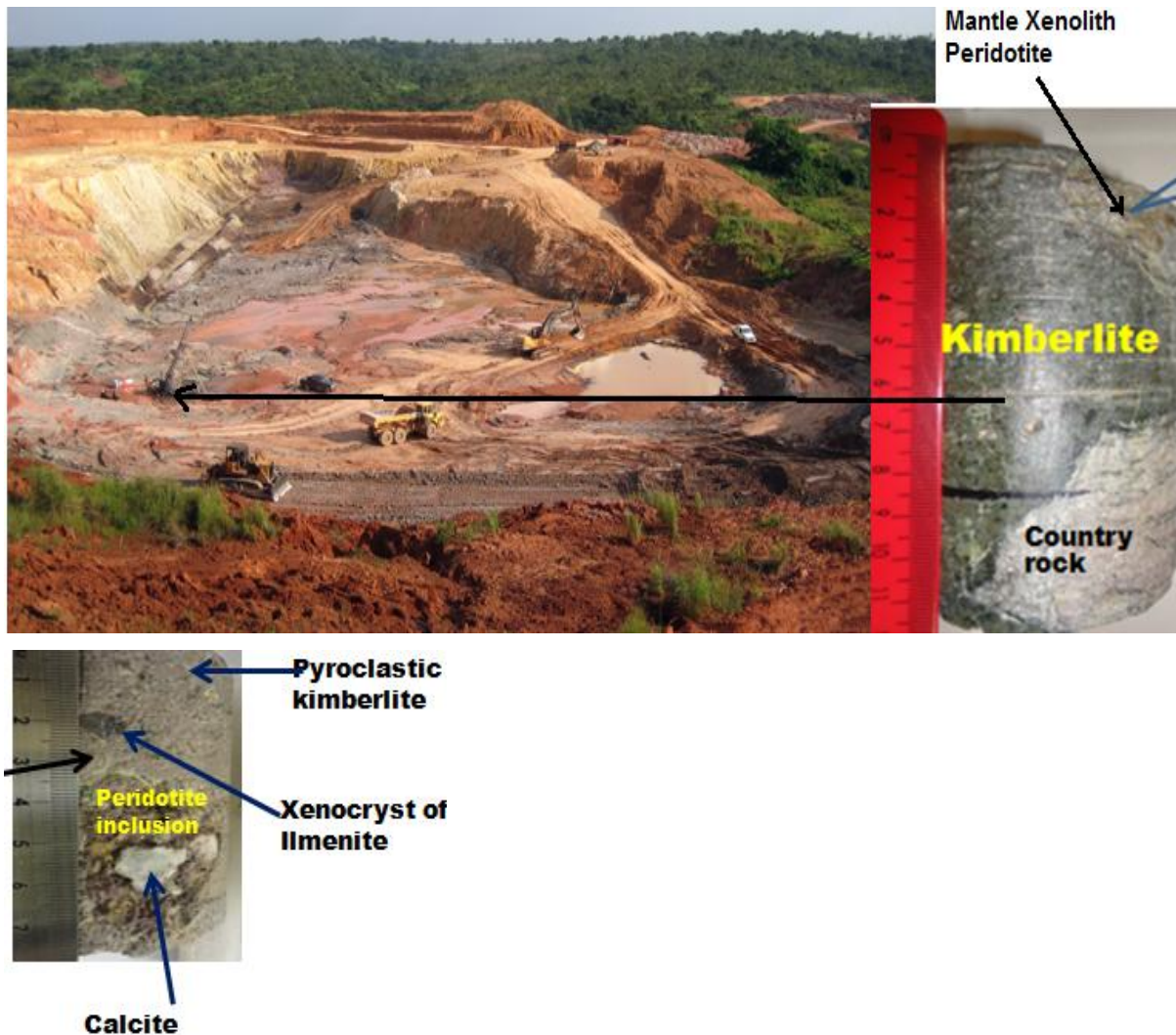


Figure 3.7. Surface diamond exploration activity at Caixepa kimberlite mine. Inset - common equigranular texture of kimberlite mantle xenolith included in diamond-bearing kimberlite rock, from Caixepa mine.

The dominant mantle xenoliths at the Camutue and Caixepa pipes are peridotite, but most of the observed olivine is serpentinised. The inequigranular texture (Figure 3.7 and 3.8) is the most dominant texture from these pipes. As seen in Figures 3.7 and 3.9, both Caixepa and Camutue pipes are covered by a several metre thick layer of Kalahari sands. It was observed that the upper part of the

pipe (crater zone) is composed of kimberlite tuffisitic breccia, gravestones, sandstone, pyroclastic kimberlite (PK), resedimented volcanoclastic kimberlite (RVK) and tuffisitic kimberlite (TK). Due to its uniform body, diatreme zones of Lunda kimberlites are characterised by the presence of numerous mantle xenoliths of different size and composition.



Figure 3.8. Photograph of a diamond-bearing kimberlite rock, from Caixepa mine (diamonds are not visible). This is a pyroclastic kimberlite core (Caixepa mine).

Several fresh (unaltered) and some minor altered rocks were obtained at variable depths (see Appendix 2). For example, olivine grains from great depths (diatreme zones, see Appendixes 1 and 2) are replaced by serpentine and white calcite (Figures 3.8). Some crater and diatreme rocks are characterized by low diamond contents (for example, those from Camatxia and Camutue mines). This is because these zones are significantly diluted by country rock fragments or other geological factors. The quality and average size of diamonds however is higher at Caixepa than any other pipe in Angola (anecdotal information obtained from local geologists and diamond evaluators), and this information is also supported by Mössbauer analysis (see Chapter Four) As illustrated in Figure 3.8, the most widely observed rocks from this pipe are poor-medium sorted with brownish and grey colour



The red coloured material is resultant of reaction/ oxidation process



Figure 3.9. Photographs of sampling activity by drilling core method at Camutue mine.

### 3. 1. 4. Camatxia and Camagico kimberlite pipes

These pipes (Camatxia, Figure 3.10, and Camagico) have similar petrographic facies to those described above for Catoca, Camutue and Caixepa mines. Most kimberlite crater facies sample rocks from these pipes present inequigranular texture, angular and rounded blocks of different sizes with irregular shapes and are generally brownish to grey in colour, with some visible minerals alteration. Mantle xenolith rocks (P-type) was found (Figures 3.10 and 3.11). Dilution processes may have affected crater rocks (tuffisitic argillaceous-sandstone, gravestones, or resedimented volcanoclastic kimberlite, tuffisitic kimberlite breccia and pyroclastic kimberlite). According to information from local geologists, most sampled pipes present a higher quality of diamond than those Catoca pipe. In contrast, Catoca pipe provides a higher volume of diamond than any other pipe in LP (see Chapters Four for more details).



Figure 3.10. Photographs of sampling activity through hammer at Camatxia diamond exploration mine. P-type are inclusions of mantle peridotite



Figure 3.11. Photograph of an inclusion of mantle xenolith (P-type) in kimberlite rock (Camatxia kimberlite).

### 3. 1. 5. Heavy concentrate (kimberlite indicator minerals) from sampled kimberlites

Diverse indicator minerals or megacrysts (Figure 3.12) were collected throughout the sampled pipes. These minerals are frequently associated with diamonds inside kimberlites (Roberts *et al.*, 2015; and Boyd and Gurney, 1986) and they are used as indicator minerals for diamond exploration (Griffin and Ryan, 1995 and Taylor *et al.*, 2000). This project highlighted that these are megacrysts minerals and they are derived at the base of lithospheric mantle or sub-continental lithospheric mantle (SCLM) of Congo craton, with thickness of >250km (Ashchepkov *et al.*, 2012) and consequently they are originated from the earlier formed magma or proto-kimberlite magma (Moore and Belousova, 2005). From an exploration point of view, the most important indicator minerals are chromite, ilmenite, garnet, olivine and Cr-diopside (Gurney *et al.*, 1993). These minerals exhibit indicative visual and compositional characteristics, making them ideal pathfinder for kimberlite, which is the main source of diamonds worldwide (Webb *et al.*, 2004; and Kamenetsky *et al.*, 2006). Garnet, ilmenite and chromite have special qualities for being more chemically resistant minerals due to their greater ability to survive weathering in the surface environment (Nowicki *et al.*, 2007). These minerals are classified as indicator minerals because they form at great pressure and high temperature under the same conditions required for diamond formation (Taylor *et al.*, 2003; and Griffin and Ryan, 1995).



Figure 3.12. Photographs of diamond indicator minerals separated from Camatxia kimberlite rock

In addition, during field work, many kimberlite indicator minerals were observed on the surface. These are assumed to be released by erosion due to washing from river- or rain- water; consequently they were deposited in rivers as part of mixture sediments (Roberts *et al.*, 2015). According to Roberts *et al.* (2015), the Mesozoic kimberlites from NE Angola are normally overlaid by Calonda Formation (CF) (Figure 3.13) sediments measuring 0.3 –2 m thick of matrix-supported gravel with intraformational and extra-basinal clasts in a fine-grained and poorly sorted muddy sandstone matrix, which is characterized by a clastic assemblage which contains pebbles and diamond indicator minerals, which are important for diamond prospecting. The CF therefore plays a key role in the context of this project by collecting the products of surface of fragmented kimberlites including diamond and its indicator minerals (Pereira *et al.*, 2013). During sampling activity, some kimberlite indicator minerals were sampled from the CF. The major implication for this geological formation in Lunda Province, is that it plays a very important role in terms of diamond exploration in Angola, and as an ore, it represents a big exploitable reserve of diamond and also provides important indicator minerals of the kimberlites search and diamonds exploration.

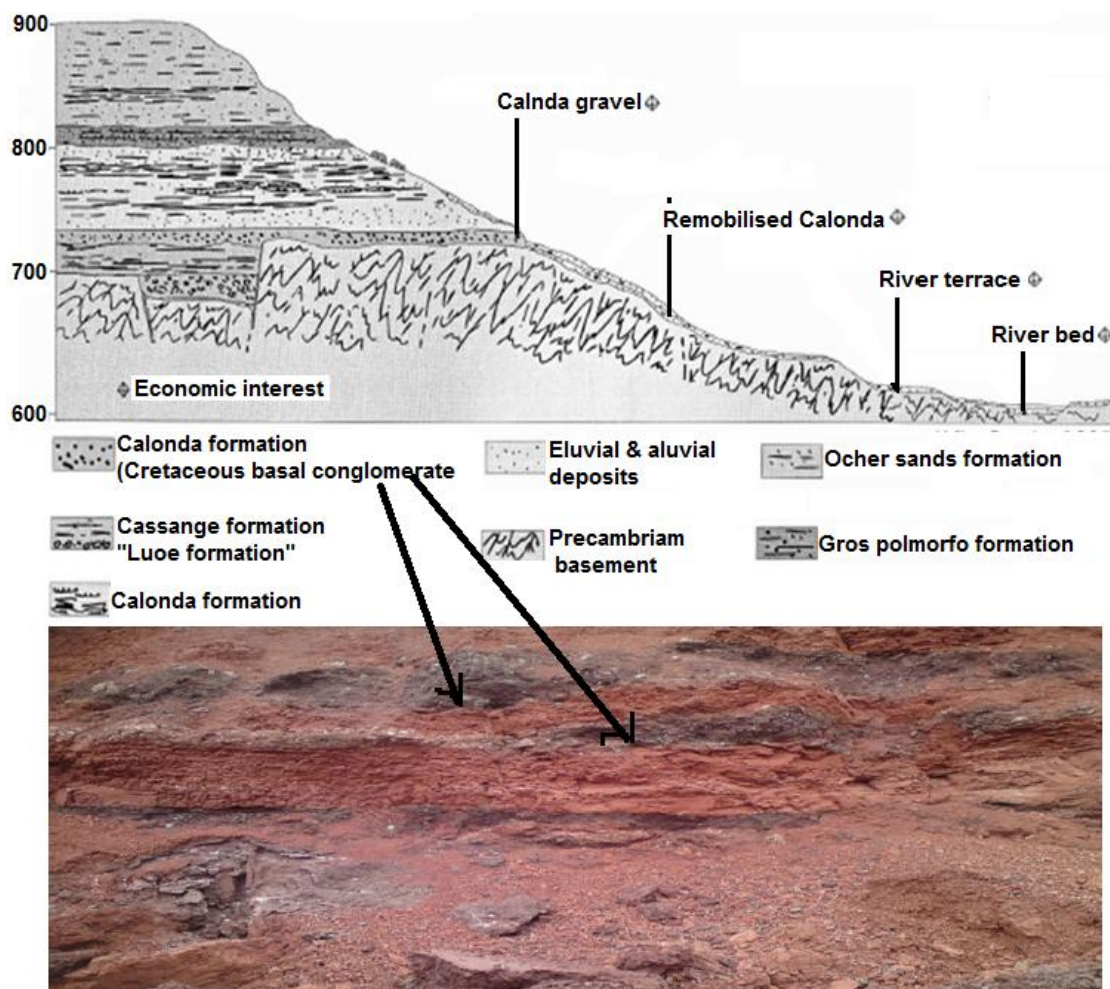


Figure 3.13. Illustration of relationship between the eluvial and alluvial diamondiferous deposits of NE Angola and the post-pliocene morphogenesis (Modified after Pereira *et al.*, 2013).

This shows that alluvial diamonds in NE Angola are located in the Calonda structure (Roberts *et al.*, 2015) which means that these diamonds are originally from magmatic kimberlites pipes, subsequently the diamonds crystals have been eroded from mother rock (kimberlites), and ultimately they are deposited in the rivers. Diamonds from CF have higher quality and are cleaner due to river transportation, than those from kimberlites.

### **3. 2. Experimental procedures, sample collection and preparation overview**

This section provides information on the sample preparation techniques and experimental methods used in this research, including petrographic analysis, Mössbauer spectroscopy, XRD, XRF, and EMPA. Figure 3.14 shows the summary process of sample collection and preparation. For Mössbauer spectroscopy, XRD and XRF, the samples were crushed carefully in a cylindrical rock-crusher, sieved to separate, resulting grains by appropriate size (>1mm and < 1mm). In addition, hand magnet and the Frantz magnetic separator methods were used to separate samples into different fractions to facilitate accurate mineral picking. A hand magnet process was basically applied to remove any strongly magnetic mineral phases present in crushed kimberlite samples, such as magnetite and pyrrhotite (an iron sulfide mineral, FeS) as these minerals could possible damage the Frantz equipment. The Frantz magnetic separator was used to separate weakly magnetic minerals in the crushed kimberlite rock, such as ilmenite, garnet, olivine and chromite by using a slope of 20° and 25° and electrical current settings at 0.4 Amps. Sample contamination, material loss, physical and chemical alteration by moisture or poor storage environment, were avoided during sample preparation as far as possible.

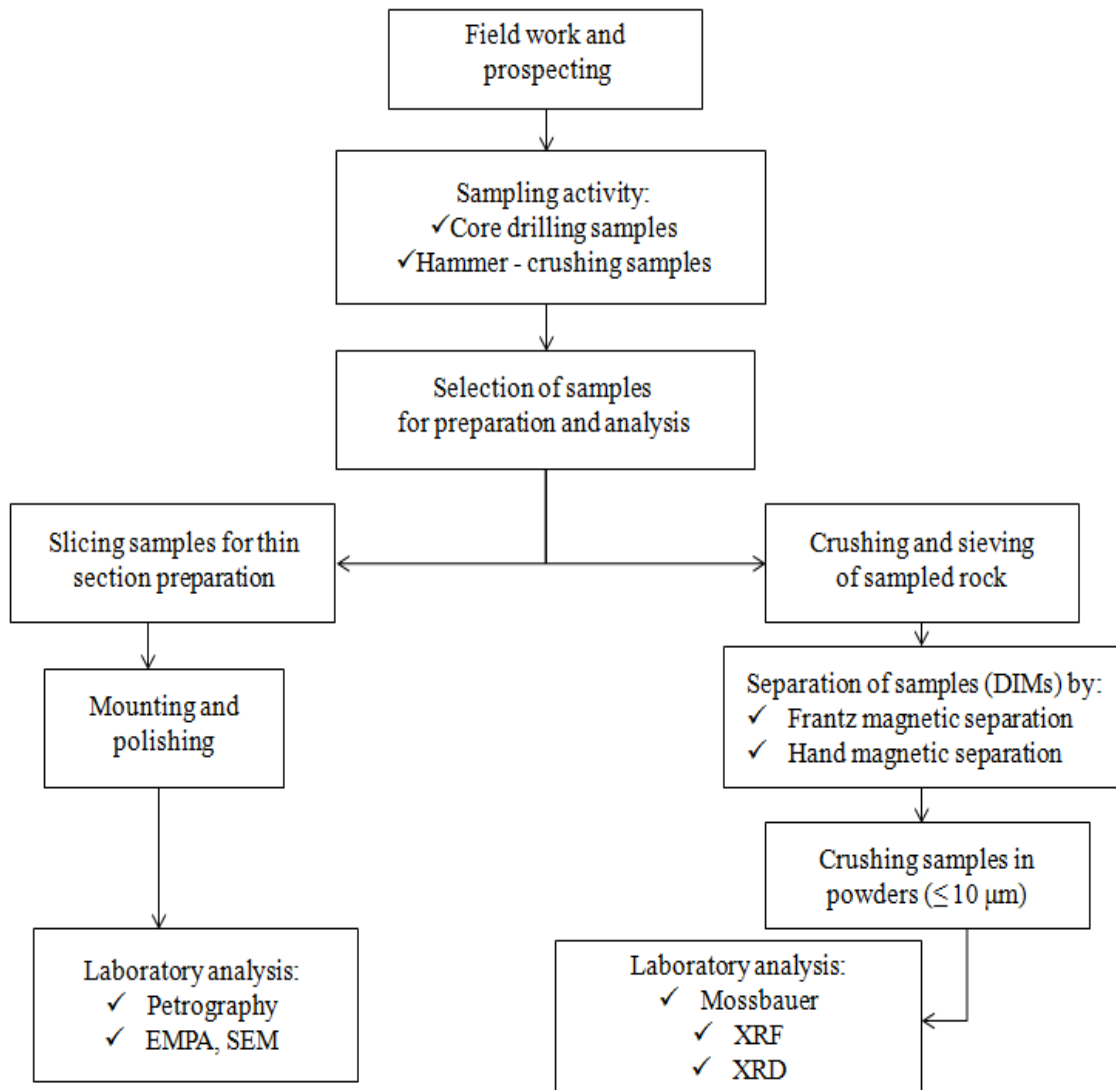


Figure 3.14. Flow-chart showing key aspects of the sample preparation process

### 3. 2. 1. Petrographic analysis

In order to obtain successful petrographic analysis, the impregnation and thin sectioning procedures used to prepare the samples are very important. The samples for this research were prepared carefully using standard procedures. For this study, more than 15 representative thin section samples from the Catoca, Camatxia, Camutue, Caixepa and Camagico kimberlite pipes were prepared using conventional polishing techniques for the preparation of polished/ non-covered thin sections (50mm×28mm, glass slide, 28μm thick) for study using reflected light and transmitted light petrographic microscopy (Figure 3.16), scanning electron microscopy (SEM) and the Electron Micro Probe Analysis (EMPA, see Section 3.5).

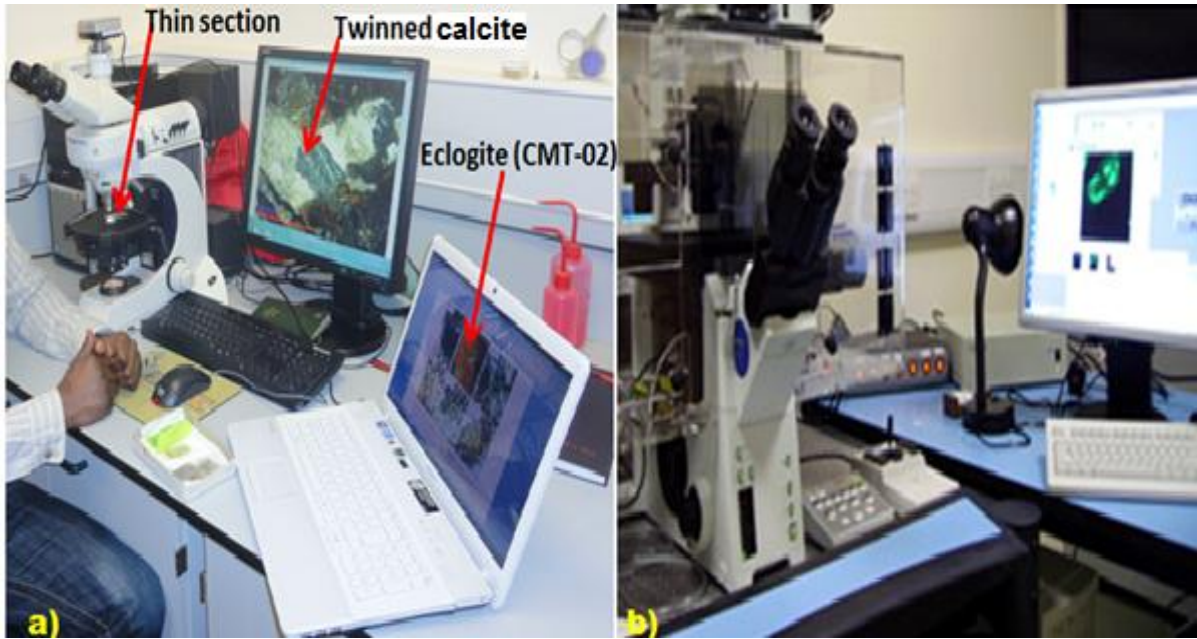


Figure 3.15. Petrographic microscopy equipment: a) Leica TCS SP5 and b) Olympus FV1000.

In addition, mineral identifications were carried out and textures studied using both optical microscopy and a Hitachi S-3600N scanning electron microscope (SEM) with a 15.0 kV accelerating voltage. The modal mineral proportions (Appendix 1) were determined using a combination of mineral identification of point count and image analysis of back-scattered SEM images for representative samples.

**The standard abbreviations used:** *Cpx* → *clinopyroxene*; *Grt* → *garnet*; *Ol* → *olivine*; *Opx* → *orthopyroxene*; *Spl* → *spinel*; *Pht* → *phlogopite*; *Ilm* → *ilmenite*; *Rut* → *rutile*; *Cab* → *carbonate*; *Sep* → *serpentine*; *Hem* → *Hematite*; *Kpht* → *kelyphite*; *Mag* → *Magnetite*

### 3. 2. 2. Mössbauer spectroscopy: theory, sample preparation and analysis methodology

#### 3. 2. 2. 1. Mössbauer spectroscopy - theory and practice

The Mössbauer effect was discovered in 1957 by Dr Rudolf Ludwig Mössbauer, who was a German physicist who studied the Mössbauer effect, or recoilless nuclear resonance (Gütlich 2005). Since then Mössbauer spectroscopy (MS) has been widely used by researchers in geoscientific environments to investigate materials contains the Fe-bearing minerals and compounds (McCammon *et al.*, 1998, 2000; Al-Rawas *et al.*, 2008; Frost *et al.*, 2004; Homonnay, 2004). One of the key reasons making iron (Fe) an important element for geological studies, is that it is the most common element that occurs in multivalent states in terrestrial deposits (Dyar *et al.*, 2006). In addition, Fe occurs in multiple oxidation states in extra-terrestrial mineral environments (Sobolev *et al.*, 1999) and these make iron a common constituent of silicate minerals in both igneous and metamorphic rocks (Ruskov *et al.*, 2010). For the mineralogist and the petrologist, investigation of site occupancies in minerals is of paramount importance. The recoilless  $\gamma$ -ray distribution has a natural line width ( $\Gamma$ ), of the order of  $10^{-8}$  eV, which is small, compared to the  $\gamma$ -ray energy, approximately  $10^4$  eV. The recoilless  $\gamma$ -rays with appropriate energy in Mössbauer spectroscopy assists in detection of minute nuclear energy level differences between nuclei within the source and absorber (Dyar *et al.*, 2006).

#### 3. 1. 2.1. Experimental procedures

As illustrated in Figure 3.16, a radioactive source, absorber (sample), detector and a drive unit which oscillates the source relative to the absorber, are the main components of a standard Mössbauer spectrometer (Dyar *et al.*, 2006). In addition, Figure 3.16 shows the horizontal transmission geometry of a Mössbauer spectrum measurement, as described by Seda (2003).  $N(v)$  is the number of counts which are detected during a certain time interval at a Doppler velocity ( $v$ ) of the Mössbauer spectrum. The  $\gamma$ -ray emitted by the source passes through the absorber, and is detected and displayed as a function of the velocity of the source. The experiment is performed by oscillating the source toward and away from the sample while varying the velocity with constant acceleration. For  $^{57}\text{Fe}$  Mössbauer spectroscopy, if the source velocity increases by 1 mm/s toward the sample, this increases the energy of the emitted photons by  $(14.413 \text{ keV}) \cdot (v/c) = 4.808 \times 10^{-8} \text{ eV}$  (Dyar *et al.*, 2006).

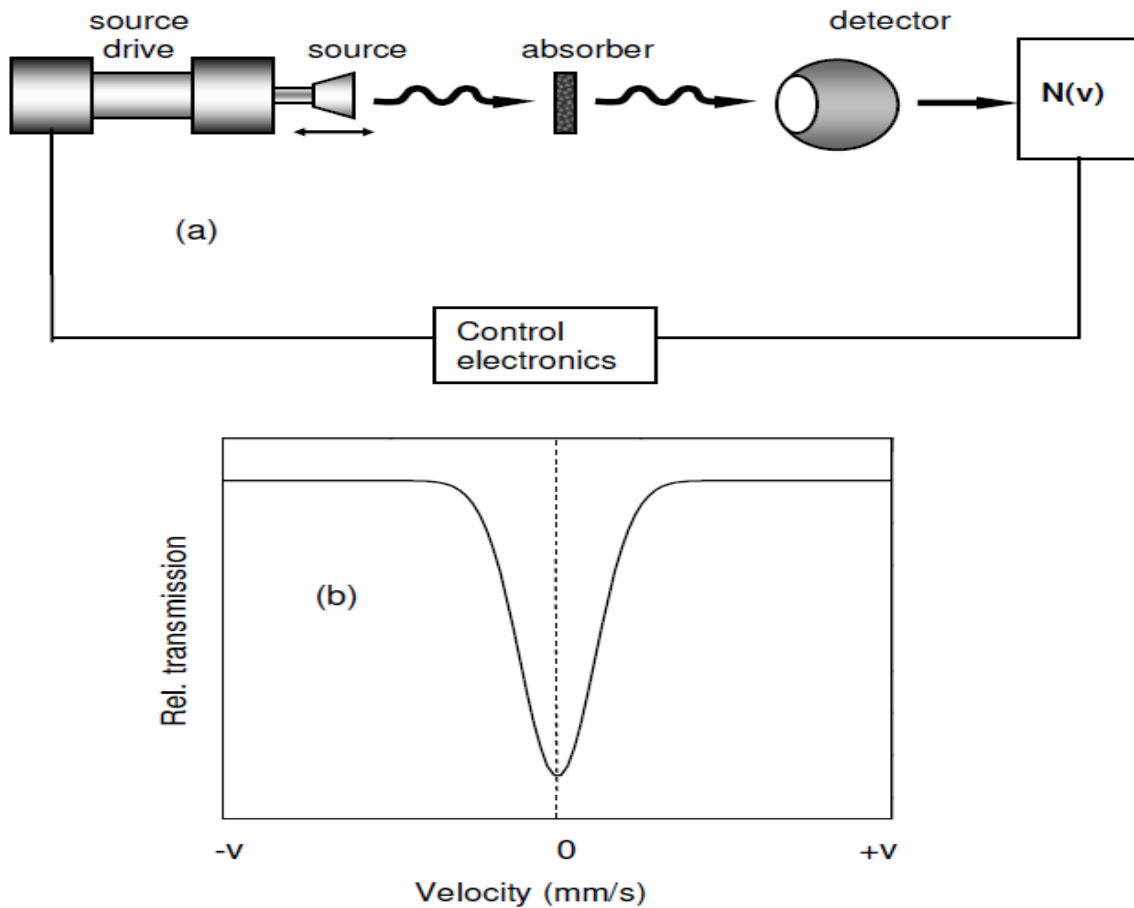


Figure 3.16. Schematic of a Mössbauer spectrometer (b) and an example of the resulting spectrum (Seda, 2003).

Figure 3.16 (b) shows no hyperfine interactions, thus the spectral line is centred at zero energy (velocity) without shift or split. It has been noted by Dyar *et al.* (2006), who investigated several earth and planetary materials, the presence of nuclear charge and its moments such as nuclear monopole interaction, quadrupole moment and magnetic dipole moment, can cause the nucleus to interact with its local environment and consequently these hyperfine interactions result in the splitting of nuclear transitions. The  $\gamma$ -rays are detected by a scintillation counter, gas proportional counter or a semiconductor detector (Duarte and Campbell, 2009). Pulses from the detector are amplified and pass through a discriminator where most of the non-resonant background radiation is rejected (Seda, 2003) and finally are fed into a multi-channel analyser which is synchronised with the oscillator drive unit with (Gütlich, 2005).

### 3. 1. 2. 2. The theory of Mössbauer spectroscopy

The resonant emission and absorption of  $\gamma$ -ray photons by nuclei of atoms is termed as the Mössbauer effect (Gutlich, 2005). The recoilless  $\gamma$ -ray distribution has a natural linewidth ( $\Gamma$ ) of the order of  $10^{-8}$  eV, which is small, compared to the  $\gamma$ -ray energy, approximately  $10^4$  eV. Recoilless  $\gamma$ -rays with appropriate energies in Mössbauer spectroscopy enable detection of minute nuclear energy level differences between nuclei within the source and absorber (Dyar *et al.*, 2006).

### 3. 2. 2. 3. The Mossbauer effect: recoil-free nuclear spectroscopy

Atoms and nuclei have excited states that consist of different electron, proton, and, neutron configurations (Erazo, 1999). These excited states are sometimes accessible from the ground states through the absorption of gamma rays (photons) but it requires highly precise and sharply defined incident gamma ray energy in order to observe resonant absorption of gamma rays by nuclei. For example, a  $^{57}\text{Fe}$  nucleus in its initial excited state can decay by emitting a photon with energy of 14.4 KeV and this photon can be absorbed by another such  $^{57}\text{Fe}$  nucleus (Dyar *et al.*, 2006).

Mössbauer spectroscopy uses solid state absorbers and emitters in gamma ray fluorescence experiments (Gutlich, 2005). The recoil energy from single nuclear decay events in a lattice can be too low to excite phonons, which means that for the purpose of recoiling, the decaying nucleus is effectively tightly bound to all the other nuclei in its crystal lattice. The resonant and recoil-free emission of gamma rays and absorption of gamma radiation by atomic nuclei bound in a solid is known as the Mössbauer effect. According to Dyar *et al.* (2006), who used Mössbauer spectroscopy to investigate solid materials including many minerals, the process in which a nucleus emits or absorbs gamma rays without loss of energy due to nuclear recoil, is described as Mössbauer effect. Resonant gamma ray fluorescence has been described by Maddock (1997) as an important tool in determining a variety of nuclear and solid state properties. The discovery of the Mössbauer effect greatly increased the accuracy and capabilities of gamma ray fluorescence. This in turn has made possible the accurate measurement of nuclear lifetimes, nuclear magnetic moments, and nuclear spins (Forder, 2004).

The Mössbauer effect shows that when atoms are held tightly in solid materials, the gamma radiation emitted by their nuclei is essentially recoil-free. This means that the emitted photon will contain the precise frequency (energy) that corresponds to the transition energy between the nuclear ground state and the excited state (Erazo, 1999). This photon with the nuclear transition energy may interact with another similar nucleus, also tightly fixed in a solid structure, and then absorption can take place. A

photon that carries the exact transition energy may also excite another nucleus. A simple schematic is shown below in Figure 3.17: according to Dyar *et al.* (2006) if the emitting and absorbing nuclei are within identical, cubic environments then the transition energies are identical and consequently will yield an absorption spectrum (Figure 3.16). According to Gutlich (2005), this resonance can take place only if the transition energy ( $E_\gamma = E_a - E_g$ ) is in the range  $5 \text{ keV} \leq E_\gamma \leq 180 \text{ keV}$ . If  $E_\gamma < 5 \text{ keV}$  there is complete non-resonant absorption and if  $E_\gamma \geq 180 \text{ keV}$ , the recoil energy will be too large and will destroy the resonance.

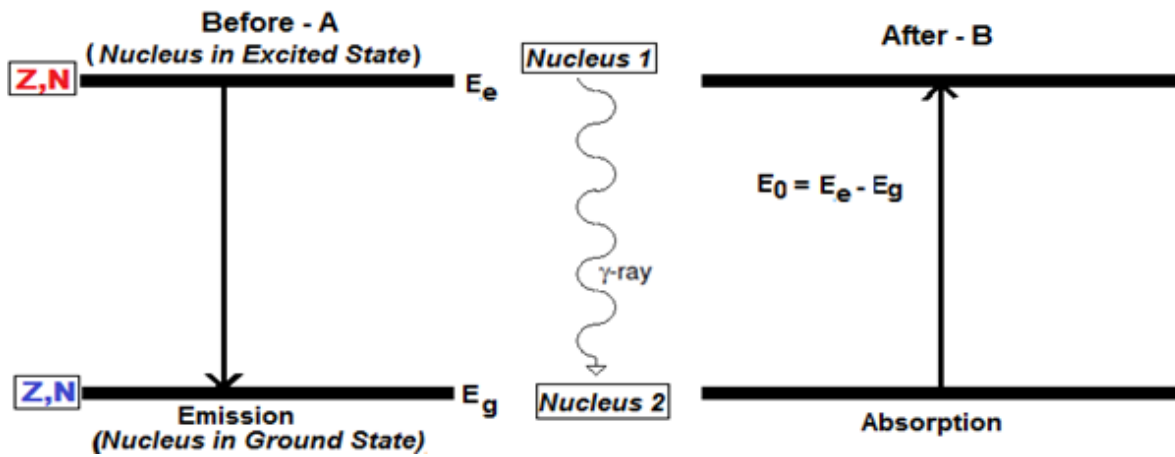


Figure 3.17. Representation of nuclear emission and absorption processes between the excited and ground nuclear states where  $E_\gamma$  is transition gamma ray energy,  $E_e$  is excited state energy and  $E_g$  is ground state energy

In a typical resonance experiment, a gamma ray is emitted by an excited nucleus and then absorbed by a nucleus in the ground state (Maddock 1997) see Figure 3.17. When emitting the gamma ray, recoil energy is lost to the recoiling nucleus but additional recoil energy is required to conserve momentum when exciting the second nucleus (Seda, 2003).  $^{57}\text{Fe}$  Mössbauer spectroscopy has a high resolution of 1 in  $10^{12}$  (Maddock, 1997). This exceptional resolution is necessary to detect the hyperfine interactions in the nucleus (Mössbauer, 2000; and Forder, 2004).

### 3. 2. 2. 4. Hyperfine interactions (HI)

Tiny energy variations (1 in  $10^{12}$  eV or  $1 \times 10^{-12}$  eV, high resolution energy) in the magnetic field at the  $^{57}\text{Fe}$  nucleus, and even distortions or asymmetries in the shape of the lattice that encloses it, can generate shifts and splitting in the absorption line. However, these alterations of the nuclear environment produce observable effects, which are called Nuclear Hyperfine Interactions (see Royal Society of Chemistry, 2016). Hyperfine interactions (Figure 3.18) are one of the aspects that make Mössbauer spectroscopy a useful analytical tool. Due to the very narrowly defined nuclear energy states, the smallest change in the energy of the photon will destroy the resonance. Mössbauer spectroscopy has proven itself as an exceptional technique to measure and detecting nuclear energy different levels (Dyar *et al.*, 2006) and the labelled numbers 1/2 and 3/2 in Figure 3.18 represent the nuclear spin. Figure 3.18 (b) represents the interaction of the nuclear quadrupole moment with the electric field gradient, splitting the nuclear energy levels. For the isotope  $^{57}\text{Fe}$ , the splitting generates individual peaks in the transmission spectrum to split into doublets obtaining a quadrupole splitting. In order for Zeeman splitting to occur, an internal magnetic field should be present at the nucleus (Seda, 2003), which will create a sextet pattern (Figure 3.18 c).

According to Mössbauer (2000), hyperfine interactions represent associations and relations among a nuclear property and appropriate electronic or atomic configurations. Therefore these hyperfine relations are important because they provide important information about electron- and spin-density distributions (Erazo, 1999). The advantage of the Mössbauer method to detect the hyperfine interactions arises from the very narrow line width of the nuclear transitions involved in this effect (Dyar *et al.*, 2006).

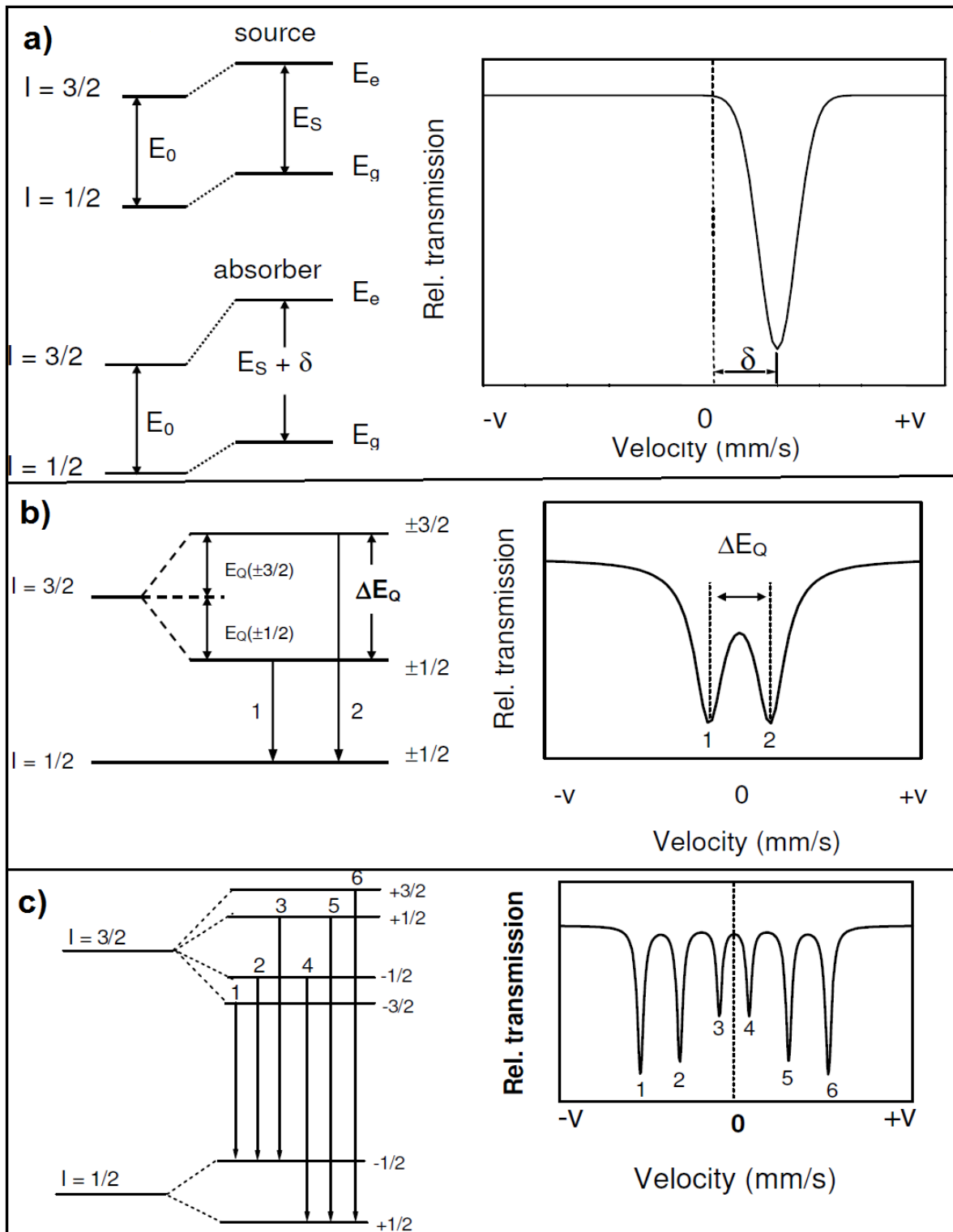


Figure 3.18. Illustration of  $^{57}\text{Fe}$  nuclear energy levels and resulting Mössbauer spectra due to (a) electric monopole interactions; (b), quadrupole interactions in the source and absorber and (c) Zeeman splitting for the excited ( $I = 3/2$ ) and ground ( $I = 1/2$ ) nuclear levels and transitions between these levels. Modified after Seda (2003).

### 3. 2. 2. 5. Key Mössbauer hyperfine parameters

Important hyperfine parameters extracted from  $^{57}\text{Fe}$  Mössbauer spectra are described below (Gütlich, 2005). Isomer shift (IS) occurs due to the electrostatic interaction between the electron charge density at the nucleus and the charge distribution of the nucleus itself over its radius. IS gives information on the oxidation state; spin state and valence state of iron (Forder, 2004) and limited information on coordination number. Ferrous ions ( $\text{Fe}^{2+}$ ) have larger positive isomer shifts than ferric ions ( $\text{Fe}^{3+}$ ). Quadrupole splitting (QS) arises from the interaction between the nuclear electric quadrupole moment and the electric field gradient (EFG) at the nucleus. QS provides information on the coordination, oxidation state, spin state and site symmetry of iron species in the sample. Linewidth (LW) provides information on crystallinity (LW tends to be narrow if the sample is strongly crystallized with single phase whereas wider LW occurs when the sample is partially or fully amorphous, Magnetic field (B). This arises when the nucleus is under a magnetic field. B gives information on the magnetic properties of the material under investigation. B is resultant magnetic field at the Fe nucleus. Mössbauer parameters IS, QS, LW (and B for magnetic phases), can help to identify the valence state and coordination or site occupancy of Fe in a given site and individual mineral, as in Figure 3.19.

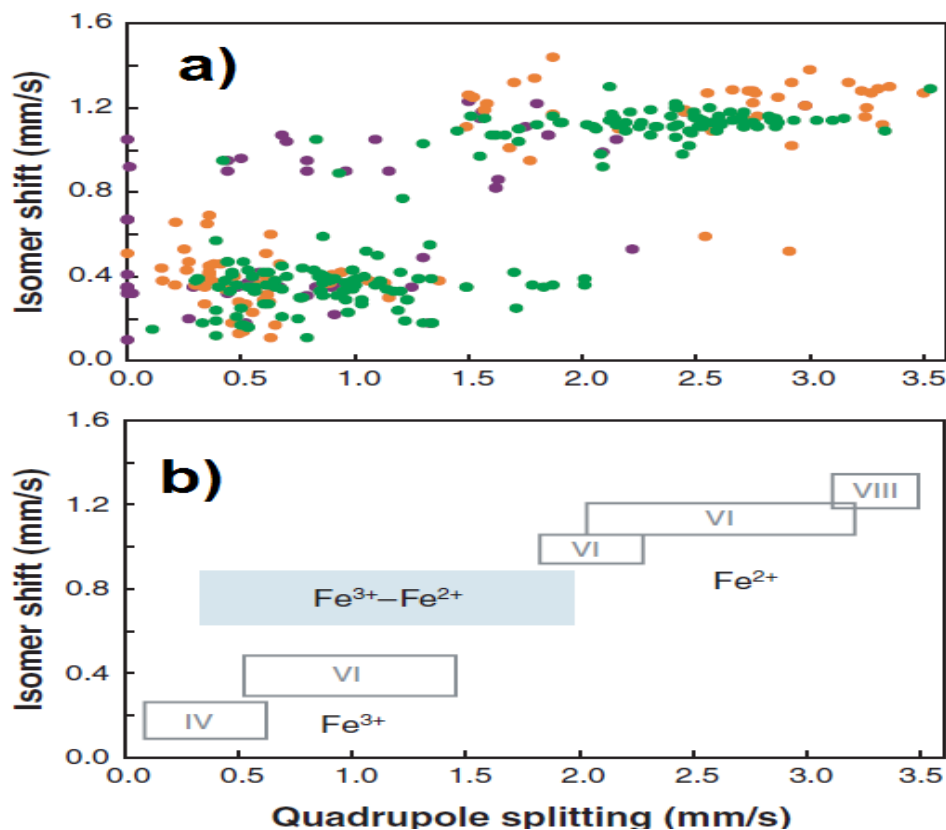


Figure 3.19. Room temperature IS vs. QS for rock-forming minerals. Purple symbols (3.5a) represent oxide phases; orange symbols represent sulphides, sulphates and phosphates; and silicate minerals are green. Figure (3.5b) shows that distinctive IS and QS ranges occur for each valence state and site occupancy of Fe. From Dyar *et al.* (2006).

### 3. 2. 2. 6. The nuclear decay scheme for $^{57}\text{Fe}$ Mössbauer spectroscopy

Radioactive  $^{57}\text{Co}$ , with a half-life of 270 days may be generated in a cyclotron and is diffused into a noble metal such as rhodium (Rh), serves as the gamma radiation source for  $^{57}\text{Fe}$  Mössbauer spectroscopy (Maddock, 1997; Forder, 2004; and Seda, 2003). As seen in Figure 3.20, the decay scheme of the  $^{57}\text{Co}$  radioactive source for  $^{57}\text{Fe}$  Mössbauer spectroscopy is a crucial process in Mössbauer spectroscopy. Forder (2004) explained that a long-lived excited state is needed to have opportunity to record the spectrum.

The  $^{57}\text{Co}$  nucleus in the radioactive source decays by multiple processes to form  $^{57}\text{Fe}$  as the daughter isotope. Electron capture from the K-shell, thereby reducing the proton number from 27 to 26, initially populates the 136 keV nuclear level of  $^{57}\text{Fe}$  with nuclear spin quantum number  $I = -5/2$ . From this  $-5/2$  energy level further decay occurs, by emission of gamma photons: 9% of the decay occurs from the  $-5/2$  nuclear energy level to the ground state ( $-1/2$ ), emitting a 136.3 keV photon. The remaining of 91% of the decay occurs in 2 stages, from the  $-5/2$  nuclear energy level to the  $-3/2$  energy level; and then from the  $-3/2$  state to  $-1/2$  ground state. It is this last decay which emits a 14.4 keV gamma photon (Dyar *et al.*, 2006). This 14.4 keV photon can then be captured by recoilless absorption by the nucleus of  $^{57}\text{Fe}$  in the sample material.

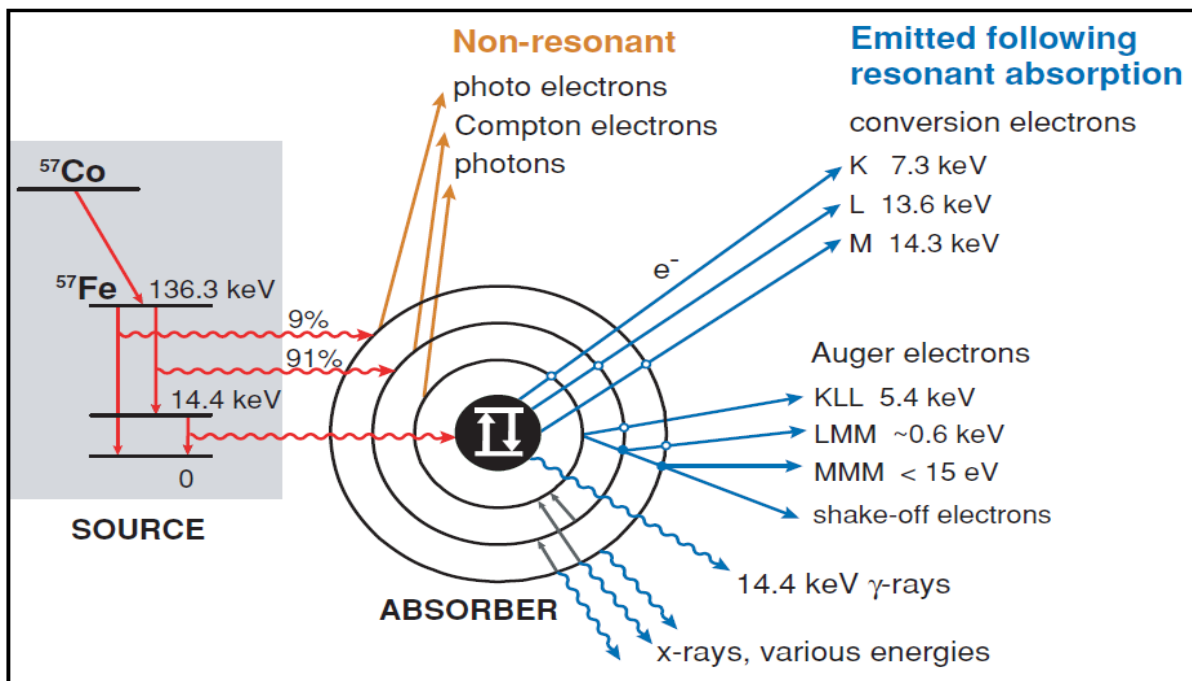


Figure 3.20. Illustration of nuclear decay scheme for  $^{57}\text{Co} \rightarrow ^{57}\text{Fe}$  and various backscattering processes for  $^{57}\text{Fe}$  that can follow resonant absorption of an incident gamma photon with different energy level (Dyar *et al.*, 2006).



Mössbauer spectroscopy provides very precise and accurate results for the oxidation state and the  $\text{Fe}^{3+}/\sum\text{Fe}$  ratio (McCammon *et al.*, 1998; Rollinson *et al.*, 2012; Sobolev *et al.*, 1999). The accuracy of Mössbauer analysis can provide determination of the oxygen fugacity within the mantle (McCammon *et al.*, 1998; Quintiliani, 2005). Note that high oxygen fugacity is a destroyer of diamond (Fedortchouk and Zhang, 2011) within the mantle and during kimberlitic eruption. The oxidation state of iron indicates the amount of oxygen present when a mineral is formed. If the environment was abundant in oxygen, assemblage minerals present will contain more oxidized iron,  $\text{Fe}^{3+}$ , whereas an oxygen-poor environment will produce assemblage mineral containing lower levels of  $\text{Fe}^{3+}$  and more  $\text{Fe}^{2+}$ . Another key aspect of the Mössbauer technique is that if the sample contains low amounts of Fe, this will require long measurement times; therefore this can be seen as one of the disadvantages of Mössbauer spectroscopy.

### 3. 2. 2. 7. Sample preparation and analytical methods

Diamondiferous kimberlite and mantle xenolith samples from 5 kimberlite pipes in Lunda province were studied using Mössbauer spectroscopy. Ilmenite, garnet and pyroxene samples were each separated from the host kimberlite rock, which was obtained from different depths of sampled kimberlite pipes (Table 4.2 in Chapter 4). In each case, this separation was carried out by first crushing representative kimberlite rock samples and sieving to < 1 mm, then using a hand-picking method to achieve very high visual purity, using an optical microscope and tweezers to visually separate the samples from the crushed surrounding rock (see Figure 3.14). This could be done since ilmenite has a distinctive dark brown colour and garnet (e.g. Almandine has a deep red colour, opaque, whereas Pyrope has deep red to black colour, transparent), and pyroxene has (dark green to black in colour, some pyroxene varieties range to light green), in contrast to the grey colour of the other constituents of kimberlite. This separation technique proved highly successful and little contaminant mineral phases were found to be present in the majority of these separated samples (see section 3.2 and Figure 3.21).

Once separation was completed, the separated samples were crushed and approximately 100mg of powdered sample with particle size < 75  $\mu\text{m}$  was mixed with 40-50 mg of graphite powder (see Figure 3.21) in order to fill a Mössbauer absorber disc to obtain a Mössbauer sample. The quantities used in this study were similar to those described by Sobolev *et al.* (1999), who stated that Mössbauer spectroscopy requires relatively large amounts of sample ( $\geq 50$  mg containing 10 wt% FeO). Although electron microprobe analysis (EMPA) has been widely used for chemical analysis (Droop 1987; Palmer 2011; Nowicki *et al.*, 2007, 2008) and for determination of  $\text{Fe}^{3+}/\sum\text{Fe}$  (McCammon and Kopylova, 2004; McCammon *et al.*, 2001), at the present time Mössbauer spectroscopy is the only

reliable method for determining accurate  $\text{Fe}^{3+}/\Sigma\text{Fe}$  ratios (Sobolev *et al.* 1999 and Rollinson *et al.*, 2012) in samples prepared for this project. The ratio  $\text{Fe}^{3+}/\Sigma\text{Fe}$  is important for accurate determination of the oxidation states of iron in indicator minerals, and thereby for estimating oxygen fugacity or partial pressure during indicator mineral formation and transport (McCammon *et al.*, 1998, 2001; and Stagno *et al.*, 2013).

Mössbauer spectra were successfully obtained from powdered homogeneous samples of ilmenite, garnet, magnetite and clinopyroxene. Samples were measured over a velocity range of  $\pm 12 \text{ mm s}^{-1}$  in order to detect any possible presence of hyperfine splitting, which, if present, would be associated with potential contaminant iron oxides minerals such as magnetite or haematite. All samples were measured at room temperature of approximately of 293 K. Calibration was performed using a natural  $\alpha$ -Fe foil, measured over the same velocity range. All centre shift and quadrupole splitting values are reported relative to this standard.

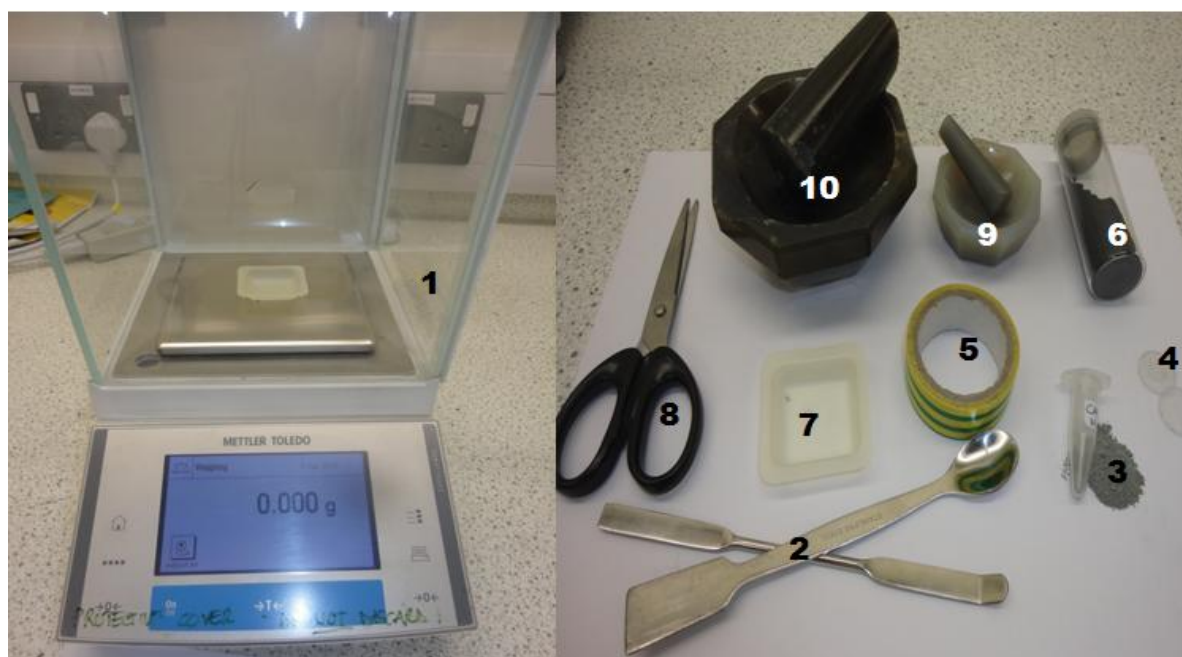


Figure 3.21. Apparatus for Mössbauer sample preparation: scales (1). The finely ground rock powder, (3) mixed in some cases with a small amount of graphite powder (6), mixed in the agate mortar and pestle (9 and 10) and then it is compressed into the disc (4) and sealed with (5) for sealing the disc. The mixture is spatulas (2) into a specific cap of sample weight (7).

Spectra were recorded on a constant acceleration Mössbauer spectrometer (Fig. 3.22) with 512 channels. Folded data were fitted with Lorentzian lineshapes using a least squares procedure with the RECOIL software as used elsewhere (Dyar *et al.*, 2006; and Waerenborgh *et al.*, 2002). All centre shifts are given relative to  $\alpha$ -iron. Uncertainties were calculated using a covariance matrix. Experimental errors were estimated as  $\pm 0.02 \text{ mm s}^{-1}$  for isomer shift and quadrupole splitting.

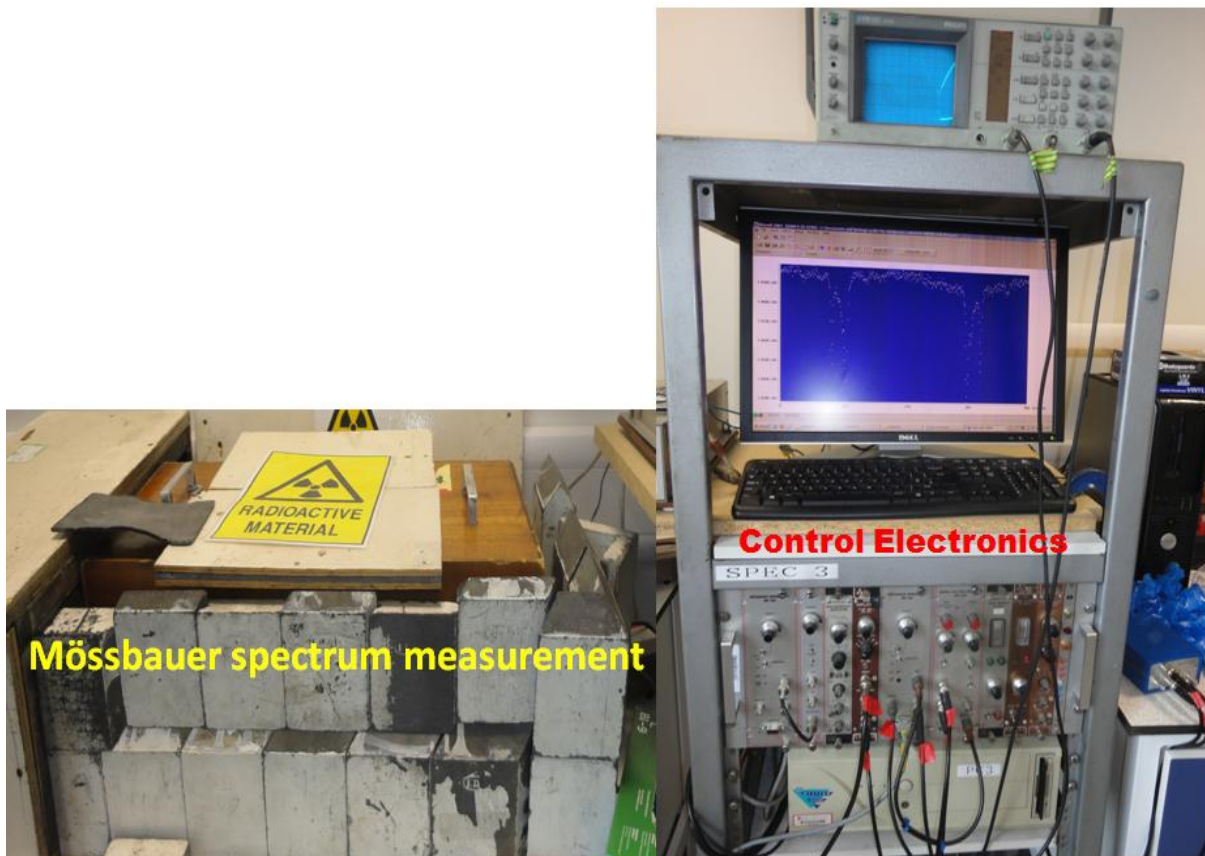


Figure 3.22. Mössbauer spectrometer used in this study

### 3. 2. 2. 8. Some advantages of Mossbauer spectroscopy

Some important advantages from  $^{57}\text{Fe}$  Mössbauer spectra are as follows : apart from the advantage for providing accurate results of oxidation state and  $\text{Fe}^{3+}/\Sigma\text{Fe}$  ratios several (Quintiliani,2005; and Rollinson *et al.*, 2012), Mössbauer researchers (Forder, 2004; Dyar *et al.*, 2006; McCammon *et al.*, 1998; and Maddock, 1997) have described the following advantages for the technique. Its high energy resolution: 1 in  $10^{12}$  eV, can assist us to study in detail the environment of the nucleus, identifying different minerals phases and then calculating the ratios present. The Mössbauer Spectroscopy technique does not affect the sample being studied – non-destructive. The lowest amount of Fe detectable in samples is approximately 10 microgrammes.

### 3. 3. X-ray diffraction, theory, sample preparation and analysis

X-ray powder diffraction (XRD) is an analytical technique used for analysis and phase identification of crystalline phase/s present in a material. Each crystalline solid has its own characteristic X-ray powder diffraction pattern which can be used as a fingerprint for its identification (Moecher, 2004). Determination and characterization of crystalline materials is a critical process in geology and in environmental and materials science studies (Moecher, 2004).

#### 3. 3. 1. Principles of X-ray diffractometry

The principles governing X-ray diffractometry are as follows: when a monochromatic beam of X-rays strikes a finely powdered sample (crystals randomly arranged) and the crystal planes in the powder sample are oriented at the Bragg angle ( $\theta$ ) to the incident beam (Moecher, 2004), diffraction occurs for these crystal planes (Figures 3.23 and 3.24). The X-rays are reflected off a plane with the angle of incidence ( $\theta$ ), which is equal the angle at which the X-rays are diffracted. The angle of diffraction is the sum of these two angles,  $2\theta$ . Diffraction occurs only when Bragg's Law (Equation 1) is satisfied condition for constructive interference (X-rays) from planes with spacing ( $d$ ).

$$2d \sin \theta = n \lambda \quad \text{Equation 1}$$

Where:

$d$  → is the spacing between layers and atoms (m).

$\theta$  → is the angle between the incident rays and the surface of the crystal.

$\lambda$  → is the wavelength of the X-rays.

$n$  → positive integer (whole number, example 1,2, 3).

The X-ray source, sample, and X-ray detector are the three key basic elements for XRD. The X-rays are generated in a cathode ray tube by heating a filament to produce electrons (Fewster, 2014; Swanson and Tatge, 1951). A detector to pick up the diffracted X-rays signal and converts the signal to a count rate which is then output to a device such as a printer or computer.

Another key aspect from Figure 3.23 is that, in order the diffraction pattern to occur, the Extra-distance (DE) in Figure 3.23 must be equal on integral number ( $n$ ) of the wavelength of the X-rays.

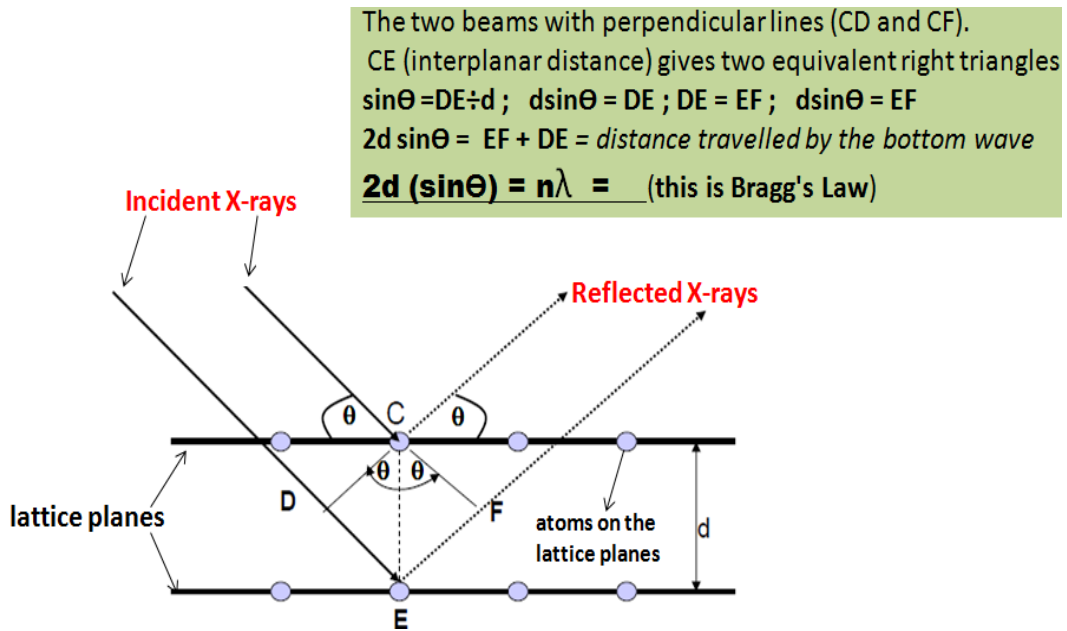


Figure 3.23. Illustration of parallel X-ray beams travelling over different distances (Adapted from Bragg diffraction.svg, 2015)

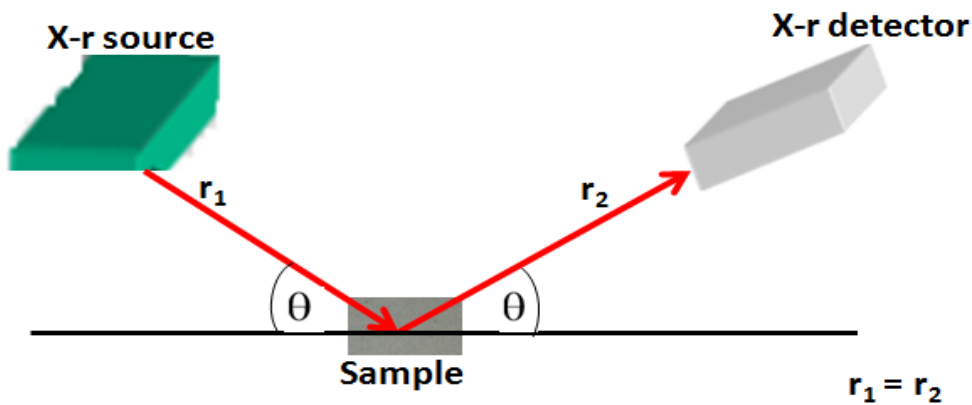


Figure 3.24. Schematic of an X-ray powder diffractometer

XRD was deployed in this project to identify different phases of crystalline material or minerals present in kimberlite and mantle xenolith rock samples. Samples were carefully crushed in a cylindrical rock-crusher and then placed in mill and milled, resulting in powdered sample. X-ray diffraction measurements were carried out using Cu-K $\alpha$  as a source on a Panalytical Empyrian instrument equipped with a sample spinner (Figure 3.25). Powder specimens were step-scanned in the ranging 10– 60  $^{\circ}2\theta$  Peak positions were determined and phase analysis was carried out using the Panalytical High Score Plus program.



Figure 3.25. X-ray diffractometer used in this study

For XRD measurements the sample should be, in theory, infinitely thick but depending on the energy of the X-ray line and the matrix of the samples, a 2 to 3 mm thickness is sufficient for operation. Samples were ground very finely using a mortar and pestle (Figure 3.21) achieving an average particle size of  $5\mu\text{m}$  with a maximum grain size of  $25\mu\text{m}$ . The accurate identification of mineral phases present in the samples was based on the mineral powder diffraction file (Pax and Stewart, 2012).

### 3. 4. X-ray fluorescence (XRF) spectrometry

As illustrated in Figure 3.26 the X-ray source, absorber (sample), and a detector are the main components of a XRF spectrometer. X-ray fluorescence enables petrologists and geochemists to obtain rock major component analyses (Si, Ti, Al, Fe, Mn, Mg, Ca, Na, K, P) and minor analyses (Sr, Ba, Sc, Y, Ce, Zr, V, Cr, Co, Cr, Cu, Ga, La, Nb, Ni, Rb, U, V, Y, Zr, Zn) for rock forming minerals (Ringwood *et al.*, 1992). Identification of elements in rocks by XRF is possible due to the characteristic radiation emitted from the inner electronic shells of the atoms under certain conditions. XRF works when an X-ray beam with energy around 20 keV, is directed at lattice planes, the beam hits the atoms and generating characteristic X-rays which is caused by the ejection of an electron from an inner shell of an atom hit by the incident x-ray and consequently an outer shell electron moves to fill the space created in the inner shell, energy in the form of an x-ray photon is emitted (Figure 3.28).

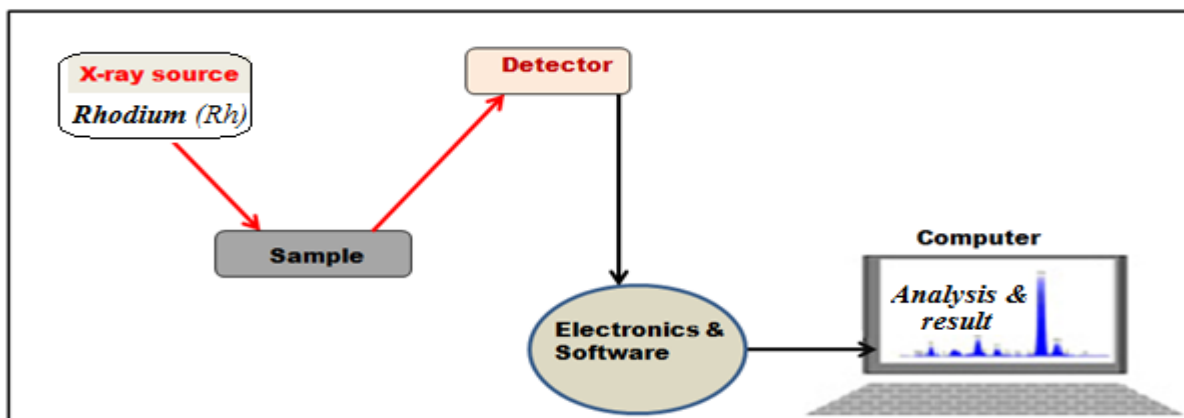


Figure 3.26. Schematic diagram of XRF instrumentation (MagiXPRO), used in this study

1. **X-ray source (Rh)**. In order to excite the atoms, primary radiation (a source of radiation) is required with sufficient energy to eject tightly held inner electrons.
2. **Detectors**, for example, a) Gas Flow Proportional b) Scintillation counters. These are used to meet the wavelength dispersive spectrometry need to have high pulse processing speeds in order to cope with the very high photon count rates that can be obtained (measuring the energy of the photons).
3. **The Analysis software** (e.g. Uniquant program) converts spectral data to direct readout of results.



Figure 3.27. XRF (MagiXPRO) analytical instrument used in this study.

The chemical compositions of rocks are crucial and are used to study several geological problems, in the context of this project these including crystallization history of kimberlites bodies or volcanic rocks, processes of formation of the sea floor, (La Tour, 1989), chemical weathering in various materials, processes of ore formation, and stratigraphic correlation of sedimentary rocks.

XRF works on wavelength-dispersive spectroscopic principles that are similar to an electron microprobe (EMPA) but the difference is that XRF is not able make analyses at the small spot sizes as EMPA (2-5  $\mu\text{m}$ ). Consequently XRF provides information on larger fractions of geological materials in order to obtain analysis. The use of sample excitation by electrons is also used in electron probe micro-analysis (EPMA). According to Brouwe (2006), XRF is based on principle that individual atoms, when excited by an external energy source, emit X-ray photons of a characteristic energy or wavelength, by counting the number of photons of each energy emitted from a sample, the elements present may be identified and quantified (Haschke, 2014). In geological rocks / materials, the analysis of major and trace elements by XRF is made possible by the behaviour of atoms when they interact with X-radiation. In order for the XRF spectrometer to work, the sample should be illuminated by an electron beam or an intense X-ray beam, and consequently some of the energy is scattered, but some is also absorbed within the sample but depends on its chemistry. The incident X-ray beam is generated from a rhodium (Rh) target (Palmer, 2011) while others elements such as Tungsten (W), Molybdenum (Mo) and Chromium (Cr) can be used (La Tour, 1989) depending on the choice of application. Electrons in the sample becomes excited when illuminated by an X-ray beam (La Tour, 1989).The excited electrons return to their ground state, emitting X-rays along a spectrum of wavelengths characteristic of each chemical element present in the sample. Normally this process take place when the materials are excited with high-energy, short wavelength radiation (e.g. X-rays), they can become ionized and if the energy of the radiation is sufficient to dislodge a tightly-held inner electron (Figure 3.11), the atom becomes unstable and an outer electron replaces the missing inner electron.

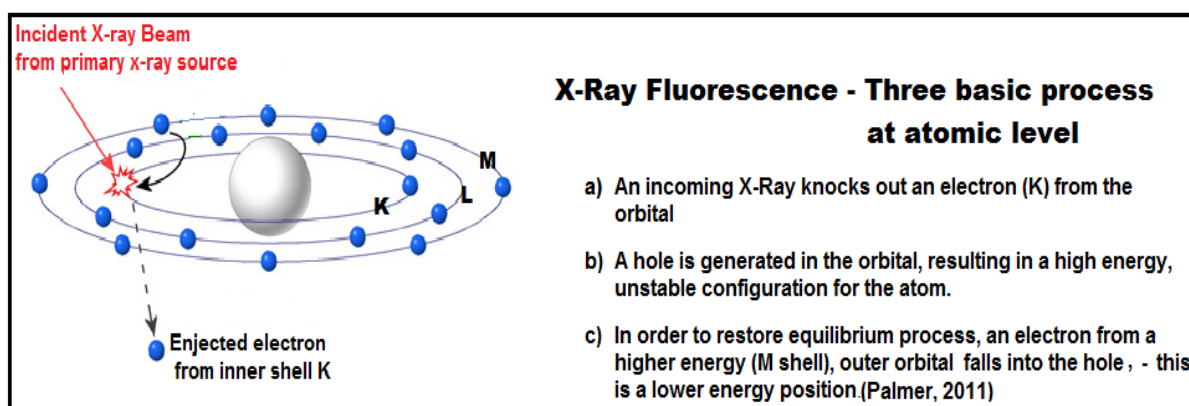


Figure 3.28. Schematic representation of X-ray fluorescence using a generic atom and generic energy levels. Illustration process of moving electrons to shells and the replacement process, (Horiba, 2016)

Energy Dispersive XRF (ED-XRF) and Wavelength Dispersive XRF (WD-XRF) are the two main types of XRF spectroscopy, which differ in the way the fluorescent X-Rays are detected and analysed (Palmer, 2011). Normally an energy dispersive (ED) spectrometer measures the energies of the emitted X-rays from the sample, by counting and plotting the relative numbers of X-rays at each energy, consequently an XRF spectrum is created. Wavelength dispersive (WD) spectroscopy measures X-ray intensity as a function of wavelength and separates the X-rays or each peak according to their wavelengths (Khan, 2011). The measured spectrum shows lines or peaks (Figure 3.29) that are characteristic of the chemical elements in the sample. Wavelength dispersive XRF is the more expensive process (La Tour, 1989), but it is crucial for quantitative rock analyses. Quantitative analysis involves determining the amount of each atom present in the specimen from the intensity of measured characteristic X-ray lines. Peaks in the XRF spectrum can arise from target element in X-ray tube (Palmer, 2011). The major difference between ED-XRF and WD-XRF techniques lies in the achievable energy (spectral) resolution. For example, WD-XRF systems can provide working resolutions between 5 eV and 20 eV, depending on their set up, whereas ED-XRF systems provide high resolutions ranging from 150 eV to 300 eV or more, depending on the type of detector used. The higher resolution from WD-XRF provides advantages in reduced spectral overlaps, so that complex samples can be accurately characterized.

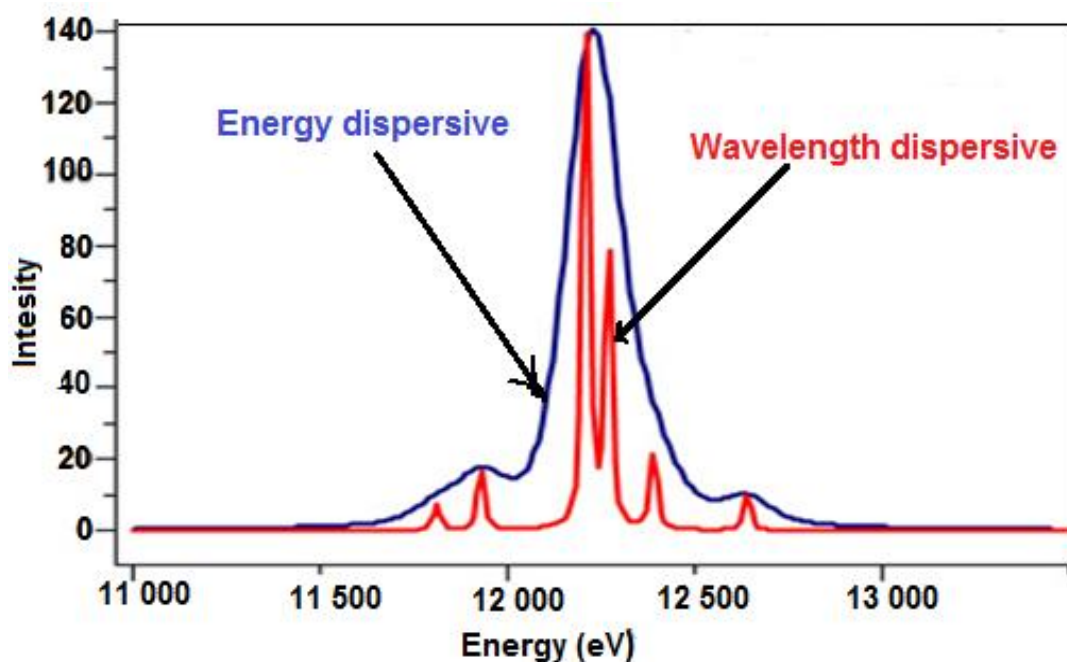


Figure 3.29. Illustration of wavelength dispersive (WD) in red and energy dispersive (ED). X-ray spectroscopy

A key aspect of WD-XRF in geochemical analysis is that if a sample contains many elements, WD-XRF, similarly to EPMA, allows the separation of a complex emitted X-ray spectrum into characteristic wavelengths for each element present (La Tour, 1989).

### 3. 4. 1. XRF, sample preparation for major and minor elements analysis

The apparatus for XRF sample preparations used in this project was similar to that described by La Tour (1989). In this particular sample preparation involves two different approaches

#### a) Approach . 1- Sample is conserved

In this method, the ground or powdered sample had no surface irregularities and was composed of sufficiently small particles for accurate measurement (Brouwer, 2010). Homogeneous powder (Figure 3.30) is placed in a pellet press and after pressing it becomes compacted, and is then placed into the XRF machine for analysis using the Semi-Quantitative Analysis (SQA) program Uniquant (software). The key advantage of this program is that it is capable of analysing a wide range of elements present in periodic table (from Sodium to Uranium). For instance, the Nickel (Ni) compound only is analysed by the SQA than QA. The drawback of the SQ analysis programme is that it is less accurate than the quantitative analysis Oxide program using the fused bead method of sample preparation.



Figure 3.30. Apparatus for preparation of pressed powder pellets for XRF: (a). Rock powder and binder were mixed using the agate mortar and pestle and then the powder sample was compressed into the die (c). The die consists of a cylindrical and base, two polished steel pellets and a plunger.

## **b) Approach - 2. Sample destroyed**

The advantage of the quantitative Oxide program with the fused bead sample preparation method is that by preparing fused beads the particle size and mineralogical effects are eliminated by making a homogeneous sample. It permits the use of synthetic standards as mean of calibration (Giles *et al.*, 1995). During this process, 1g of ground sample was mixed with 10 g of lithium tetraborate and heated in a furnace to 1180°C, (Figure 4.27 in section 4.5) to dissolve the sample and transform into a fluid melt then cooling to a rigid sample disc and placing in the XRF spectrometer (Panalytical Magix-Pro) for analysis. Lithium tetraborate is used for fused bead manufacture as it does not absorb X-rays at energies overlapping those of elements heavier than fluorine, e.g. can be considered X-ray transparent for the purposes of XRF analysis. This analysis programme produces quantitative analysis results for 18 major elements (see section 4.5) and its result is more accurate than those from SQA.

## **3. 5. Electron Probe Microanalysis (EMPA)**

An electron probe micro-analyser (EMPA) (Sobolev *et al.*, 1999) is a micro-beam instrument used primarily for the chemical analysis of very small solid samples and for mapping and imaging compositional differences (Keulen *et al.*, 2009). A finely focused (approx. 1µm) beam of electrons is directed onto a flat polished thin section specimen (Figure 3.31), however, the interaction volume of analysed sample is greater because the electron interaction volume in a specimen increases with the incident beam energy (Chatterjee, 2012) which means that high energy greater interaction volume. The interaction volume can vary according to the characteristic or type of samples under investigation. For example, X-ray beam pass through when the analysed material/samples are light, therefore the interaction volume increase, whereas if the samples are denser or heavy opaque materials, the interaction volume is reduced, because the X-ray beam will not pass through in the sample, more electrons. The high energy electrons ionize the inner shells of the target elements in the sample. The working principle of EMPA is based on wavelength-dispersive X-ray spectroscopy (Chatterjee, 2012), similar to WD-XRF (Czyzycki *et al.*, 2009; and Brouwer, 2010). EMPA uses Bragg's law (Moecher, 2004) to determine the energy spectrum of X-rays permitting identification of the wavelengths unique to every element and identifying which elements comprise a specific analysed sample. EMPA data are usually calibrated using well-established standards (Palmer, 2011) for each element, and can be highly accurate and precise. EMPA (Figure 3.32) therefore provides quantitative information about the chemical composition of a sample (Keulen *et al.*, 2009) which is used in understanding processes and chemical composition of the mantle lithosphere (McCammon, 2005).

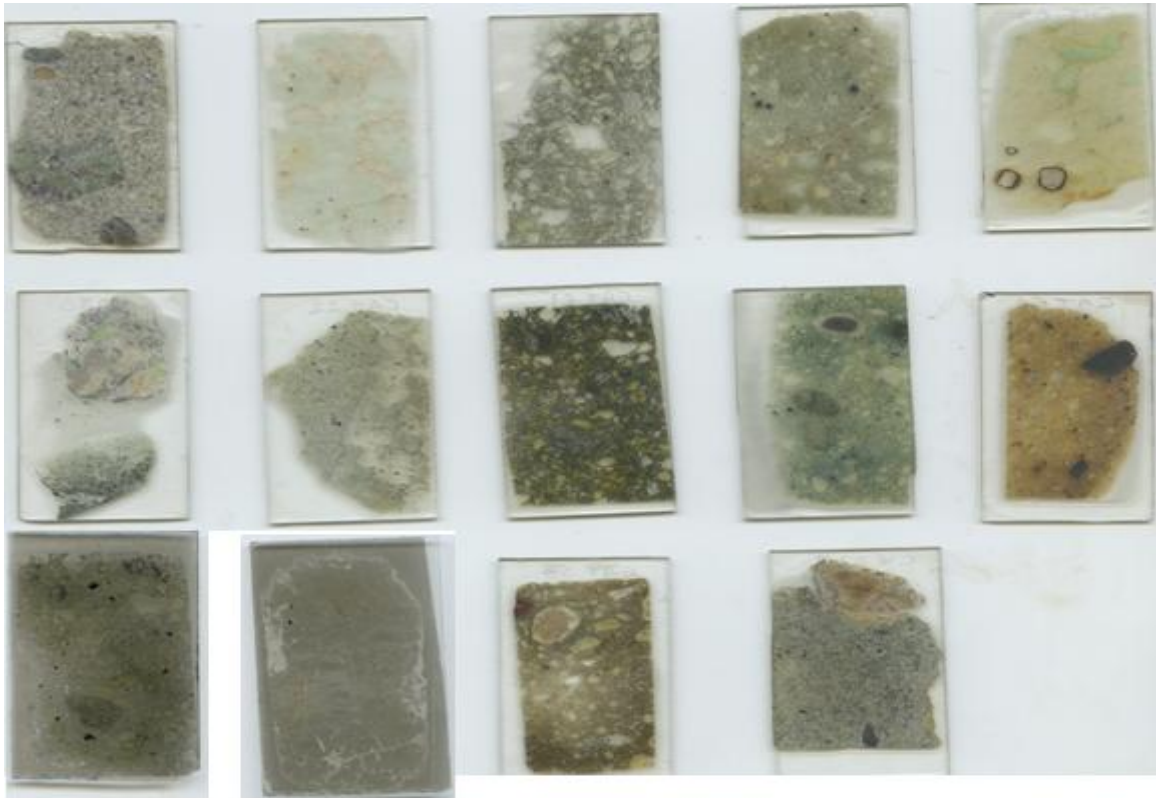


Figure 3.31. Polished thin sections 28  $\mu\text{m}$  thick on glass slides (50mm $\times$ 28mm) for used for EMPA, SEM, reflected light and transmitted light microscopy.

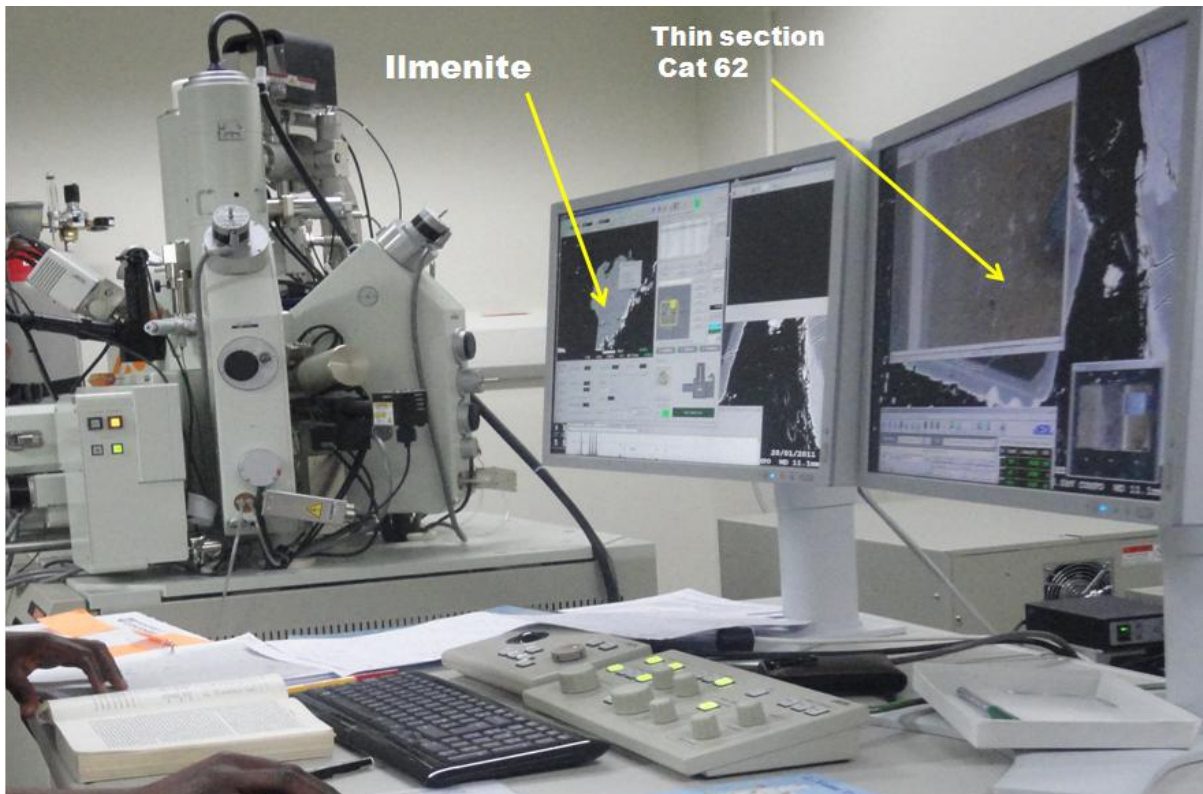


Figure 3.32. JEOL JXA-8230 electron microprobe analysis (EMPA) instrument used in this study.

EMPA analysis, shown in Chapter 4, was carried out at University of Leeds. The JEOL JXA8230 EMPA instrument is equipped with a tungsten source and 5 wavelength dispersive spectrometers. The combination of up to 5 wavelength dispersive X-ray spectrometers (WDS) and dispersive X-ray spectrometer (EDS) combined Electron Probe Micro analysis (EMPA) with a new PC-based operating environment for easy data acquisition and analysis featuring spectral imaging provide the most efficient and accurate analysis of data (Palmer, 2011). The analysis was conducted using Probe for Windows software produced and marketed by Probe Software Inc. EMPA is crucial due to its ability to acquire precise, quantitative elemental analyses at very small "spot" sizes approximately 1  $\mu\text{m}$ , by wavelength-dispersive spectroscopy (Chatterjee, 2012). The JXA-8530F operates on PC Windows for data acquisition and analysis. The PC-based operation facilitates rapid and easy analyses at high magnification (up to 40,000x) and identifies the features of interest, and then analyse the composition of those features. The technique will also identify trace elements or bulk contaminants.

## Chapter Four . Results

The results presented in this section detail the study of selected diamond indicator minerals, their oxidation states, crystalline phases, petrography, viscosity modelling and how they are related with oxygen fugacity in the Lunda lithospheric mantle.

### 4. 1. Petrographic analysis

The following section demonstrates the result of the investigation of the thin sections taken from samples detailed in the Appendixes 1, 2 and 5. The analysis was carried out through petrography using optical microscopy. A better understanding of the nature of the Lunda province lithosphere is based on the analysis of both mantle xenoliths and kimberlite rocks. Note that the results are presented according to their analysis techniques and their mantle origin as follows: such as, and. In this way, results for each experimental technique have been ordered as follows:

1. **Eclogite and peridotite (harzburgite or lherzolites) mantle xenoliths;** these are primary mantle rocks (e.g. samples Cat 18; CMT – 05; CAT – 22; CMT – 01; CMT – 02; CM 003; CMG 002. Mantle Xenoliths samples are important as they provide a wide key data/information regarding the mantle conditions and the genesis of diamond.
2. **Megacrysts or rocks formed by metasomatism in mantle related to the primitive or protokimberlite magma** (e.g. ilmenite and garnet minerals analysed in the Mossbauer spectroscopic and EMPA techniques). In addition, some megacrysts from the kimberlites rock samples were observed and analysed (e.g. Samples: CAT- 61; CAT 59; CM-CW 045 (7) and CAT 58. This project made the important observation that these megacrysts are formed from an earlier formed magma or proto-kimberlite magma or the ascent of primitive/precursor kimberlite magma (proto-kimberlite) that crystallised in pegmatitic veins structure, dykes, in the magma conduit or networks, probably at the based of the lithospheric mantle depths > 250km (Ashchepkov *et al*, Mahotkin *et al*, 2000; 2012 Shirey, and Shigley, 2013 and ) and subsequently transported them to the Earth surface (see section 4.2 for more details). The genesis of pro-tokimberlites megacrysts have been studied by Shchukina *et al*, (2006); Giuliani *et al*, (2013); Moore and Belousova, (2005), Wyatt, (1979); Kornprobst, (1984); Moore and Lock, (2001) ; Mitchell, (1973; 1977) and Agee *et al*, (1982)
3. **Kimberlites magma/rocks, groundmass, xenocryst and evidence of fluid rections.**  
(e.g. carbonate groundmass, veins and fluid reactions from samples CAT 59; CAT 58 ; CM-CW 045 (7); CAT- 61) as well as from EMPA results in Figures 4.26.4.27 and 4.28

Note that for some techniques (XRF, XRD and viscosity modelling) samples did not arise for all categories (1, 2 and 3 above). This has been noted in the appropriate sections.

#### 4. 1. 1. CAT-18 from Catoca kimberlite pipe.

This sample represents the primary mantle rock (eclogite mantle xenoliths) in the Lunda lithosphere province. Several diamond researchers (Shirey and Shigley, 2013; Dobosi and Kurat, 2009; Stachel *et al*, 2009; Maruoka *et al*, 2004; Stachel and Harris, 2008; Stachel, 2003; Stachel *et al* 2003; 2005 and Job, 2004) have concluded that the origin of the vast majority of the mantle of eclogites are from the subducted oceanic crust beneath the major cratons of the world (Taylor *et al*, 2003 and Taylor *et al*, 2000, see Figures 2.10 and Figure, 2.17).

As shown in Figure 4.1, based on the petrographic investigations, the sample Cat-18 was classified as a bimineralic eclogite (e.g. the rock is composed mainly of garnet (Grt) and clinopyroxene (Cpx) and with minor oxide mineral such as rutile (Rut)). The bimineralic mantle eclogites as been also studied by Jacob, 2004). During the petrographic analysis process for this study, it was observed that the xenocryst minerals (Grt, Cpx and Rut) present in this rock sample are supported by a groundmass of fine-grained carbonate and serpentine materials which are products of kimberlite magma. Most grains of garnets and clinopyroxenes exhibit irregular fractures, as shown for example in Figure 4.1 for samples Cat18-a and 18-c. Some fractures in the garnet (sample, Cat18-d) contain reddish reaction rims filled between gaps with kelyphite, this is an indication of metasomatic fluid. Texturally this appears to represent a replacement of garnet; it may also represent a kimberlite magma process. Also the kelyphite texture is found in spinel /ilmenite (sample Cat18-a). Despite exhibiting a well-developed cleavage, the clinopyroxene in sample Cat18-e also exhibits mechanical (probably shear) deformation, which may be due to kimberlite emplacement or high shear forces within the mantle. Also sample Cat18-b shows two different stages of pyroxene formation (growth phenomena). The presence of spinel in sample Cat-18a and rutile in sample Cat18-e as host minerals or earlier-formed minerals has led to the interpretation that these were incorporated within the late Cpx- poikilitic texture. There is a reaction rim / metasomatic event, between host Cpx and and guest spinel (sample Cat18-a). A serpentinisation process is also present in this rock. The petrographic evidence supports the interpretation that the studied mantle lithospheric rocks experienced metasomatic events and oxidation, probably within the mantle, before, during or after kimberlite emplacement, but this is difficult to determine precisely, due to the complex process of kimberlite emplacement (Heaman *et al.*, 2003; and Field *et al.*, 2008). According to Stachel *et al.* (2003, 2005), mantle xenolith rocks are transported by kimberlite magma and these rocks constrain the formation depths of these magmas to the deep or the base of the cratonic mantle lithosphere (Griffin and Ryan 1995; Robinson *et al.*, 1989). Mechanical disaggregations of xenoliths yields a suite of xenocrysts which are characteristic of most kimberlites (Russell *et al.*, 2012).

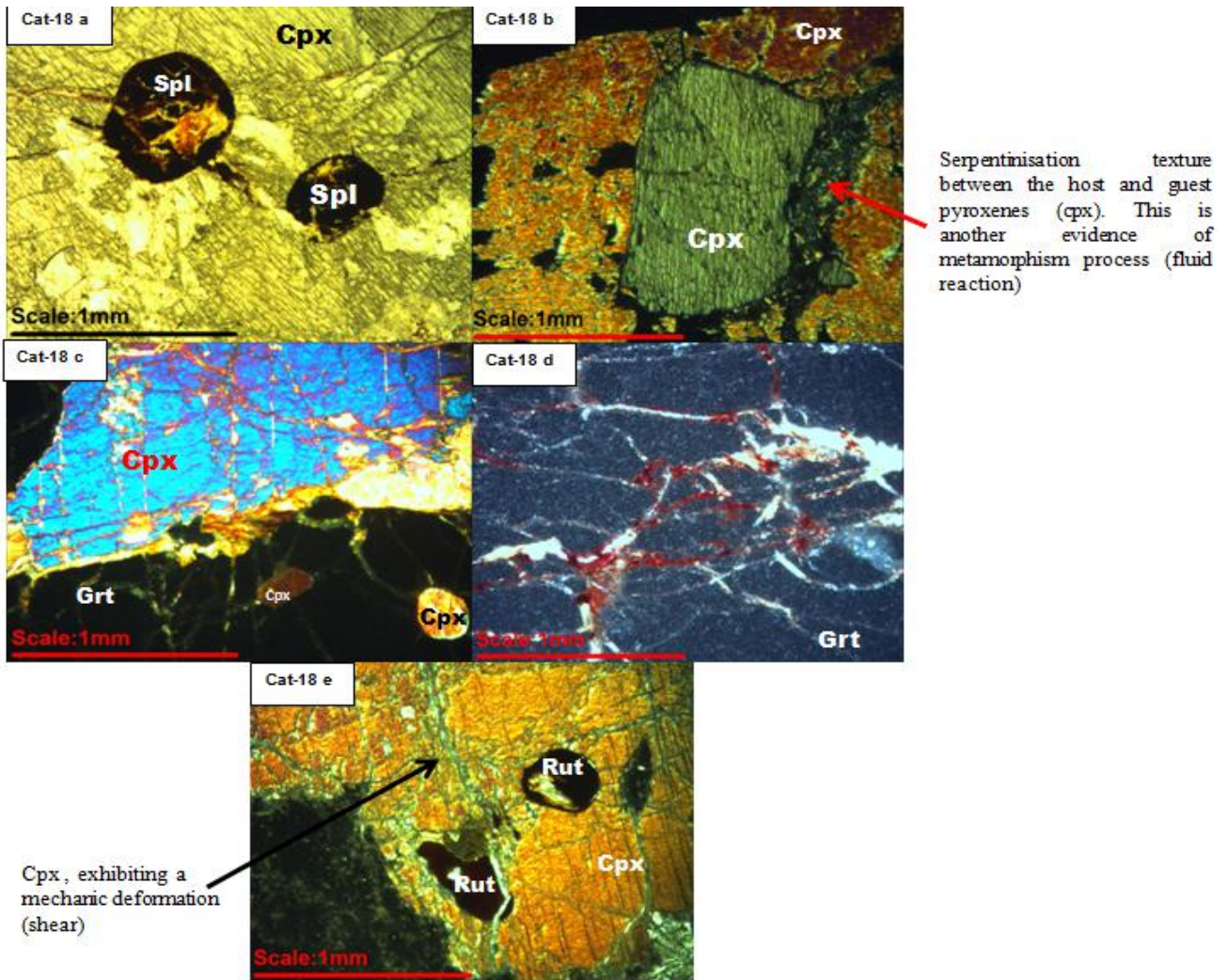


Figure 4.1. Transmitted-light optical microscopy images of thin sections of E-type rock mantle xenoliths with mineral assemblages from Catoca kimberlite sample Cat-18. Indicator row 1 shows serpentinisation texture between the host and guest clinopyroxenes (Cpx) and Indicator row 2 shows Cpx, exhibiting mechanical deformation (shear).

#### 4. 1. 2. CAT - 22 Mantle xenoliths (eclogite) included in the kimberlite rock

The most dominant minerals in this rock (Figure 4.2) are garnet, and pyroxene (clinopyroxene). Also minor oxide minerals (ilmenite  $\leq 1$  vol. %) were found (sample CAT-22b, see Appendix 1). The phlogopite and twinned calcite with cleavage features (sample Cat-22d) are interpreted to be a secondary mineral phase. The fine brown material along fractured Cpx and Grt is probably kelyphite. This rock (Figure 4.2) presents a complex deformation process. There are several rims providing evidence of kelyphite around the primary minerals (garnet and pyroxene), which indicates this rock has been highly transformed due to the metasomatic replacement event. The kelyphite present in this rock has been formed after the formation of the host rock minerals (olivine, pyroxene, and

spinel/ilmenite). The phenocrysts minerals are supported by a mixture of groundmass of kelyphite and fine grained materials of olivine.

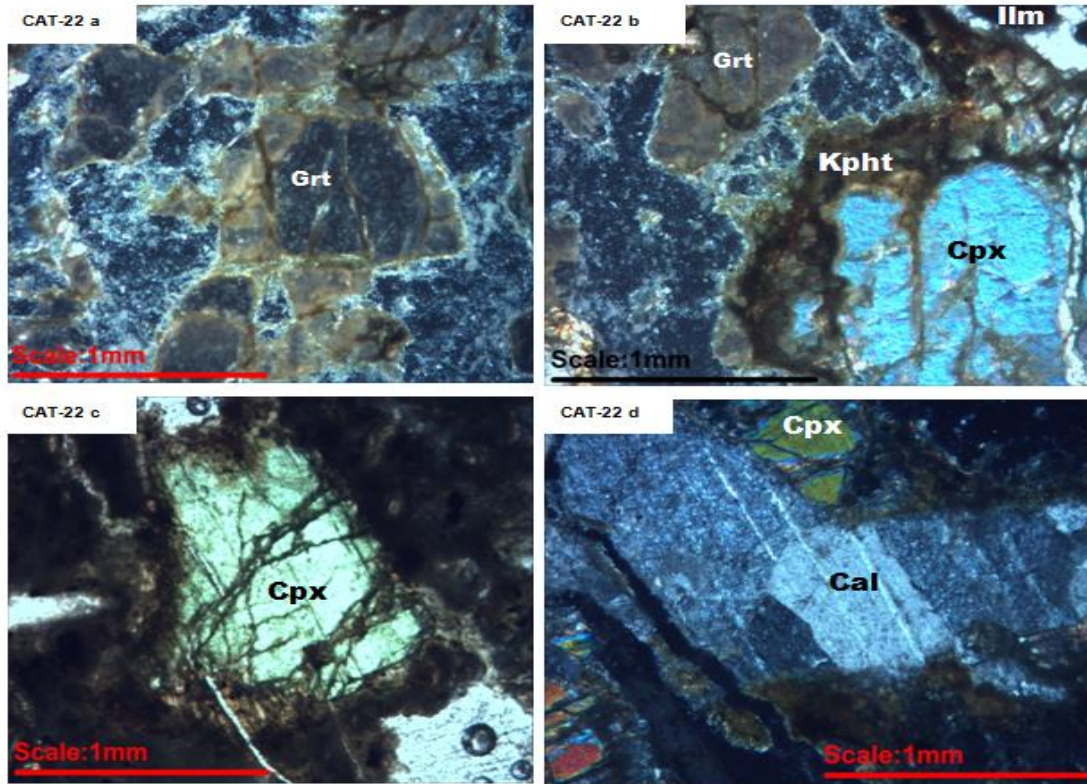


Figure 4.2. Mineral assemblages in thin section samples from petrographic and geochemical analyses of mantle xenolith P-types (CAT-22, from Catoca pipe.)

#### 4. 1. 3. CMT – 05 Mantle xenoliths (eclogite) from Camatxia pipe

This rock (Cmt-05 in Figure 4.3) is described as mantle xenolith peridotite which is mainly composed of clinopyroxene, garnet, serpentised olivine (Cmt-05g), and very small amount of orthopyroxene (see the occurrence % and grain size in Appendix 1). This rock shows high oxidation/metasomatose process and the symplectite texture is visible on cracked megacrysts of olivine (sample Cmt-05) and Opx- Cpx (CMT 05b). The garnet grain (Cmt 05a) shows two different zones (inner and outer) with kelyphite texture, and appears to represent a replacement of garnet texture by other minerals such as pyroxenes and iron rich minerals (e.g. spinel and amphibole), at low pressure environments.

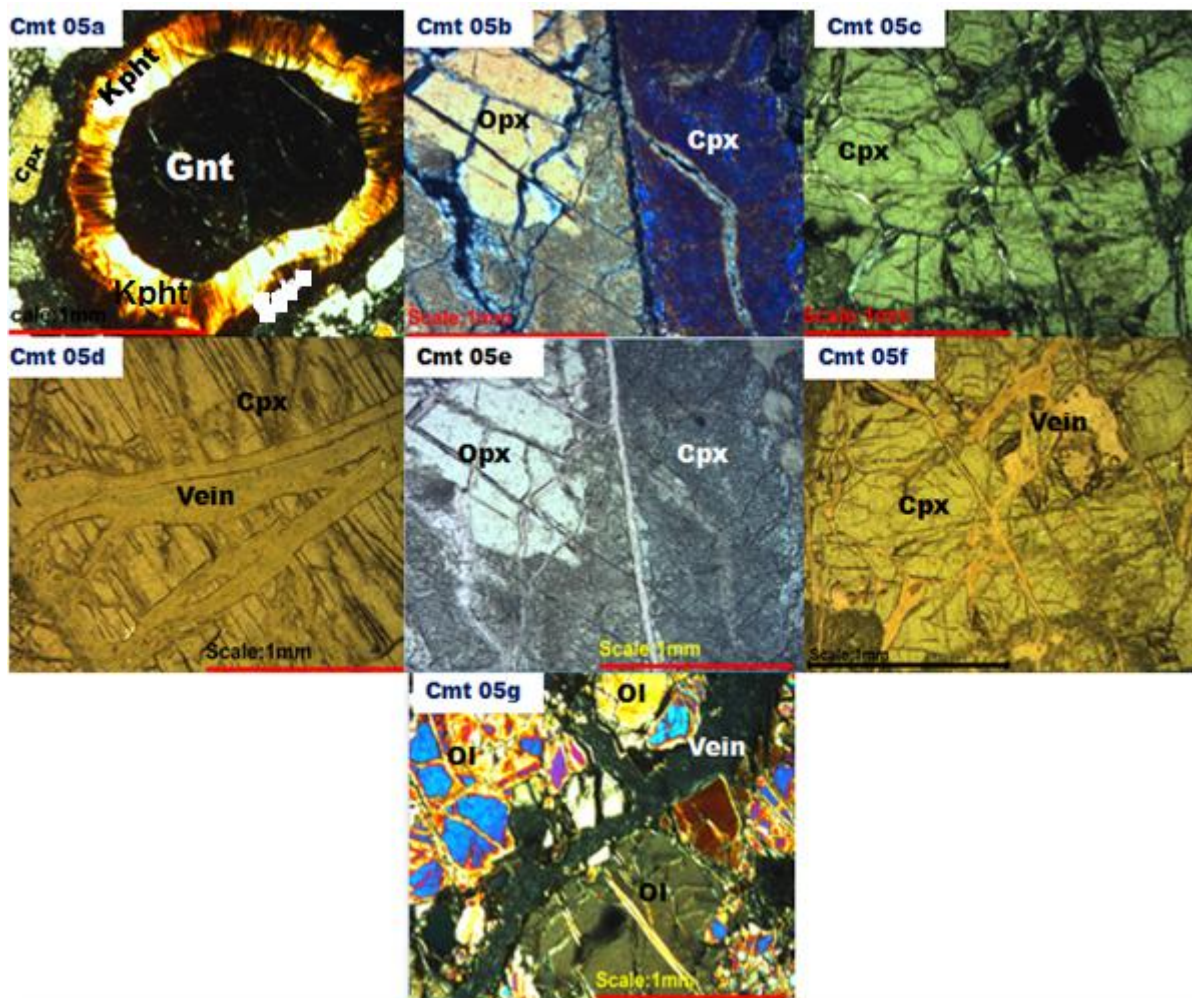


Figure 4.3. Transmitted-light optical microscopy and mineral assemblages in thin section from petrographic and geochemical analyses of mantle xenolith P-types (Cmt-05).

The examined mantle peridotite (Figure 4.3) shows irregular veins (width 0.2 - 0.4mm) filled with very fine serpentine (brown and hydrated magnesium silicate) and white carbonate materials (sample Cmt 05d and Cmt 05g). These are indicative of penetration of rich fluid phases in the diamond peridotite mantle. It is understood that most of the silicate minerals in this rock are disaggregated with several irregular fractures, probably due to kimberlite emplacement.

The evidence of kinetics of the oxidation/reduction on garnet (Cmt-05a) and Cpx (Cmt 05d and f), suggest that the oxidised fluid or melt has infiltrated in the mineral assemblages, and the existing oxygen in the fluids may have reacted with mineral (garnet for instance) that contains  $Fe^{2+}$  to produce  $Fe^{3+}$  (McCammon *et al.*, 2001). The red-brown isotropic rim material (Cmt 05a) may have resulted from an oxidation process which formed kelyphite. This evidence of oxidation processes is indicative of mantle metasomatic and disequilibrium events that have affected the primary minerals (Cmt-05a, b and 5g) are the porphyroblastic and inequigranular textures (Figure 4.3, sample Cmt-05a and 05g), are dominant textures, but the groundmass is composed of serpentine.

#### **4. 1. 4. CMT - 01 Mantle xenoliths (eclogite) from Camatxia pipe**

Olivine, clinopyroxene, serpentine, spinel/ilmenite and phlogopite are dominant minerals in this rock (Figure 4.4 but hematite or kelyphite have also been found (sample CMT 01d). This rock shows high levels of oxidation / metasomatic process. The observed processes of oxidation / metasomatic fluid / melts in the diamond indicators minerals at Camatxia kimberlite are pieces of critical evidence that may also have negative impact in terms of diamond preservation conditions within the Lucapa structure. Xenocryst grains of olivine (CMT 01a) and clinopyroxene (Cmt 01 c and e) are fragmented, and also these grains contain several veins filled by fine grained materials of serpentine. The symplectite texture is visible along the veins within cracked megacrysts of olivine (samples CMT 01f) and Cpx (CMT 01e). The grain sizes vary (see Appendix 1). Based on the microscopic study of the sampled pipes, this suggests that the observed symplectite texture in the rock may be derived from the breakdown of unstable mineral phases; by reaction between adjacent phases; or by decomposition of a single phase (for example, Cpx, CMT-01c and e). Another important texture found in this rock is the porphyritic or phyrlic texture, in which the ilmenite is set with fine grained olivine (CMT 01a). Sample CMT-01c shows two different stages of mineral formation (growth phenomena). For instance the xenocryst of ilmenite is an earlier-formed mineral by protokimberlite magma. This is because ilmenite is included in fine grained Cpx (CMT-01c) and it may be referred to as a poikilitic texture. Also this texture is observed at CMT-01g (where Olv may be formed earlier than Sep), and most xenocryst minerals from this rock are supported by a mixture groundmass of serpentinitised olivine and fine grained materials of clinopyroxene (e.g. CMT-01e).

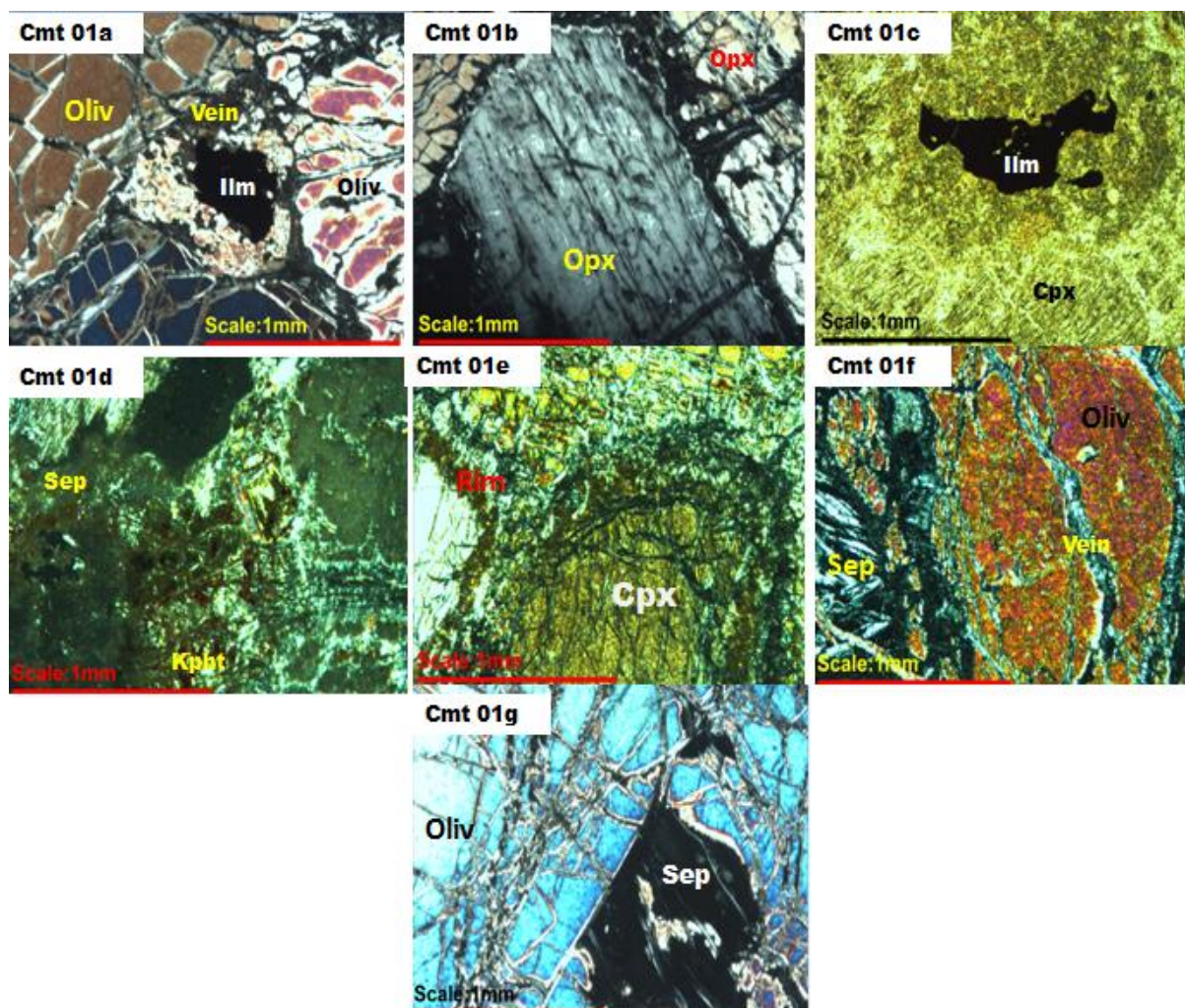


Figure 4.4. Transmitted-light optical microscope images of thin section analysis. Mineral assemblages in thin section from petrographic and geochemical analyses of the mantle xenolith P-types (CMT 01), photographs illustrating textures of CMT - 01.

#### 4. 1. 5. CMT - 02 mantle xenoliths (peridotite) from Camatxia kimberlite.

As shown in Figure 4.5, mantle xenoliths (peridotite) from the Camatxia kimberlite pipe (sample Cmt-02) were also examined by polarised light optical microscopy. Results show that this sample is composed mainly of carbonate, clinopyroxene, garnet spinel/ilmenite and red-brown isotropic mineral (possibly highly oxidised ilmenite, which may have been the origin of hematite, (sample Cmg-02 e). Porphyroblastic to inequigranular is the main texture for this rock (samples Cmg-02a and c). Again, these samples show evidence (samples Cmg-02 b and c) of infiltration of metasomatic fluid/melts into the diamondiferous lithospheric mantle beneath the Congo craton, which may have converted the primary diamond indicator minerals into variably oxidised kelyphitization assemblages comprised of a fine dark brown matter of clinopyroxene, spinel, and serpentine which texturally appears to represent a replacement of garnet (sample Cmg-02 b). The kelyphite (sample Cmg-02 b) probably

consists of intergrowth of brown spinel and pyroxenes (Opx or Cpx). Note that kelyphite forms as the result of partial re-equilibration of the garnet during its rise to the surface in hot kimberlite magma (Kerr *et al.*, 1997) where the effects of heating and lowering of pressure caused transformation of the garnet to a lower pressure assemblage of spinel and pyroxenes. Both analysed mantle peridotite (sample CMT-02, Figure 4.5) and eclogite (sample CAT 18 in Figure 4.1) are described as principal rocks in which diamonds grow in the mantle. This means that a single crystal of diamond in kimberlite is considered to be released from eclogite or peridotite through mechanical disaggregation during eruptive transport to the earth's surface (Shirey *et al.* 2013 and Stachel and Harris 2009).

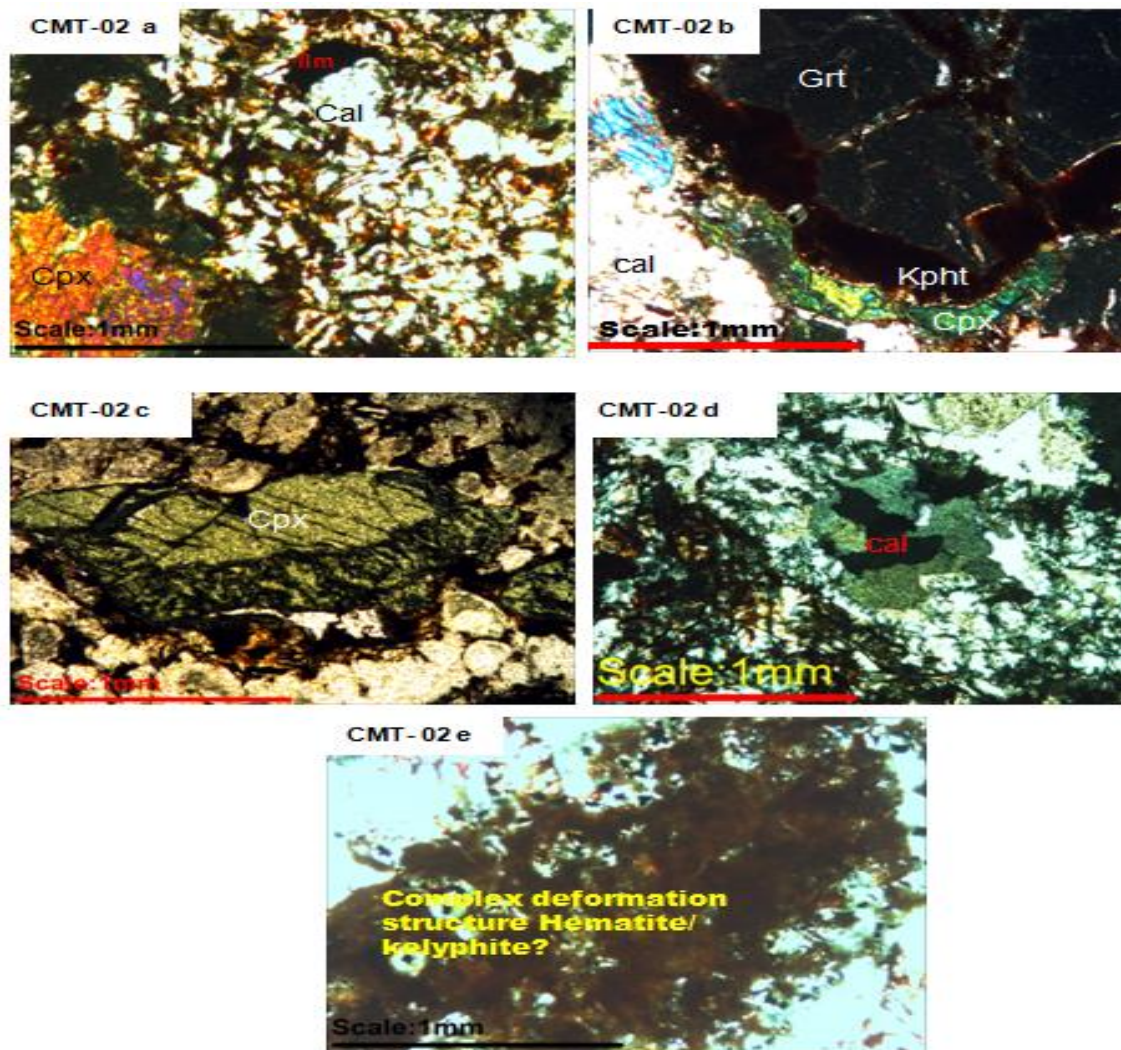


Figure 4.5. Transmitted-light optical microscopy images of thin section mineral assemblages from petrographic and geochemical analyses of mantle xenolith eclogite (CMT-02), illustrating textures of kimberlite rock.

Kerr *et al.* (1997) explained that kelyphite is a reaction product that develops around garnet minerals as result of reactions in the source regions of the xenoliths from the mantle and interaction of the

garnets with kimberlite magma. This means that the reacted zones of garnet probably reflect the original mineralogy (pyroxene and spinel) before these minerals were modified to kelyphite. Note that the shear deformation observed on Cr-diopside (sample, CMT-02c) is further evidence of pressure related/mechanical deformation that occurred within the local lithosphere mantle and this deformation process (cracking), possibly occurred during the emplacement phase of the Camatxia kimberlite. The evidence that dissolution has taken place is around the cracked Cr-diopside (sample CMT-02 c).

#### **4. 1. 6. CM 003 mantle xenoliths (peridotite) from Camutue kimberlite,**

As shown in Figure 4.6, sample Cm 003 can be classified as peridotite. The rock is composed mainly of the minerals garnet (Grt) and olivine (Olv), serpentine (Sep), and minor clinopyroxene (Cpx) and with kelyphite present in rock (Cm 003c and Cm 003e). Note that due to the metasomatic events, the observed olivine has been broken-down, serpentinised and consequently transformed into a fine grained kelyphite structure (sample Cm 003 e). Furthermore, it has been found that the replacement process of serpentine has obscured the original crystal of olivine (sample Cm003c, d, and e) in the rock, especially overprinting the original fine clastic matrix, as well as the original groundmass texture in kimberlite. The megacryst minerals of this rock are supported by a complex mixture of kelyphite, calcite, and serpentine as groundmass.

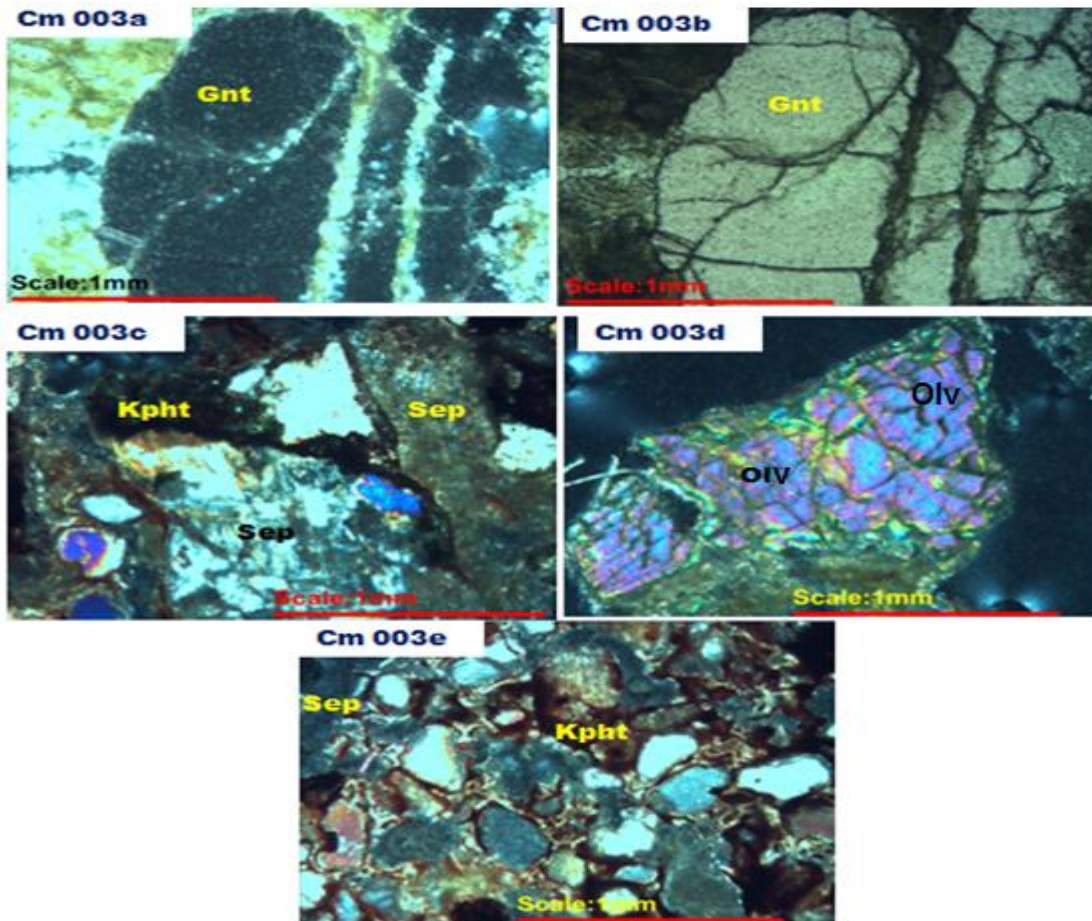


Figure 4.6. Transmitted-light optical microscope images of thin sections analysis. Mineral assemblages in thin section from petrography and geochemistry analyses of P-type (Cm-003), photographs illustrating textures of kimberlite rock.

#### 4. 1. 7. CMG 002 Mantle xenoliths (peridotite) from Camagico kimberlite

As shown in Figure 4.7, mantle xenoliths (peridotite) from the Camagico kimberlite pipe (sample Cmg-002) were also examined by polarised light optical microscopy. Results show that this sample is composed mainly of garnet, perovskite/spinel, carbonates and serpentinised olivine (with two different growth period textures noted at Cmg-002g). Olivine is clearly the dominant mineral, but the groundmass is composed of a complex mixture of fine particles of carbonates and serpentine. The rock exhibits a complex formation texture. This indicates that the rich fluid phase affected the primary mantle minerals (as shown, for example, for olivine, garnet and ilmenite in Cmg-002a and c) consequently these diamond indicators minerals (Griffin and Ryan, 1995; Robinson *et al.*, 1989; Gurney and Zweistra, 1995) have been into variably oxidised kelyphitization, serpentinization assemblages (samples Cmg 002a and Cmg 002c).

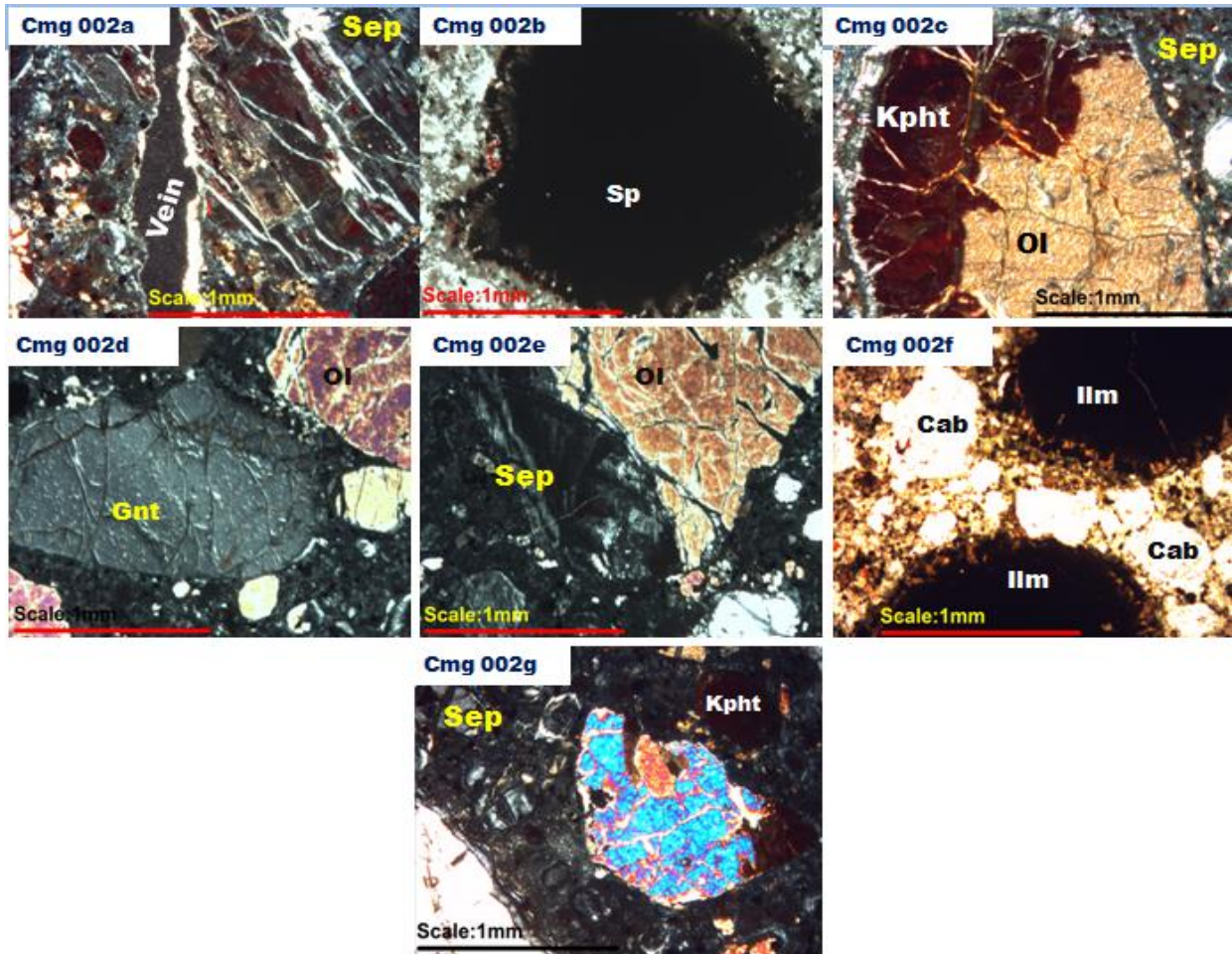


Figure 4.7. Transmitted-light optical microscopy images of thin sections of mantle xenolith with mineral assemblages from Camagico kimberlite sample Cmg-002; Sep = serpentine, Sp = spinel, Kpht = kelyphite, Gnt = garnet, Ol = olivine, Ilm = ilmenite, Cab = Carbonates.

#### 4. 1. 8. CAT- 61 Catoca kimberlite (pyroclastic kimberlite- PK)

In this particular rock (Figure 4.8) carbonate, olivine, garnet, orthopyroxene, clinopyroxene and phlogopites are the most dominant minerals (see the occurrence % and grain size in Appendix 1), and the oxide minerals (spinel and ilmenite) are less abundant. The rock presents porphyroblastic (samples Cat-61a, and Cat-61c in Figure 4.8) to inequigranular texture (samples Cat- 61 b, and e in Figure 4.8). The uncommon equigranular texture was caused by violent eruptions in the kimberlite magma (Sparks *et al.*, 2006; Skinner, 2008; and Scott Smith *et al.*, 2008). Sample Cat-61 d presents features closer to an equigranular texture. In addition, this sample shows evidence of secondary processes, which are indicative of disequilibrium of primary silicate assemblages from mantle equilibrium and serpentinization of olivine (samples Cat- 61 b and c), phlogopite (sample Cat- 61 e), and a fine grained brown rim around Gt. Serpentine occurs as pseudomorphs of olivine macro/microphenocrysts (sample

Cat - 61b) and is dispersed in the groundmass. The presence of serpentinisation reactions (sample Cat-61b) can be interpreted as evidence of low to moderate ambient temperatures. This is supported by White *et al.* (2012), who showed the maximum temperatures for serpentinisation reactions to be approximately 500°C.

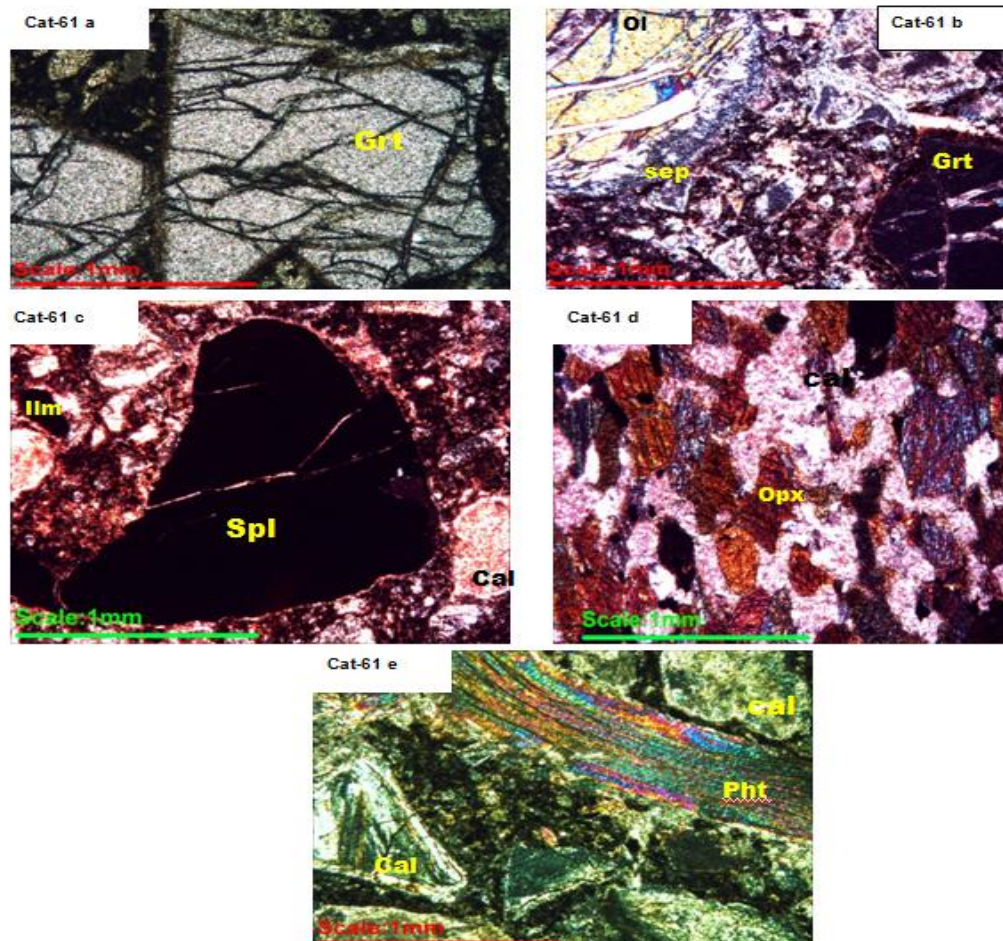


Figure 4.8. Transmitted-light optical microscopy images of thin sections of Lunda province mantle xenolith with mineral assemblages from Catoca kimberlite, garnet exhibiting mechanical deformation.

The brown thin-rimmed materials on the cracks/fractured megacryst of garnet are indicative of possible melt infiltration /oxidation reactions during kimberlite emplacement (Cat-61a in Figure 4.8) and the rims appear to be made of fine materials of pyroxene. This rock is from hypabyssal facies at great depths (> 600m deep, see Appendix 2). The carbonate activity observed in kimberlite samples (Cat- 61e, Figure 4.8) may have played a negative role in diamond preservation within the Lucapa graben. This statement is consistent with McCammon *et al.* (2001) and Fedortchouk *et al.* (2007) who explained that increasing carbonate activity within the kimberlite mantle would increase the degree of diamond reaction with the melt, consequently causing the resorption of diamond. The possible zonation features on the carbonate materials, detected in sample Cat-61c (Figure 4.8) leads to the interpretation that fluids with different compositions infiltrated this rock, probably over different time scales (Emery and Marshall, 1989). As shown in Figure 4.8, xenocryst minerals of garnet, olivine,

pyroxene, phlogopite including the isotropic minerals spinel and ilmenite (sample Cat-61e) are supported by a groundmass of carbonates and fine grained materials of serpentine. Based on kimberlite terminology recommended by Scott Smith *et al.* (2008) and Cas *et al.* (2008), this rock can be interpreted and classified as a pyroclastic kimberlite (see hand specimen description in Appendix 2).

#### **4. 1. 9. CAT 59. Kimberlite rock. Tuffisitic kimberlite breccia (TKB), Catoca pipe**

This rock is TKB generated at a depth of 345 m. According to the analysed result (Figure 4.9), carbonate, serpentine, phlogopite, clinopyroxene, and spinel/ilmenite are the dominant rock constituent minerals. The CAT 59 also contains inclusion of peridotite. A poikilitic or symplectite texture was detected at samples (Cat 59c and Cat 59b). This is interpreted as showing that carbonate and phlogopite are intergrowth minerals. The alteration in rocks, for example the presence of serpentine, is resultant in olivine (with sub-polymorph feature- sample CAT 59g). Petrographic analysis has led to the conclusion that carbonate (e.g. calcite) is considered as the groundmass which supports megacryst minerals (e.g. Grt, Pht, Ilm and Cab). Many of the carbonates found in the kimberlite rocks are products of carbonatite and kimberlite magmas (Cas *et al.*, 2008). In this particular case of Lunda kimberlites, however, much of the carbonates analysed, suggests being secondary products. The microscopic analysis results - in cross polarised light, demonstrates that phlogopite grains are rich in iron showing a red/blue colour (Cat 59a). The modification of minerals structure at sample Cat 59h, presents complex metamorphic events that occurred in NE Angolan kimberlites. The implication is that the presence of carbonate activities in this rock may have a negative impact in diamond preservation or grade in the pipe this is because when kimberlite rocks and peridotite mantle are subjected to significant metasomatism, leading in increasing of Ca content, which are indicative of resorption process of diamond and the increasing of carbonate activities in mantle have been described to be linked with significant increases in oxygen fugacity (Griffin and Ryan, 1995) and therefore it is assumed that the presence of significant carbonate activities in Lunda mantle may have increased the potential for diamond resorption at Catoca and Camagico kimberlites. This result is also consistent with the work of Nowicki *et al.* (2007) who explained that when mantle xenoliths are subjected to significant metasomatism, it normally increases the Ca content and reduces the proportion of G10 peridotite garnet.

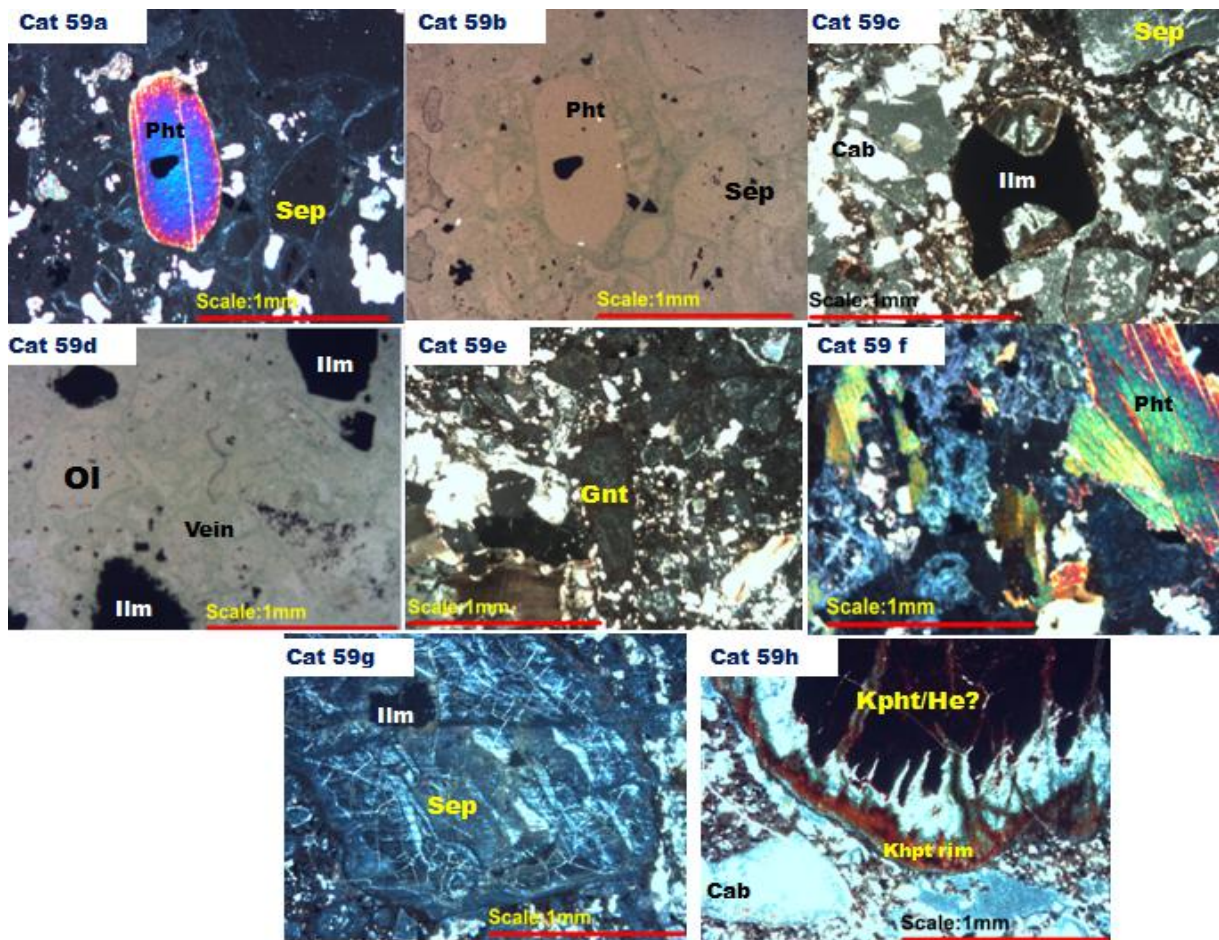


Figure 4.9. Transmitted-light optical microscope images of thin section analysis. Mineral assemblages in thin section from petrography and geochemistry analyses. Tuffisitic kimberlite breccia (TKB), CAT 59, photographs illustrating textures of kimberlite rock.

#### 4. 1. 10. CM-CW 045 (7) pyroclastic kimberlite (PK), with inclusion of mantle xenoliths (from Camutue pipe)

As demonstrated in Figure 4.10, this section is pyroclastic kimberlite (PK) from diatreme facies of the Camutue kimberlite pipe. The petrographic analysis shows evidence of serpentinised olivine with poikilitic texture (Cm-CW045-7d). This texture simply refers as a growth phenomenon, not exsolution or replacement. Note that phlogopite and ilmenite/spinel are minor minerals in this rock. Olivine is clearly the dominant mineral and garnet is also one of the main mineral components in this rock. More than 70% of this rock has been altered by several reactions (Cm, Cw 045-7e).

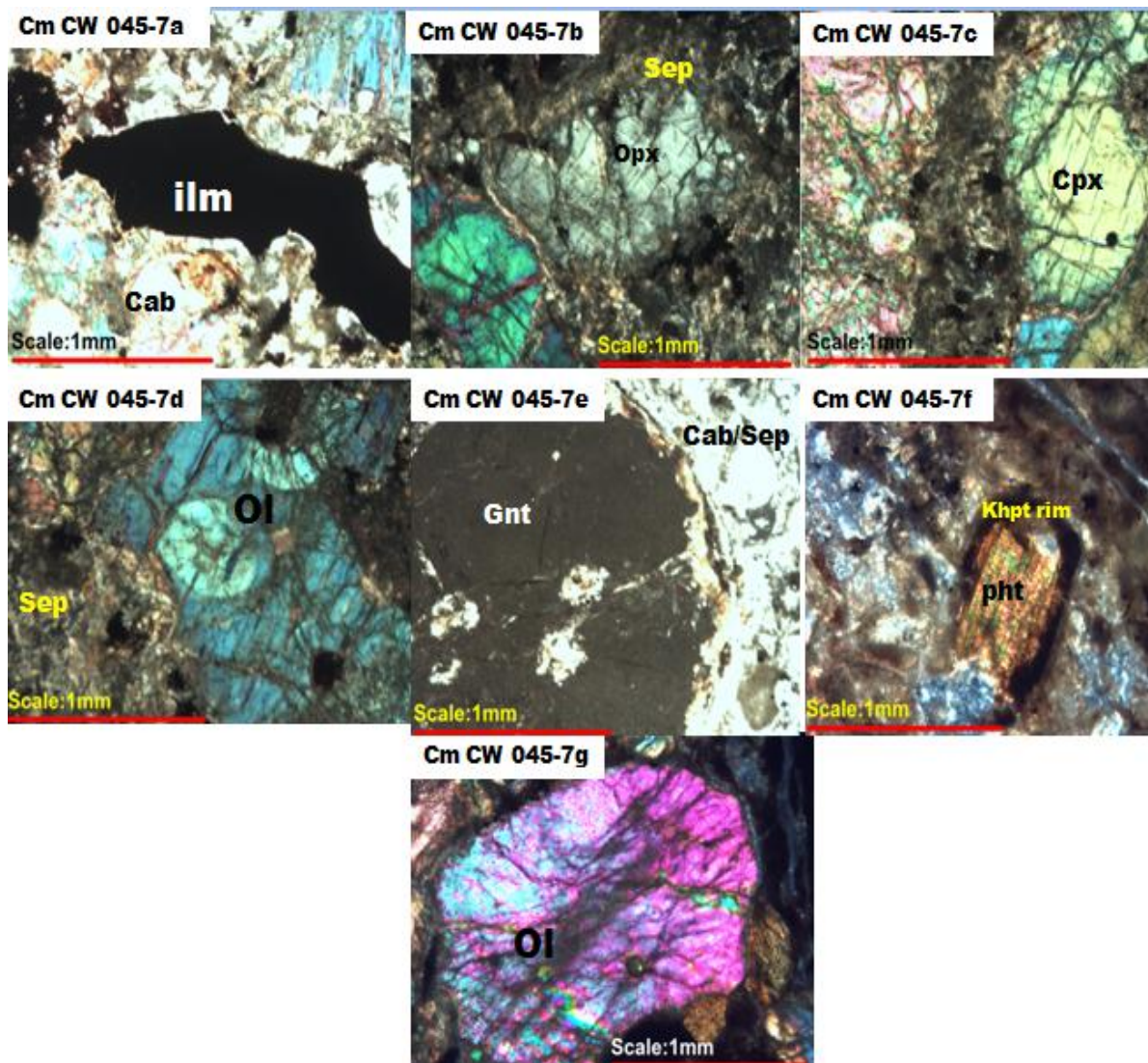


Figure 4.10. Transmitted-light optical microscopy images of thin section analysis of pyroclastic kimberlite rock (CW045-7, Camutue), with minerals assemblages from Camutue kimberlite sample Cm/Cw 45; Sep = serpentine, Sp = spinel, Kpht = kelyphite, Gnt = garnet, Ol = olivine, Ilm = ilmenite, Cab = Carbonates.

After a detailed analysis, the result from thin section (Figure 4.10), it is shown that the groundmass is composed of a complex mixture, associated with fine grained products of serpentine, carbonate and kelyphite (samples Cm Cw 045-7a, c, d, e, and f). Some garnets grains are rounded with well-developed kelyphite rims but the garnet deformation process is similar to those garnet lherzolites from Namibian kimberlites (Hanaus-I and Louwrensia kimberlites) that lack diamonds as described by Mitchell (1984). What is crucial in a geological context is that Namibian kimberlites are barren in diamond whereas the Angolan pipes are rich in diamond. The main reason of this difference is that the Namibian pipes are barren in nature because they are derived from off-cratonic kimberlites within the graphite stability field (Boyd and Gurney, 1986) and also Namibian pipes are located within mobile belts (Batumike *et al.*, 2009) and are younger in age (Nixon, 1995).

#### 4. 1. 11. CAT 58 Coherent kimberlite (CK) from Catoca pipe

The examined hand specimen (Figure 4.11) of this kimberlites sample shows a texture from inequigranular to porphyritic and fragmental in appearance and this contains abundant angular to rounded crustal and xenoliths. This rock is derived from hypabyssal facies- deep dyke formation material at depth approximately > 540 m (see Appendix 2 for additional information). The dominant minerals from Figure 4.11 are serpentine, carbonate, phlogopite, pyroxene, and spinel/ilmenite. From a very close naked eye analysis and evaluation it is notable that the megacrysts of serpentine and opaque minerals show poikilitic or symplectite texture (where carbonate is intergrowth). Serpentine is resultant from alteration of pyroxene and olivine (with sub-polymorph feature). This rock presents evidence of complex fluid reaction events, where the serpentinised olivine or pyroxene may have reacted with fluid from mantle source to generate hematite or kelyphite. Note that the groundmass is mainly composed by fine grained carbonate minerals.



Figure 4.11. Diamond-bearing kimberlite rock from Catoca mine (diamonds are not visible). Also illustrates the porphyritic texture on Catoca kimberlite rock.

Based on field work investigation (rock examination and morphology of emplacement of kimberlite magma, and petrology study), it can be explained that the kimberlites bodies of NE- Angola are products of multiple intrusive and extrusive magmatic events (Figures 3.27), and are recognised as distinctive kimberlites facies (Table.4.1). The kimberlite rock texture and classification (Table 4.2) from this research are consistent with those reported previously in literature (Webb *et al.*, 2004; Cas *et al.*, 2008; Field and Scott Smith, 1998; and Kjarsgaard, 2007).

Pipe Zone	Pipe infill. Textural interpretation	Kimberlite geological facies Terminology
Crater Zone	1. Pyroclastic kimberlite (PK) 2. Resedimented volcanoclastic kimberlite (RVK)	Crater facies
Diatreme Zone	3. Massive volcanoclastic kimberlite (MVK) 4. Tuffisititic kimberlite breccias, (TKB) 5. Hypabyssal kimberlite (HK).	Diatreme facies
Root zone	6. Hypabyssal kimberlite (HK).	Hypabyssal facies

Table 4.1. Summary of kimberlite petrography of LP and its terminology.

Based on petrographic analysis and field work activity, it was observed that crater, diatreme and root zone have different shapes and contrasting material filling in the zones (Figure 3.4 in section 3.1.3), suggesting that these zones were formed by varying process within the one overall emplacement event (Field *et al.*, 2008). For instance, Scott Smith (1999) explained that the root zone may have been formed by stopping the magmatic process, whereas the diatreme by fluidisation and finally the crater was zone formed by explosive breakthrough (violent events). Though dykes or hypabyssal kimberlites have been found in some Angolan kimberlites, (example at Catoca mine), they are less common than crater and diatreme facies rocks (Boyd and Danchin, 1980). After a detailed rock examination, it can be highlighted from this project the petrographic facies of kimberlites from Lunda-provinces described here, are similar to those from across the world such as Canada, Brazil (Pimenta Bueno kimberlite), South Africa (Wesselton and Premier kimberlites), Orapa kimberlite (Botswana) and Australian pipes, described by several researchers (Mitchell, 1991; Field and Scott Smith, 1998; Scott Smith, 2008; Field *et al.*, 2008; Masun and Scott Smith, 2006; Mitchell *et al.*, 2008; and Cas *et al.*, 2008).

Order	Sample Ref.	Name of Pipes	Borehole for Sample	Depth, M	Name of Rock.	Kimberlites Facies/Zones	Ages of Angolan Kimberlites
1	Cat-18	Catoca	Mina NE	horizon. 930 m,	Mantle eclogitic ( bimineralic eclogite)	Crater	Lower- Cretaceous 115-144 Ma
2	Cat-22	Catoca	047/35-1	508.2	Mantle eclogitic included in kimberlite	Diatreme	Lower- Cretaceous 115-144 Ma
3	Cat-29	Catoca	047/35-1	595.9	Mantle peridotitic (Iherzolite), P-type	Diatreme	Lower- Cretaceous 115-144 Ma
4	Cat-58	Catoca	050/37	543,0	Coherent Kimberlitte (CK)	Diatreme	Lower- Cretaceous 115-144 Ma
5	Cat-59	Catoca	033/35	344.4	Tuffisitit kimberlite breccias (TKB)	Crater	Lower- Cretaceous 115-144 Ma
6	Cat- 67	Catoca	037/34	612.8	Coherent Kimberlitte (CK)	Hypabyssal facies	Lower- Cretaceous 115-144 Ma
7	Cat-60	Catoca	Mine NW	horiz. 900 m	Pyroclastic Kimberlite. (PK).	Crater	Lower- Cretaceous 115-144 Ma
8	Cat-59	Catoca	033/35	344.4	Tuffisitit kimberlite breccia (TKB).	Diatreme	Lower- Cretaceous 115-144 Ma
9	Cat-61	Catoca	Mine SW	horiz. 900 m	Pyroclastic Kimberlite. (PK).	Crater	Lower- Cretaceous 115-144 Ma
	Cat 253	Catoca	CAT	250	Peridotitic and PK	Diatreme	Lower- Cretaceous 115-144 Ma
10	CX	Caixepa	CX012	60.8	Pyroclastic Kimberlite (PK) .	Crater	Lower- Cretaceous 115-144 Ma
11	CX	Caixepa	CX022	30	Pyroclastic Kimberlite (PK) .	Crater	Lower- Cretaceous 115-144 Ma
12	CX	Caixepa	CX12	54.9	Pyroclastic Kimberlite (PK) .	Crater	Lower- Cretaceous 115-144 Ma
13	CX	Caixepa	CX009	57	Pyroclastic Kimberlite (PK) .	Crater	Lower- Cretaceous 115-144 Ma
14	CX	Caixepa	CX030	76.7	Pyroclastic Kimberlite (PK) .	Crater	Lower- Cretaceous 115-144 Ma
15	CM	Camutue	CW045	140.6	Pyroclastic Kimberlite (PK) .	Diatreme	Lower- Cretaceous 115-144 Ma
16	CM	Camutue	CW045	114	Pyroclastic Kimberlite (PK) .	Diatreme	Lower- Cretaceous 115-144 Ma
17	CM	Camutue	CM N1 and P-TYPE	~ 50	Pyroclastic Kimberlite (PK) and P-TYPE	Crater	Lower- Cretaceous 115-144 Ma
18	CM	Camutue	CW45CM MG	114	Pyroclastic Kimberlite. (PK).	Diatreme	Lower- Cretaceous 115-144 Ma
19	CMG	Camagico	CMG 171	116	Tuffisitit kimberlite breccia (TKB).	Diatreme	Lower- Cretaceous 115-144 Ma
20	CMG	Camagico	CMG 60	111	Tuffisitit kimberlite breccia (TKB).	Diatreme	Lower- Cretaceous 115-144 Ma
21	CMG	Camagico	CMG 006	87	Pyroclastic Kimberlite (PK) .	Crater	Lower- Cretaceous 115-144 Ma
22	CMG	Camagico	CMG 002	50	Pyroclastic Kimberlite (PK) .	Crater	Lower- Cretaceous 115-144 Ma
23	CMG	Camagico	BH	43	Pyroclastic Kimberlite (PK) .	Crater	Lower- Cretaceous 115-144 Ma
24	CMT	Camatxia	MZ	110	Pyroclastic Kimberlite (PK) .	Diatreme	Lower- Cretaceous 115-144 Ma
25	CMT	Camatxia	CMT 01	71	Mantle xenoliths, eclogite	Crater	Lower- Cretaceous 115-144 Ma
26	CMT	Camatxia	CMT 1 –Y	62	P- TYPE	Crater	Lower- Cretaceous 115-144 Ma
27	CMT	Camatxia	CMT 02	95	Pyroclastic Kimberlite (PK) .	Diatreme	Lower- Cretaceous 115-144 Ma
28	CMT	Camatxia	CN	130	Pyroclastic Kimberlite (PK) .	Diatreme	Lower- Cretaceous 115-144 Ma

Table 4.2. Summary of selected samples. All are the same age.

## 4. 2. Megacrysts origins

The sampled megacryst suites (ilmenite, olivine, garnet, and pyroxene) or mantle xenolith materials brought to the surface by kimberlites and other alkaline volcanic rocks, have played a crucial role in providing information about the composition and the evolution of the continental upper mantle. This project has highlighted that the lithospheric mantle beneath Angolan Archean craton is composed mostly of mantle xenolith peridotites (lherzolite and harzburgite), eclogites and minor pyroxenites. The lithospheric mantle peridotites are residues of extensive partial melting of harzburgites and possibly dunites (Stachel *et al.*, 1998; Sobolev *et al.*, 1969; and Shchukina *et al.*, 2006). The similar megacrysts /xenoliths used in this research have also been described by Giuliani *et al.* (2013) as resulting from the ascent of primitive/precursor kimberlite magma (proto-kimberlite) that crystallised in the magma conduit at lithospheric mantle depths. The examined megacrysts (from mantle lherzolite, harzburgite and eclogite) beneath the Congo Craton, for this project, sampled by kimberlite magma vary in size (up to 45 cm diameter) and they appear to have crystallised at high pressures of approximately 45–55 kbar (Giuliani *et al.*, 2013) at depths equivalent to the lithosphere–asthenosphere boundary (Harte and Gurney, 1981). On basis on information from radiogenic (Sr–Nd–Hf) isotope systematic of kimberlitic megacrysts, Giuliani *et al.* (2013) explained that the asthenospheric mantle is the origin for the megacryst magmas that were consequently contaminated by Achaean lithospheric material sampled by kimberlites magma.

The megacrysts used for this research occurred as individual crystals or intergrown grains of the same or different megacryst minerals showing partial re-crystallization, compositional zoning, and textures of polycrystalline megacrysts. All of these features suggest that megacrysts formed metasomatically before the emplacement of kimberlite magma.

Despite a number of efforts being made by several researchers to study Angolan kimberlites, there is still uncertainty and no clear a picture of the composition of the lithospheric mantle. One reason for this problem may be Angolan government regulations, which have not helped the lithospheric mantle beneath the Lunda diamondiferous province to be fully characterized in mantle sections beneath kimberlite and megacryst occurrences. There are relatively few studies on the variations in mantle minerals and composition of lithospheric mantle of Lunda provinces.

Based on geochemical, mineralogical and petrographic studies , this project has proposed and concluded with confidence that megacrysts such as ilmenite, orthopyroxenes, olivine, garnet and clinopyroxene found in Lunda kimberlites pipes, which were used for this project, are derived at the base of lithospheric mantle or sub-continental lithospheric mantle (SCLM) of the Congo Craton, with thickness of > 250km (Ashchepkov *et al.*, 2012) and consequently they originated from the earlier magma or proto-kimberlite magma (Moore and Belousova, 2005). The contamination and magma mixing process has made the chemical analysis of these megacrysts to be more complex.

However, the evidence from veins observed from the analysed megacrysts (olivine, clinopyroxene, garnet and ilmenite) are interpreted as post-date deformation events (see thin section results in Chapter Four). Most of the analysed garnet harzburgite, eclogite and other mantle peridotite minerals (e.g olivine and pyroxene) are mostly metasomatised.

Based on EMPA results from this research, the presence of Mn- ilmenites (the Lucapa mantle rock) can be interpreted as being the result of interactions of kimberlite with local meteoric waters. This statement is supported by the work of Wyatt (1979) who concluded that Mn-ilmenites in the Premier kimberlite in South Africa were formed during post-magmatic interaction of the Premier kimberlite with rain water; and the country rock is the source of Mn. These megacrysts may have crystallised in pegmatitic vein structures, dykes, or networks in the mantle from melts derived from the magma that subsequently transported them to the Earth's surface. Vein features on ilmenites have also been reported by Kornprobst (1984). Another crucial interpretation from the origin of these megacrysts is that they are the result of the crystallization of liquids trapped prior to kimberlite eruption (Figures 2.9 and 2.10). This model is similar to that described by Moore and Lock (2001), who studied the megacryst suite for South Africa and Botswana kimberlites: the megacryst suite crystallised in pegmatitic veins from small volumes of liquid injected into a fracture network in the thermal aureole surrounding the main kimberlite magma reservoir in the mantle prior to eruption.

The analysed mantle peridotite (harzburgite and possibly lherzolite) and eclogite all showed evidence of deformation (see Chapter Four). However, these results suggest that deformation of Angolan mantle xenoliths or megacrysts by metasomatic agents may have taken place at the base of the lithospheric mantle or during ascent of kimberlite magma to the surface / eruption. Deformations of megacrysts at the base of the lithospheric mantle or during ascent of kimberlite have been also described by Moore and Lock (2001); and by Moore and Belousova (2005). It can be argued that carbonate and alkali-carbonate melts, H<sub>2</sub>O, CO<sub>2</sub>, CH<sub>4</sub>, CO, H<sub>2</sub> and O<sub>2</sub> are the most important metasomatic agents that affect the Earth's mantle rocks (Zhang and Duan (2009)). According to Giuliani *et al.* (2013) carbonate melts play a prominent role in metasomatism of mantle rocks and minerals because experimental studies have revealed that carbonate melts are the first product of partial melting of carbonated peridotites and eclogites (Wallace and Green, 1988) and carbonate melts can be derived from liquid immiscibility in CO<sub>2</sub>-rich silicate or silicate-carbonate melts (Giuliani *et al.*, 2013).

Phlogopite and amphibole minerals were detected and analysed throughout thin sections in this project. The presence of phlogopite and amphibole in mantle xenoliths has been described by Bell *et al.* (2005) and Shchukina *et al.* (2016) as metasomatic products.

Understanding the genesis of the ilmenite megacrysts is complex and problematic (Kornprobst, 1984). Some researchers have pointed out that megacrysts or macrocrysts of ilmenite have crystallised in a

protokimberlite melt (Mitchell, 1977) which implies that they could be early crystallising pre-intrusion phenocrysts in the recent kimberlite magma. However, Kornprobst (1984) noted that ilmenite macrocrysts could be also formed in a liquid derived from partial melting of mantle peridotite, which is dissimilar to kimberlite, and are thus considered xenocrysts. One of the reasons that make understanding the origin of ilmenite megacrysts problematic is that it is questionable whether the megacrysts and concentrates are derived from disaggregated ilmenite-bearing metasomatised peridotites because, according to Kornprobst (1984), the metasomatic ilmenites are richer in chromium (Cr) than the megacrysts/macrocrysts.

The fact that ilmenite occurs in mantle xenoliths (Kornprobst, 1984) indicates that it is xenocrystic to kimberlites. Ilmenite was among most abundant oxide phases found in Lunda kimberlites, and it is present both as a megacryst (e.g size  $\geq 0.5$  cm with shape sub-rounded and anhedral grains) and as a groundmass mineral. Ilmenite megacrysts studied in this project exhibit rounded anhedral to subhedral shapes which are attributed to abrasion during emplacement of the kimberlite magma. The origin of the large crystals of ilmenites from Catoca, Camatxia, Camagico, Caixepa and Camutue kimberlite pipes is associated with proto-kimberlitic liquid. This statement is consistent with Agee *et al.* (1982), who explained that ilmenite is an extremely rare minor constituent of mantle xenolith peridotite, and the size of the ilmenite megacrysts (0.5-1.5 cm) is much larger than the grain size expected from disaggregated peridotite. When the ilmenite megacrysts display a correlation of increasing Fe<sub>2</sub>O<sub>3</sub> with decreasing MgO, it can be attributed to fractional crystallization. Giuliani *et al.* (2013) explained that ilmenites have crystallised from cementing phases crystallised from a S-bearing Ti-Fe-K-rich ultramafic silicate melt, derived from an ascending primitive or proto-kimberlite melt, which was later modified by wall rock assimilation and / or magma mixing, porphyroclast dissolution and crystal fractionation processes.

It has been confirmed by Mitchell (1977) on the basis of on textural, geochemical, and mineralogical studies, that magnesian ilmenite phases are the earlier phenocrysts in protokimberlite formed by partial melting of a mica-rich lherzolite. According to Kornprobst (1984), ilmenite does exist in the mantle as veins or pegmatites, which may have developed as an aureole around the embryonic proto-kimberlite or as metasomatic from preceding the upward migrating magma. On basis of his study, Kornprobst (1984) explained that in the emplacement of the ilmenite and its associated minerals, it is assumed that the ilmenite megacrysts are correlated to an early phase of mantle brecciation prior to the main eruption of the kimberlite magma. Mitchell (1973) proposed that magnesian ilmenite crystallizes from melts unusually rich in Ti and Mg (protokimberlite) formed by small amounts of partially melting lherzolite mantle that involved Ti-rich mica, chrome diopside, and garnet.

A similar situation of antiquity is linked to the genesis of diamond. The majority of diamond crystals found in kimberlite pipes are derived from either a peridotitic or an eclogitic paragenesis, and are

considerably older than the host kimberlite (Nixon, 1995; Richardson, and Harris, 1997), which means diamonds are mantle xenocrysts sampled at the time of kimberlite emplacement. This statement is consistent with the work of Mahotkin *et al.* (2000) who explained that megacrysts of clinopyroxene, garnet and ilmenite are derived at the base of the lithospheric mantle (250-300 km depth; Shirey and Shigley, 2013) from primitive or proto-kimberlite magmas separated from the sublithospheric convecting mantle at depth of several hundred km. This project has highlighted that the mode of formation of the megacryst suite also has important implications for understanding the origin of deformed peridotite (sheared peridotites, Moore and Lock, 2001) or eclogite (Moore and Belousova, 2005) which occur as xenoliths in kimberlites.

It has been explained by Kornprobst (1984) that the peridotite suite reflects shearing at the base of the lithosphere at depths of approximately 200 km (Mahotkin *et al.* 2000), where the chemical boundary separates this unit from the underlying asthenosphere.

Several lines of field, petrographic, chemical and experimental studies have provided evidence that the megacrysts of ilmenite have crystallized from protokimberlite magma (Kornprobst, 1984). The geochemical results from analysed megacryst garnets (for example, sample Cat -18) shows high chemical contents of  $Al_2O_3$  (17-24 wt %), indicating that these garnet megacrysts originated from eclogite mantle xenoliths. It can be surmised that the analysed garnet megacrysts were not crystallized directly from the kimberlitic melt because kimberlite melts contain very low  $Al_2O_3$  (1-2 wt.%) so they cannot crystallize any significant amount of garnet (Shchukina *et al.*, 2016). Also kimberlitic melts are rather carbonatitic in composition (Kamenetsky *et al.*, 2009) and therefore they do not crystallize garnet, although they can assimilate peridotitic and eclogitic minerals during ascent (Shchukina *et al.*, 2016; and Sobolev *et al.*, 1969), and after their formation kimberlite magmas are erupted in a short time span (Shchukina *et al.*, 2016).

### 4. 3. Mössbauer spectroscopy

Mössbauer spectroscopy has been widely used and discussed in the geological literature. The following section shows the results of the investigation by Mössbauer spectroscopy of the sampled kimberlite rock. The high sensitivity of Mössbauer spectroscopy is due to its ability to detect the extremely small changes in nuclear energy levels that result from changes in chemical state or the magnetic or electronic environment which surrounds the  $^{57}\text{Fe}$  atoms. The ability to provide accurate Fe redox ratios using Mössbauer spectroscopy (McCammon *et al.*, 1998; Quintiliani, 2005; Rollinson *et al.*, 2012; and Sobolev *et al.*, 1999) leads this technique to be special in diamond research environments.

The ilmenite samples studied in this project are natural samples from different kimberlite rock facies. Apart from being an indicator mineral in the diamond exploration environment that this project highlights ilmenite ( $\text{FeTiO}_3$ ) was also selected because accurate redox ratios ( $\text{Fe}^{3+}/\sum\text{Fe}$ ) obtained from Mössbauer spectroscopy for ilmenite, is provide crucial information of the origin and genesis or diamond preservation conditions (Gurney *et al.*, 1993; Gurney and Zweistra, 1995; and Kozai and Arima, 2005) Note. Further discussion is provided in Chapter Five. Ilmenite with low  $\text{Fe}^{3+}/\sum\text{Fe}$  ratios is associated with higher diamond contents than those with more ferric iron ( $\text{Fe}^{3+}$ ). Another important aspect for using ilmenite is the information it provides about the oxygen fugacity. According to Gurney and Zweistra, (1995) high oxygen fugacity is the main diamond destroyer, but its evaluation depends critically on  $\text{Fe}^{3+}/\sum\text{Fe}$  (McCammon *et al.*, 1998).

#### 4. 3. 1. Ilmenite indicator minerals

Figures 4.12; 4.13 and 4.14 show three Mössbauer spectra of ilmenites and their redox ratios are presented in tables 4.3, 4.4 and 4.5. The difference is the spectra of these ilmenite in Figures 4.12 and 4.13 compared to the spectra presented in Figures 4.14 (CAT59HM1), 4.16 (CMT 58) and 4.17 (CAT59HM1 CAT=MY001C) is that where  $\text{Fe}^{3+}$  in ilmenite is in a multiphase environment. For samples CMT 58, CAT59HM1, CAT=MY001C, CAT 59 d, CMT 253 and CMT 58, it was not possible to calculate the iron redox ratio of the ilmenite phases because these were multiphase materials with relatively low abundances of ilmenite and high abundances of amphibole. Separation of the respective ilmenite and amphibole  $\text{Fe}^{3+}$  components in Mössbauer spectra proved impossible as their hyperfine parameters (CS, QS and LW) are closely similar (Gunter *et al.*, 2003; Das *et al.*, 1996; Gibb *et al.*, 1969; Virgo *et al.*, 1988; and Waerenborgh *et al.*, 2002). For these spectra one  $\text{Fe}^{3+}$  doublet was fitted to the combined ilmenite and amphibole  $\text{Fe}^{3+}$  contributions. Consequently it was not possible to separately assess the  $\text{Fe}^{3+}$  content of the ilmenite phases from Mössbauer data but we have provided upper limits of the redox ratio (see Tables 4.5; 4.7; 4.8; 4.9; 4.10 and 4.11) by

assuming that all  $\text{Fe}^{3+}$  in the relevant doublets arises from the ilmenite phase. This presents an "upper redox boundary" and by no means quantifies the iron redox ratio in these phases.

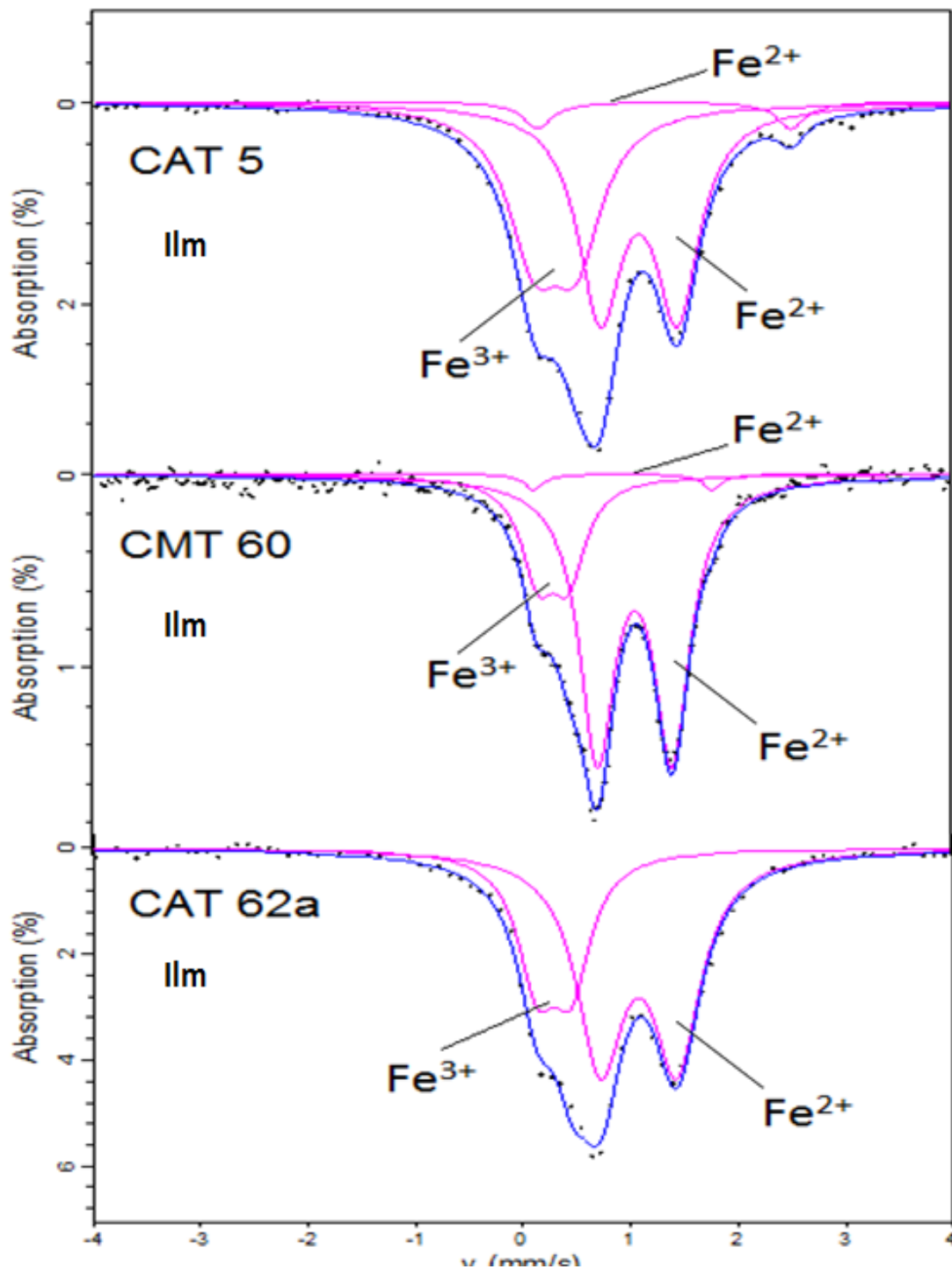


Figure 4.12. Fitted room temperature Mössbauer spectra of ilmenite inclusion samples from diamondiferous pipes Catoca (CAT-5, CAT 62a) and Camatxia (CMT 60). Data were fitted with  $\text{Fe}^{2+}$  and  $\text{Fe}^{3+}$  doublets as shown.

Sample	Fe <sup>2+</sup>				Fe <sup>3+</sup>				Redox Ratios
	CS mm/s ±0.02	QS mm/s ±0.02	W mm/s ±0.02	Area % ±1	CS mm/s ±0.02	QS mm/s ±0.02	W mm/s ±0.02	Area % ±1	Fe <sup>3+</sup> /ΣFe ±0.02
CAT 62a Ilm phase	1.07	0.71	0.26	67.4	0.28	0.32	0.22	32.6	0.32
CMG 60 Ilm phase	1.05	0.69	0.19	73.6	0.30	0.28	0.19	24.1	0.24
CMT 60 Amp phase	0.93	1.66	0.19	2.3	-	-	-	-	-
CAT 5 Ilm phase	1.08	0.71	0.24	53.7	0.31	0.39	0.29	41.9	0.41
CAT5 Amp phase	1.32	2.36	0.15	4.4	-	-	-	-	-

Table 4.3. Room temperature fitted Mössbauer hyperfine parameters of ilmenite and amphibole inclusions.

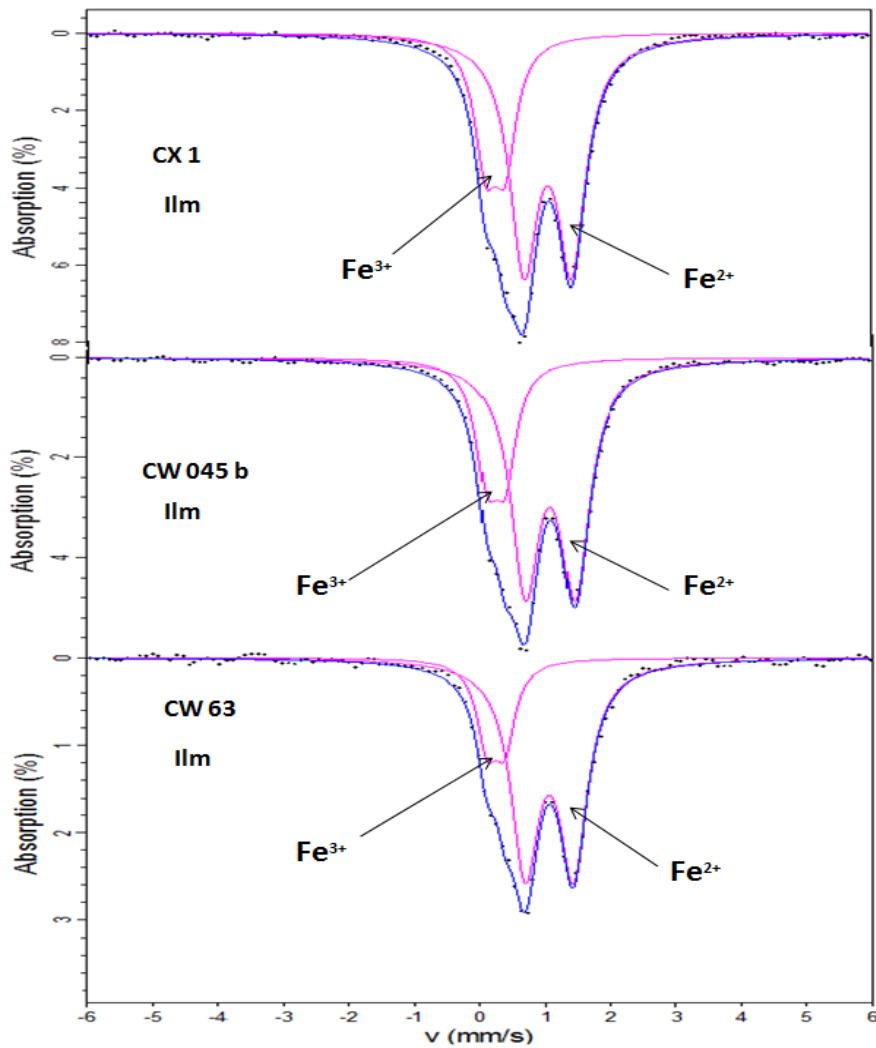


Figure 4.13. Fitted room temperature Mössbauer spectra of ilmenite inclusion samples from two diamondiferous pipes of Caixepa (CX1) and Camutue (CW045b CW 63). Data were fitted with Fe<sup>2+</sup> and Fe<sup>3+</sup> doublets as shown.

Sample	Fe <sup>2+</sup>				Fe <sup>3+</sup>				Redox Ratios
	CS mm/s ±0.02	QS mm/s ±0.02	W mm/s ±0.02	Area % ±1	CS mm/s ±0.02	QS mm/s ±0.02	W mm/s ±0.02	Area % ±1	Raw Fe <sup>3+</sup> /ΣFe ±0.02
Camutue & Caixepa pipes									
CW045b	1.06	0.74	0.26	73.7	0.24	0.27	0.20	26.3	0.26
CX1	1.06	0.72	0.26	70.8	0.26	0.29	0.21	27.2	0.27
CW 63	1.06	0.73	0.26	78.3	0.24	0.27	0.19	21.7	0.21

Table 4.4. Room temperature hyperfine parameters of mineral inclusions (ilmenite) from Caixepa (CX1) and Camutue (CW045b) determined from Mössbauer spectroscopy, (CS→ centre shift; QS→ quadrupole splitting, W→ half width, half maximum line width).

As illustrated in Figure 4.14, both spectra show (CAT 67NMM and CAT59HM1) fitting for minerals inclusion, of amphibole and ilmenite. Sample CAT 67NMM was fitted with Fe<sup>2+</sup> and Fe<sup>3+</sup> for amphibole, whereas sample CAT59HM1 despite the amphibole is main component, but it contains small amount of ilmenite which was fitted with doublet 1. The presence of the ilmenite in Mössbauer is also supported by XRD result. It can be assumed that Fe<sup>3+</sup> for ilmenite (sample CAT59HM1) may share same area for Fe<sup>3+</sup> of amphibole (sample CAT59HM1). However, it is difficult to establish precisely the amount of Fe<sup>3+</sup> in sample (CAT59HM), due to the sample being multiphase materials and the hyperfine parameters (CS, QS and, W) are much closer, almost the same.

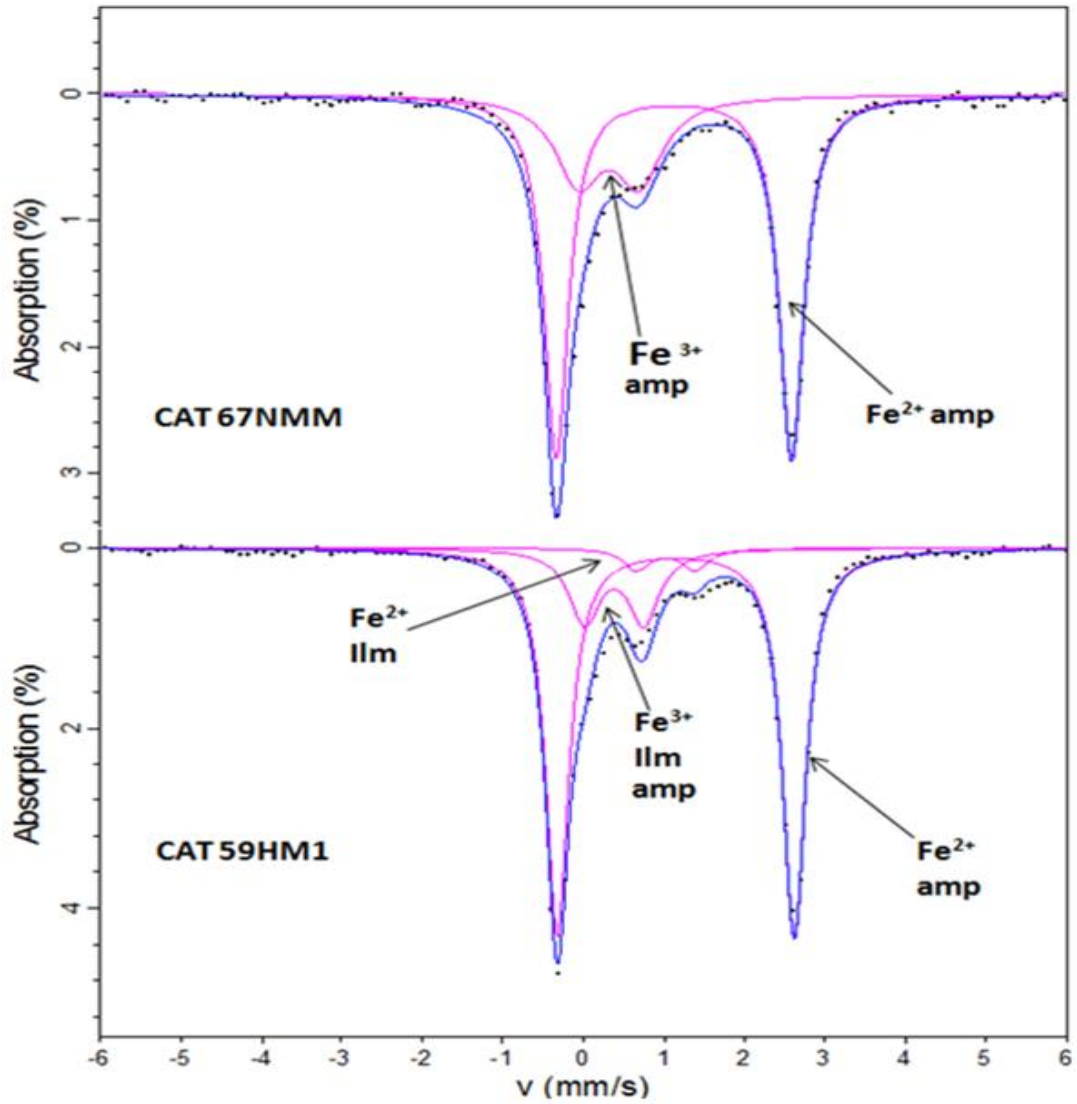


Figure 4.14. Room temperature Mössbauer spectra of ilmenite and amphibole mineral inclusions from diamondiferous pipe Catoca (samples CAT 67NMM and CAT59HM1).

Samples	Fe <sup>2+</sup>				Fe <sup>3+</sup>				Redox Ratios Fe <sup>3+</sup> /ΣFe ±0.02
	CS mm/s ±0.02	QS mm/s ±0.02	W mm/s ±0.02	Area %	CS mm/s ±0.02	QS mm/s ±0.02	W mm/s ±0.02	Area %	
CAT 67NMM and CAT 59 HM1	1.12	2.92	0.18	69.8	0.31	0.75	0.40	30.2	0.31
CAT 67NMM Amp phase									
CAT 59 HM1 Ilm + Amp	1.02*	0.73*	0.20*	4.9	0.38*	0.78*	0.23*	19	0.79
CAT 59 HM1 amphibole phase	1.14	2.94	0.17	76					0.20

Table 4.5. Room temperature hyperfine parameters of mineral inclusion (ilmenite amphibole) from samples (CAT CAT 67NMM) (CAT 59 HM1) multiphase minerals, determined from Mössbauer spectroscopy, (CS→ centre shift; QS→ quadrupole splitting, W→ half width at half maximum).

### 4. 3. 2. Garnet and pyroxene and indicator minerals

The redox ratio of pyroxene was obtained by assuming that both  $\text{Fe}^{2+}$  contributions share the same area or overlap (see Figure 4.15 and table 4.6). This statement is more compatible with the work of McCammon *et al.* (1998) and Vieira *et al.* (1983), who found  $\text{Fe}^{2+}$  for both doublets in clinopyroxene with equal area, while all garnet spectra (CAT 67, CMT05 and CMT 01) were fitted to one  $\text{Fe}^{2+}$  doublet and one  $\text{Fe}^{3+}$  doublet according to conventional models (Sobolev *et al.*, 1999).

	<b>Kimberlite names</b>	<b>Garnet redox ratios (<math>\text{Fe}^{3+}/\Sigma\text{Fe}</math>)</b>
1	Catoca CAT 67 (Gnt)	0.08
2	Camatxia CMT 05 (Grt)	0.34
2	Camatxia CMT 01(Cpx)	0.46
4	Camatxia CMT 01 (Grt)	0.63

Table 4.6. Summary of redox ratio for pyroxene and garnet diamond indicator mineral inclusions

The interesting aspect from sample CMT 01, Figure 4.15, is that the sample is a multiphase material; therefore, it is hard to tell precisely the amount of  $\text{Fe}^{3+}$  for garnet present in sample (CMT 01). In addition, the hyperfine parameters (CS, QS and, W) are almost similar much closer, almost the same with the clinopyroxene. Based on these facts and interpretation, it can be explained that the calculated redox ratio of 0.63, in tables 4.6 and 4.7, is not only for garnet, because the  $\text{Fe}^{3+}$  for garnet is in the mixture environment, together with clinopyroxene, thus it is more difficult for an effective interpretation.

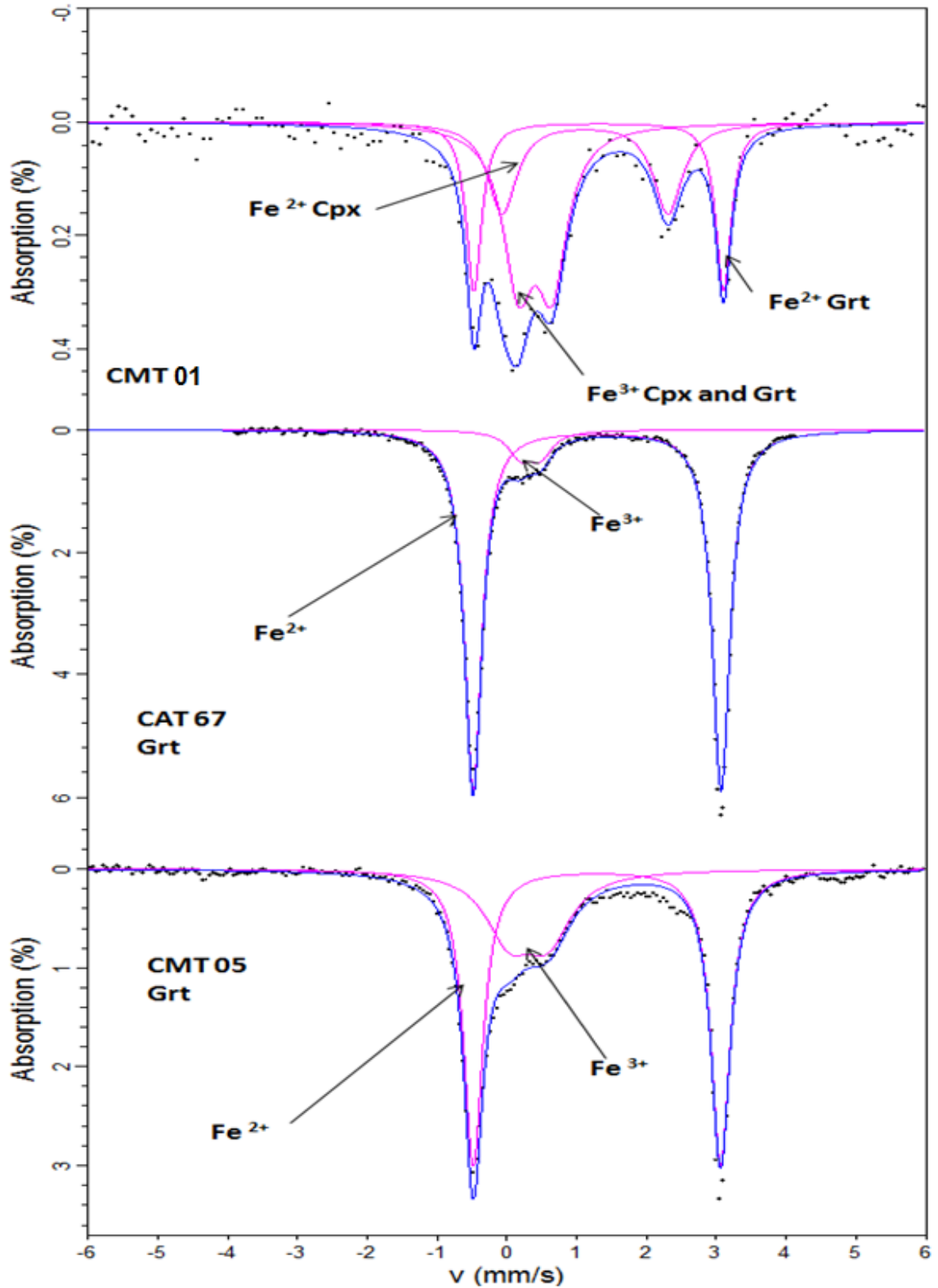


Figure 4.15. Fitted room temperature Mössbauer spectra of garnet inclusion samples from diamondiferous pipes Catoca (Garnet - CAT- 67 Grt) and Camatxia pipe (Garnet - CMT 05 Grt, CMT01 and pyroxene - CMT01). Data were fitted with  $\text{Fe}^{2+}$  and  $\text{Fe}^{3+}$  doublets as shown.

Samples	Fe <sup>2+</sup>				Fe <sup>3+</sup>				Redox, Ratios
	CS mm/s ±0.02	QS mm/s ±0.02	W mm/s ±0.02	Are a % ±1	CS mm/s ±0.02	QS mm/s ±0.02	W mm/s ±0.02	Are a % ±1	Fe <sup>3+</sup> /ΣFe ±0.02
CAT 67 Grt	1.28	3.53	0.15	91.4	0.33	0.29	0.21	8.6	0.08
CMT 05 Grt	1.28	3.53	0.16	65.9	0.30	0.56	0.40	34.1	0.34
CMT 01 (Grt)	1.31	3.57	0.13	26.9	0.40	0.48	0.26	46.5	0.63
CMT 01 Cpx (Fe <sup>2+</sup> for both 2 doublet )	1.11	2.37	0.24	26.7					0.46

Table 4.7. Room temperature hyperfine parameters of mineral inclusions (garnet, and clinopyroxene) determined from Mössbauer spectroscopy, (CS→ centre shift; QS→ quadrupole splitting; W→ half width, half maximum line width. Samples (CMT 05 Cpx and CMT 05 Grt) are from Camatxia pipe whereas CAT 67 Grt is from Catoca pipe

As shown in Figure 4.16 and Table 4.8 data were fitted with Fe<sup>2+</sup> and Fe<sup>3+</sup> doublets (1 and 2) for sample CAT 67M were fitted as amphibole and these parameters are similar to those published by Gunter *et al.* (2003) and Waerenborgh *et al.* (2002), whereas sample CMT 58 contains a small amount of ilmenite which was fitted with doublets 2 and 3, these values are comparable to Gibb and Greenwood (1969). Sample CAT 67M is also complex, multiphase with magnetite and amphibole being major components. It can be assumed that Fe<sup>3+</sup> for ilmenite (sample CMT58) may share the same area for Fe<sup>3+</sup> of amphibole (sample CMT58).

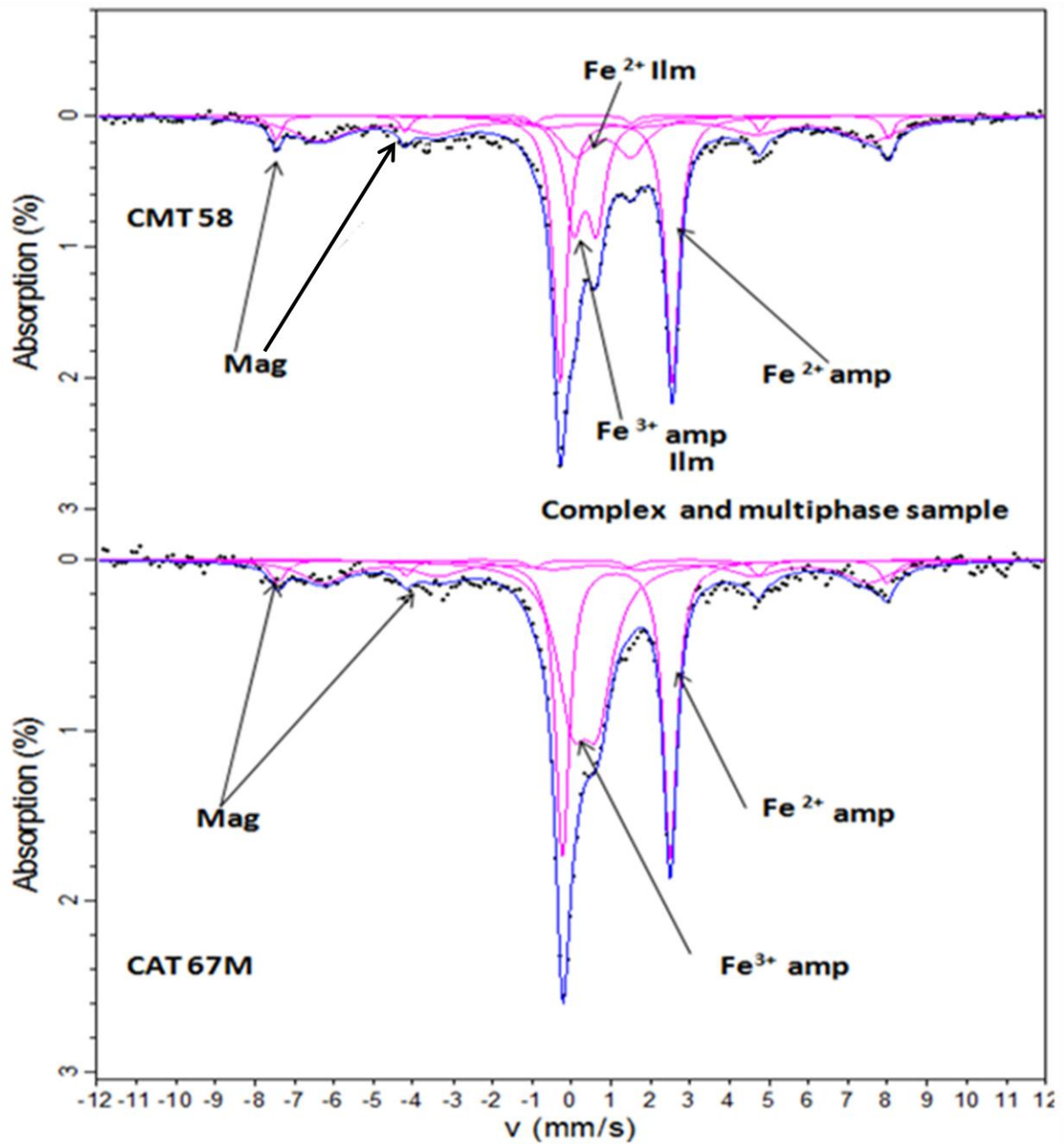


Figure 4.16. Room temperature Mössbauer spectra of complex mineral inclusions of magnetite and pyroxene, samples from diamondiferous pipes of Camatxia (CMT 58) and Catoca (CAT 67M).

Sample	Fe <sup>2+</sup>				Fe <sup>3+</sup>				Redox Ratio
	CS mm/s ±0.02	QS mm/s ±0.02	W mm/s ±0.02	Area % ±1	CS mm/s ±0.02	QS mm/s ±0.02	W mm/s ±0.02	Area % ±1	Fe <sup>3+</sup> /ΣFe ±0.02
Paramagnetic Sites									
Doublet 1 (CAT 67M) Amp phase	1.13	2.72	0.21	37.4	0.34	0.64	0.46	36.7	0.49
Doublets 1 & 2 (CMT 58) ilm+ amph	1.24	0.64	0.19	3.1	0.21	0.71	0.31	44.2	<0.93
Magnetic Sextets									
Magnetic Sextets	CS mm/s	w+ mm/s	H (T)	Area %					Area %
Sextet 1 (CAT 67 M)	0.28	0.24	47.8	6.5					99.9
Sextet 2 (CAT 67 M)	0.63	0.74	42.7	19.3					
Sextet 1 (CMT 58)	0.27	0.29	49.5	16.3					
Sextet 1 (CMT 58)	0.67	0.87	46	17					

Table 4.8. Room temperature fitted hyperfine parameters of mineral inclusions (ilmenite, amphibole and magnetite) for samples CAT 67M and CMT 58, with isomer shift (CS), quadrupole splitting (QS) line width of the high velocity peak (w+), low and high velocity line widths (w-/w+) = 1 to keep equal, line width of the most intense sextet peak (w3), effective hyperfine field (H) and relative site intensities area.

Figure 4.17 and Table 4.9 show the spectra were fitted with 2 major minerals present such as, Magnetite and Amphibole, and also with possible presence of minor inclusions of ilmenite. The spectra of sample CAT59d was fitted doublets Fe<sup>2+</sup> and Fe<sup>3+</sup> for parameters of amphibole; these values are in agreement with Gunter *et al.* (2003) and Waerenborgh *et al.*, (2002). A doublet with an isomer shifts of 1.01 and 1.07 mm/s relative to metallic iron, quadrupole splitting of 0.75 and 0.73 mm/s, corresponds to ferrous iron (Fe<sup>2+</sup>) in ilmenite and other doublets with an isomer shifts 0.32 mm/s and quadrupole splitting of 0.55 mm/s corresponds to ferric iron (Fe<sup>3+</sup>) in ilmenite. See table 4.9. These parameters (Fe<sup>3+</sup>) are comparable with Jancik and Mashlan (2002). Both spectra (CAT59d and CAT=MY001C) show sextets, which were fitted as magnetite (see table 4.9). XRD results for sample (CAT59d) support the presence of small amount of ilmenite in these samples.

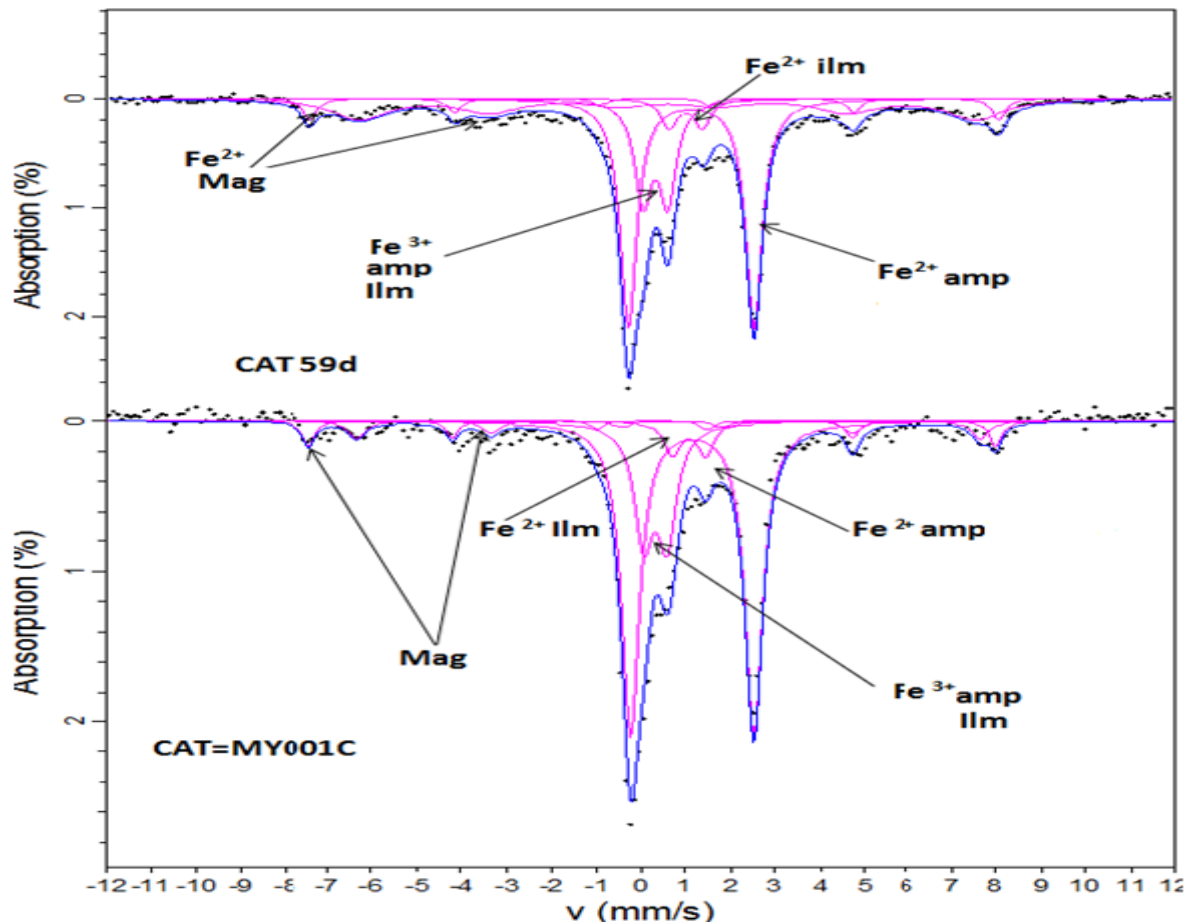


Figure 4.17. Room temperature Mössbauer spectra of amphibole and magnetite inclusions from diamondiferous pipe (CAT 59d) and (CAT=MY001C), with possible presence of Ilmenite in the sample.

Samples	CS mm/s ±0.02	Fe <sup>2+</sup>			Fe <sup>3+</sup>				Redox Ratios Fe <sup>3+</sup> /ΣFe ±0.02	
		QS mm/s ±0.02	W mm/s ±0.02	Area % ±1	CS mm/s ±0.02	QS mm/s ±0.02	W mm/s ±0.02	Area % ±1		
Paramagnetic Sites										
CAT 59 d Possible Ilm phase	1.01*	0.75*	0.22*	5.2	0.32*	0.55	0.23*	18.2	0.77	
CAT 59 d Amp phase	1.13	2.82	0.22	43					0.29	
MY001C Ilm phase	1.07*	0.73*	0.22*	5.7	0.32*	0.52*	0.25	22.4	0.79	
MY001C Amp	1.13	2.75	0.24	59					0.27	
Magnetic sites										
Magnetic site (CAT 59 d)	CS mm/s		w+ mm/s	H (T)	Area	-	-			
Sextet 1	0.30	-	0.19	48.8	6.7	-	-	-	-	-
Sextet 2	0.60	0.61	0.7	43.3	26.1	-				
Magnetic site MY001C	CS mm/s	ε	w+ mm/s	H (T)						
Sextet 1	0.27	-0.017	0.16	47.7	6.4					
Sextet 2	0.67	-0.016	0.23	43.3	6.3					

Table 4.9. Room temperature fitted Mössbauer hyperfine parameters of mineral inclusions (ilmenite, amphibole, magnetite) from samples CAT 59 d and CAT=MY001C. Values with \* were fixed during the fitting process.

As demonstrated in Figure 4.18, the fitted spectrum for the sample (CMT 253) is complex, due to the multi-phase minerals present. It was fitted as magnetite with 2 sextets, which is a characteristic for magnetite (Waerenborgh *et al.*, 2002). The same sample also contains inclusion of ilmenite and amphibole, both with small areas (see fitting parameters and redox ratios in Table 4.10). However, sample (CX 12N) was fitted as hematite with 1 sextet.

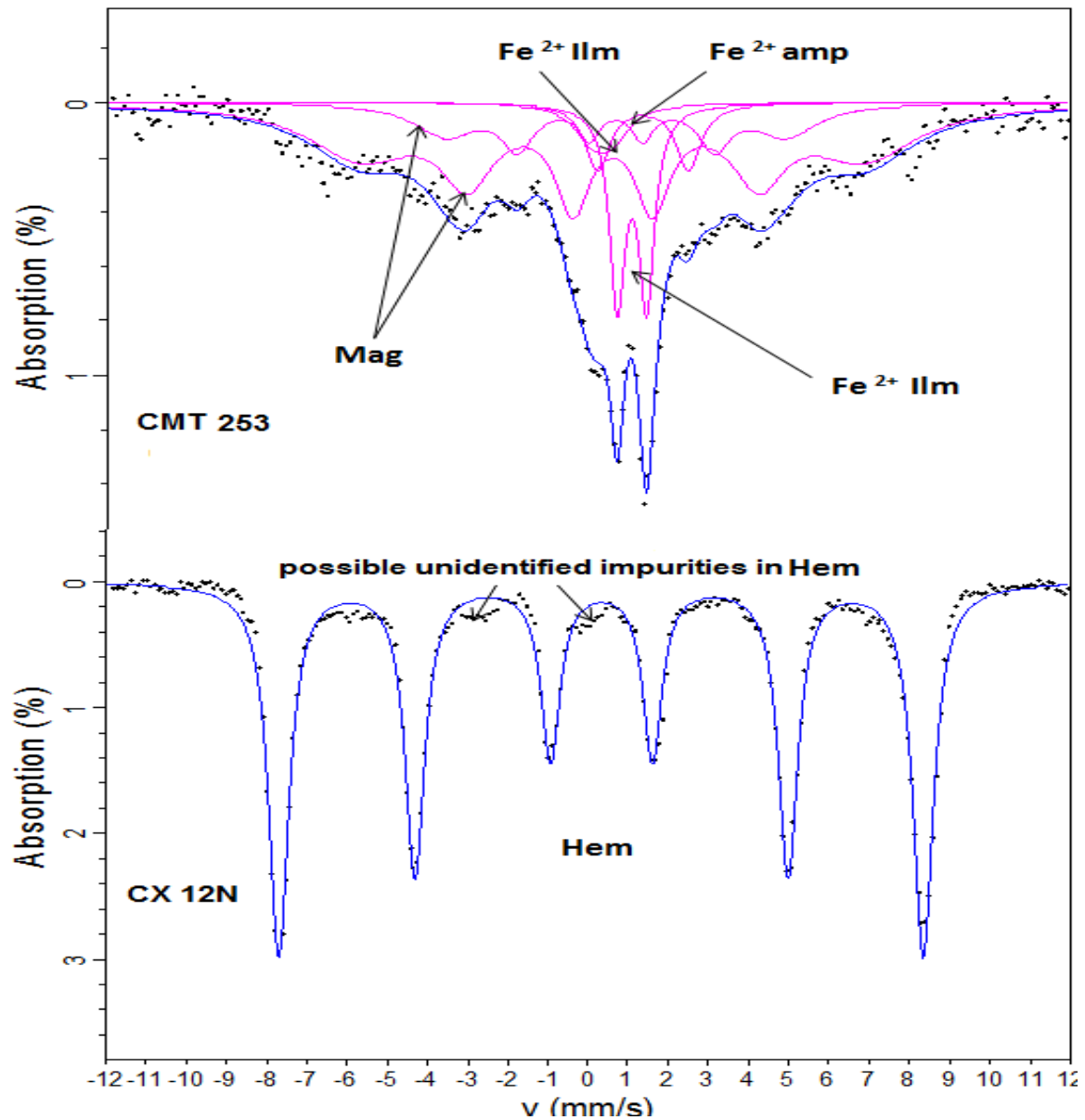


Figure 4.18. Room temperature fitted Mössbauer spectra of amphibole, ilmenite and magnetite inclusions from diamondiferous pipe of Camatxia (CMT 25, poorly magnetic phase) and hematite inclusion from Caixepa pipe (CX 12N). Possible presence of ilmenite in the sample.

Samples	Fe <sup>2+</sup>				Fe <sup>3+</sup>				Redox Ratio
	CS mm/s ±0.02	QS mm/s ±0.02	W mm/s ±0.02	Area % ±1	CS mm/s ±0.02	QS mm/s ±0.02	W mm/s ±0.02	Area % ±1	Fe <sup>3+</sup> /ΣFe ±0.02
Paramagnetic Sites									
CMT 253 Ilm phase	1.07*	0.73*	0.23*	13.7	0.32*	0.52*	0.52*	4.8	0.25
CMT 253 Amph phase	1.34	2.26	0.38	7.4					
Magnetic Sites									
Magnetic Sextets	CS mm/s	w+ mm/s	H (T)	Area %	CS mm/s	w+ mm/s	ε mm/s	H (T)	Area %
Sextet 1 (CMT 253)	0.59	0.53	38.9	56.0					
Sextet 2 (CMT 253)	0.67*	0.32	26.3	18.0					
Sextet 1 (CX 12N)	-	-	-	-	0.32	0.28	-0.006	49.6	100.0

Table 4.10. Room temperature hyperfine parameters of mineral inclusions (ilmenite, amphibole and magnetite) for Camatxia (CAT 253) and Caixepa (CX 12N) samples. Isomer shift (CS), quadrupole splitting (QS) line width of the high velocity peak (w+), low and high velocity line widths (w-/w+) = 1 to keep equal, line width of the most intense sextet peak (w3), effective hyperfine field (H) and relative site intensities area.

In Figure 4.19, the sample (CX 022) was fitted as hematite parameters with 2 sextets, which is not usual because Hematite contains one sextet (Waerenborgh *et al.*, 2002; and Greenwood and Gibb, 1971). The possible origin of the two sextets in this particular sample can be explained that the original magnetite was probably transformed into hematite through progressive oxidation of structural Fe<sup>2+</sup> to Fe<sup>3+</sup> (Santana *et al.*, 2001). See Chapter 5 for further interpretation and discussion for the reason why this hematite was fitted with 2 sextets. This sample also contains minor' inclusions of ilmenite, (see parameters and redox ratios in Table 4.11). But sample CX (027) in the same Figure 4.19 was fitted as magnetite.

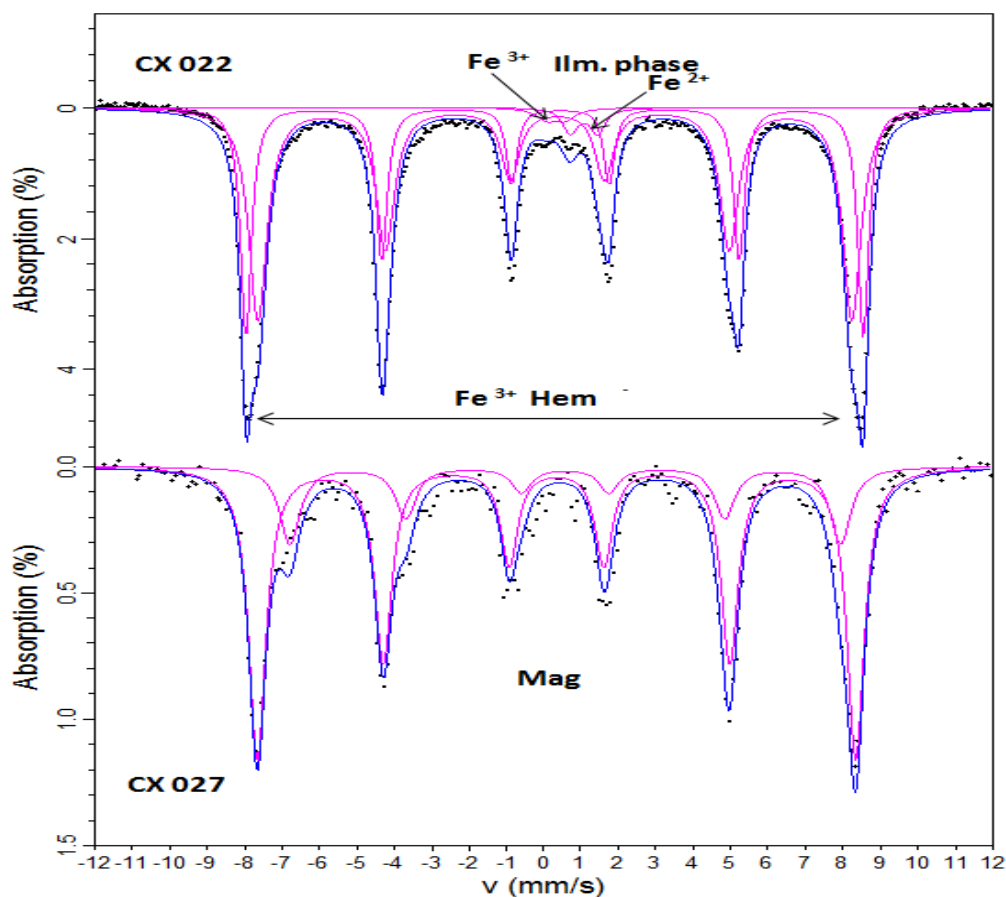


Figure 4.19. Room temperature fitted Mössbauer spectra of hematite (Hem) sample (CX 022) and magnetite (Mag), sample CX 027) inclusions from diamondiferous pipe of Caixepa.

Sample	Fe <sup>2+</sup>					Fe <sup>3+</sup>				Redox Ratio Fe <sup>3+</sup> /ΣFe ±0.02
	CS mm/s ±0.02	QS mm/s ±0.02	W mm/s ±0.02	Area %		CS mm/s ±0.02	QS mm/s ±0.02	W mm/s ±0.02	Area %	
Doublets 1 & 2 (CX 022)	1.07 *	0.73 *	0.25 *	2.9	----- -	0.32 *	0.52 *	0.35 *	1.8	0.37
Magnetic Sextets										
Magnetic Sextets	CS mm/s	w+ mm/s	ε mm/s	H (T)	Are a %	CS mm/s	w+ mm/s	ε mm/s	H (T)	Area %
Sextet 1 (CX 022)	-	-	-	-	-	0.32	0.29	-0.03	49.1	58.2
Sextet 2 (CX 022)	-	-	-	-	-	0.36	0.17	-0.07	51.1	37.1
Sextet 1 (CX027)	0.33	0.29	0	49.5	76.3	-	-	-	-	-
Sextet 2 (CX 027)	0.57	0.87	0	45.6	23.8	-	-	-	-	-

Table 4.11. Room temperature Mössbauer spectra of hematite (Hm) sample (CX 022) and magnetite (Mt), sample CX 027) inclusions from diamondiferous pipe of Caixepa. Data were fitted to two doublets Fe<sup>2+</sup> and Fe<sup>3+</sup> for ilmenite sample at CX 022 and sextets for Hematite and Magnetite.

Another complex result comes from sample (CW 0045D) in Figure 4.20. The result is complex because the sample is a multi-phase material with possibly more than 3 minerals (Hematite, Magnetite, ilmenite and amphibole). The fitting, carries notable uncertainty due to the poor signal (see more discussion in Chapter 5)

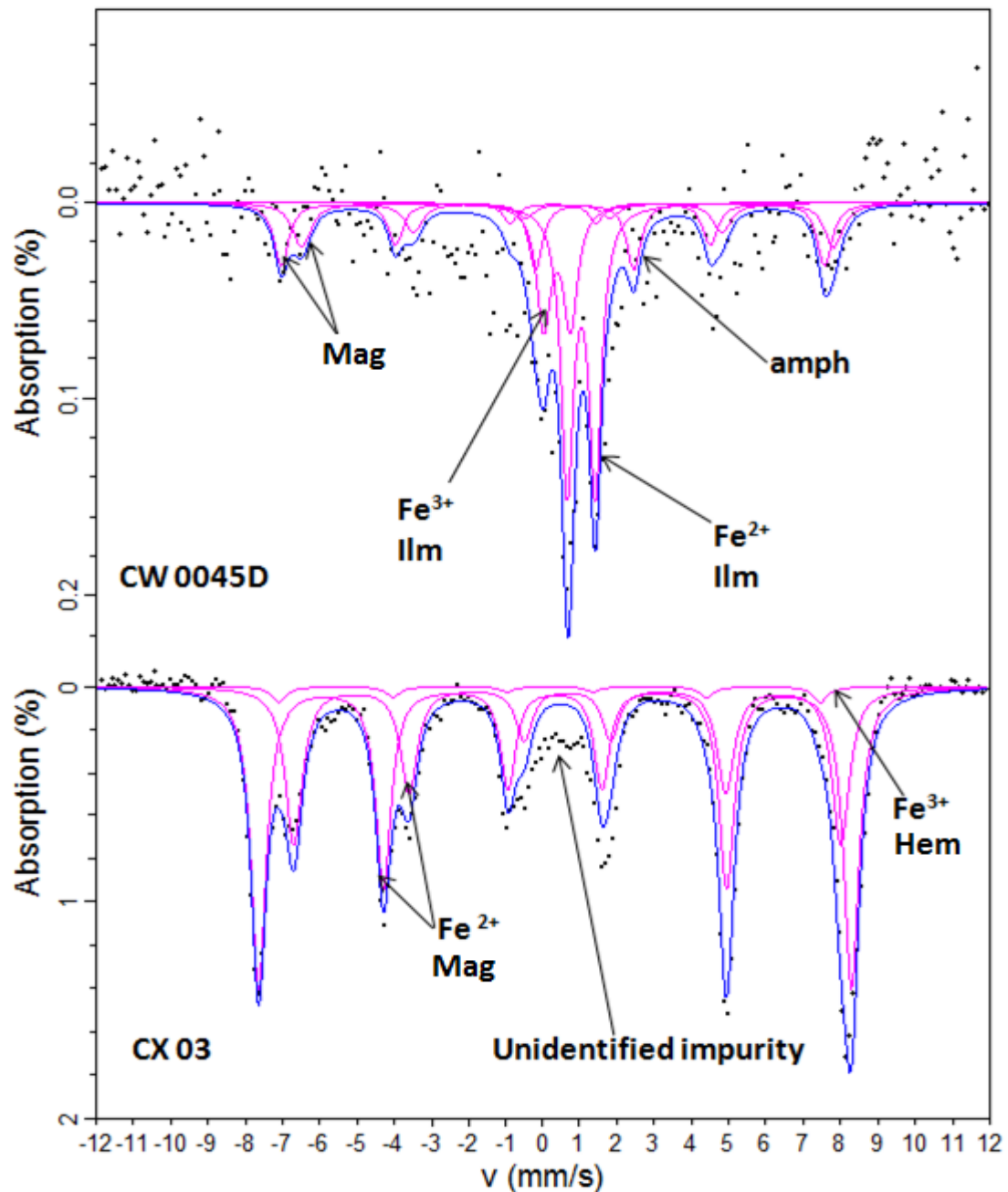


Figure 4.20. Room temperature fitted Mössbauer spectra of hematite (Hm) and ilmenite in sample (CW 0045D) from Camutue and magnetite (Mt) and hematite (Hm), sample (CX 03) from Caixepa diamondiferous pipes.

Samples	Fe <sup>2+</sup>				Fe <sup>3+</sup>				Redox Ratios
	CS mm/s ±0.02	QS mm/s ±0.02	W mm/s ±0.02	Area % ±1	CS mm/s ±0.02	QS mm/s ±0.02	W mm/s ±0.02	Area % ±1	Fe <sup>3+</sup> /ΣFe ±0.02
Paramagnetic Sites									
CW 0045D ilm phase	1.03*	0.80*	0.20*	19.7	0.45*	0.50	0.25*	11.5	0.36
CW 0045D Amph phase	0.82	2.50*	0.30*	25					0.31
Magnetic sites									
Magnetic site CW0045D	CS mm/s	εε	w+ mm/s	H (T)	Area %	-	-	-	-
Sextet 1	0.67*	0	0.30*	44.3	17.0	-	-	-	-
Sextet 2	0.27*	0	0.24*	45.2	19.0	-	-	-	-
Magnetic site CX03	CS mm/s	εε	w+ mm/s	H (T)		-	-	-	-
Sextet 1(Mag)	0.32	0	0.24	49.3	60.8	-	-	-	-
Sextet 1(Mag)	0.65	0	0.27	45.5	35.9	-	-	-	-
Sextet 2(Hem)	0.18	0	0.24*	45*	3.3	-	-	-	-

Table 4.12. Room temperature hyperfine parameters of mineral inclusions (hematite, magnetite, amphibole and ilmenite) Room temperature hyperfine parameters of mineral inclusion from Camutue (CW0045D) and Caixepa (CX 03) pipes determined from Mössbauer spectroscopy (CS→ centre shift; QS→ quadrupole splitting; W→ half width at half maximum). The parameters with asterisks were fixed during the fitting process.

<b>Order</b>	<b>Pipe D</b>	<b>Mössbauer</b>		<b>XRD</b>	<b>XRF</b>	<b>Viscosity</b>
Order	Depth, (m)	Name of Kimberlites	Sample Reference	Sample Reference	Sample Reference	Sample Reference
		Catoca pipe				
1	70	Catoca	CAT 62	Cat 62		
2	205	Catoca	CAT 115		CAT 115	
3	543	Catoca	CAT 58	Cat 58	CAT 58	
4	344	Catoca	CAT 59		CAT59 (3) IL	
5	613	Catoca	CAT 67	Cat 67	CAT67HM CAT67NMM	CAT 67
6	506	Catoca	CAT 50	Cat 50	CAT 50FM CAT 50HM CAT 50 IL	
7	300	Catoca	CAT 313		CAT 313	
8	250	Catoca	CAT 253		CAT 253	
9	191	Catoca	CAT 38		CAT 38	
10	115	Catoca	CAT 5			
11	70	Catoca		Cat 18	CAT 18	CAT 18
12	191	Catoca			CAT 38	
13	100	Catoca			CAT 63	
14	100	Catoca			CAT 61	
16		Caixepa pipe				
16	30	Caixepa	CX 022	CX 022	CX022	
17		Caixepa	CX 023			
18		Caixepa	CX 027	CX 027	CX 027	CX027
19	61	Caixepa	CX 012 & 012N			
20	57	Caixepa	CX009 and CX1		CX012	
21		Camutue Pipe				
22	110	Camutue	CM N (ca. novo)		CMN CAMUTUE	
23	140	Camutue	CW 045b		CM=CW45	CM=CW45
24	115	Camutue	CW 0045D	CW 0045D		
25	114	Camutue	CW 0045	CW 0045	CW45CM MG	
26	55	Camutue (CM)	CM			
27		Camatxia pipe				
28	95	Camatxia	CMT	CMT 02	CMT02	CMT02
29	122	Camatxia	CMT 05 CPX			
30	130	Camatxia	CN(c. novo)			CMT006
32	111	Camatxia	CMT 60	CMT 60	CMT 60 CMT 60 IL	CMT60
33	87	Camagico pipe Camagico	CMG	CMG 006	CMG006	
34	116	Camagico	CMG	CMG 171	CMG171	CMG171

Table 4.13. Summary of samples studied using advanced spectroscopic techniques

#### 4. 4. X-ray diffractometry (XRD) results

The XRD results are organised and presented according to phases. Many of the sample were not analysed by XRD, this is due to the limited amount of powder sample obtained from homogeneous mineral after being crushed. In most of these cases, samples were preferentially analysed directly by Mössbauer spectroscopy

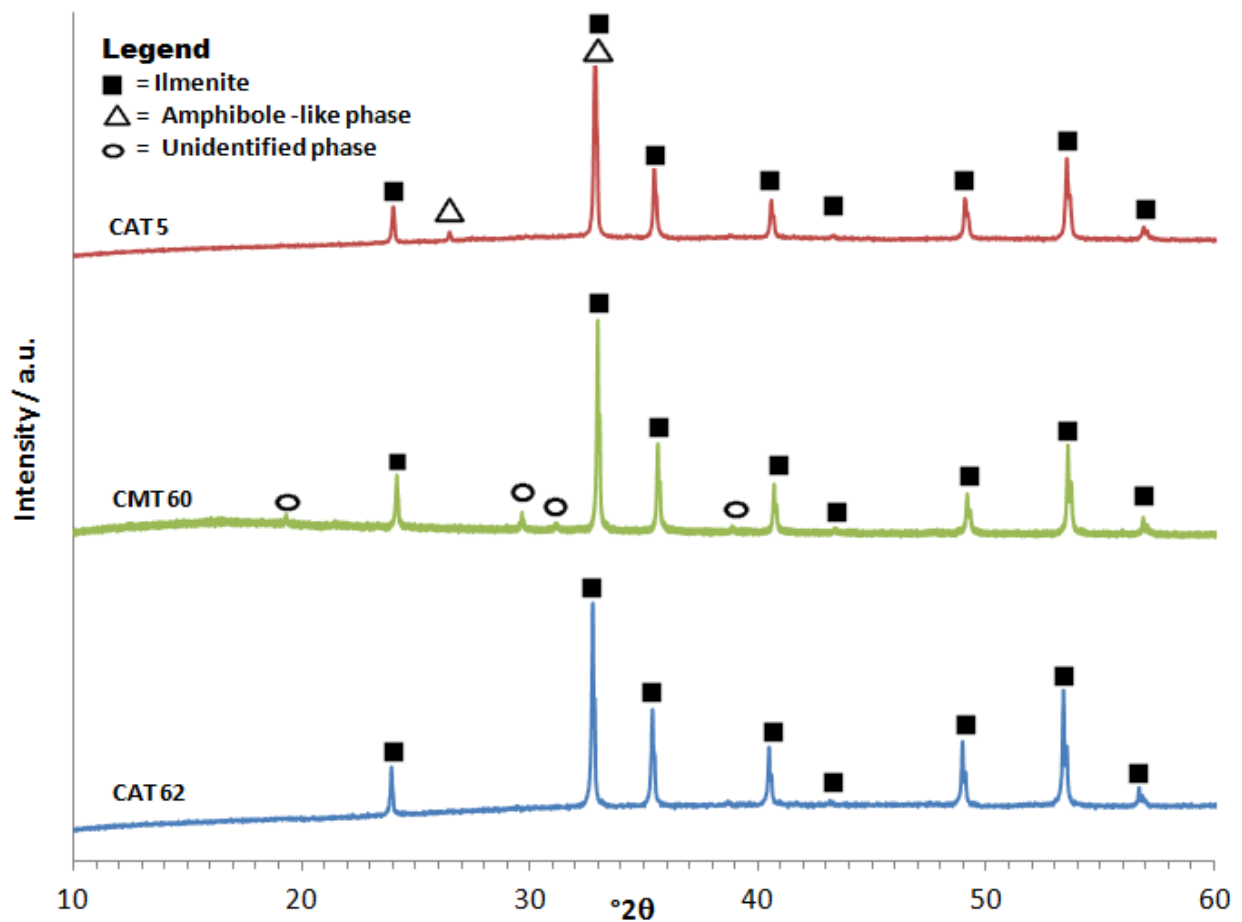


Figure 4.21. X-ray diffraction patterns of crystalline materials present in and studied kimberlite samples from Catoca pipe, samples CAT5 (order 10) and CAT62 (order 1) and Camatxia pipe sample CMT60 (order 32).

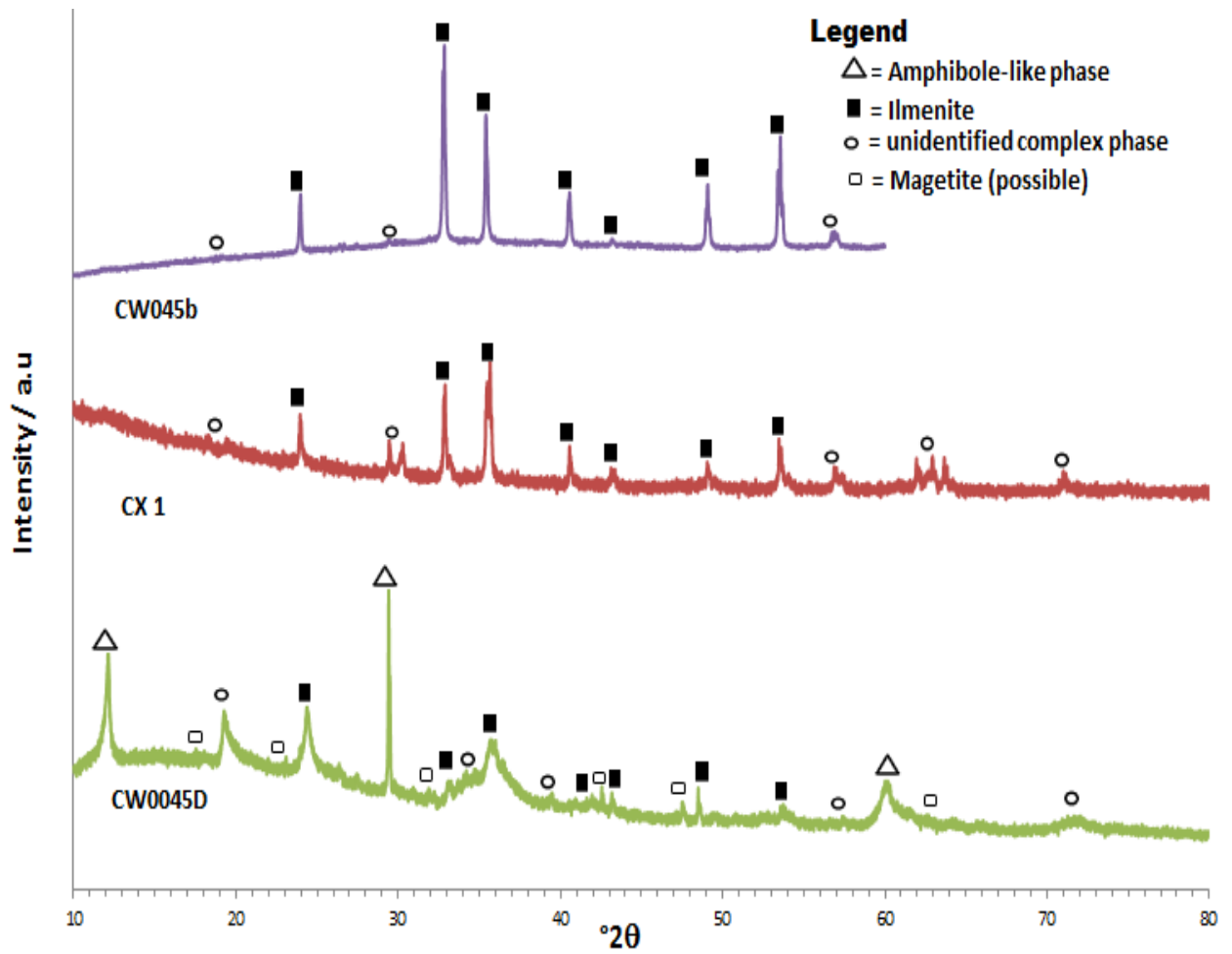


Figure 4.22. X-ray diffraction patterns of crystalline materials present and studied kimberlite samples from Camutue pipe, samples CW0045D (order 24), CW045b (order 23) and Caixepa pipe, sample CX 1 (order 20).

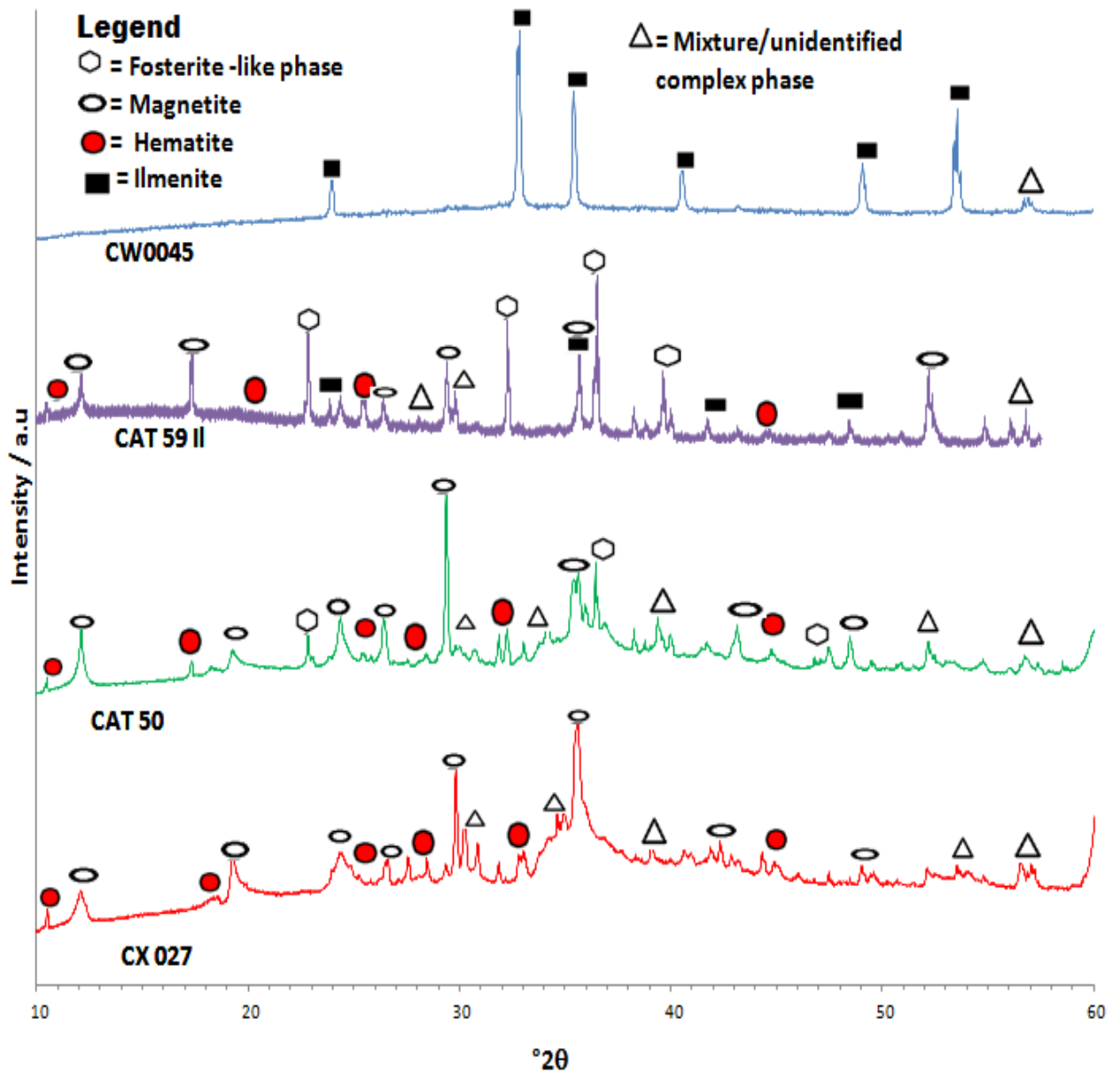


Figure 4.23. X-ray diffraction patterns of complex crystalline materials present in studied kimberlite samples from Caixepa pipe, samples CX027 (order 25), CX027 (order 18) and Catoca pipe, samples CAT 50 (order 6); CAT 59 ilm (order 6).

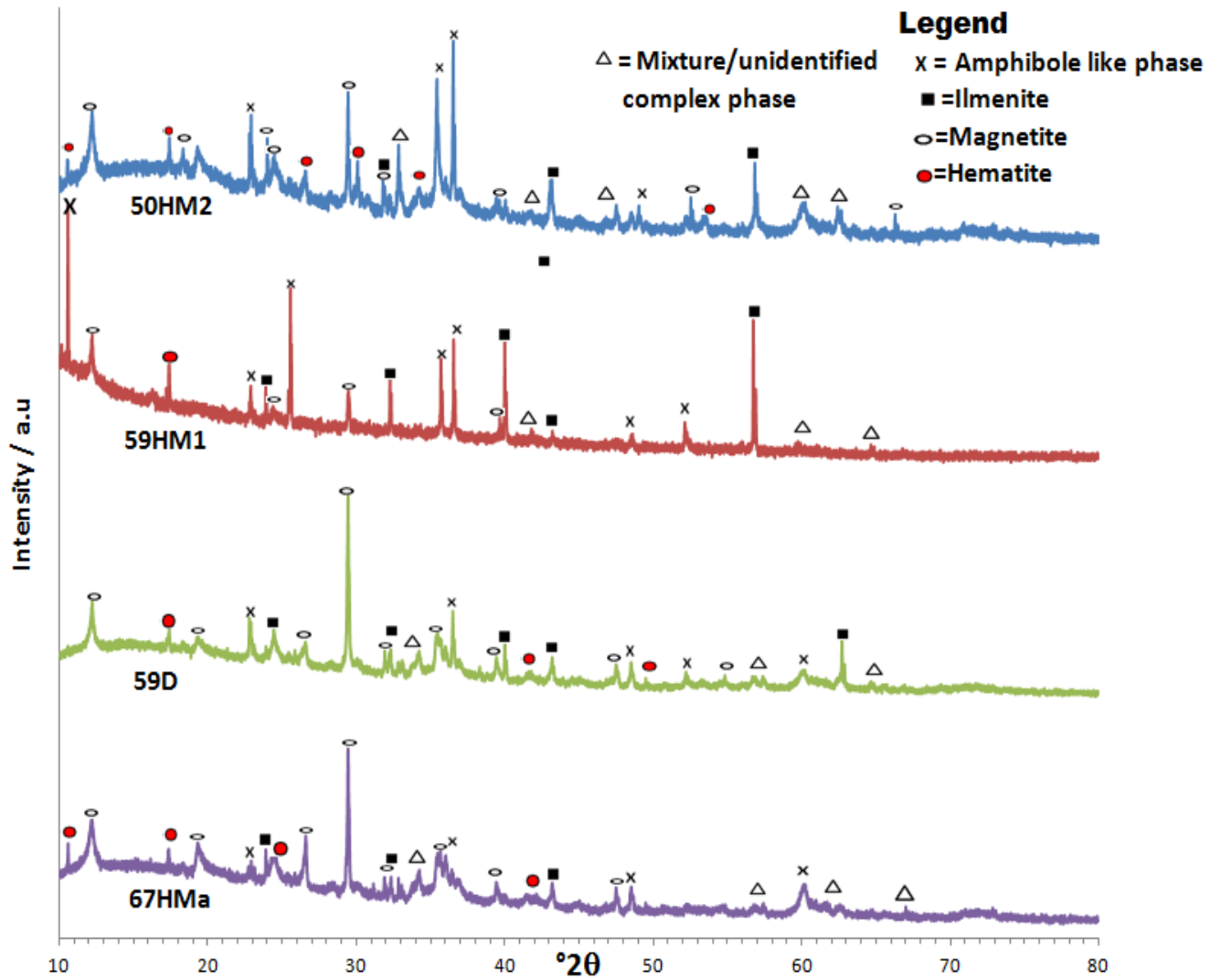


Figure 4.24. X-ray diffraction patterns of crystalline materials present in studied kimberlite samples from Catoca pipe, samples CAT 67HMa (order 5); 50HM2 (order 6), 59HM1 and 59D. This ilmenite contains minor inclusion of amphibole and an unidentified complex phase.

#### 4. 5. XRF (X-ray fluorescence) spectroscopy



Figure 4.25. Application process and sample preparation method for XRF analysis. Kimberlite rock (a), powdered rock (b), high temperature furnace instrument (c), melted powder rock ready (d) - for XRF analysis

Wt %	Sample CMN	Sample CAT 63	Sample CAT 38	Sample CX 027	Sample CAT 50	Sample CAT 313	Sample CAT 115	Sample CAT 253	Sample CAT 38
Na <sub>2</sub> O	0.00	0.05	0.27	0.18	0.76	0.67	0.21	0.14	0.41
MgO	10.48	10.15	14.02	32.85	36.11	5.34	6.01	8.36	10.72
Al <sub>2</sub> O <sub>3</sub>	0.62	0.21	0.58	3.93	3.74	0.26	0.47	0.36	0.35
SiO <sub>2</sub>	8.12	1.20	9.38	37.17	33.00	2.35	1.95	3.50	6.75
P <sub>2</sub> O <sub>5</sub>	0.03	0.04	0.09	0.38	1.39	0.12	0.00	0.08	0.05
SO <sub>3</sub>	0.00	0.00	0.00	0.21	0.20	0.04	0.00	0.02	0.03
K <sub>2</sub> O	0.02	0.01	0.08	0.37	1.05	0.04	0.01	0.05	0.00
CaO	1.03	0.18	0.72	3.82	6.48	0.47	0.40	0.21	1.01
TiO <sub>2</sub>	9.09	41.79	16.61	2.14	1.14	27.76	31.75	26.63	18.93
V <sub>2</sub> O <sub>5</sub>	0.31	0.49	0.41	0.05	0.03	0.56	0.63	0.57	0.42
Cr <sub>2</sub> O <sub>3</sub>	0.50	1.33	1.49	0.21	0.16	0.68	1.18	0.81	1.71
MnO	0.17	0.39	0.37	0.24	0.24	0.58	0.18	0.36	0.29
Fe <sub>2</sub> O <sub>3</sub>	69.23	43.41	55.12	17.98	14.84	60.02	55.97	57.88	58.46
ZnO	0.03	0.02	0.02	0.02	0.01	0.01	0.01	0.01	0.02
SrO	0.00	0.00	0.00	0.09	0.15	0.00	0.00	0.00	0.00
Y <sub>2</sub> O <sub>3</sub>	0.00	0.00	0.00	0.00	0.00	0.00	0.00	0.00	0.00
ZrO <sub>2</sub>	0.05	0.07	0.07	0.03	0.04	0.16	0.22	0.15	0.08
BaO	0.00	0.00	0.06	0.09	0.13	0.04	0.00	0.00	0.05
Total	99.67	99.34	99.28	99.74	99.46	99.10	98.99	99.13	99.28

Table 4.14. Semi- quantitative XRF analysis results (Fused bead) of kimberlite samples.

Wt %	Sample CAT 67	Sample CMT006	Sample CMT60	Sample CX027	Sample CMT02	Sample CMG171
Na <sub>2</sub> O	0.40	0.07	0.02	0.25	0.12	4.01
MgO	28.80	46.28	32.27	24.55	2.42	15.70
Al <sub>2</sub> O <sub>3</sub>	3.24	1.04	1.84	3.83	1.43	5.66
SiO <sub>2</sub>	32.66	40.72	34.95	39.89	80.19	39.16
P <sub>2</sub> O <sub>5</sub>	0.78	0.06	0.17	0.34	0.07	0.35
SO <sub>3</sub>	0.30	0.29	0.25	0.24	0.27	0.52
K <sub>2</sub> O	1.51	0.05	0.10	0.20	0.14	0.11
CaO	7.43	0.44	3.20	5.59	5.56	8.39
TiO <sub>2</sub>	1.09	0.06	1.26	1.01	0.09	2.17
V <sub>2</sub> O <sub>5</sub>	0.02	0.01	0.03	0.01	0.02	0.02
Cr <sub>2</sub> O <sub>3</sub>	0.12	0.48	0.15	0.11	0.52	0.07
Mn <sub>3</sub> O <sub>4</sub>	0.21	0.16	0.16	0.15	0.08	0.20
Fe <sub>2</sub> O <sub>3</sub>	10.11	7.37	11.53	9.75	3.93	9.72
ZnO	0.00	0.02	0.00	0.00	0.00	0.01
SrO	0.10	0.00	0.01	0.05	0.01	0.11
Y <sub>2</sub> O <sub>3</sub>	0.01	0.01	0.08	0.10	0.10	0.08
ZrO <sub>2</sub>	0.01	0.01	0.09	0.11	0.10	0.11
BaO	0.10	0.01	0.03	0.04	0.01	0.13
Total 1	86.86	97.04	86.15	86.22	95.06	86.50
LOI	13.55	5.49	15.11	13.78	6.24	11.76
Total 2	100.41	102.53	101.26	100.00	101.30	98.26

Table 4.15. Quantitative analyses ( Fused Bead) and Loss on Ignition ( LOI) measurement. Note that the Total 1 was obtained through the XRF before the calculation of Loss On Ignition (LOI) and Total 2 was obtained after the LOI.

#### 4. 6. EMPA (Electron micro probe -analysis)

The alteration characteristics of these diamond indicator minerals (ilmenite, garnet and pyroxene) from the studied diamond deposits were investigated by optical and electron probe microanalysis (EMPA). Optical microscopic and EMPA studies revealed that the alteration of these minerals proceeded along grain fractures and boundaries resulting in an amorphous (lacking a clear structure / not crystalline) to microcrystalline assemblage. The studied megacrysts have rounded anhedral to subhedral shapes which are attributed to abrasion during emplacement of the kimberlite magma. This study also reveals that the alteration of ilmenite and garnet leads to unstable phases, with complex elemental distribution patterns samples CAT 5 in Figures 4.26 (a, b and d) and CAT 62 in Figure 4.27 (c). The analysed megacrysts (Figures 4.26 and 4.27) occurred as individual crystals or intergrown grains of the same or different megacryst minerals showing partial re-crystallization, compositional zoning, and textures of polycrystalline megacrysts, all these features suggest megacrysts formed metasomatically before the emplacement of kimberlite magma. The origin of these magacrysts are associated with proto-kimberlite magma (see section 4.2) for more details), which

imply that they could be early crystallising pre-intrusion phenocryst in the recent kimberlite magma (Mitchell, 1977 and Kornprobst, 1984).

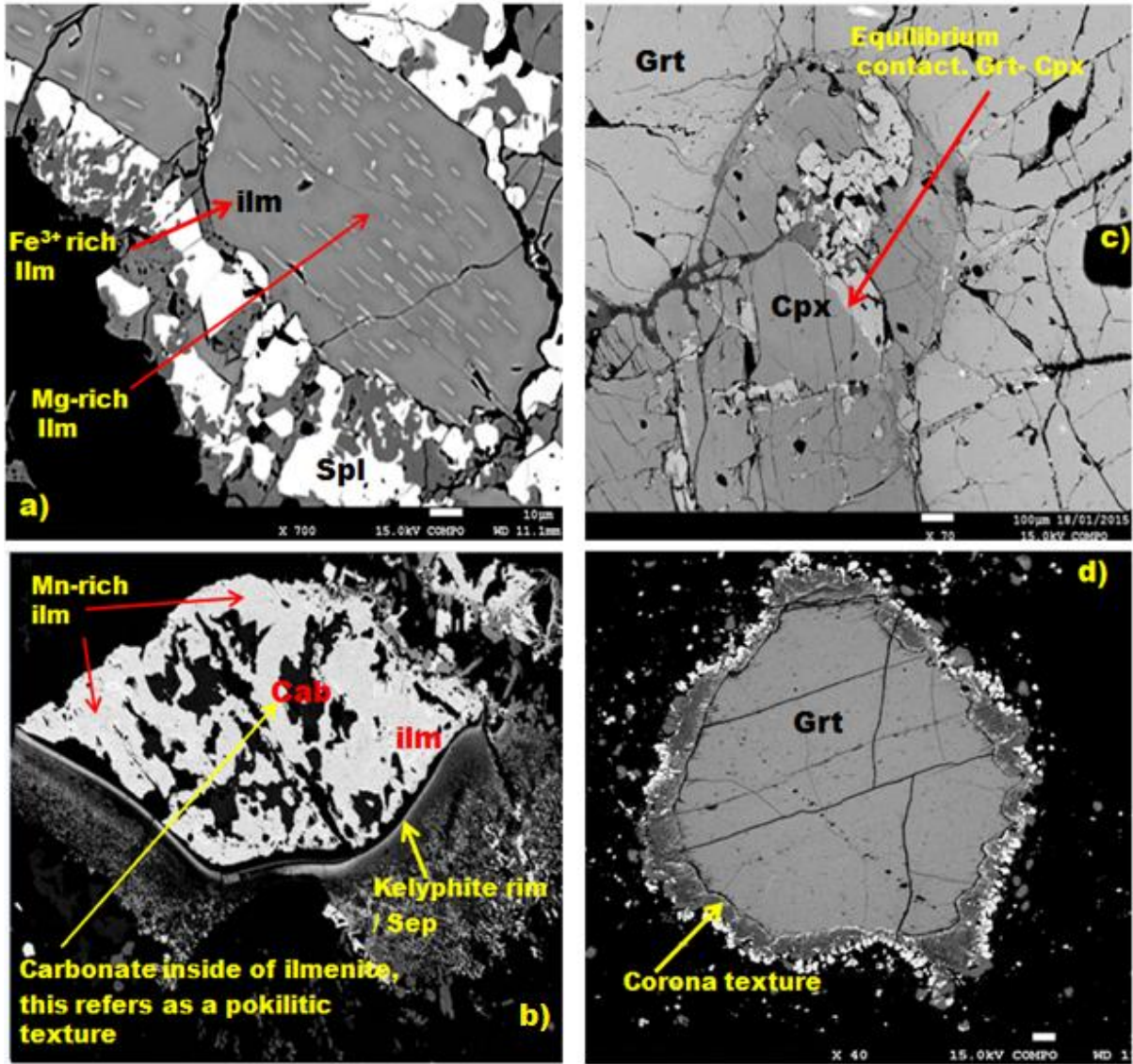


Figure 4.26. Electron Probe Micro-Analysis (EPMA), backscattered electron images (sample CAT 5) showing the mineral assemblage and metasomatic alterations processes in mantle-derived ilmenite, spinel and garnet/pyroxene. Replacements of ilmenite (a, b) and Garnet (c) and equilibrium contact between Grt and Cpx (d). Strongly anisotropic ilmenite and spinel.

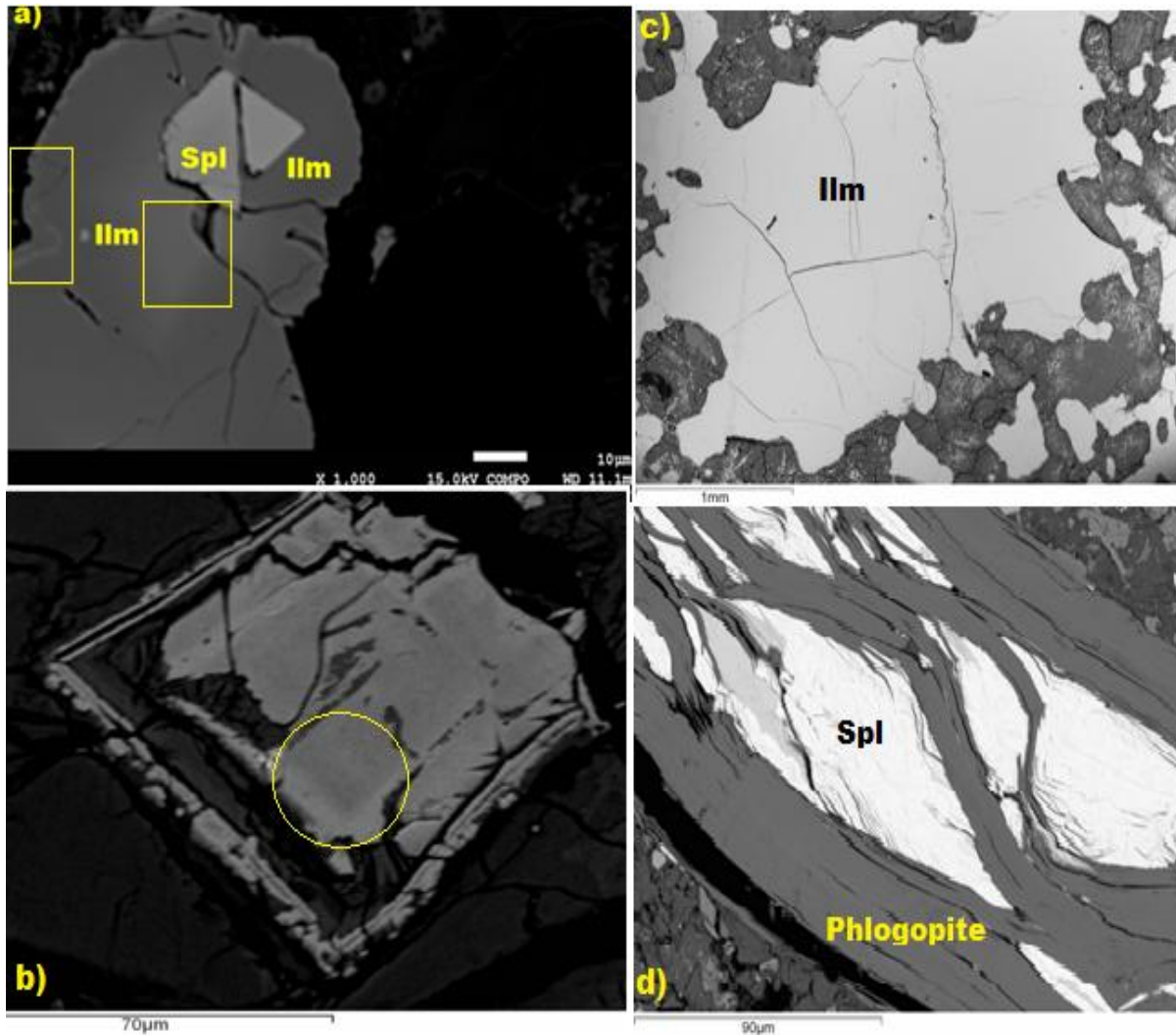


Figure 4.27. Electron Micro Probe -Analysis (EMPA), backscattered electron images (sample CAT 62) showing the mineral assemblage and metasomatic alterations processes in mantle-derived ilmenite and spinel (NE Angola). Replacements of ilmenite (a, b, c) and equilibrium contact between Ilm and Spl is at samples (a). Zoning features on Ilm are indicated in rectangle, square signs in sample (a) and Carbonate in circle sign at sample (b). Mechanical and chemical deformation at sample (d)

As demonstrated in Figure 4.28 the EMPA analytical results reveal that sample CX 030 consists of garnet, pyroxene, ilmenite, spinel, olivine and carbonate and phlogopite but serpentine and phlogopite has been found as less dominant minerals. This rock shows evidence of metasomatic alteration where the oxides minerals are altered (e.g. sample CX 030 b). Porphyritic or phyrict texture has been also identified, at samples CX 030a and 030b where phenocrysts of pyroxene and spinels are set in a fine-grained or intergranular matrix of carbonate and serpentine. These very fine grained materials are interpreted as groundmass which consequently supports the megacrysts. It is interesting to see that a hydrothermal texture is also present in this rock, where pyroxene (a,b) ilmenite and garnet (c) are undergoing replacement process, the newly forming minerals being difficult to discern due to the fluid reaction, and may have different chemical compositions from the pre-existing ones. Similar texture has been studied by El-Shazly (2004).

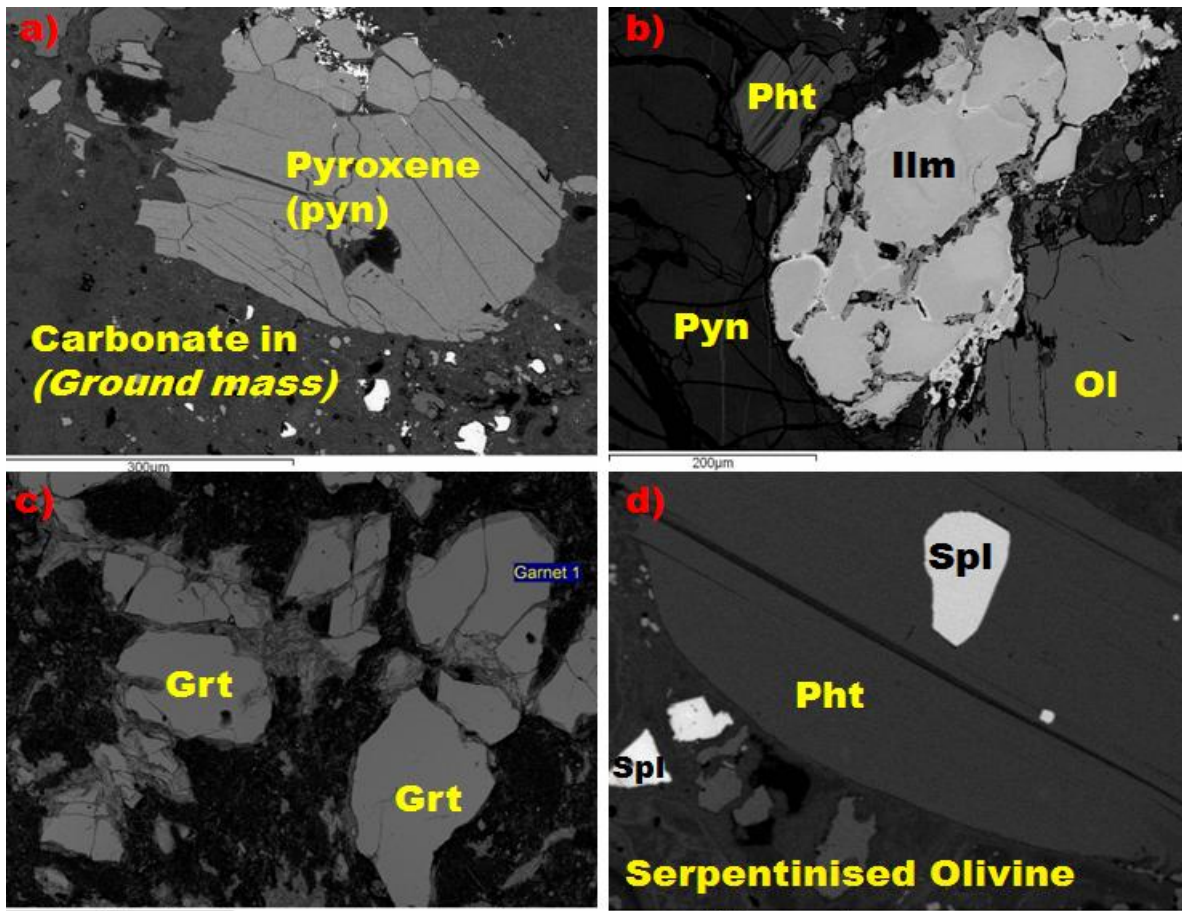


Figure 4.28. Backscattered electron images Analysis of kimberlite rock from Caixepa pipe (sample CX 030), showing the mineral assemblage and metasomatic alteration processes in mantle-derived ilmenite, spinel and garnet/pyroxene with replacement of ilmenite (a, b); garnet (c); and equilibrium contact between garnet and clinopyroxene (d). Images show strongly anisotropic ilmenite and spinel. Grt = garnet; Olv = olivine; Pyn = pyroxene; Spl = spinel; Pht = phlogopite; Ilm = ilmenite; Cab = carbonate; Sep = serpentine

**Table 4.16. EMPA of major chemical elements of ilmenite crystals from diamondiferous pipes of Catoca samples (Cat 62 and Cat 5) and Camatxia sample (CMT 60)**

<b>Catoca samples</b>										
<b>Sample name</b>	<b>TiO<sub>2</sub> wt.%</b>	<b>Al<sub>2</sub>O<sub>3</sub> wt.%</b>	<b>Cr<sub>2</sub>O<sub>3</sub> wt.%</b>	<b>Fe<sub>2</sub>O<sub>3</sub> wt.%</b>	<b>FeO wt.%</b>	<b>MnO wt.%</b>	<b>MgO wt.%</b>	<b>CaO wt.%</b>	<b>Total wt.%</b>	<b>Fe=Fe O wt.%</b>
CAT 5	38.55	0.00	2.18	26.43	25.22	0.24	5.13	0.01	97.83	49.01
CAT 5	38.41	0.00	2.13	26.83	24.71	0.24	5.34	0.01	97.74	48.86
CAT5	38.76	0.00	2.16	25.25	26.42	0.22	4.57	0.01	97.48	49.15
CAT 5	38.96	0.00	2.15	25.05	25.44	0.20	5.25	0.01	97.09	47.99
CAT 5	38.63	0.95	2.18	27.62	23.08	0.36	6.31	0.00	99.21	47.94
CAT 62	39.04	0.00	2.18	24.79	26.50	0.19	4.67	0.01	97.49	48.81
CAT 62	38.20	0.00	2.08	28.61	23.43	0.30	5.92	0.01	98.62	49.18
CAT 62	39.26	0.16	2.18	24.98	25.47	0.27	5.35	0.01	97.73	47.96
CAT 62	38.75	0.92	2.14	25.13	25.58	0.22	5.02	0.01	97.88	48.20
CAT 62	40.22	0.68	2.24	24.23	21.76	0.29	7.88	0.02	97.38	43.57
CAT 62	41.63	0.00	2.34	18.41	28.26	0.22	4.98	0.02	95.95	44.83
CAT 62	41.52	1.75	2.36	18.99	27.89	0.17	5.15	0.01	97.96	44.99
CAT 62	41.70	0.26	2.41	18.74	27.99	0.19	5.15	0.01	96.62	44.86
CAT 62	41.73	0.00	2.38	18.01	27.59	0.29	5.36	0.02	95.48	43.80
CAT 62	41.31	0.00	2.36	19.41	27.69	0.19	5.15	0.02	96.22	45.16
CAT 62	41.35	0.69	2.31	18.45	27.67	0.24	5.13	0.05	95.99	44.28
CAT 62	41.30	0.00	2.28	18.70	28.58	0.19	4.63	0.03	95.81	45.41
CAT 62	41.35	0.69	2.31	18.45	27.67	0.24	5.13	0.05	95.99	44.28
CAT 62	41.20	0.03	2.29	18.37	28.67	0.17	4.56	0.03	95.40	45.20
CAT 62	41.27	0.00	2.33	18.6	28.45	0.21	4.68	0.02	95.73	45.25
CAT 5	37.78	0.04	0.27	27.73	25.94	1.31	3.76	0.01	96.88	50.90
CAT 5	38.34	0.27	0.31	27.01	26.96	0.27	4.04	0.01	97.29	51.27
<b>Continue of Table 4.16. EMPA of major chemical elements of ilmenite crystals. Catoca samples (Cat 62 and Cat 5)</b>										
CAT 5	37.99	1.07	0.29	27.38	27.33	0.18	3.72	0.01	98.01	51.97
CAT 5	37.76	0.03	0.26	28.22	26.66	0.37	3.87	0.00	97.24	52.06
CAT 5	37.69	0.03	0.26	28.51	26.37	0.38	4.01	0.01	97.28	52.02
CAT 5	37.35	0.00	0.28	29.03	24.45	1.90	4.02	0.03	97.11	50.58
CAT 5	38.14	0.00	0.25	26.98	26.93	0.19	4.01	0.00	96.55	51.22
CAT 5	37.66	0.00	0.25	28.10	26.14	0.80	3.87	0.02	96.87	51.43
CAT 62	36.36	0.00	1.33	36.05	15.15	0.36	9.61	0.02	98.95	47.60
CAT 62	36.13	0.04	1.32	34.68	17.17	0.34	8.37	0.01	98.14	48.38
CAT 62	35.97	0.00	1.32	32.27	22.18	0.20	5.55	0.01	97.59	51.23
CAT 5	36.01	0.00	1.33	30.17	25.20	0.15	3.91	0.01	96.86	52.35
CAT 5	37.73	0.00	0.20	29.06	27.03	0.24	3.74	0.01	98.04	53.19
CAT 5	37.64	0.00	0.19	29.44	26.96	0.21	3.73	0.00	98.23	53.45
CAT 5	37.83	0.00	0.19	29.10	27.12	0.14	3.80	0.00	98.21	53.31
CAT 5	37.319	0.00	0.15	29.38	26.64	0.20	3.75	0.00	97.49	53.08

CAT 5	37.64	0.00	0.19	29.39	26.39	0.27	4.03	0.00	97.95	52.84
CAT 5	37.81	1.40	0.19	29.18	26.93	0.19	3.81	0.01	99.66	53.19
CAT 5	37.13	0.00	0.34	30.73	26.23	0.18	3.88	0.00	98.59	53.88
CAT 5	37.20	0.00	0.32	30.62	26.44	0.15	3.83	0.01	98.61	54.00
CAT 5	37.20	0.00	0.34	30.57	26.51	0.16	3.78	0.01	98.65	54.02
CAT 5	37.40	0.00	0.35	29.92	26.76	0.14	3.77	0.00	98.40	53.68
CAT 5	37.17	0.00	0.33	30.51	26.40	0.15	3.83	0.01	98.46	53.86
CAT 62	39.65	0.20	0.20	23.50	27.85	0.76	3.94	0.01	96.15	49.00
CAT 62	39.43	0.00	0.25	23.96	28.51	0.23	3.75	0.00	96.18	50.07
CAT 5	38.54	0.00	0.19	28.37	24.41	2.23	4.48	0.01	98.25	49.95
CAT 5	36.62	0.00	2.02	29.11	24.42	0.62	4.40	0.00	97.27	50.62
CAT 5	36.64	0.93	2.08	29.05	25.49	0.13	4.06	0.00	98.51	51.64
CAT 5	36.81	0.19	2.01	29.01	25.35	0.46	4.04	0.01	98.00	51.46
CAT 5	36.75	0.65	1.98	29.53	24.43	0.67	4.43	0.00	98.53	51.00
CAT 62	46.68	0.08	2.44	11.45	29.28	0.38	6.88	0.00	97.27	39.59
CAT 62	45.78	0.35	2.52	12.45	30.45	0.33	5.76	0.01	97.79	41.66
CAT 62	46.41	0.12	2.49	12.80	27.34	0.81	7.57	0.01	97.65	38.86
CAT 62	45.53	0.00	0.98	13.54	31.14	0.26	5.33	0.01	96.86	43.33
CAT 62	46.15	0.48	0.96	14.04	28.83	0.27	6.88	0.01	97.76	41.47
<b>Continue of Table 4.16. EMPA of major chemical elements of ilmenite crystals Catoca samples (Cat 62 and Cat 5)</b>										
CAT 62	46.13	0.00	0.95	11.95	32.11	0.26	5.04	0.02	96.58	42.87
CAT 5	36.82	0.00	0.91	30.45	25.74	0.22	3.95	0.00	98.24	53.14
CAT 5	36.92	0.00	0.89	30.36	25.42	0.61	4.00	0.01	98.27	52.74
CAT 5	37.12	0.00	0.86	30.85	24.30	0.60	4.74	0.00	98.53	52.06
CAT 5	35.51	0.97	0.51	32.75	26.10	0.17	3.15	0.00	99.24	55.58
CAT 5	35.07	0.00	0.49	33.73	25.10	0.14	3.53	0.01	98.08	55.45
CAT 5	34.54	0.00	0.46	34.54	23.93	0.20	3.85	0.03	97.60	55.01
CAT 5	35.79	1.56	0.52	33.67	23.19	0.11	4.94	0.00	99.90	53.49
CAT 5	35.38	0.04	0.20	34.00	26.21	0.21	3.02	0.01	99.11	56.81
CAT 5	35.03	0.00	0.19	34.29	25.92	0.22	3.00	0.00	98.68	56.77
CAT 5	35.62	0.00	0.17	33.61	26.17	0.20	3.17	0.01	98.97	56.41
CAT 5	34.64	0.01	0.53	34.47	25.17	0.12	3.28	0.01	98.26	56.19
CAT 5	34.62	0.62	0.58	33.56	25.39	0.18	3.08	0.01	98.14	55.60
CAT 5	35.64	0.00	0.62	29.01	27.35	0.11	2.55	0.01	95.36	53.46
CAT 5	34.50	0.91	0.58	34.79	23.58	0.30	3.99	0.01	98.71	54.89
CAT 62	43.56	0.00	1.60	17.24	28.75	0.14	5.70	0.03	97.15	44.27
CAT 62	46.72	0.00	1.87	14.48	26.80	0.25	8.35	0.02	98.57	39.84
CAT 62	45.38	0.00	2.27	14.85	27.86	0.25	7.08	0.02	97.80	41.23
CAT 62	47.52	0.00	2.26	13.13	25.19	0.32	9.61	0.03	98.13	37.01
CAT 62	45.70	0.00	2.26	14.52	26.01	0.37	8.16	0.05	97.22	39.08
CAT 5	38.76	0.00	0.51	27.74	26.9	0.18	4.32	0.00	98.50	51.91
CAT 5	38.55	0.00	0.45	28.29	26.75	0.20	4.32	0.01	98.58	52.21
CAT 5	38.78	1.54	0.56	27.99	26.81	0.19	4.34	0.01	100.3 6	52.00

CAT 5	38.78	0.00	0.49	27.99	27.02	0.24	4.27	0.00	98.83	52.22
Cat 62	41.26	1.015	0.35	23.56	21.79	0.30	8.35	0.04	96.78	43.00
Cat 62	37.40	0.88	1.80	29.11	25.37	0.21	4.51	0.00	99.34	51.57
CAT 5	37.08	0.00	1.73	29.35	25.05	0.22	4.52	0.00	98.01	51.47
<b>Continue of Table 4.16. EMPA of major chemical elements of ilmenite crystals. Catoca samples (Cat 62 and Cat 5)</b>										
CAT 5	37.41	0.00	1.80	29.07	25.40	0.22	4.48	0.00	98.46	51.57
CAT5	37.36	0.00	1.79	29.07	25.35	0.19	4.523	0.00	98.32	51.51
CAT 5	36.69	0.07	0.78	30.96	25.96	0.17	3.832	0.00	98.52	53.82
CAT 5	36.65	0.00	0.77	31.39	25.86	0.16	3.872	0.00	98.78	54.11
CAT 5	36.57	0.00	0.79	31.20	25.81	0.17	3.872	0.010	98.45	53.89
CAT 5	36.63	0.00	0.84	31.15	25.92	0.22	3.812	0.00	98.62	53.96
CAT 5	36.85	0.65	0.82	30.54	26.17	0.17	3.782	0.01	99.09	53.66
CAT 62	35.34	0.00	1.93	32.38	24.14	0.17	4.183	0.01	98.19	53.28
CAT 5	35.20	0.00	1.91	32.35	24.31	0.16	3.962	0.01	98.04	53.42
CAT 62	35.33	0.00	1.86	32.39	24.20	0.18	4.132	0.01	98.14	53.34
CAT 62	35.42	0.24	1.96	32.36	24.46	0.16	4.042	0.00	98.70	53.59
CAT 5	35.80	0.00	1.85	31.71	24.74	0.17	4.062	0.01	98.41	53.28
<b>Continue of Table. 4.16. EMPA of major chemical elements of ilmenite crystals. Camatxia sample (CMT 60)</b>										
<b>Sample name</b>	<b>TiO<sub>2</sub> wt.%</b>	<b>Al<sub>2</sub>O<sub>3</sub> wt.%</b>	<b>Cr<sub>2</sub>O<sub>3</sub> wt.%</b>	<b>Fe<sub>2</sub>O<sub>3</sub> wt.%</b>	<b>FeO wt.%</b>	<b>MnO wt.%</b>	<b>MgO wt.%</b>	<b>CaO wt.%</b>	<b>Total wt.%</b>	<b>Fe=FeO wt.%</b>
CMT 60	47.42	0.00	0.64	16.61	25.87	0.45	9.09	0.02	100.23	40.82
CMT 60	47.13	0.53	0.67	16.65	25.44	0.55	9.14	0.04	100.22	40.42
CMT 60	47.40	0.00	0.67	17.07	24.97	0.49	9.54	0.02	100.32	40.34
CMT 60	47.47	0.61	0.65	16.82	25.23	0.52	9.41	0.03	100.89	40.36
CMT 60	54.63	0.00	0.00	5.97	27.37	0.73	11.74	0.02	100.56	32.74
CMT 60	54.75	1.25	0.00	5.17	29.88	0.30	10.65	0.04	102.08	34.53
CMT 60	55.31	0.00	0.01	4.81	28.78	0.54	11.39	0.04	100.96	33.11
CMT 60	54.87	0.85	0.00	5.78	28.29	0.61	11.42	0.03	101.90	33.49
CMT 60	53.57	0.00	0.03	7.79	27.10	0.75	11.34	0.04	100.69	34.11
CMT 60	51.43	0.00	1.05	11.75	22.90	0.67	12.63	0.02	100.63	33.48
CMT 60	51.21	0.69	1.00	11.58	22.92	0.73	12.51	0.02	100.77	33.34
CMT 60	51.29	0.25	1.05	11.50	23.08	0.68	12.47	0.02	100.47	33.43
CMT 60	51.51	0.28	1.02	11.61	23.20	0.72	12.48	0.05	101.00	33.66
CMT 60	51.54	0.00	1.00	11.31	23.12	0.69	12.58	0.03	100.38	33.30
CMT 60	46.34	0.00	0.06	18.89	25.67	0.36	8.72	0.02	100.16	42.67
CMT 60	50.63	0.00	0.02	12.23	27.08	0.54	9.99	0.04	100.61	38.09
CMT 60	51.45	0.00	0.01	11.11	26.84	0.55	10.546	0.03	100.62	36.84
CMT 60	54.41	0.00	0.00	6.48	27.35	0.71	11.64	0.04	100.71	33.18
CMT 60	55.08	0.23	0.00	4.80	28.23	0.57	11.58	0.04	100.60	32.560
CMT 60	45.50	0.00	0.06	20.53	25.62	0.46	8.26	0.04	100.57	44.09
CMT 60	45.59	0.00	0.09	21.09	23.64	0.72	9.16	0.09	100.62	42.63
CMT 60	52.99	0.07	1.20	9.96	22.16	0.94	13.51	0.27	101.26	31.13
CMT 60	53.20	1.30	1.07	9.79	22.21	0.95	13.67	0.18	102.50	31.02
CMT 60	52.80	0.48	1.04	9.61	22.99	0.97	13.05	0.10	101.20	31.65

CMT 60	52.96	0.07	1.23	9.12	23.26	0.96	12.94	0.17	100.87	31.47
CMT 60	52.88	0.00	1.32	9.20	23.35	1.08	12.87	0.04	100.89	31.63
CMT 60	52.58	0.00	1.29	9.47	23.34	1.04	12.74	0.05	100.67	31.87

Table 4.16. Summary of Electron Probe Micro-Analysis (EPMA) of major chemical elements of ilmenite crystals from diamondiferous pipes. Catoca samples (Cat 62 and Cat 5) are in normal text and the Camatxia sample (CMT 60) is in italic text.

The lower Ti and excess Fe<sup>3+</sup> observed in the analysed ilmenite sample (Table 4.16), reflects the evidence of oxidised ilmenite. The oxidised sample of ilmenite was also studied by Waerenborgh *et al.* (2002). The EMPA chemical analysis results (Table 4.16) are comparable with reported previously in the literature for natural ilmenite (Gibb and Greenwood, 1969).

As shown in table 4.16 mineral chemistry by EMPA (electron micro probe -analysis) revealed some reduction of TiO<sub>2</sub>, MgO, Al<sub>2</sub>O<sub>3</sub>, Cr<sub>2</sub>O<sub>3</sub>, MnO and CaO, in the altered products ilmenite grains probably during weathering/transformation leading to the formation of leucoxene. According to (Deysel, 2007), leucoxene is fine granular material which is formed through extensive transformation or weathering of ilmenite that removes iron and increases the titanium content of the mineral grains (Rao and Rao, 1965).

Despite the analysed rock (CAT-18, see Table 4.17) is being considered as a mantle eclogite rock, but a group of cluster analyses of mantle lherzolite (peridotite) garnet data which is rich in Cr (see Table 4.17) were identified in this rock (CAT-18). For example the analysed garnet data Cr<sub>2</sub>O<sub>3</sub> (7.61%); Cr<sub>2</sub>O<sub>3</sub> (7.60%); Cr<sub>2</sub>O<sub>3</sub> (7.50%); Cr<sub>2</sub>O<sub>3</sub> (6.90%) and Cr<sub>2</sub>O<sub>3</sub> (6.85%) they may be from lherzolic garnet (G9). This result is in the agreement of lherzolites or G9 garnets analysed by Gurney and Moore, (1993). The low magnesium oxides analysed in this sample, e.g analysed data MgO (2.38%); MgO (2.34%); MgO (2.32%); MgO (2.35%) with elevate percentage of FeO (see Table 4.17) are interpreted as a almandine garnet or crustal garnet. This rock CAT 18 ( see Figure 3.5 (a)) is primary mantle rock, formed at great depth and lately transported by kimberlite magma from deep mantle depth to the surface, conqently some minor inclusion of the cluster of almandine garnet or crustal garnet are present in the CAT 18. It is questionable that some analysed data with low FeO content of 3-4% are probably classified as garnets

Table. 4.17 EMPA analysis of garnet for mantle xenoliths, E-type (Cat-18), Catoca pipe.

FeO wt.%	MnO wt.%	MgO wt.%	CaO wt.%	TiO <sub>2</sub> wt.%	SiO <sub>2</sub> wt.%	Al <sub>2</sub> O <sub>3</sub> wt.%	Cr <sub>2</sub> O <sub>3</sub> wt.%
11.66	0.32	19.55	3.22	0.09	41.75	23.25	0.08
11.97	0.31	19.51	3.16	0.15	41.58	23.20	0.04
11.86	0.32	19.53	3.15	0.15	41.47	23.20	0.08
11.89	0.32	19.59	3.14	0.14	41.57	23.23	0.08
11.26	0.36	19.87	3.27	0.10	41.78	23.22	0.11
12.00	0.30	19.36	3.15	0.15	41.63	23.19	0.05
3.25	0.04	12.87	16.87	0.37	54.6	5.98	0.11
3.33	0.06	12.79	16.60	0.39	54.74	6.22	0.14
3.23	0.04	12.91	16.85	0.37	54.68	5.95	0.10
3.21	0.04	12.68	16.68	0.40	54.85	6.26	0.05
12.07	0.33	19.36	3.16	0.14	41.53	23.15	0.04
11.76	0.30	19.55	3.12	0.14	41.76	23.03	0.06
11.43	0.29	19.72	3.14	0.10	41.62	23.28	0.09
11.92	0.32	19.50	3.13	0.12	41.60	23.17	0.09
11.97	0.31	19.47	3.13	0.13	41.66	23.18	0.04
11.82	0.28	19.50	3.10	0.15	41.71	23.15	0.04
11.81	0.33	19.56	3.13	0.16	41.68	23.12	0.07
11.89	0.31	19.56	3.14	0.13	41.66	23.13	0.07
11.72	0.31	19.73	3.15	0.11	41.69	23.16	0.12
11.57	0.34	19.55	3.21	0.10	41.59	23.24	0.08
3.21	0.06	12.62	16.51	0.37	54.93	6.36	0.12
3.22	0.04	12.84	16.77	0.38	54.73	6.00	0.17
36.90	0.20	2.38	3.75	0.05	37.11	21.08	0.00
36.72	0.22	2.34	3.92	0.05	37.11	20.93	0.00
36.40	0.22	2.32	4.20	0.07	37.18	21.10	0.02
36.36	0.22	2.35	4.18	0.06	37.12	20.98	0.01
3.40	0.03	8.16	12.18	0.33	54.92	11.75	0.02
3.52	0.01	8.32	12.30	0.38	54.92	11.35	0.03
3.60	0.04	8.37	12.31	0.38	54.92	11.42	0.04
16.23	0.28	12.29	8.36	0.30	40.19	22.14	0.00
16.46	0.27	12.55	7.80	0.30	40.21	22.14	0.01
16.52	0.27	12.53	7.79	0.30	40.19	22.08	0.02
16.46	0.28	12.52	7.76	0.28	40.22	22.24	0.01
16.54	0.26	12.22	8.43	0.31	40.19	22.27	0.02
16.39	0.28	12.51	7.98	0.23	40.04	22.51	0.03
16.31	0.29	11.57	9.26	0.21	40.17	22.07	0.03
16.28	0.28	11.55	9.27	0.20	39.98	22.27	0.02
16.25	0.28	11.58	9.19	0.21	40.07	22.29	0.01
16.37	0.28	12.00	8.67	0.28	40.13	21.92	0.03
16.26	0.28	11.74	8.93	0.21	40.25	22.30	0.01
16.35	0.26	11.86	8.95	0.22	40.31	22.38	0.01
16.45	0.28	12.55	7.87	0.31	40.21	22.28	0.03

FeO wt. %	MnO wt. %	MgO wt. %	CaO wt. %	TiO <sub>2</sub> wt. %	SiO <sub>2</sub> wt. %	Al <sub>2</sub> O <sub>3</sub> wt. %	Cr <sub>2</sub> O <sub>3</sub> wt. %
16.51	0.27	12.54	7.89	0.29	40.40	22.14	0.03
16.52	0.29	12.41	8.32	0.30	40.33	22.15	0.03
16.38	0.26	12.38	8.06	0.28	40.22	22.25	0.03
15.32	0.61	15.45	5.26	0.20	40.30	20.53	2.47
15.34	0.65	15.18	5.52	0.20	40.49	20.29	2.37
15.46	0.65	15.11	5.66	0.22	40.25	20.38	2.26
8.73	0.40	20.51	4.33	0.26	41.47	22.22	2.02
8.75	0.42	20.71	4.35	0.26	41.94	21.77	2.12
11.62	0.24	18.12	5.52	0.57	41.45	21.85	0.04
11.75	0.24	18.13	5.57	0.57	41.44	21.85	0.09
11.73	0.26	18.16	5.51	0.58	41.38	21.84	0.09
11.72	0.24	18.13	5.58	0.56	41.63	21.87	0.08
7.91	0.45	19.48	5.64	0.09	41.43	17.64	7.61
7.92	0.42	19.36	5.63	0.10	41.11	17.77	7.60
7.93	0.43	19.52	5.55	0.09	40.49	18.15	7.50
8.95	0.46	18.71	5.69	0.24	41.10	18.02	6.90
8.94	0.48	18.95	5.66	0.24	40.61	18.07	6.85
36.5	0.20	2.39	3.99	0.06	37.13	20.92	0.00
36.4	0.23	2.40	3.92	0.04	36.95	21.05	0.00

Table 4.17. EPMA analysis of garnet (wt %) sample reference: CAT 18

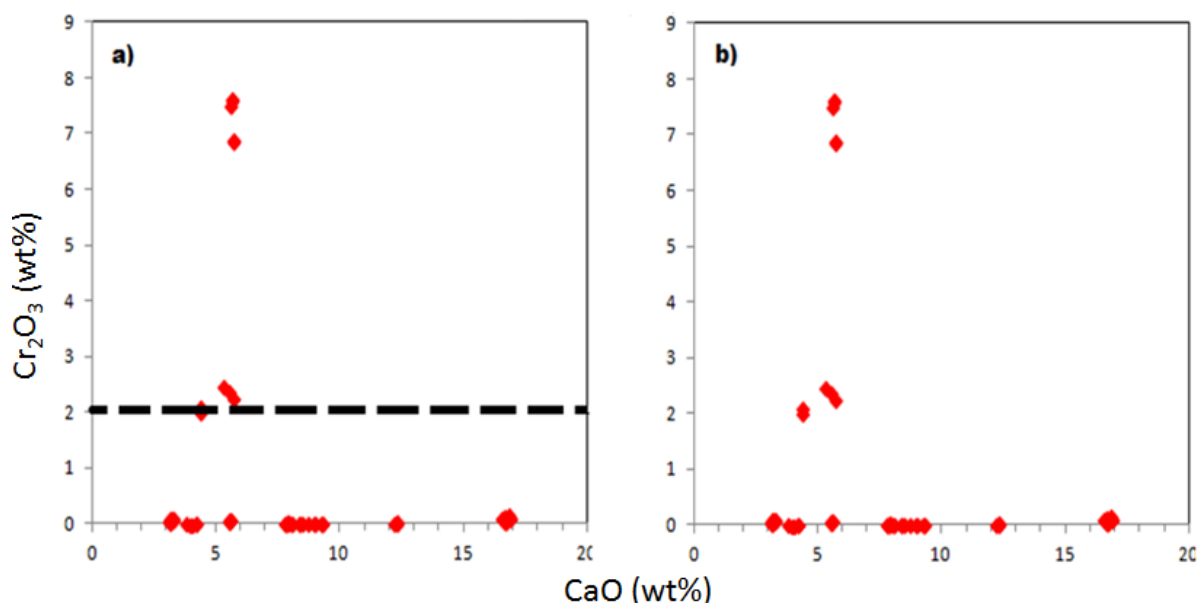


Figure 4.29. Plot of Cr<sub>2</sub>O<sub>3</sub> versus CaO content for diamond inclusion garnets from locality of Catoca. The horizontal line drawn at 2 wt. % Cr<sub>2</sub>O<sub>3</sub> is only used as an arbitrary division between eclogitic (< 2 wt. % Cr<sub>2</sub>O<sub>3</sub>) and peridotitic (>2 wt.% Cr<sub>2</sub>O<sub>3</sub>) garnets.

Despite mantle peridotite dominating in Lunda province, this new finding (Figure 4.29) indicates, that Angolan diamonds are also associated with the eclogite mantle (Table 4.17). The previous study of Correia and Laiginhas (2006) showed that Angolan diamonds are associated with the peridotitic mantle, and with the eclogite garnet ( $< 2$  wt %  $\text{Cr}_2\text{O}_3$ ). In contrast this new finding (Figure 4.29) clearly demonstrates that Angolan eclogite diamond garnet contains ( $\geq 2$  wt%  $\text{Cr}_2\text{O}_3$ ). This result is in agreement with the work of Cookenboo and Grütter (2010), who pointed out that the eclogite garnet field have  $>2.0\%$   $\text{Cr}_2\text{O}_3$ . The observed high percentage of CaO ranging between 3.5% - 16.9% and 00.9% - 0.58%  $\text{TiO}_2$  and 3.2 - 36.9 % FeO of analysed eclogite garnet (Table 4.17), leads to the conclusion that these garnets are derived from diamond field and this classification criteria can be used as main target of diamond exploration in order to discriminate the eclogite diamond garnet and crustal garnet. The crustal garnets can have very low CaO contents ( $< 1.0$  wt%; Cookenboo and Grütter, 2010) and garnet eclogite has high % FeO and low  $\text{TiO}_2$ , (Table 4.17 and Figure 4.30). This result is also in agreement of the work of Schulze (1997).

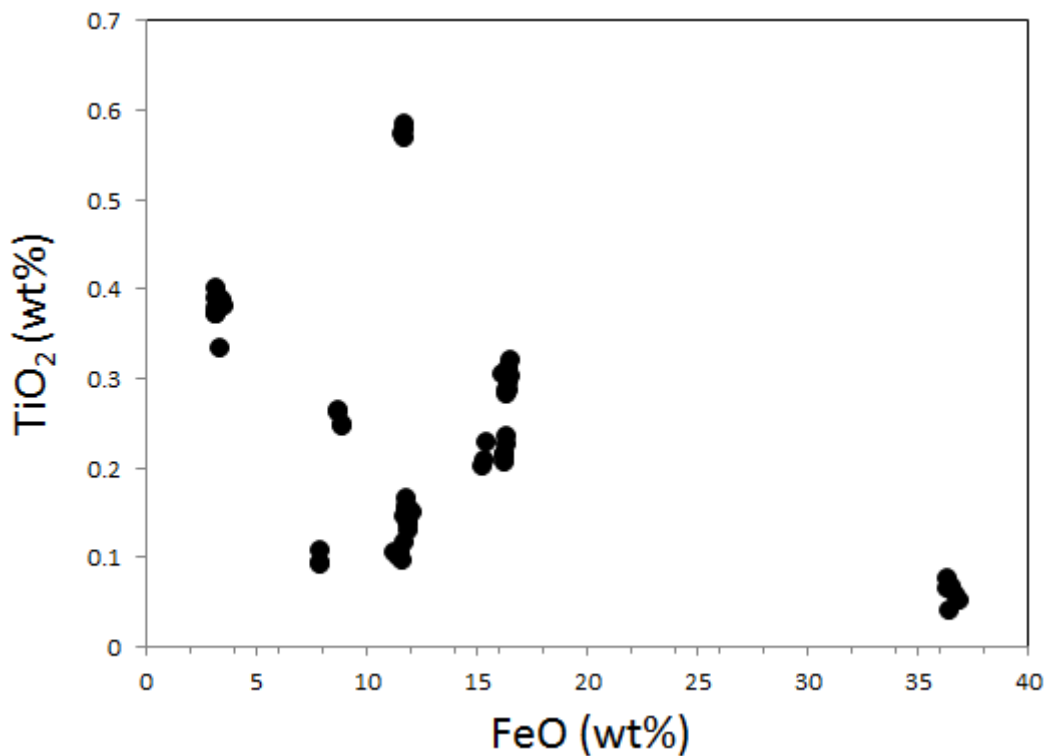


Figure 4.30. Plot of  $\text{TiO}_2$  versus FeO content for diamond inclusion garnets of eclogite (sample CAT18) from Catoca kimberlite.

As demonstrated in Figures 4.31, 4.32 and 4.33, ilmenite from three pipes has different composition. When redox ratio ( $\text{Fe}^{3+}/\sum\text{Fe}$ ) was plotted against major chemical components ( $\text{Cr}_2\text{O}_3$ ,  $\text{TiO}_2$  and  $\text{MgO}$ ), the results show that ilmenite for Catoca pipe has high redox ratios ranging from 0.3 to 0.95 Although having 2.2% of  $\text{Cr}_2\text{O}_3$ , (Figure 4.31) and 5.5 -6.1 % of  $\text{MgO}$  (Figure 4.32) but even so, its redox ratio

is still high enough for the lower survival of diamonds during their journey to surface. The evidence indicates the resorption process to be active and high, consequently leading to the poor diamond preservation condition at Catoca pipe. But the situation is different at Camutue, Caixepa and Camatxia, where the redox ratio mostly is less than approximately 0.3. It can be assumed that some minors impurities in ilmenite sample (Figures 4.31, 4.32 and 4.33) for the Caixepa and Camutue may have influenced the redox ratio to be slightly high at 0.32 when it is plotted against major chemical elements Cr<sub>2</sub>O<sub>3</sub> (2.2%), TiO<sub>2</sub> (39%) and MgO (4.7%). The decrease in TiO<sub>2</sub> content (39%) for these ilmenites is due to an alteration (oxidation, excess Fe<sup>3+</sup>) process in the original crystal of ilmenite. This statement is supported by the work of Gibb and Greenwood (1969) that studied ilmenite and explained that lower Ti in natural ilmenite is associated with an oxidation process. As demonstrated in Figures 4.31, 4.32 and 4.33, it is interesting to see the redox ratio (Fe<sup>3+</sup>/ΣFe) is low, 0.2 for ilmenite of Camatxia pipe, presenting variation in Cr<sub>2</sub>O<sub>3</sub>, TiO<sub>2</sub>, and MgO against Fe<sup>3+</sup>/ΣFe. The increase in MgO for Camatxia ilmenite is a good indication factor for diamond preservation conditions in this region. This statement is in agreement with the works of Nowicki *et al.* (2007).

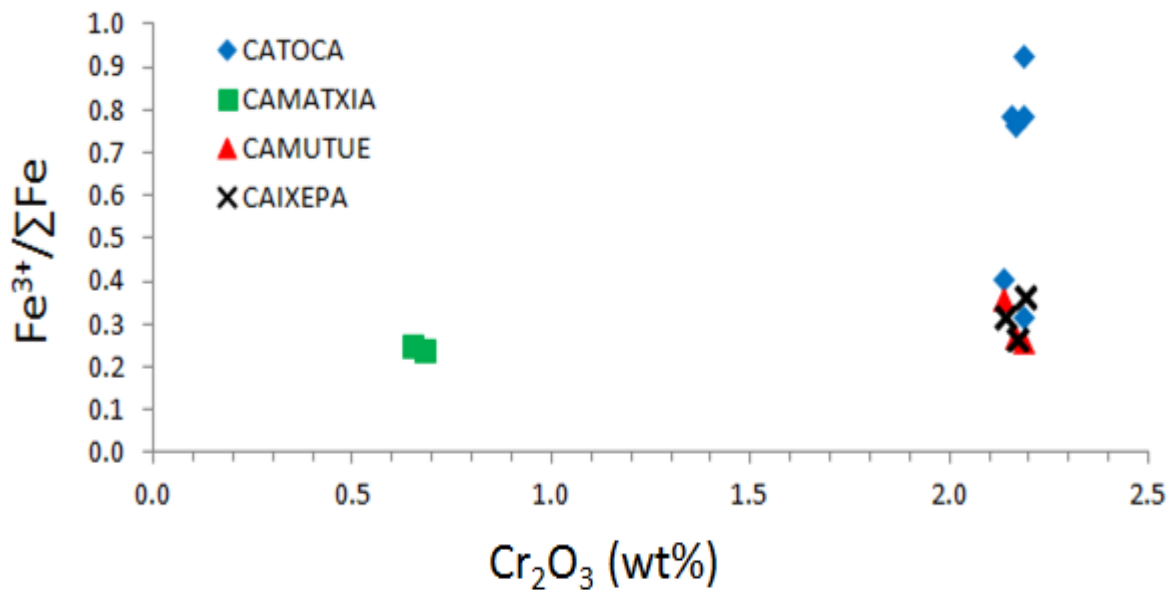


Figure 4.31. Plot of Cr<sub>2</sub>O<sub>3</sub> content against Fe<sup>3+</sup>/ΣFe (iron redox ratio) of ilmenite diamond indicator minerals.

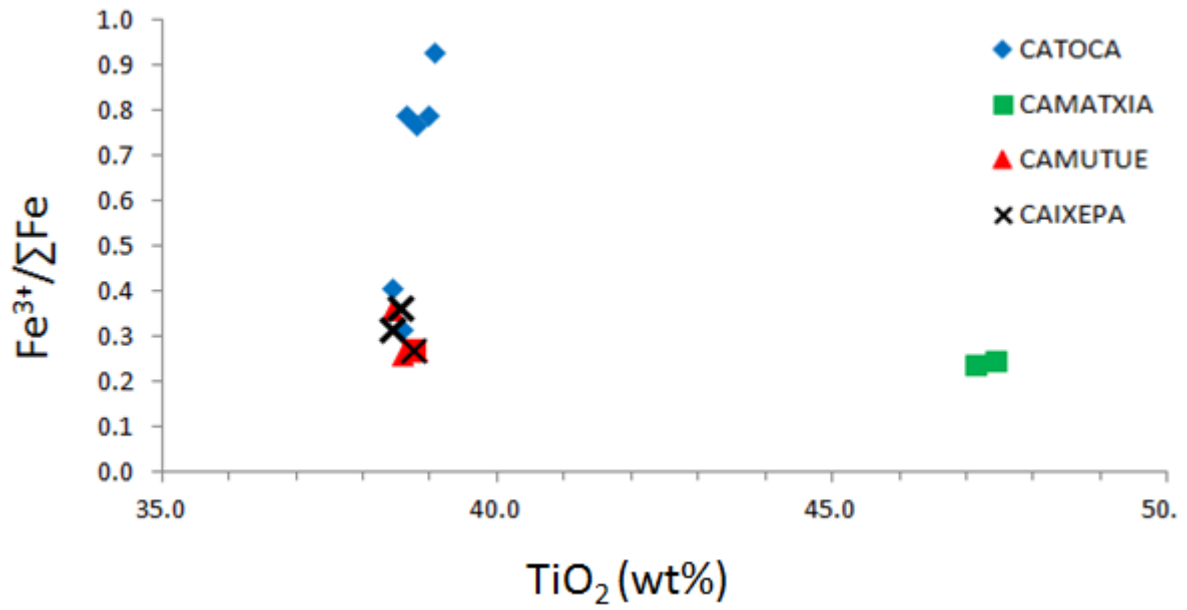


Figure 4.32. Plot of TiO<sub>2</sub> content against Fe<sup>3+</sup>/ΣFe (iron redox ratio) of ilmenite diamond indicator minerals.

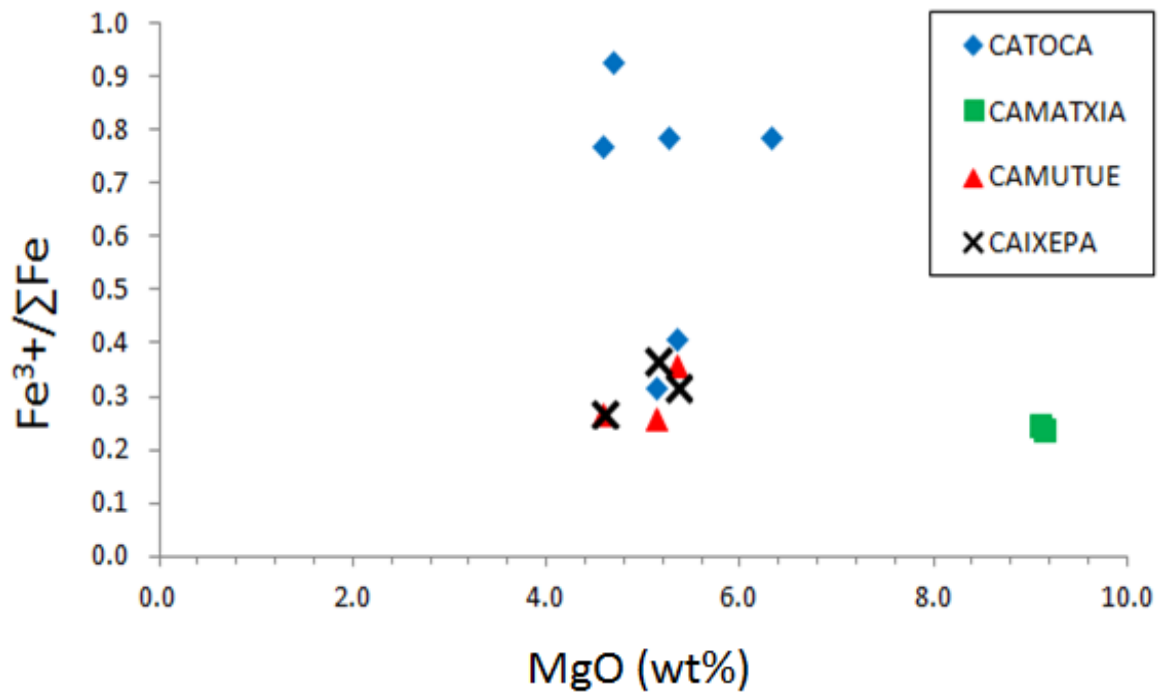


Figure 4.33. Plot of MgO content against Fe<sup>3+</sup>/ΣFe (iron redox ratio) of ilmenite diamond indicator minerals.

#### 4. 7. Diamond heterogeneous mantle model

The model presented here was developed using calculations of diamond carats per hundred tonnes of rock that each pipe produce and possible percentages of diamond brought to the Earth`s surface by kimberlite (Figure 4.34). These are confidential data that were provided by local geologists and mining engineers. The developed model that supports the view that the observed variations in diamond grade (Table 4.18) and / or abundance in Lunda provinces are associated with the heterogeneous mantle, so each kimberlite pipe has sampled and transported different amounts of diamond from the deep mantle. Results show that the Catoca pipe is the richest pipe as this pipe has sampled more diamond deep mantle source than any active kimberlite in the Lucapa graben.

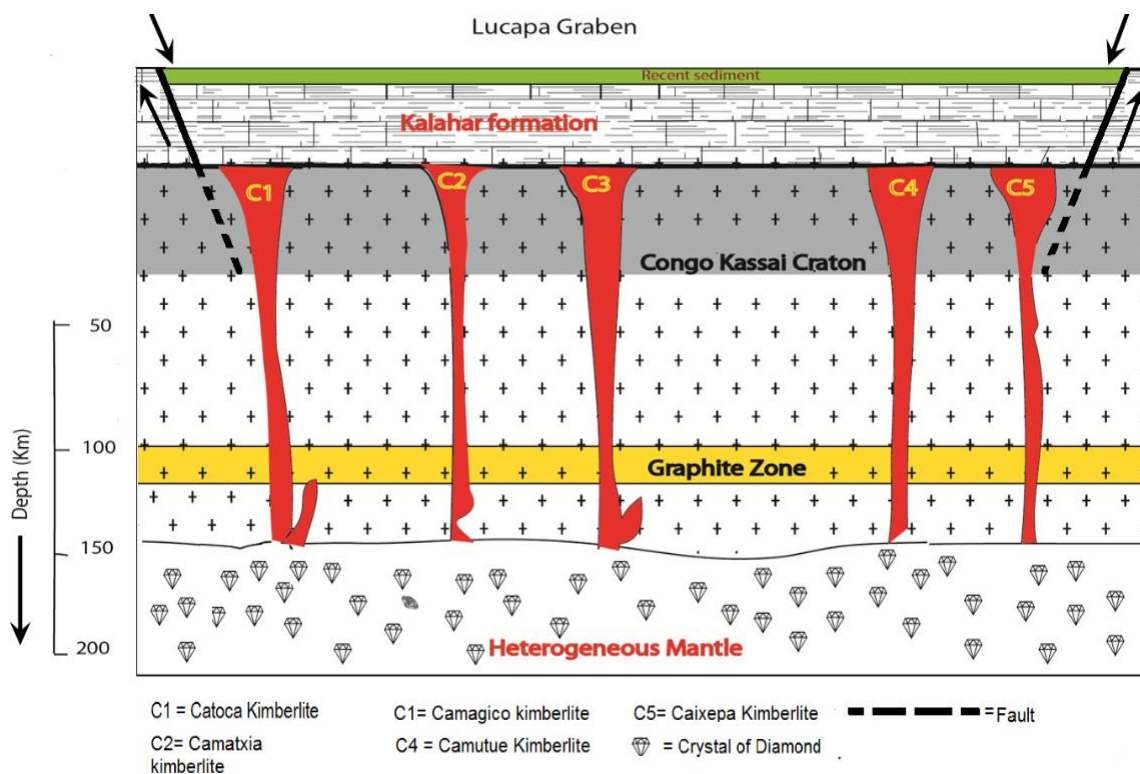


Figure 4.34. Developed heterogeneous model for diamondiferous kimberlites, Western Africa (NE Angola) showing relative locations of 5 principal pipes investigated in this study.

Kimberlite pipes	Quantity diamond each Mine production in 100 tonnes	Diamond % on surface
Catoca pipe	65-720 ct/100t	$0.14 \times 10^{-4} \%$
Camatxia pipe	0.07 - 0.45 ct/t = 7-45 ct/100t	$0.9 \times 10^{-6} \%$
Camutue pipe	0.085-0.6ct/t = 8.5-60 ct/100t	$0.12 \times 10^{-4} \%$
Caixepa pipe	0.06-0.39ct/t = 6-39 ct/100t.	$0.78 \times 10^{-5} \%$
Camagico pipe	0.06-0.085ct/t = 6-8.5 ct/100t...	$0.17 \times 10^{-5} \%$

Table 4.18. Grade variations of diamonds from a single pipe. Shows diamond carats per hundred tonne of rock that each pipe produces, and possible percentages of diamond brought to surface by kimberlite. Source of information: local geologists in NE Angola.

#### 4. 8. Diamond preservation model for sampled kimberlites

This section presents discussion and new findings regarding diamond grade variation, quality, and size distributions observed between kimberlite pipes in the Congo Craton. In addition, an indication of oxygen fugacity for the sampled diamondiferous kimberlites and how this information can be used to the benefit of diamond mining companies in future exploration and further recommendations are provided. This model was developed based on the chemical composition of ilmenite as a criterion for the preservation of diamond index in NE Angola.

Ilmenite ( $\text{FeTiO}_3$ ) is one of the iron-bearing minerals with iron naturally occurring in the two oxidation states ( $\text{Fe}^{3+}$  and  $\text{Fe}^{2+}$ ). For this reason it is a good candidate for studying the redox ratio  $\text{Fe}^{3+}/\sum\text{Fe}$  (McCammon *et al.*, 1998) and can be used for *in situ* studies under pressure (Seda and Hearne, 2004). In addition, this mineral is commonly found as a rock inclusion in kimberlites and volcanic rocks, and it is generally used as an indicator mineral in the diamond exploration environment (Wyatt *et al.*, 2004 and Keulen *et al.*, 2009). The oxidation state of the ilmenite mineral inclusions is, therefore, indicative of the oxidation state of the host kimberlite assemblage, which in turn determines the origin and genesis or diamond preservation conditions (Gurney *et al.*, 1993; Gurney and Zweistra, 1995; and Kozai and Arima, 2005). The preservation of diamond during kimberlite ascent to the surface is the crucial parameter in determining diamond grade within kimberlite pipes and the rate at which diamond crystals were resorbed depends mostly on oxygen fugacity (McCammon *et al.*, 1998; McCammon *et al.*, 2001; Fedortchouk and Canil, 2009). Estimation of the potential for diamond resorption by kimberlites is primarily based on the geochemical composition of megacryst ilmenite (Harvey *et al.*, 2001). It has been revealed by Nowicki *et al.* (2007) that in many cases the average ferric iron ( $\text{Fe}^{3+}$ ) content of ilmenite megacryst populations can be related to the extent of diamond resorption and consequently it has significant impact on diamond content, size-distribution and value in the exploration of kimberlite deposits (4.35).

As discussed by Gurney and Zweistra (1995), the presence of magnesium (Mg) in ilmenite can be used as a guide for the existence of diamond in kimberlite pipes. This research elucidates further understanding of diamond preservation and indicates that, in terms of diamond prospecting and exploration, the presence or absence of magnesium (Mg) in ilmenite as an indicator mineral is not an effective method to conclude whether host kimberlite pipe economically supports diamond mining (Yambissa *et al.*, 2014). A clear example of this case arises from the diamondiferous kimberlite of Catoca, for which, as shown in Figure 4.35, the majority of chemical analysis (Table 4.16) of Catoca ilmenite with an average  $< 6$  wt% MgO, places the Catoca pipe between the poor diamond preservation zone (3) to the no preservation zone (5) according to Nowicki *et al.* (2007) and Gurney

and Zweistra (1995), but in contrast the Catoca kimberlite pipe is the richest diamondiferous pipe in NE Angola. The new findings from this study are that different diamond fields may appear to obey different rule sets with respect to diamond preservation condition by using ilmenite criteria. The presence of high volumes of diamond at Catoca mine may be associated with mantle richness in diamond itself. This statement can be supported with the evidence from Table 4.18. Catoca kimberlite is the richest diamond pipe in NE Angola and the fourth largest diamond production mine in the world. Despite the Catoca pipe being the richest in diamond within the Lunda diamondiferous zone, but the results suggest (shown in Figure 4.35) poor diamond preservation conditions. This is another crucial factor which can be interpreted to be associated with the possibility of its mantle being more mineralized and richer in diamond than predicted on the basis of the  $\text{Fe}_2\text{O}_3$  vs  $\text{MgO}$  plot in Figure 4.35. This result is supported by the work of Bataleva *et al*, (2012) who explained that all amount of C can be oxidized by  $\text{Fe}^{3+}$  to  $\text{CO}_2$  or carbonates only in rocks depleted with carbon.

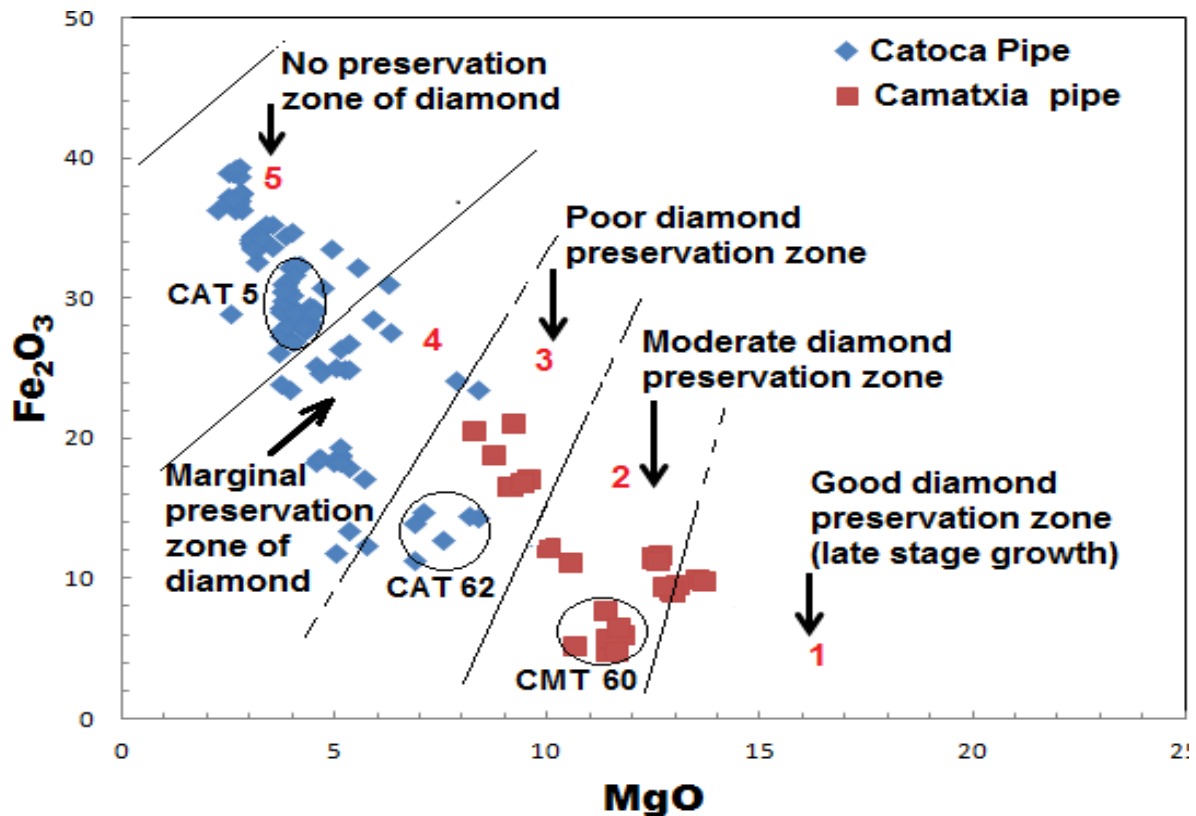


Figure 4.35. Preservation of diamond index model and illustration the composition of ilmenite  $\text{Fe}_2\text{O}_3$  vs  $\text{MgO}$  in wt % (Catoca and Camatxia kimberlite pipes).

The major implication from the interpretation of EMPA data for the complex ilmenite formation processes demonstrated for the Catoca and Camatxia kimberlites is that even with increased ferric iron,  $\text{Fe}^{3+}$ , and the lack of the original Mg-rich the ilmenite at Catoca pipe, the presence or mineralization of diamond within Lucapa graben kimberlites cannot be ruled out.

#### 4. 8.1. Classification of Angolan kimberlites based on ilmenite criterion

The investigated geochemistry of ilmenite of the sampled kimberlites, suggests that Angolan pipes fall in the kimberlite ilmenite environment, according to the Figures 4.36 and 4.37. The geochemical results are within this classification based on the work of Haggerty and Tompkins (1983). As illustrated on Figure 4.36 kimberlitic ilmenite is mostly dominated by solid solutions among three end-member components ( $\text{FeTiO}_3$ ;  $\text{MgTiO}_3$  and  $\text{Fe}_2\text{O}_3$ ). This is because the oxidation state of iron in the two end-members (ilmenite and hematite) is either  $\text{Fe}^{2+}$  or  $\text{Fe}^{3+}$ , and the stability of any composition within ilmenite ternary components should depend on  $f\text{O}_2$  (Haggerty and Tompkins, 1983). A precise classification and identification of the ilmenite source lithology, especially in kimberlite deposits where ilmenite is used as an indicator mineral, can provide a positive impact including effective geological/mineral study for the area, diamond quality evaluation index and direct cost savings in diamond exploration programmes. Anomalies can be easily recognized because non-kimberlitic ilmenites usually exhibit very low  $\text{Cr}_2\text{O}_3$  contents of approximately 0.5 wt% (Wyatt *et al.*, 2003).

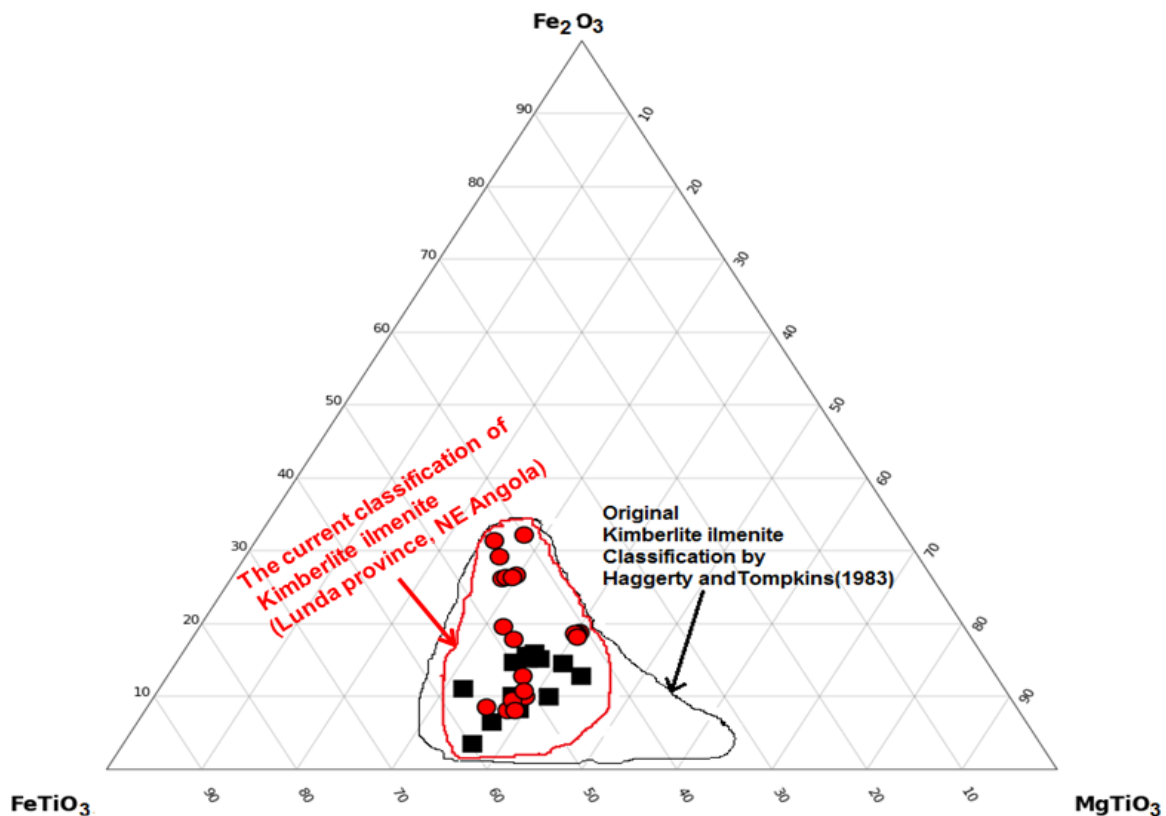


Figure 4.36. Ternary diagram showing the field of kimberlite ilmenite composition from Western Africa (NE Angola, samples Cat 5, Cat 62 in red colour and CMT 60 in back colour), plotted as function of hematite, ilmenite and geikeilite.

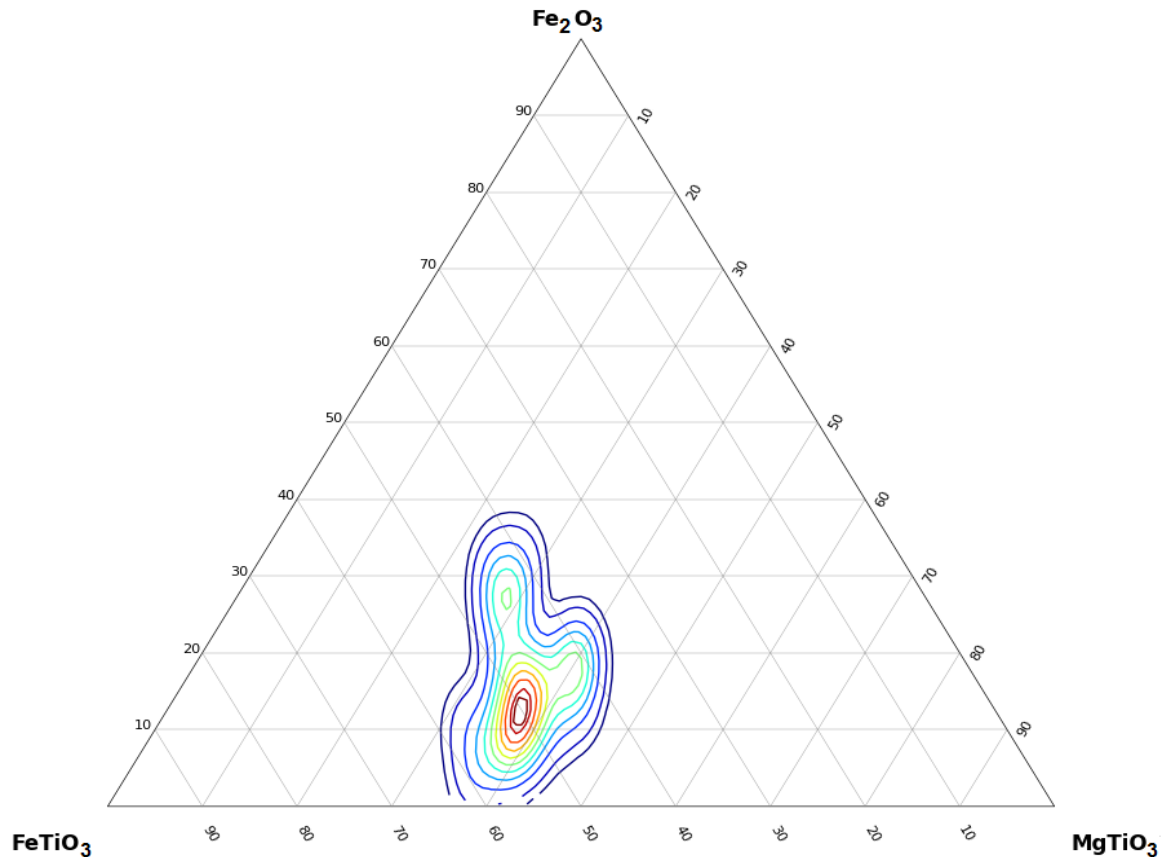


Figure 4.37. Ternary diagram showing the contour lines field of kimberlite ilmenite composition from Western Africa (NE Angola) plotted as function of hematite, ilmenite and geikeilite.

#### 4. 9. Viscosity model for sampled kimberlite rocks

The purpose of viscosity modelling in this research was to try to generate a better understanding of the causes of the variations in diamond abundance /quality (including absorption) and grades observed among the studied pipes from NE Angola. The quality and grade variation and diamond distribution is also linked to the speed of kimberlitic magma used to transport diamond crystals from deep source mantle to the surface. According to Sparks *et al.* (2006), kimberlite magma with lower viscosity can enable an exceptional rapid transport of diamond from the deep source mantle region to the surface, which is a crucial process for diamond survival (Wilson and Head, 2007). This viscosity model assists geologist/petrologists and mineralogists to understand the behaviour of kimberlite magma or silicate melts (Shaw, 1972) and the dynamic and violent eruption style of kimberlite magma. The viscosity model used in this research is similar to that described by Bottinga and Weill (1972), temperature dependence of viscosity in the compositional silicate melts (Persikov, 2007), which is a strong viscosity model for this project, because this model deals with chemical complex geological system (for example kimberlite melt emplacement events) (Shaw, 1972). The assumption made in this model is that for example this viscosity modelling deal with atmospheric pressures, and therefore it gives

only relative viscosities of one kimberlite magma versus another, also the model does not include allowance for the presence of water, CO<sub>2</sub> or other volatiles in the magma, effect of pressure, so there are several sources of uncertainty which make the viscosity modelling more qualitative than quantitative. Another important limitation associated with the viscosity of the analysed kimberlite rock/magma for this project, is lack of pure liquid or original composition of kimberlite magma/fluid, make the result unrepresentative of the viscosity of the kimberlite magma. This is because kimberlite magma/rocks are mostly contaminated magma/rocks (Sparks, 2013 and Sparks *et al*, 2006) containing several pieces of other materials/rocks, different phases, therefore kimberlite magma has Non-Newtonian behavior of fluids which is caused by several factors/ contaminated material/ inclusion of foreign materials. The shear force influence the viscosity of the fluid to change (Sparks *et al*, 2006; 2009) this occurs when the shear force is applied to non-Newtonian fluids.

Nevertheless it provides a useful comparative tool for considering compositional effects of different sampled kimberlites. The application of the viscosity calculation in this project is concerned primarily with geological applications, and several chemical composition representative of the magmatic range or kimberlite rock sample from different mantle depths are used. The appropriate samples have been selected in order to calculate the viscosity and the necessary approximations according to the equation 2 from Bottinga and Weill (1972). Major chemical compositions of representative magmatic/igneous rocks are provided in weight percent (wt %) together with the mole percentages and mole fractions in table 4.19 (also see Appendix 4) of the components required for the viscosity calculation. See discussion in section 5.7.

Weight %	CAT 67	CMT 006	CMT 60	CX 027	CMT 02	CMG 171	CM=CW45	CAT 50
Na <sub>2</sub> O	0.40	0.07	0.02	0.25	0.12	4.01	1.21	0.76
MgO	28.80	46.28	32.27	24.55	2.42	15.70	20.29	36.11
Al <sub>2</sub> O <sub>3</sub>	3.24	1.04	1.84	3.83	1.43	5.66	4.65	3.74
SiO <sub>2</sub>	32.66	40.72	34.95	39.89	80.19	39.16	38.72	33
P <sub>2</sub> O <sub>5</sub>	0.78	0.06	0.17	0.34	0.07	0.35	0.12	1.39
K <sub>2</sub> O	1.51	0.05	0.10	0.20	0.14	0.11	0.39	1.05
CaO	7.43	0.44	3.20	5.59	5.56	8.39	4.90	6.48
TiO <sub>2</sub>	1.09	0.06	1.26	1.01	0.09	2.17	0.24	1.14
Mn <sub>3</sub> O <sub>4</sub>	0.21	0.16	0.16	0.15	0.08	0.20	0.11	0.16
Fe <sub>2</sub> O <sub>3</sub>	10.11	7.37	11.53	9.75	3.93	9.72	7.18	0.24
<b>Mole %</b>								
KAlO <sub>2</sub>	2.07	0.29	0.13	0.29	0.18	0.15	0.63	1.30
NaAlO <sub>2</sub>	0.83	0.54	0.04	0.54	0.24	8.78	2.83	1.43
CaAl <sub>2</sub> O <sub>4</sub>	0.60	2.10	1.07	2.10	0.66	0.69	1.59	0.77
MgAl <sub>2</sub> O <sub>4</sub>	0.00	0.00	0.00	0.00	0.00	0.00	0.00	0.00
K <sub>2</sub> O	0.00	0.00	0.00	0.00	0.00	0.00	0.00	0.00
Na <sub>2</sub> O	0.00	0.00	0.00	0.00	0.00	1.39	0.00	0.00
CaO	7.99	4.58	2.60	4.58	5.55	10.16	4.75	5.97
MgO	46.40	40.91	51.70	40.91	3.77	26.48	36.58	52.31
MnO	0.19	0.20	0.19	0.20	0.18	0.20	0.21	0.17
FeO	5.69	5.89	5.66	5.89	5.51	5.96	6.36	5.12
TiO <sub>2</sub>	0.88	0.84	1.01	0.84	0.06	1.84	0.21	0.83
SiO <sub>2</sub>	35.30	44.60	37.57	44.60	83.80	44.29	46.81	32.07

Table 4.19. Composition of representative kimberlite magma types used in sample viscosity calculation. Data from XRF analyses. CAT 67, CAT60→Catoca pipe; CX027→Caixepa pipe; CMG171→Camagico pipe; CM=CW45→Camutue pipe and CMT006, CMT02→Camatxia pipe.

$$\ln \eta = \sum X_i D_i \quad \text{Equation 2}$$

where:

$\eta$  → the Newtonian viscosity coefficient

$D_i$  → an empirical constant associated component  $i$  over a restricted range of SiO<sub>2</sub> concentration

$X_i$  → the mole fraction of oxide component

As seen in Figure 4.38, viscosity modelling results demonstrate that at temperatures of ca. 1500°C all samples such as Camutue (CM=CW45); Catoca (CAT – 50; CAT-67), Camatxia CMT-60 and Camagico (CMG17) and Caixepa (CX027) exhibit modelled viscosities of  $1.5 \pm 1$  Poise and at lower temperature of 1200°C all samples provide modelled viscosities of  $3 \pm 1$  Poise, which means that there is not a great difference in viscosity for a given temperature between samples, except Camatxia

sample CMT02 which has a very different viscosity from the other samples. This is clearly due to the high content of silicon oxide ( $\text{SiO}_2 = 80.19\%$ ) and low magnesium oxide ( $\text{MgO} = 2.42 \text{ wt } \%$ ) observed in this sample (Table 4.19) compared with the others. Viscosity is determined mainly by  $\text{SiO}_2$ ,  $\text{Al}_2\text{O}_3$ ,  $\text{MgO}$  and  $\text{CaO}$  content in magmas. This is supported by Giordano *et al.* (2008) and Moussallam *et al.* (2016), who stated that these major chemical elements influence magma viscosity (Sparks *et al.*, 2009). When the temperature decreases from  $1450^\circ\text{C}$  to  $1250^\circ\text{C}$  the viscosity increases (see table 4.20 and 4.21). Higher levels of silica in magma cause higher viscosity due to the presence of strong Si-O bonds. When water is present in magma it has the ability to break Si-O bonds and therefore the viscosity decreases (Dingwell and Virgo, 1988; Giordano *et al.*, 2008; Petford, 2009).

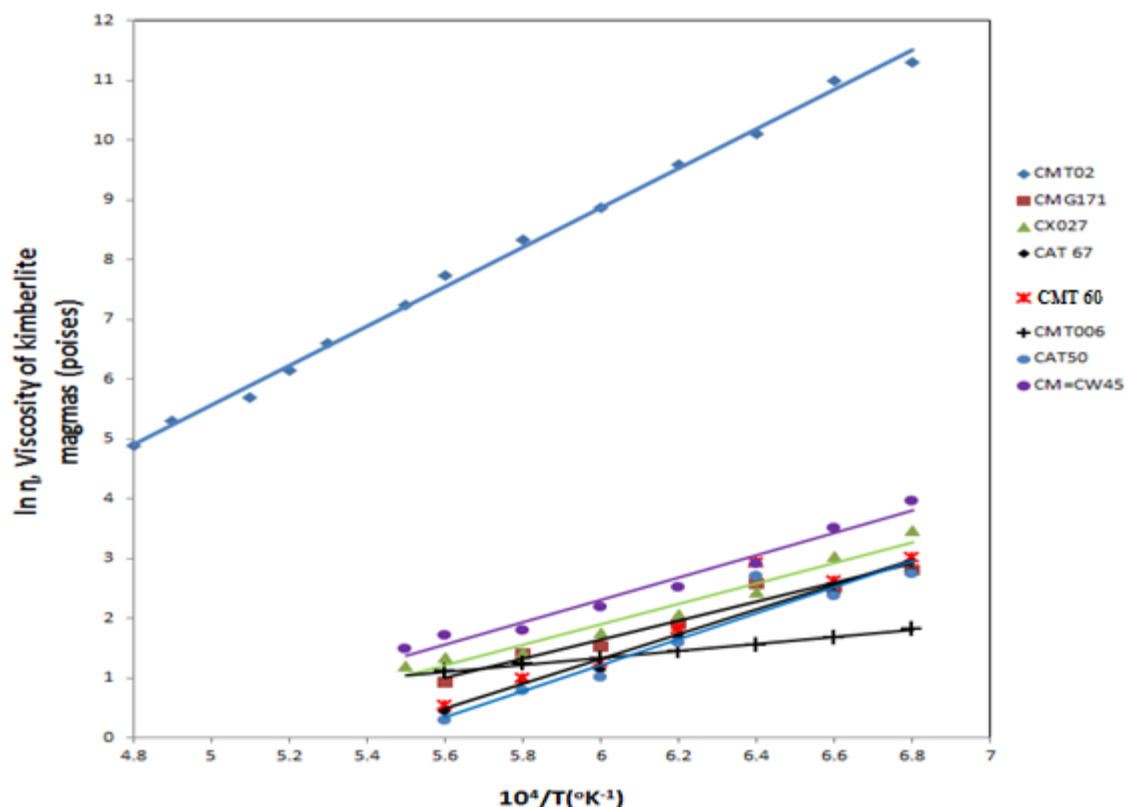


Figure 4.38. Calculated viscosities for typical kimberlite magmatic melts. The plotted points correspond to viscosities calculated at 50°C intervals according to the Table 2.

Temperature (°C and °K <sup>-1</sup> )		log (η /Poise)							
T. °C	10 <sup>4</sup> /T (°K <sup>-1</sup> )	CMT 02	CAT 67	CMT 60	CM= CW04 5	CMG 171	CX 027	CAT 50	CMT 006
1197.6	6.800	11.31	2.79	3.02	3.97	2.82	3.46	2.75	1.83
1242.2	6.600	10.98	2.41	2.62	3.51	2.52	3.03	2.37	1.68
1289.5	6.400	10.10	2.70	2.93	2.96	2.59	2.43	2.70	1.56
1339.9	6.200	9.58	1.69	1.83	2.52	1.91	2.06	1.60	1.44
1393.7	6.000	8.86	1.15	1.26	2.20	1.53	1.75	1.02	1.33
1451.1	5.800	8.33	0.95	0.98	1.81	1.41	1.42	0.79	1.24
1512.7	5.600	7.74	0.44	0.54	1.70	0.93	1.35	1.11	1.11
1545.2	5.500	7.25	1.42	1.79	1.49	1.28	1.20	1.50	1.06
1613.8	5.300	6.61	1.43	1.77	1.47	1.43	1.15	1.46	1.16
1650.1	5.200	6.16	1.41	1.69	1.1	1.42	0.79	1.43	1.08
1687.8	5.100	5.70	0.48	0.68	0.95	0.83	0.68	0.41	1.00
1687.8	4.900	5.31	0.26	0.44	0.72	0.64	0.46	0.17	0.94
1810.3	4.800	4.89	0.130	0.31	0.52	0.51	0.29	0.05	0.86

Table 4.20. Calculated viscosities for studied kimberlite magmas samples using model from Bottinga and Weill (1972).

Modelled viscosity data of kimberlite melt/magmas Modelled using the viscosity model of Bottinga and Weill (1972)													
Temperature		log ( $\eta$ /Poise)											
Temp. / °C	$10^4/T$ (°K <sup>-1</sup> )	Model Data(2)	Graphic data(2A)	Model data (3)	Graphic data (3A)	Model Data (4)	Graphic Data (4A)	Model data(5)	Graphic data(5A)	Model Data (6)	Graphic data(6A)	Graphic data(1)	Graphic data(1A)
1197.6	6.8	8.56	8.6	6.93		6.17	6.18	3.15	3.16	2.93	3	12.46	13.4
1242.2	6.6	7.79	7.8	6.09	6.1	5.53	5.50	2.73	2.70	2.50	2.5	11.81	12.6
1289.5	6.4	7.32	7.3	5.45	5.5	4.53	4.50	3.00	3.00	2.89	2.9	11.00	12
1339.9	6.2	6.91	6.9	4.88	4.9	3.92	3.90	1.93	1.90	1.69	1.7	10.27	11
1393.7	6.0	6.32	6.3	4.43	4.4	3.51	3.50	1.37	1.40	1.06	1	9.61	10.5
1451.1	5.8	5.83	5.9	4.00	4	2.91	2.90	1.08	1.10	0.74	0.7	8.98	9.5
1512.7	5.6	5.46	5.5	3.80	3.7	2.70	2.70	0.66	0.68	0.31	0.3	8.40	9.1
1545.2	5.5	5.17	--	-	-	2.19	2.20	1.88	-	1.81	-	7.82	8.4
1613.8	5.3	4.89	-	-	-	2.49	-	1.89	-	1.18	-	7.16	7.5
1650.1	5.2	4.44	-	-	-	2.07	-	1.80	-	1.11	-	6.67	7.2
1687.8	5.1	4.08	-	-	-	1.80	-	0.83	-	0.93	-	6.18	6.5
1687.8	4.9	-	-	-	-	1.03	-	0.59	-	0.85	-	5.75	6.1
1810.3	4.8	-	-	-	-	1.26	-	0.45	-	0.77	-	5.31	5.6

Table 4.21. Validation of viscosity model. Temperature depending viscosity data used for validation of viscosity model by comparing the calculated viscosity with those published viscosity data (graphic data).

#### 4. 10. Results from studied crystals of diamond from Catoca kimberlite

After a detailed examination of some natural crystal of diamonds from kimberlites of NE Angola, the optical result shows they contain evidence of resorption characteristics on their surfaces, such as trigonal etch-pits on faces, hillocks, and striation, and sharp steps along the edges (Figure 4.39), with tetrahexahedroid texture (poorly-preserved facets due to extreme resorption). Similar diamond deformation features have been described by Arima and Kozai (2008); Fedortchouk *et al.* (2007) and Zhang *et al.* (2015). All of these deformation characteristics of diamond are interpreted as products of interaction with their host magma during ascent and the effects of interactions with oxygen (e.g. Robinson *et al.*, 1989). The sampled crystals of diamond (Figure 4.39) show tetrahedral morphologies, reflecting a complex history of growth and rounded shape due to dissolution. Similar diamond morphologies or kimberlite induced resorption features have been described by Fedortchouk *et al.* (2007). As shown in Figure 4.39, these diamond show yellowish colours which are assumed be associated with the common impurity observed of nitrogen, in various states of aggregation (Orlov, 1973). This is consistent with Tappert and Tappert (2011) who described that normally the diamond in its pure form is colourless, but due to the imperfections, impurities of nitrogen, and inclusions of mantle xenolith minerals, it can exhibit colouration. These factors have a negative influence on the market price of diamonds.

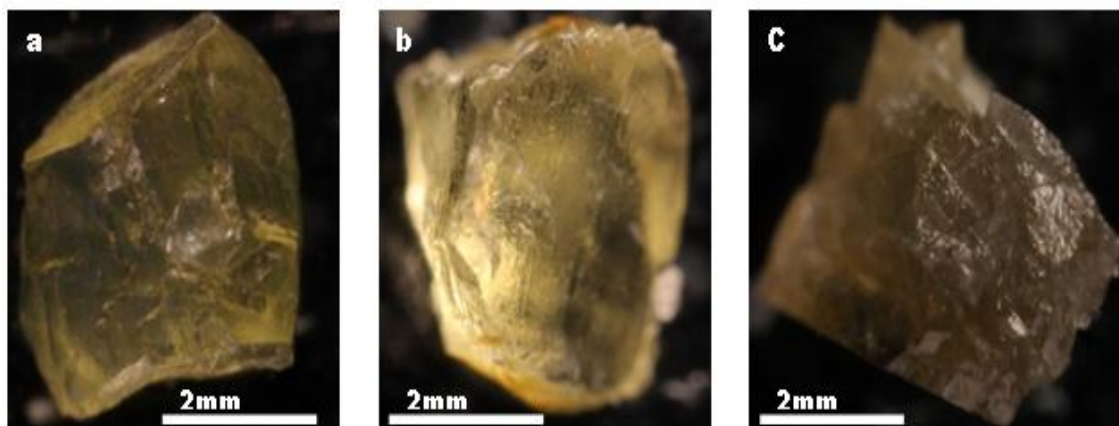


Figure 4.39. Diamond surface textures resulting from late stage etching process, poor quality. Photographs taken on optical microscope.

The conductive geothermal or surface heat flow of  $38\text{mW/m}^2$  (megawatts per square meter) for the lithospheric mantle beneath the Lunda kimberlite province calculated by Castillo-Oliver, *et al.* (2011) has been considered to be high enough for diamond formation (Stachel, *et al.*, 2003). The question arising is whether there is additional information that can be obtained to ensure a clearer understanding of diamond preservation within Lunda province. This question is addressed in the results and discussion relating to Mössbauer and petrographic analyses; and the heterogeneous mantle model and diamond preservation model.

## Chapter Five . Discussion

This chapter elucidates and provides discussion of the results from all advanced analytical methods used in this research, namely petrography, Mössbauer spectroscopy, XRD, XRF and Electron Probe Micro Analysis (EPMA). Some of the crucial interpretations and discussion of microscopic petrographic analyses are provided in Chapter Four (section 4.1), and the hand specimens for petrographic analysis are considered in Chapter 3, Section 3.1.6 for the field work. The results of viscosity modelling of the sampled kimberlite magma, diamond resorptions, diamond preservation model and ilmenite kimberlite classification, are discussed in this chapter.

### 5. 1. Discussion - petrography of the sampled diamondiferous kimberlites.

Petrographic studies of kimberlite rocks are crucial in terms of both scientific and economic importance. In an economical context, kimberlite deposits are the most important source of economically mined diamonds in NE Angola and across the world. Apart from sampling and transporting diamonds to the Earth's surface, eclogite garnet and peridotite mantle xenoliths are derived from depths greater than any other igneous rock type (Ringwood *et al.*, 1992) The Angolan kimberlites also have scientific importance by providing information on the composition of the deep mantle (400–650 km) and the melting processes that occurred between the cratonic continental lithosphere (Congo Craton) and the underlying convecting asthenospheric mantle (Creighton *et al.*, 2008).

In order to understand the petrography of kimberlites from NE Angola, mantle xenoliths (P-type and E- type) and kimberlite rocks have been analysed systematically. As mentioned above, mantle xenoliths (peridotite and eclogite) are the primary mantle rocks. The samples have been well characterised and the study has provided indications (e.g. mineral deformation) of the history of formation of the materials by using specific textural characteristics such as structure, fabric, phase assemblage, phase relationships, reaction textures and chemical compositions (also see Appendices 1 and 2). But the problem encountered during analysis is that the variations in mineralogy and major and trace element contents make it more difficult to constrain a primary kimberlitic melt composition (Mitchell *et al.*, 2008; Cas *et al.*, 2008; Masun and Scott Smith 2006). The studied kimberlite rocks from Lucapa Graben contain mantle derived peridotite (found at Camagico, Camutue, Caixepa Camatxia mines) and eclogite (mostly found at Catoca mine) xenoliths and xenocrysts of micro-ilmenite, spinel and garnet, xenoliths of Precambrian basement and rocks from the Phanerozoic period (Boyd and Danchin, 1980). Gneiss and granites were found to be the most dominant country rock, (Dirks *et al.*, 2003; Robles Cruz *et al.*, 2008, 2009; and Pereira *et al.*, 2003).

Throughout the petrographic study, it was observed that the sampled and examined kimberlite rocks are contaminated by the material of intruded rocks and are strongly transformed by hydrothermal-metasomatic processes (see Chapter Three). It can be shown that metasomatic processes were accompanied by changes in mineralogy, which are assumed to be due to the high-energy mechanism of controlled kimberlite emplacement. This breaks up the abundant minerals released from xenolith fragmentation during eruption, including the phenocryst minerals, alteration of previously formed minerals and pieces of pre-existing kimberlite, and changes in temperature and pressure. These factors have all strongly contributed to the NE Angolan kimberlite rocks being challenging to interpret texturally, mineralogically, and compositionally.

After careful interpretation of the data obtained from the studied samples, the conclusion drawn is that both hand specimen and thin section analyses of peridotite, eclogite and kimberlite are complicated by the fact that the mantle rocks in the Lucapa Graben have experienced processes of metasomatic episode or later alteration. The interesting aspect from the analysed primary diamond indicator minerals such as garnet, olivine, ilmenite, chromite and pyroxenes, reflect these later alteration or redox reactions. These mineral reactions can be interpreted as being crucial indicators of how the rich fluid phases affected the primary mantle minerals, as shown in Chapter 4. For example the thin section results of olivine, garnet and ilmenite in samples CMT 01; CW045-7; CM 003; CAT 59; CMG-002; and CMT-05 and Cat 18 show that they are transformed into variably oxidised kelyphitization /serpentinization assemblages mainly comprised of a fine dark brown matter of clinopyroxene, spinel, and serpentine. Particularly clear evidence of this can be seen in sample CMT-05. In addition, the original mantle has been altered or modified from the original minerals into secondary formation phases, and other factors such as high oxygen fugacity, metasomatoses events and heterogeneous mantle are interpreted as major causes of diamond grade variation and quality within Lunda provinces. This can be supported by the work of Harvey *et al.* (2001) who noted that altered fluid agents (H<sub>2</sub>O, CO<sub>2</sub>) can affect the original diamonds structure, resorption (Robinson *et al.* 1989) or can impose conditions sufficiently oxidising to cause diamond breakdown to carbonate or even to CO<sub>2</sub> (Gurney *et al.*, 1993; and Fedortchouk *et al.*, 2005). The metasomatic agent such as carbonate carbonate melts play a prominent role in mantle metasomatism, because experimental studies (Giuliani *et al.* 2013) have shown that carbonate melts are the first product of partial melting of carbonated peridotites and eclogites and consequently these melts have high mobility under mantle conditions. The Carbonate melts can also derive from liquid immiscibility in CO<sub>2</sub>-rich silicate or silicate-carbonate melts (Giuliani *et al.* 2013)

In connection to the problem associated with diamonds in Lunda provinces, the petrographic information on the studied kimberlitic rock is crucial. The sampled crystals of diamond from Catoca pipe (Figure 4.39) contain resorption features. According to the Boyd and Gurney (1986), at depths in

the Earth corresponding to pressures greater than the graphite to diamond transition the mantle (see Figure 2.14), diamond may not be stable (Nowicki *et al.*, 2007). It can be argued here that the processes of metasomatism evidenced from the rock studied rocks in this project, Lunda lithospheric mantle, may impose conditions sufficiently oxidising to cause diamond breakdown to carbonate or CO<sub>2</sub> (Harvey *et al.*, 2001) or resorption. The result from this research (see Chapter 4), show indications of oxidation processes within the sampled kimberlite magma, leading to the interpretation that some diamond crystals from Lunda kimberlites have experienced resorption processes (Figure 4.39) or may have been converted to graphite or CO<sub>2</sub> due to high oxygen fugacities.

The kimberlite rock texture and classification from this research are consistent with those reported previously in literature (Webb *et al.*, 2004; Cas *et al.*, 2008; Field and Scott Smith, 1998 and Kjarsgaard, 2007). Another interesting aspect which can be argued here is that despite the study of examined rock textures creating much difficulty in interpretation, further important information on mineral chemistry and composition can help provide clues about the formation process. In order to avoid petrographic misinterpretation, the sampled mantle rocks (Lunda- diamond province) used in this project have been analysed systematically in detail. The study of ore polished thin section / microscopy involves not only the identification of individual mineral grains, but also the interpretation of diamondiferous kimberlite and mineral textures and their formation processes (see Chapter 3 and 4).

The textures described in this research from thin section, hand specimen and EMPA analyses are important aspects of the study of rocks and economical ores deposits. This is because these textures provided evidence of the nature of processes such as initial ore deposition, post-depositional, mineral re-equilibration or metamorphism, deformation, as well as meteoric weathering (Cas *et al.*, 2008; Field and Scott Smith, 1998). According to Kjarsgaard (2007) who studied kimberlite rocks, the recognition and interpretation of rock textures are tools necessary for understanding the processes involved in the genesis and post depositional history of kimberlite deposits, which in turn is very important for prospecting for economic ore bodies. For example the exsolution textures observed in the studied sample (Figure 4.26 and Figure 4.27) are indicative of a slow or intermediate cooling rate whereas the identifying of equilibrium mineral assemblages such as spinel and ilmenite (Figure 4.26) are necessary for understanding phase relations and the correct interpretation of geothermometric studies (Nowicki *et al.*, 2007).

Many lines of evidence indicate that metasomatic silicate rich phases of subcontinental lithospheric mantle have caused, the resorption on diamond (Stachel and Harris, 2009; Nowicki *et al.*, 2007). These fluid agents (CH<sub>4</sub> and CO<sub>2</sub>) are complex due to the alteration of primary mantle minerals assemblages (Zhang *et al.*, 2015). The results from this project confirm the presence of infiltration of

metasomatic agents in the sampled rock (Figure 4.11). Therefore, the infiltration of metasomatic or silicate rich fluids (CH<sub>4</sub> - bearing rich fluid, CO<sub>2</sub>-rich fluid and carbonatitic melt) or even hydrothermal fluid (H<sub>2</sub>O) phases, into diamondiferous lithosphere mantle beneath of Congo Kassai craton, has converted/transformed the original mantle peridotite into variably oxidized rock, these including phlogopite, serpentised olivine, kelyphite rims on garnets (Figures 4.4 and 4.5) and carbonates. This statement is also supported by evidence from the crystals of diamond studied here (Figure 4.39). Increasing carbonate activities in the diamondiferous mantle in NE Angola would also increase the degree of diamond reaction with metasomatic fluids, consequently causing the resorption of diamond crystals even at oxygen fugacities below the reaction boundary (McCammon *et al.*, 2001).

There are many questions concerning diamond genesis. One of the crucial elements is the composition of the natural diamond crystallization environment which is critically seen as one of the principal questions in the problem of diamond genesis (Palyanov and Sokol 2009). However, the main source of information about the composition of mantle and information about the crystallization of diamond come from the mineral and fluid inclusions in diamond which are studied in this project. For example the studied mineral inclusions (garnet, olivine, pyroxene and ilmenites) used in this research are also the same minerals that have been used in order to determine the diamond paragenesis (Stachel, 2003) and to estimate the P–T– and oxygen fugacity conditions (Gurney *et al.*, 1993; Stachel and Harris, (2007) whereas the fluid inclusions may provide direct information about the composition of the crystallization (Palyanov and Sokol 2009). It can be highlighted from this project that understanding these processes is important for diamond exploration and assessing the potential diamond grade of kimberlites from NE Angola.

Several carbonate layers have been observed throughout this study (see thin sections result in Chapter four). The question arising is, what sort of information can be taken from these carbonate layers within the Lunda lithosphere mantle? According to McCammon *et al.* (2001) the activity of carbonate within the system increases with increasing oxygen fugacity until the reaction boundary is reached, at that point the carbonate activity becomes unity. In addition the increase of carbonate activity with mantle has negative impact on diamond survival (McCammon *et al.*, 2001). Because the minerals and kimberlite mantle rocks of the Congo craton (NE Angola) have experienced oxidation processes, it is possible to say that many crystals of Lunda diamonds have been absorbed and this resorption may possibly have taken place in both lithospheric mantle and during kimberlite emplacement. In addition, this statement is supported by Harvey *et al.* (2001), who explained that diamond has less chance to survive if the kimberlite magma is highly oxidising.

One of the dominant alteration processes in the Lunda kimberlites intrusions is the serpentinisation of olivine and the presence of fluid agents within the NE Angola lithosphere. One of the most notable

and clear alteration features is that olivine crystal pseudomorphs can be distinguished from surrounding zones of amorphous serpentine (sample Cat- 61 b, from Figure 4.2). Based on petrographic analyses, the texture observed in sample Cat- 61 b suggests that the groundmass phases, in particular the kimberlite carbonate minerals, have been replaced by serpentine (Webb *et al.*, 2004), which implies an open chemical system in which components such as CaO and CO<sub>2</sub> have been removed by a fluid phase (White *et al.*, 2012). The process of serpentinisation reactions have been suggested to take place at low ambient temperatures with the maximum temperatures approximately 500°C (White *et al.*, 2012).

Throughout sampling activity, picroilmenite was one of the most collected minerals. It can be argued here that many of the picroilmenites (e.g. Figure 3.12) observed in NE Angolan pipes may not be related with the diamondiferous mantle. This suggestion is comparable with the work of Alyмова (2012), who also suggested that the majority of picroilmenites (solid solution between geikielite-MgTiO<sub>3</sub> and ferroilmenite) from kimberlites is not associated with the diamondiferous mantle rock. Because non - kimberlite ilmenite contains low contents of Cr<sub>2</sub>O<sub>3</sub> ( $\leq 0.5$  wt.%) (Wyatt *et al.* 2003), it is important to characterise and carry out a comprehensive study the chemistry of ilmenite before the conclusion is reached about diamond preservation condition.

Throughout the field-based examination in Lunda provinces, it was noticed that the occurrence of diamondiferous pipes show several petrographic kimberlites rocks, and their mineralised body can be sub-divided into main stages such as pyroclastic kimberlite (PK), resedimented volcanoclastic kimberlite (RVK), volcanoclastic kimberlite (VK), and Tuffisitic kimberlites breccias (TKB) (see table 3.3). These stages dominate kimberlites rocks within the two main geological facies (Crater and Diatreme) in the Angolan pipes (Pervov *et al.*, 2011; Pereira *et al.*, 2003; Robles-Cruz, *et al.*, 2008).

Understanding the textures and emplacement processes of kimberlites is important as it improves the degree of confidence in any predictions of economic potential of kimberlite bodies (Scott Smith, 2010). The kimberlite pipes from Lunda provinces contain mantle derived peridotite and eclogite (e.g. as found at Catoca, Camatxia, Caixepa and Camutue kimberlite pipes) xenoliths and xenocrysts of indicator minerals (spinel, garnet, picro-ilmenite) along with xenoliths of Precambrian basement and rocks from the Phanerozoic period. Note that gneisses and crystalline schists were found as the most dominant country rocks within Lunda pipes. Angolan kimberlites present similar petrography features to those from North-western Saskatchewan (Canada) described by Harvey *et al.* (2001).

During field work, kimberlites and many mantle xenoliths (eclogite and peridotite) were collected in the crater zones at Catoca, Camatxia, Camagico, Camutue, and Caixepa. The presence of these rocks in the Crater zones from Lunda provinces pipes, however, is interpreted as suggesting that this zone

may have survived the erosion. This suggestion is supported by work of Ganga *et al.* (2003) and Pereira *et al.* (2003), who described that diatreme kimberlites with preserved crater zones are characteristic for the Lunda provinces but dikes and sills (Hypabyssal facies kimberlite) are also known (for example at Catoca, Appendix 2).

In terms of an occurrence mode shape, the majority of the pipes from Lunda provinces show different shaped structures (e.g. see Section 3.1.6), including elliptical or circular, irregular, with variable shape dimensions probably due to the mode of formation and with minor erosion cycle on crater zones. However, pipes such as Catoca and Camafuca-Camazambo form the exception in this area as these are much larger in size and less eroded (Pereira *et al.*, 2003).

From field based investigations, it was noticed that most of the sampled kimberlite rocks from crater zones are poorly sorted and include tuffs and tuff breccias (pyroclastic deposits) containing fragments of kimberlite, country rock and mantle - derived xenoliths. In many cases, graded beds and depositional features seem to be absent, thus leading to the interpretation that such tuffs are primarily products of airfall materials. Following recognition by Nixon (1995), kimberlites in Lunda provinces have survived erosion within confined crater zones, and consequently preserve crater facies that have been filled with diamondiferous, coarse to fine reworked kimberlite pyroclastic deposits, interstratified with shale and sandstones also having kimberlites components. Similar rock sediments have been finding in the kimberlites pipes located in Kaapvaal Craton (Field *et al.*, 2008; Skinner and Clement, 1979). The Lunda pipes have attracted interest as they contain diamonds, garnet peridotite and eclogite mantle xenoliths.

In contrast, diatreme facies present a different case. The most common rocks observed and analysed are tuffisitic kimberlite breccias containing pelletal lapilli, abundant angular to rounded country rock inclusions (variable size, see Appendix 2), and discrete and fractured grains of olivine, garnet and ilmenite mega- and macrocrysts, set in a fine-grained matrix of microcrystalline carbonate, diopside and serpentine (Wilson and Head, 2007). The rounded clasts (pelletal lapilli) materials observed from sampled pipes can be interpreted to be formed as the magma fluids intrude into earlier volcanoclastic infill materials within diatreme zones (Mitchell, 1986; and Kamenetsky *et al.*, 2011).

## 5. 2. Discussion - Mössbauer spectroscopy

The following discussion is more to illustrate the promising nature of Mössbauer spectroscopy in diamond research than to deliver firm conclusions, since a great many sample analyses from each kimberlite pipe would need to be carried out to enable certainty. Mössbauer Spectroscopy (MS) has been widely used in several geoscientific environments to investigate materials containing Fe-bearing minerals (McCammon *et al.*, 1998, 2000; Al-Rawas *et al.*, 2008; Frost *et al.*, 2004). Determination of the ratio of the oxidation states of iron, often presented as  $\text{Fe}^{3+}/\Sigma\text{Fe}$ , (Virgo *et al.*, 1988), or  $\text{Fe}^{3+}/\text{Fe}^{2+}$  (Seda and Hearne, 2004) from rock-forming minerals is an important method in the study of iron bearing materials (e.g. ilmenite, pyroxene and garnet). This is because accurate redox ratios obtained from Mössbauer spectroscopy of deposited minerals can potentially provide key information about their weathering history (Seda and Hearne, 2004; Homonnay, 2004) and the diagenesis of these materials after deposition at a particular location.

With regard to the origin of megacrysts or macrocrysts of garnet, pyroxene, ilmenite used in all analytical methods from this research, this project highlights those that have crystallised from protokimberlite melt which imply that they could be early crystallising pre-intrusion phenocryst in the recent kimberlite magma. This statement is consistent with the work of Mahotkin *et al.*, (2000) who explained that megacrysts of clinopyroxene, garnet and ilmenite are derived at base base of lithospheric mantle depths (250-300 km, Shirey, and Shigley, 2013) from primitive or protokimberlite magmas separated from sub-lithospheric convecting mantle at several hundreds of kilometres depths within the mantle. See furthermore discussion in section 4.2.

Ilmenite ( $\text{FeTiO}_3$ ) is commonly found as a rock inclusion in kimberlites and volcanic rocks (Wyatt *et al.*, 2004), and it is generally used as an indicator mineral in diamond exploration environments (Keulen *et al.* 2009). Here we have used ilmenite as an indicator mineral because its' iron naturally occurs in two oxidation states ( $\text{Fe}^{3+}$  and  $\text{Fe}^{2+}$ ) and the ratio of these two oxidation states vary under different geological conditions. For this reason it is a good candidate for studying redox conditions in different geological environments (Seda and Hearne, 2004).

Tables 5.1 presents a summary of the analysed redox ratios of ilmenite from samples taken from all five diamondiferous kimberlite pipes studied. These results and fitted Mössbauer parameters (CS, QS, and LW) are consistent with Mössbauer data for natural ilmenite reported previously in the literature (Virgo *et al.*, 1988; Waerenborgh *et al.*, 2002; Tronche *et al.* 2010; Seda and Hearne, 2004; Dyar *et al.*, 2006; Gibb *et al.*, 1969; Das *et al.*, 1996; and Jancik and Mashlan, 2002). Small variations may be observed between data sets - the reasons for variation may be associated with geological factors, such as different pressures, temperatures, depths, environments and metasomatoses/alteration processes,

within sampled kimberlite pipes, all of which can impact upon iron oxidation state and environment within kimberlites. According to Dyar *et al.* (2006), CS is a very sensitive parameter to the oxidation state and coordination number of iron in the sample. According to Bancroft (1979), the CS in silicate minerals decreases as the Fe coordination number decreases to about 0.2 mm/s. This statement is also supported by Dyar *et al.* (2006) who explained that CS values predictably decrease with increasing *s*-electron density around the nucleus which mean that so they also depend on the type and bond lengths of ligands coordinated to the Fe atoms. All Mössbauer spectral measurements were carried out at room temperature, which was measured by thermometer at  $296 \pm 2$  K for all measurements. The redox ratio results ( $\text{Fe}^{3+}/\Sigma\text{Fe}$ ) are provided in Table 5.1 and fitted spectra are presented in section 4.31.

In order to validate the ilmenite criteria/model for diamond preservation condition, (Figure 4.35, presented in Chapter four) and the observed levels of diamond resorption (Figure 4.34, in Chapter Four) from the sampled kimberlites, Mössbauer spectroscopy was carried out in this research to analyse and determine the redox ratios, ( $\text{Fe}^{3+}/\Sigma\text{Fe}$ ) for the different ilmenites, and consequently these ratios were used as a means of estimating  $f\text{O}_2$  during formation and ascent of kimberlite.

Mössbauer spectra, shown in Chapter Four, were successfully fitted with:

- ✓ Two hyperfine doublets, for example (CAT- 67 Grt), (CMT 05 Grt), and (CAT-62a), (CX1) and (CW045b), (CW 63), (CMT 01), (CX1), (CX027);
- ✓ Three hyperfine doublets (CAT59HM1), (CAT 67NMM), (CMT58), (CX 022); (CW0045D); (CAT 59d); (CAT=MY001C), (CAT 67M), (CMT 253), (CMT 60), CAT 5;
- ✓ One hyperfine doublet was fitted at sample CX12N, and interpreted as hematite mineral.

Pure ilmenite phases were fitted with one doublet for  $\text{Fe}^{2+}$  and one for  $\text{Fe}^{3+}$ . The third doublets fitted to the spectra (CAT-5) and (CMT-60) for ilmenite samples, were necessary in order to provide robust fits, and can be attributed to  $\text{Fe}^{2+}$  present in the second phases (amphiboles) confirmed by XRD to be present in these samples (see XRD results, Figure 4.21). A complex case with the presence of minor inclusions of amphibole and magnetite within an ilmenite sample was observed for sample CW 0045D in Figure 4.20. This result confirms once again that the sampled kimberlite ilmenite has been modified and oxidised from its original form. Highly oxidised ilmenite samples are suggestive of poor diamond preservation conditions. The oxidation state of iron indicates the amount of oxygen present when a mineral is formed. If the environment was abundant in oxygen, assemblage minerals present will contain oxidized iron,  $\text{Fe}^{3+}$ , whereas the reducing environment will have more  $\text{Fe}^{2+}$ . The amount of oxygen present influences the elements that interact in magma, as well as which minerals form; this is known as oxygen fugacity ( $f\text{O}_2$ ).

Appropriate papers from the previous published works using Mössbauer spectroscopy in advanced diamond research, were used in this project in order to compare and consequently to validate the calculated redox ratios of the ilmenite studied samples. In this study, the iron redox ratio, expressed as  $\text{Fe}^{3+}/\sum\text{Fe}$ , e.g.  $\text{Fe}^{3+}/(\text{Fe}^{3+} + \text{Fe}^{2+})$ , was calculated from appropriate sub-spectral areas. The results are consistent with published data for kimberlites and indicate a range of oxygen partial pressures during kimberlite formation and ascent for different pipes (Tables 5.1 and 5.2). These results support the main original project hypothesis concerning diamond grade variation and surface abundance.

The iron redox ratios in ilmenite inclusions from the sampled kimberlites have been fundamentally important as they have provided qualitative estimates of the oxygen fugacity in the studied kimberlite pipes. This statement is supported by a substantial body of literature which shows that iron redox ratio ( $\text{Fe}^{3+}/\text{Fe}^{2+}$  or  $\text{Fe}^{3+}/\sum\text{Fe}$ ) depends critically on oxygen fugacity (McCammon *et al.*, 1998; Quintiliani, 2005; Fedortchouk and Zhang, 2011, Fedortchouk and Canil, 2009). It can therefore be confidently concluded that the resorption of diamond and its grade variation within different volcanic kimberlite pipes depends strongly on oxygen fugacity. Note that the spectral areas of the  $\text{Fe}^{2+}$  and  $\text{Fe}^{3+}$  components in the Mössbauer spectra for ilmenites, garnets and spinels presented in Chapter 4 have been used to calculate the iron redox ratio  $\text{Fe}^{3+}/\sum\text{Fe}$  (McCammon *et al.*, 2001; Virgo *et al.*, 1988; Waerenborgh *et al.*, 2002). It was assumed that the recoil-free fractions of  $\text{Fe}^{2+}$  and  $\text{Fe}^{3+}$  are equal based on literature evidence for a  $\text{Fe}_{1-x}\text{Ti}_{2-x}\text{O}_5$  solid solution (Guo *et al.*, 1999). However, there is also evidence suggesting that the recoil-free fractions of  $\text{Fe}^{2+}$  and  $\text{Fe}^{3+}$  components may differ (de Grave and Alboom, 1991; and Eeckhout and de Grave, 2003), and this may have led to a systematic overestimation of  $\text{Fe}^{3+}/\text{Fe}^{2+}$ . Here only uncorrected data are presented (i.e.  $f=1$ , see Table 5.2). It is noted that for some of the compounds investigated by de Grave and Alboom (1991) and Eeckhout and de Grave (2003) are synthetic and so it is expected that their recoil-free fractions may be slightly different from those of the natural minerals that have been studied in this project (ilmenite, garnet, pyroxene and amphiboles), owing to the presence of impurities in the natural samples.

For samples CMT 58, CAT59HM1, CAT=MY001C and CAT 59 d it was not possible to calculate the iron redox ratio of the ilmenite phases present in these samples because they were multiphase materials with relatively low abundances of ilmenite and high abundances of amphibole. Separation of the respective ilmenite and amphibole  $\text{Fe}^{3+}$  components in the Mössbauer spectra proved impossible as their hyperfine parameters (CS, QS and LW) are closely similar (Gunter *et al.*, 2003; Das *et al.*, 1996; Gibb *et al.*, 1969; Virgo *et al.*, 1988; and Waerenborgh *et al.*, 2002). For these spectra one  $\text{Fe}^{3+}$  doublet was fitted to the combined ilmenite and amphibole  $\text{Fe}^{3+}$  contributions. Consequently it was not possible to separately assess the  $\text{Fe}^{3+}$  content of the ilmenite phases from Mössbauer data and so there is no measured ilmenite iron redox ratio available for these samples. We have provided upper limits of the redox ratio (Tables 5.1) by assuming that all  $\text{Fe}^{3+}$  in the relevant

doublets arises from the ilmenite phase. This presents an "upper redox boundary" and by no means quantifies the iron redox ratio in these phases

Calculated		Comparable Data From Literature	
Kimberlite names	Ilmenite redox ratio ( $\text{Fe}^{3+}/\Sigma\text{Fe}$ )	References	Ilmenite ( $\text{Fe}^{3+}/\Sigma\text{Fe}$ )
Camatxia (CMT 60)	0.24	Virgo <i>et al.</i> 1988	0.244
Camutue (CW045b)	0.26	Virgo <i>et al.</i> 1988	0.265
Camatxia (CMT 253)	0.25	Virgo <i>et al.</i> 1988	0.192
Camutue (CW 63)	0.25	Virgo <i>et al.</i> 1988	0.244
Catoca (CAT 62a)	0.32	Waerenborgh <i>et al.</i> 2002	0.31
Catoca (CAT 5)	0.41		
Caixepa (CX1)	0.27	Waerenborgh <i>et al.</i> 2002	0.21
Camutue (CW 0045D)	0.36		
Caixepa (CX 022)	0.37		0.3-0.4
Catoca (CAT 59 d)	$0 < \text{Fe}^{3+}/\Sigma\text{Fe} < 0.77$	N/A	N/A
Catoca (CAT=MY001C)	$0 < \text{Fe}^{3+}/\Sigma\text{Fe} < 0.79$	N/A	N/A
Catoca (CAT59HM1)	$0 < \text{Fe}^{3+}/\Sigma\text{Fe} < 0.79$	N/A	N/A
Catoca (CMT58)	$0 < \text{Fe}^{3+}/\Sigma\text{Fe} < 0.93$	N/A	N/A

Table 5.1. Comparison of redox ratios obtained for Lunda ilmenite mineral inclusions with literature values for ilmenites obtained from Portugal and South Africa.

It is noted that in the some kimberlite ilmenites studied here, high  $\text{Fe}^{3+}/\Sigma\text{Fe}$  ratios are associated with low/moderate MgO contents (Figure 4.33). The sampled kimberlite pipes and their examined rocks that contain ilmenites with low  $\text{Fe}^{3+}/\Sigma\text{Fe}$  ( $< 0.27$ ) and high MgO contents, such as sample CMT 253, CW 63, CX1, CW045b and CMT-60, are believed to have crystallized early in ascent and thus under low  $f\text{O}_2$  conditions (Virgo *et al.*, 1988; Gurney and Zweistra, 1995; Nowicki *et al.*, 2007) and consequently has a higher chance for diamond survival, whereas CX03, CW0045D, CX022), CAT5, CAT59d, CAT=MY001C, CAT59HM1 and CAT58 with  $\text{Fe}^{3+}/\Sigma\text{Fe} > 0.32$  are more oxidised (Table 5.1). This evidence is also consistent and it is supported by the results in Figure 5.1. The two doublets fitted to the ilmenite spectra are typical of  $\text{Fe}^{2+}$  and  $\text{Fe}^{3+}$  in natural ilmenites and clearly show significant differences in the redox ratio,  $\text{Fe}^{3+}/\Sigma\text{Fe}$  between the different samples. Redox differences from natural ilmenites have also been reported by Gibb and Greenwood (1969); Seda and Hearne, (2004); Virgo *et al.* (1988); and Gunter *et al.* (2003).

Mössbauer spectroscopy results from spectra for CMT-60, CX1 and CW045b in Figures 4.12;4.13 and Tables 4.3 and 4.4, show that their ilmenites are considerably more reduced than the CAT-62a and CAT-5 ilmenites, as demonstrated by its higher  $\text{Fe}^{3+}/\Sigma\text{Fe}$  ratios of 3.05; 2.80 and 2.59 compared with 2.06 and 1.28. The Mössbauer results for CMG-60, CX1 and CW045b are dominated by  $\text{Fe}^{2+}$  which is indicative of more reducing environments during formation and ascent, compared with samples CAT-62a and CAT-5.

Ilmenites with a high  $\text{Fe}^{3+}/\Sigma\text{Fe}$  ratio are associated with higher resorption of diamond than those with lower  $\text{Fe}^{3+}/\Sigma\text{Fe}$  ratios, i.e. more ferrous iron ( $\text{Fe}^{2+}$ ). The lower  $\text{Fe}^{3+}/\Sigma\text{Fe}$  ratios in ilmenites from three of the diamond deposits studied here (Caixepa, Camutue and Camatxia) gives a strong indication of good diamond preservation conditions. However, the Catoca samples, with their higher  $\text{Fe}^{3+}/\Sigma\text{Fe}$  ratios, suggest relatively poor diamond preservation conditions with higher levels of diamond resorption. In reality the resorption is high in the Catoca diamondiferous kimberlites, which is consistent with this view. However, the Catoca mine still produces the highest abundance of diamond from all of the sampled and studied kimberlite pipes in this study. This suggests that, despite the high levels of resorption in the Catoca diamonds, the Catoca heterogeneous mantle was rich in diamonds prior to ascent. The crucial evidence from both EMPA and Mössbauer spectroscopy for the Camutue, Caixepa, and Camatxia kimberlite pipes can be directly linked with their high diamond quality and lower oxygen fugacity,  $f\text{O}_2$ , during formation and ascent of the kimberlite magma. The main implication from this result is that the resorption of diamonds is high when the mantle or kimberlite magma contains ilmenites with high  $\text{Fe}^{3+}/\Sigma\text{Fe}$  ratios, and consequently this phenomenon leads to lower diamond survival, and lower quality of those diamonds which do survive (Nowicki *et al.* 2007). To summarise - more reduced ilmenites are indicative of higher diamond survival rates, with higher-quality diamonds surviving; and more oxidised ilmenites are indicative of lower diamond survival rates, with lower-quality diamonds surviving. The Catoca results can be explained if the Catoca heterogeneous mantle was particularly rich in diamond prior to ascent. The obtained results and evidence of diamond grade variation and quality from studied samples in this project have also been supported and confirmed by local mining geologists and mineralogists in NE Angola with whom this author has spoken directly, although their evidence cannot be reported here for commercial / confidentiality reasons.

Due to the complexity of emplacement of diamondiferous kimberlite deposits and consequently the high degree of alteration that many pipes experienced during volcanic emplacement (Kjarsgaard, 2007), the application of mineral geothermometers and oxygen barometers for the estimation of temperature and oxygen fugacity ( $f\text{O}_2$ ) in kimberlite magmas is usually not feasible (Fedortchouk and Canil, 2004). However, there are possible measures of redox conditions and  $f\text{O}_2$  in kimberlite

deposits, these are Fe redox ratio  $\text{Fe}^{3+}/\sum\text{Fe}$  in the ilmenite (Table 5.1.) and chemical composition (Table 4.16, Figure 4.35 and Figure 5.1). According to Nowicki *et al.* (2007), differences in the  $\text{Fe}^{3+}/\sum\text{Fe}$  ratio in ilmenite are indicative of different  $f\text{O}_2$  during kimberlite formation and ascent (also McCammon *et al.* 1998; 2001). Increased oxygen fugacity is the main diamond destroyer (Gurney and Zweistra 1995). The ilmenite samples, for this research, present different levels of  $\text{Fe}^{3+}$  and different redox ratios  $\text{Fe}^{3+}/\sum\text{Fe}$  (Table 5.1). These are indications that the sampled kimberlite ilmenites from NE Angola have been modified and oxidised, to differing degrees, from their original states. This is supported by EMPA and petrographic results from this project. This result is also supported qualitatively by evidence from both optical microscopy and electron microprobe analysis in Chapter Four. It is therefore argued that  $^{57}\text{Fe}$  Mössbauer spectroscopy can be used to qualitatively (perhaps quantitatively) estimate  $f\text{O}_2$  for different kimberlite pipes and consequently assist geologists and mineralogists to effectively evaluate and differentiate between economical and non-economical diamond deposits. The complexity of Mössbauer spectroscopy results for the studied samples may be associated with several geological factors such as different kimberlite emplacement environment / facies, different magnetic / iron-containing phases present in samples, fluid reaction processes, and alteration. The values of fitted parameters from Mössbauer spectra obtained in this study are similar to those published by several authors (Luth *et al.*, 1990; Virgo *et al.*, 1988; Waerenborgh *et al.*, 2002; Gibb *et al.*, 1969; Dyar *et al.*, 2006; and McCammon *et al.*, 1998) The oxidation state of the ilmenite mineral inclusions studied here are, therefore, a good indicator of the oxidation state of the host kimberlite assemblage, which in turn determines the origin and genesis of diamond (Seda and Hearne, 2004).

Figure 4.14 shows the spectrum for sample (CAT 67NMM), fitted with parameters  $\text{Fe}^{2+}$  (CS=1.12; QS = 2.92; W= 0.18) and  $\text{Fe}^{3+}$  (CS = 0.31; QS = 0.75; W= 0.40) for the amphibole. These parameters are within agreement with those previously published by Gunter *et al.* 2003 and Waerenborgh *et al.* (2002). But the more complex sample spectrum for CAT 59HM1 is due to the minor inclusion of ilmenite in the analysed sample. The presence of the ilmenite in Mössbauer analysis (CAT 59HM1) is also supported by XRD results for this sample. The spectrum was fitted with amphibole as the main component. The second doublet for ilmenite inclusions shows an excess in  $\text{Fe}^{3+}$  which is a crucial indication of high oxygen fugacity, consequently a more oxidised environment (poor preservation conditions of diamond). This makes interpretation difficult. For example, due to the complexity of the sample and it being more oxidised, and lack of  $\text{Fe}^{2+}$  in the sample. It can be assumed that the  $\text{Fe}^{2+}$  may be present in very small amounts and it may be possible that  $\text{Fe}^{2+}$  is in the amphibole phase and not the ilmenite phase in this sample. An excess of  $\text{Fe}^{3+}$  in ilmenite has been described by Nowicki *et al.* (2007) to be associated with high resorption diamond environments.

As demonstrated in Figure 4.15 and Table 4.7, the garnet spectra were fitted with one Fe<sup>2+</sup> doublet and one Fe<sup>3+</sup> doublet according to conventional models (Sobolev *et al.*, 1999). The Mössbauer spectra for both samples (CAT 67 Grt and CMT 05 Grt) show similar degrees of asymmetry. Both samples CAT 67 Grt and CMT 05 Grt show the same asymmetric feature in the Fe<sup>2+</sup> doublet as in Almandine garnet (Fe<sub>3</sub>Al<sub>2</sub>Si<sub>3</sub>O<sub>12</sub>) (Dachs *et al.*, 2012). The measurements show that this almandine has a small Fe<sup>3+</sup> doublet with an area of 8.6% of the total Fe, which is the stoichiometric almandine composition (Dachs *et al.*, 2012). The fits show a small asymmetry, overestimating the signal at -0.5 mm s<sup>-1</sup> and underestimating it for the signal at +3 mm s<sup>-1</sup>, in the quadrupole doublet. The cause of this asymmetry of the Fe<sup>2+</sup> doublet could have different possible sources, which have been widely reported (Bull *et al.*, 2012; Cerná *et al.*, 2000; and Dachs *et al.*, 2012), as follows:

1. Partial substitution of Fe<sup>2+</sup> by Mg<sup>2+</sup> which can change the hyperfine parameters and paramagnetic relaxation of Fe<sup>2+</sup> in the dodecahedral site. According to Cerná *et al.* (2000) the IS and QS of Fe<sup>2+</sup> in the dodecahedral sites are large compared to other minerals values of Fe<sup>2+</sup>. These large values could be indicative of the high spin ferrous iron in a highly ionic state. It is interesting to see the values of IS (1.28mm/s) and QS (3.53mm/s) from the studied almandine garnet sample (Table 4.7) of this project are in agreement to those reported by Armbruster *et al.* (1992) and Cerná *et al.* (2000). According to Cerná *et al.* (2000), who studied similar materials, the commonly observed asymmetry in quadrupole doublets in the room temperature spectra has its origin on the paramagnetic relaxation of Fe<sup>2+</sup> in the dodecahedral position. The degree of spectral asymmetry is approximately the same for both samples and, as noted above, it may depend on Mg<sup>2+</sup> (Fe<sup>2+</sup>) content in dodecahedral site (Armbruster *et al.*, 1992), and this reflects the characteristic for spin-spin relaxation. This statement is supported by Cerná *et al.* (2000), who explained that the asymmetry of Fe<sup>2+</sup> doublets in almandine-pyrope is induced by spin-spin paramagnetic relaxation, which means that this asymmetry depends on Mg<sup>2+</sup> content in dodecahedral sites and is induced by spin-spin paramagnetic relaxation of ions in dodecahedral sites.
2. Spectral asymmetry is often associated with intensities for a single crystal absorber, which are not the same in all crystal directions. The observed asymmetry may therefore be associated with sample preparation and preferred orientation of sample absorbers (Garg, 1980).
3. The third possible cause of the asymmetry in the CAT 67 Grt and CMT 05 Grt spectra (Figure 4.15) is the Goldanskii-Karyagin effect (Mansel and Vogl, 1976; Garg 1980; and Bull *et al.*, 2012). The Goldanskii-Karyagin effect (GKE) is anisotropy of the recoilless fraction in minerals or solid materials. If the Mössbauer nucleus is within a non-cubic crystal site then it can have anisotropic mean-square vibrational amplitude and the recoil-free fraction will

depend on the orientation of the gamma ray relative to the site coordinate axes of the absorbing nucleus (Dickson *et al.*, 2005). The equivalent recoilless fractions are anisotropic and consequently Goldanskii-Karyagin effect is manifested by an asymmetric quadrupole doublet in polycrystalline absorbers (Bull *et al.*, 2012). To give an example of this in relevant minerals, GKE is exhibited in the Fe<sup>2+</sup> quadrupolar doublet produced by some almandine garnets (Bull *et al.*, 2012; and Dachs *et al.*, 2012).

Several workers have disagreed over the causes of the spectral asymmetry in almandine garnets. For example, Cerná *et al.* (2000) stated that the asymmetry of the lines in almandine garnet does not change in the spectra taken at different orientations of the absorber to the incident gamma rays and similar areas of the two resonant lines, therefore the asymmetry cannot result from a Goldanskii-Karyagin effect whereas Bull *et al.* (2012) stated that the Goldanskii-Karyagin effect was manifested by an asymmetric quadrupole doublet in almandine garnet absorbers if the equivalent recoilless fractions are also anisotropic in different direction (Dickson and Berry, 2005). It is not possible, from the data available for our samples, to establish which of these explains the observed behaviour; however, our results are entirely consistent with those from the relevant literature for garnets. Also Figure 4.15 illustrates another multi-complex fitted sample (CMT 05 Cpx) with possibility of existence of more than three minerals present (Garnet, clinopyroxene and magnetite or hematite) which has generated some fitting problem, despite a successful result for the analysis and fitting. The parameters of doublets 1 and 3 were fitted as clinopyroxene (Fe<sup>2+</sup> and Fe<sup>3+</sup>) and they are in agreement with those previously published by Sobolev *et al.* (1999); Viera *et al.* (1983); and McMammon *et al.* (1998). The fitted parameters of garnet are consistent with those reported previously in the literature (Dyar *et al.*, 2006; McMammon *et al.*, 1998; Luth *et al.*, 1990; and Sobolev *et al.* 1999). The major difference from others authors is that pyroxene has been fitted with three doublets but in contrast, the pyroxene for this research was fitted with 2 doubles (one for Fe<sup>2+</sup> and another one for Fe<sup>3+</sup>).

The pyroxene samples used by Viera *et al.* (1983) and McMammon *et al.* (1998) contain more Fe<sup>2+</sup> and very small amounts of Fe<sup>3+</sup> whereas the pyroxene sample (CMT05Cpx) for this project contain high amounts of Fe<sup>3+</sup> which means that the samples are more oxidised and much of Fe<sup>2+</sup> may possibly have been transformed to Fe<sup>3+</sup>. The fitting analysis for sample CMT05Cpx has led to the conclusion that this sample may contain some minor inclusions of hematite or magnetite. Due to the limited signal to noise ratio it was difficult to fit spectra for both minerals. It can be assumed that the Fe<sup>3+</sup> for garnet is probably very small and may be in the same area of Fe<sup>3+</sup> for clinopyroxene but it is difficult to specify the exact amount. The iron redox ratios for garnet (Table 5.2) are indicative of low oxygen fugacity in the Camatxia pipe, this is consistent with the lower oxygen fugacity garnet from George Creek, Colorado Wyoming Province, (McCammon *et al.*, 1998).

Calculated		Published in Literature	
Kimberlite names	Garnet redox ratio (Fe <sup>3+</sup> /ΣFe)	Garnet (Fe <sup>3+</sup> /ΣFe)	References
Catoca CAT67(Gnt)	0.08	0.03	McCammon <i>et al.</i> , 1998
Camatxia CMT01(Grt)	0.63	0.07	McCammon <i>et al.</i> , 1998
Camatxia CMT05(Grt)	0.34	>0.10,	Luth <i>et al.</i> ,1990
Camatxia CMT01(Cpx)	0.46		

Table 5.2. Comparison of redox ratios obtained for Lunda garnet mineral inclusions with literature values for garnet obtained from South Africa kimberlites

As shown in Figure 4.16 and Table 4.8, Mössbauer fitting parameters of spectra for sample CAT - 67M were fitted with amphibole as a major component, and also the presence of Fe<sup>3+</sup> and Fe<sup>2+</sup> in magnetite (spinel) mineral, detected as sextets, with effective hyperfine fields (H) of 47.8 T and 42.7 T (tesla). These values are much closer to those published by Maddock, (1997). It can be argued that these magnetic field (Tesla) values may give some indication that this Magnetite may have been under transformation process into hematite during evolution through oxidation of structural Fe<sup>2+</sup> to Fe<sup>3+</sup>, which implies altered rock (Santana *et al.* 2001).

As shown in Figure 4.16 and Table 4.8, data were fitted with Fe<sup>2+</sup> and Fe<sup>3+</sup> doublets (1 and 2) for sample CAT 67M were fitted as amphibole and this parameters are similar to those published by Gunter *et al.* (2003) and Waerenborgh *et al.* (2002) whereas sample CMT 58 contains a small amount of ilmenite which was fitted with doublets 2 and 3, these values are comparable to Gibb and Greenwood (1969). Despite minor inclusion of ilmenite was detected, at sample CMT58 but it is hard to tell the precisely position whether the Fe<sup>3+</sup> is for ilmenite or amphibole. It can me assumed that Fe<sup>3+</sup> for ilmenite (sample CMT58) may share the same area for Fe<sup>3+</sup> of amphibole (sample CMT58).

The ilmenite from sample CMT 58 contains higher levels of Fe<sup>3+</sup> which is not usual. According to Gibb *et al.* (1969), lower abundance of Fe<sup>2+</sup> in natural ilmenite is due high Fe<sup>3+</sup> in the kimberlite. Based on evidence from Mössbauer spectral analysis (sample CMT 58), the high Fe<sup>3+</sup> in the sample is indicative of strongly oxidising processes that occurred within the sampled mantle. The combination of the observed industrial (lower) diamond quality from the Catoca mine and the results presented here indicate that the Catoca kimberlite pipe is more oxidised than the other kimberlite pipes, resulting in high diamond resorption (poor diamond preservation environment).

As seen in Figure 4.17 and Table 4.9, both Catoca samples are complex, multiphase samples. Doublet 1 for sample CAT 59d was fitted with the parameters for amphibole and these values are in agreement

with Waerenborgh *et al.* (2002). Doublets with centre shifts of 1.01 and 1.07 mm/s relative to metallic iron, quadrupole splitting of 0.75 and 0.73 mm/s, corresponds to ferrous iron ( $\text{Fe}^{2+}$ ), and other doublets with an isomer shifts of 0.32 and 0.32 mm/s and quadrupole splitting of 0.52 and 0.55 mm/s correspond to ferric iron ( $\text{Fe}^{3+}$ ). These values are also in agreement to those published by Jancik and Mashlan, (2002). Sextets 1 and 2 were fitted with parameters of magnetite (Maddock, 1997 and Waerenborgh *et al.*, 2002).

As shown in Figure 4.18, the fitting of this sample (CMT253) is complex and may be due to several factors associated with mineral samples, such as distribution or orientation of particle size in magnetic phases, with regard to the incident gamma rays, and orientation of the magnetization with the gamma rays can affect the peak intensity. Doublets 1 and 2 were fixed and fitted as ilmenite (Table 4.10) and component 3 was fitted as amphibole. The results are in reasonable agreement with Waerenborgh *et al.* (2002). The spectrum is dominated by magnetic phases. Fitting parameters for hematite were attempted but did not work during the fitting process. It can be explained by the complexity of the spectrum, the fitting strategy used was to allow the linewidth ( $w$ ) to vary differently to magnetic fitting where usually ratio  $w1/w3=1$  and  $w2/w3=1$ . In order for the fitted spectrum to be reasonable and well fitted, the ratio of linewidth was increased ratio to 3 ( $w1/w3=3$ ) and  $w2/w3$  to 1.5. The main problem associated with this spectrum is probably due to the distribution or orientation of particle size in magnetic phase and composition of the sample. It is interesting to observe that a relatively low-intensity magnetic and low  $H$  (magnetic hyperfine field) spectrum parameter, appears in the altered rock samples, which is assigned to linked  $\text{Fe}^{3+}$  in spinel sites (Santana *et al.*, 2001). The  $H$  is lower compared to those values from Santana *et al.* (2001); and Waerenborgh *et al.* (2002). Again, the reason of  $H$  for sample (CMT 253) to have lower value could be probably due to factors mentioned already above, at the beginning of section 5.2. According to Santana *et al.* (2001) when the rock samples are weathered or altered, it tends to have higher  $H$ , ranging from 41.7 - 56.3 T.

The spectrum for sample CX 12N provides good quality data (Figure 4.18) and was fitted as hematite. The result seems to be reasonable with expected field ( $H=49.6$  T for hematite) which is comparable to those published by Waerenborgh *et al.* (2002). It was not possible to fit the second sextet for magnetite because due to the fitting problem (it could not fit properly). Another key aspect is that due to the very small amount of mineral powder, it was not possible to carry out further XRD analysis.

The spectrum for sample CX 022 in Figure 4.19 indicates a multiphase and complex material but at the same time the fitting result is interesting. The spectrum was fitted with parameters of hematite with 2 sextets, which is not usual. When the spectrum was fitted with parameters for magnetite, no fit was obtained. Then, the Mössbauer spectrum was fitted as hematite and the result was sensible. However, hematite has been widely fitted with one sextet (Dickson, and Berry, 2005; Greenwood and Gibb, 1971; Waerenborgh *et al.*, 2002). Based on the analysis and interpretation for this particular

sample, it can be assumed that the original magnetite was probably transformed into hematite through progressive oxidation of structure  $\text{Fe}^{2+}$  to  $\text{Fe}^{3+}$  but this transformation may not be completed yet. The magnetic field values ( $H=49.1$  T and  $H=51.1$  T) are comparable and supported the works of Santana *et al.* (2001) who explained that during petrogenesis (origin) the magnetite can be transformed into hematite via an oxidation process. Sample (CX (027) in Figure 4.19 contains minor inclusion of ilmenite fitted with values for doublets 1 and 2 (Table 4.11) that are similar to those for natural ilmenite published by Das *et al.* (1996) and Gibb *et al.* (1969).

Another complex result arose with sample CW 0045D in Figure 4.20. The result is complex because the sample is a multi-phase material with more than 3 minerals (hematite, magnetite, ilmenite and amphibole). The fitting quality is therefore not high; this is may be due to the poor signal obtained during the MB sample analysis on instrument. This estimated fitting values to give indication of the present phase in rock (ilmenite, and amphibole) all fitted as doublets sites. Probably both hematite and magnetite also may be present due to the two sextet's features, whereas the spectrum for sample CX03 from Caixepa diamondiferous pipe was fitted as magnetite (Maddock, 1997).

### **5. 3. X-ray diffractometry (XRD)**

X-ray powder diffraction (XRD) has been widely discussed in the geological literature (Gibb *et al.* 1969). In order to validate the phases present in samples for the purpose of Mössbauer spectroscopy, X-ray powder diffraction (XRD) was used for phase identification of crystalline materials present in the samples studied, for example (Figure 4.21), CAT 5, CAT-62 and CMT 60. Complex multi-phase samples (magnetite, hematite, ilmenite, amphibole and unidentified elements) were also analysed. These were samples CW045B, CX1 and CW0045D in Figure 4.22; samples CW0045, CAT59i1, CAT50 and CX027 in Figure 4.24; and samples CAT50HM2, CATHMa, CAT50HM1 and CAT 59D in Figure 4.24. Each crystalline solid has its own characteristic X-ray powder diffraction pattern which can be used as a fingerprint for its identification (Moecher 2004). Determination and characterization of crystalline materials is a critical process in geology and in environmental and materials science studies (Moecher 2004). As expected, due to the complexity of kimberlite formation and its emplacement during ascent to surface (Kamenetsky *et al.*, 2006; Cas *et al.*, 2008), some XRD results show the presence of multiphase materials, which makes interpretation more difficult. However, many XRD patterns show that the dominant phase was ilmenite, amphibole, hematite and / or magnetite. As explained in Section 4.3, due to the very small amounts of mineral powder available, this had to be prioritised for Mossbauer spectroscopy and therefore it was not possible to carry out XRD analysis for certain samples. To summarise, XRD analysis proved very useful for this project, due to the following reasons:

- a. Phase identification of a crystalline materials/minerals present in the complex kimberlite rocks and in the peridotite and eclogite sampled mantle.
- b. Once the minerals phases have been identified, then this process can assist or guide to select the right samples for Mössbauer spectroscopy analysis

The main mineral phases detected in CMT-60, CAT 62a and CAT 5, were ilmenite and hematite. Other phases identified contained iron oxide and silicon oxide. As expected, hematite, magnetite, together with ilmenite, were the main phases observed in studied rock, although low-intensity diffraction peaks show that a number of phases were detected in CMT 60.

#### **5. 4. Electron Micro Probe Analysis (EMPA)**

Major-element compositions were determined by JEOL JXA8230 Electron Micro Probe Analysis (EMPA) and using the four-spectrometer CAMECA SX-50, in the School of Chemical and Process Engineering at the University of Leeds. All silicate and oxide analyses were run using an accelerating voltage of 15kV, a nominal beam current of 30nA and a focussed beam. Note that Quantitative analysis (tables 4.16 & 4.17) was accomplished by measuring the intensity of the characteristic wavelengths for each element present in the polished thin sections (50mm×28mm) samples. The application of EMPA in this project is important as it provides the total chemical composition of Fe present in the rock. Based on this fact Mössbauer does not tell the total amount of iron present.

Again, the interpretations of the result from EMPA analysis are complicated by the fact that the mantle rocks in the Lucapa Graben have experienced later alteration, and the garnet, olivine; ilmenite chromite crystals chemistry also reflects these later redox reactions. As demonstrated on Figure 4.30, most examined mantle ilmenite from all sampled kimberlite pipes show a complex process of formation. The exsolved ilmenites and replacement phases are abundant with alterations along the border and discontinuities Figure 4.26 (a and b), and ilmenite, which apparently exsolved parallel to rhombohedral directions Figure 4.26 (a). The Textural evidence of replacement of Fe<sup>3+</sup> rich homogeneous ilmenite is probably due to the action of fluids reaction, and it may appear to be derive by mantle metasomatism under at high oxygen fugacity environment. In addition, this process may take place when ferric (Fe<sup>3+</sup>) rich ilmenite (dark grey) reacted with melt under reducing conditions, consequently generating a slightly light Mg-rich ilmenite (Robles-Cruz *et al.*, 2009). The presence of Mn rich ilmenite (sample an in Figure 4.26) is a product of the reaction of lately melts, for instance fluid rich in Carbon dioxide (CO<sub>2</sub>). The major implication from the interpretation of this complexity of ilmenite formation process is that even having presence of more ferric Fe<sup>3+</sup> and lack of the original Mg-rich ilmenite, as result it cannot be ruled out the presence or mineralization of diamond within Lucapa graben kimberlites. A poikilitic texture is also found where the host-oikocryst

of ilmenite Figure 4.26 (b) contains inclusions carbonate. Due to the complexity process of ilmenite replacement (Figures 4.26; 4.27; 4.28) it is difficult to establish the timing and whether this replacement was produced before kimberlite emplacement. It can be however, confirmed that petrographical texture (Kelyphite or corona texture) is a late stage deformation process at Figure 4.26 (b) and (d). This texture is simply referred to a fine-grained, fibrous intergrowth of multiple mineral phases including amphibole, pyroxene and spinel, forming a rim surrounding garnet and also similar texture was detected at ilmenite Figures 4.26 (b) and Figure 4.28 (b) and (c). Normally this texture takes place under lower pressure environment. Mechanical and chemical deformation was detected at sample (b) in Figure 4.27.

Though the samples have experienced metasomatic processes, the primary mineral assemblages, from both E-types and P-types, are considered to be sourced from – equilibrated mantle (Nowicki *et al.*, 2007), and nothing has proved contrary from this investigation, therefore this is a good sign, principally for calculation of geothermobarometry of diamond formations based on coexisting mineral pairs and for determination of oxygen fugacity which is a critical parameter for diamond preservation. Due to retaining their mantle-equilibrated assemblages during and subsequent to transportation by kimberlite magma, mantle xenoliths have provided direct history information of the mantle source environment in which they formed (see Figures 3.5). Based on the mantle hypothesis, the examined eclogites (Figure 3.5 Cat 18), suggests to be generated by high-pressure crystallization from peridotite generated magmas (Barth *et al.*, 2001) that rise through the lithosphere. The combination of the hand specimen descriptions and petrography examination suggest that kimberlite rocks from Lunda province, NE Angola present evidences that they are formed through different facies these including, the crater, diatremes and hypabyssal. In addition, the evidence of diamond grade distinction from the working model (Figure 4.34.), laboratory investigation, and a work experience as a mineralogist and geologist, have led to the interpretation that kimberlite pipes from LP present a variation of diamond contents within sampled kimberlite mantle and it is also evidenced on Figure 4.35.

The examined petrography evidences (for example high pressure deformed phlogopite by the growth of spinel, Figure 4.27, sample (d) and dissolution deformation of ilmenite Figure 4.27 (c), clearly show that ilmenite (sample c) is transformed through solvent/solution process, consequently re-deposited in very fine materials as secondary minerals in various combinations of carbonates, sulphates, or even in phosphates. Based on evidences of examined thin section, it can be highlighted that this alteration process on ilmenite is not exsolution. According to Haggerty and Tompkins, (1983), who studied the similar material (kimberlitic ilmenite), they explained that exsolution, in mineralogy for example in ilmenite, is a process through which an initially homogeneous solid solution (e.g. in this case is ilm) separates into at least two different crystalline minerals without the addition or

removal of any materials (e.g. see light oriented exsolution lamellae in an ilmenite host megacryst. The light oriented lamellae in ilmenite are the intergrowths of titaniferrous spinel (ulvospinel, titanomagnetite or magnetite; Latfard, 1995). Normally this take place when the solute (a substance, e.g. Spl) that is dissolved in another substance (a solvent, e.g. ilm), forming a solution.

It can be discussed from this project that the observed crystallographically oriented spinel lamellae in Figure 4.26 (a) has occurred in some megacrysts of ilmenite are probably due to the result of ilmenite-spinel solid solution. This argument can be supported also by Rao and Rao (1965), who studied the exsolution lamellae in an ilmenite host. His work explained that the Ilm-spl solid solution, can be originated due to replacement of some of the  $Ti^{4+}$  ions in the ilmenite structure by  $Cr^{3+}$  (0.63Å),  $Al^{3+}$  (0.51 Å) and  $Fe^{3+}$  (0.64 Å)  $Fe^{2+}$  (0.74 Å) by  $Mg^{2+}$  ions. From Figure 4.30, it can be evaluated that, due to the formation of picrotite or spinel  $(Mg, Fe)(Al, Fe, Cr)_2O_2$ , elongated in [111] directions, and oriented parallel to the [0001] plane of ilmenite, the oxygen positions in these planes normally coincide in ilmenite structures (Rao and Rao (1965). The sort of exsolution observed in this Figure 4.26 can be interpreted to be from lower to intermediate cooling rate or temperature (stability of the solution) which result in formation of spinel, whereas the solid-solution between hematite (hm) and ilmenite occur at high temperature (Craig, 2001).

The zoning texture observed in Figure 4.27 (c) is crucial deformation evidence that can yield considerable information on the paragenetic history of sampled kimberlite rocks. The observed zoning feature in Figure 4.27 (b) may be the resultant from the mineral this mineral being unable to maintain chemical equilibrium with magma during rapid cooling. According to Frank and Raymond (1986) the chemical zoning develops when minerals exist in solid solution series that crystallise with different compositions at different temperatures. It can be discussed that the zoning features in samples (a) and (b) in Figure 4.31 may support evidence of chemical compositions are incompatible in rock (chemical variations) and the incorporation of hydrothermal fluids in kimberlite deposit, change in local pressure and temperature environment at different period of the time of growth (Shore and Fowler, 1996). Normally the core of mineral represents a high temperature original composition and the rim a lower temperature composition of the mineral. All these alteration evidences described above lead to conclusion that sampled kimberlite mantle rock have been strongly affected through metasomatic events.

The compositions of mantle derived ilmenite from diamondiferous kimberlites sources have been compiled from selected published thin section and evaluated in terms of their major element compositions at University of Leeds. Based on chemical compositional, this project has concluded that the ilmenites belong to kimberlite source, having composition 4.5 to 7 wt.% MgO (Catoca pipe) and 8 to 13wt. MgO% (Camagico pipe) which represents the compositional range of ilmenite from

kimberlites. The crustal ilmenites contains  $\leq 4$  wt. % MgO (Harvey *et al.*, 2001). The high percentage of 14 wt.% MgO and low 4 -15 wt.% Fe<sub>2</sub>O<sub>3</sub> from Camagico pipe, reflect good indication for diamond quality reservoir and preservation condition compared to those from Catoca pipe with 4.5 wt.% MgO and 12- 38 wt.% Fe<sub>2</sub>O<sub>3</sub> according to diagram 4.35 and Table 4.16.

The process of distinction of ilmenites derived from kimberlitic versus non-kimberlitic rocks is crucial process in the context of diamond exploration in regions in which ilmenites are present in relatively low abundance but where the ilmenites are the dominant kimberlitic indicator mineral (Harvey *et al.* 2001). The chemical composition 1 - 3.9 wt.% Cr<sub>2</sub>O<sub>3</sub> and 4.5- 16 wt.% MgO of ilmenite is similar to those described by Wyatt *et al.* (2004) from on-craton group I kimberlites from South Africa, but the presence of lower < 1 wt.% Cr<sub>2</sub>O<sub>3</sub> at Catoca pipe is indication of diamond resorption process have taken place.

## 5. 5. Discussion of studied diamond heterogeneous mantle

It is interesting to see the result for developed model from this project (Figure 4.34.) demonstrates and supports the view/hypothesis for observed variations in diamond grade (Table 4.18) and abundance within Lunda Province (NE Angola) which clearly, is associated with the heterogeneous mantle. This means that each kimberlite pipe has sampled & transported different amount of diamond from deep mantle to the surface. It can be explained in details that the results from developed model (Figure 4.34), from this project also support the main of the original project hypotheses concerning diamond grade variation and surface abundance (Table 4.18) and or abundance within Lunda provinces, which are associated with the heterogeneous mantle, consequently each kimberlite pipe has sampled & transported different amount of diamond from deep mantle with depth more than 660 km (Stachel *et al.*, 2005, Ringwood *et al.*, 1992 and Dasgupta, 2013) to the surface. Based on this result, it can be discussed that Catoca pipe is the richest pipe among of them because this pipe has sampled more diamond deep mantle source than any active kimberlite in the Lucapa graben.

The result from Figure 5.1 indicates that Catoca pipe produce more diamond per tonne of kimberlite rock and yet that it is also is more oxidised than the other three kimberlite pipes studied here. The calculated possible percentages of diamond within each pipe transported to the surface are presented in table 4.18. This result is useful because it can be used in the future to measure the redox conditions and estimate  $fO_2$  for economical diamond deposit exploration. In addition, this result is consistent with the new finding from other analytical methods (EMPA and Mössbauer) which shows that Catoca kimberlite is more oxidised with high  $0.41 > Fe^{3+}/\sum Fe$  than other kimberlites studied here. Also it is evidenced on Figures 4.12; 4.13 and Tables 4.3; 4.4.

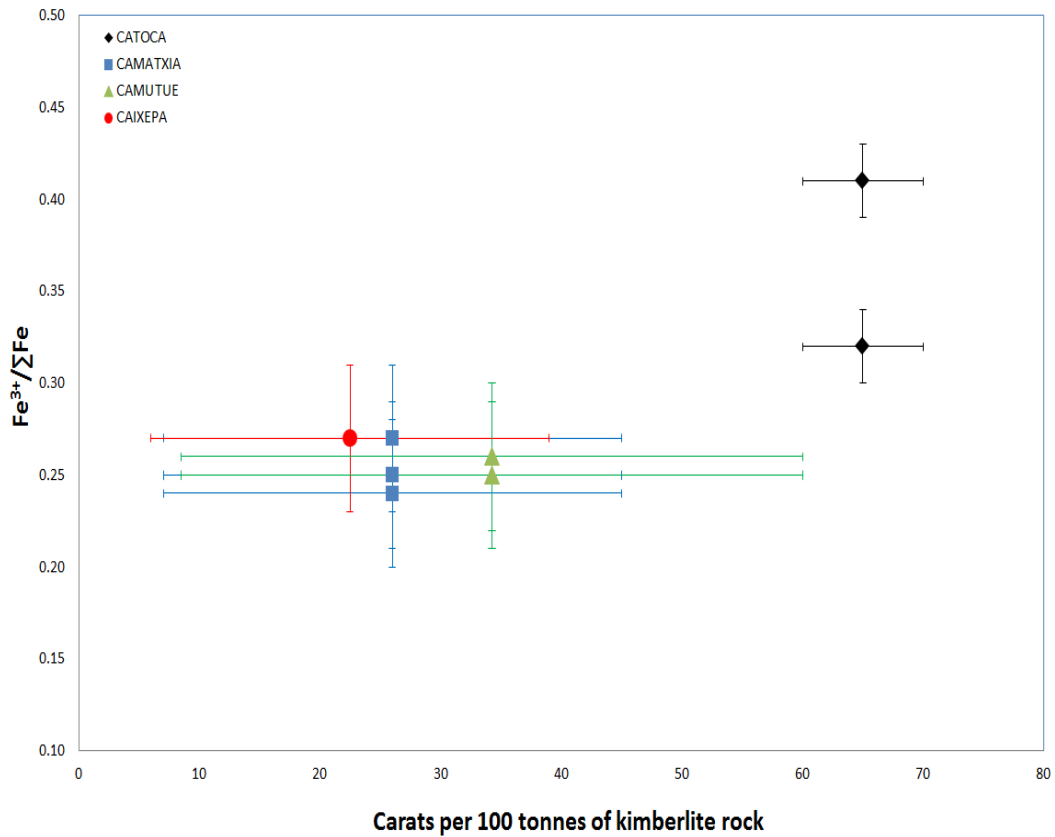


Figure 5.1. Redox ratio vs carats/100 tonnes of kimberlite rock

## 5. 6. Discussion of diamond preservation model for sampled kimberlites

The observed low diamond quality from Catoca pipe and high measured  $Fe^{3+}/\Sigma Fe$  ratio of indicator minerals is consistent with the model of Gurney and Zweistra (1995). The result from this research (Figure 4.35) supports the use of ilmenite redox ratios to measure diamond quality (Fedortchouk and Zhang, 2011, Robinson *et al.* 1989). Applying this model to the other four pipes studied here indicates that their average diamond quality would be greater than for Catoca diamonds on the basis of lower measured iron redox ratios in the ilmenite indicator minerals from these four pipes and it is also evidenced on Figures 4.32; 4.33; and 5.1 which shows that Catoca kimberlite is more oxidised with high  $0.41 > Fe^{3+}/\Sigma Fe$  than other kimberlites studied here. The present author worked at Catoca mine as a diamond selector, mineralogist and geologist. The author has personally observed the high fraction of poor quality diamonds at Catoca mine. Furthermore, verbal communications collected by the author from local geologists and miners at the Camutue, Camatxia, Caixepa and Camagico diamond mines indicate a higher quality of diamond from these four pipes than from the Catoca pipe. However, diamonds and kimberlites from the other four pipes have not been studied academically and consequently no literature evidence is currently available that supports the author's observations and verbal information from local geologists.

## **5. 7. Viscosity model for sampled kimberlite magmatic rocks and its implication on diamond survival within Lunda province**

### **5.7.1. Overview and discussion**

This section provides a brief review of viscosity and a discussion of the results of viscosity modelling of selected kimberlite magmas and how this may assist estimation of the possible speed of transportation of the sampled kimberlite which carried diamond to the Earth's surface.

Despite various attempts at viscosity prediction with some success (e.g. Shaw 1972), the detailed viscosity studies of Bottinga and Weill (1972) revealed an easily-applied method of modelling the viscosity of multicomponent silicate mixtures relevant to rock forming compositions. The present research used the model of Bottinga and Weill (1972) in order to estimate the high temperatures viscosity of the kimberlites studied here. The purpose of this was to investigate possible factors, reasons or explanations for the variations in diamond abundance and / or quality (including resorption) and grades observed between the five different studied kimberlite pipes.

The previous viscosity studies of Dingwell and Virgo, 1988; Giordano *et al.*, 2008; Petford, 2009; Bottinga and Weill, 1972; and Wilson and Head 2007, have demonstrated that magma viscosity is a crucial factor that might have influenced the diamond quality and grade variation in economical kimberlite deposits. There has been considerable work on parametrization of the viscosity of silicate and magmatic melts as a function of major element composition (Persikov, 2007; Persikov and Bukhtiyarov, 2013; and Shaw, 1972). From a dynamic point of view, various aspects of viscosity of kimberlite magma eruptions can provide critical information for the understanding of magmatic or igneous processes, such as melt migration in source regions, magma mixing, flow differentiation by crystal fractionation, convection process in magma chambers, dynamics and style of eruptions, flow characteristic mechanism, the rate of cooling of magmatic intrusion and extrusion, as well as the speed that kimberlite magma transports diamond crystals to the Earth's surface. These phenomena are critically dependent upon viscosity of magmatic fluid. Quantitative evaluation of any of these igneous processes can start with the estimation by modelling of the viscosity of kimberlite / silicate melts within a relevant range of temperatures and compositions (Shaw, 1972; Bottinga and Weill, 1972).

The viscosity modelling carried out here was validated by comparing the calculated viscosity data for the studied Angolan kimberlites with the published data for other relevant magmas from Bottinga and Weill (1972). Results show satisfactory agreement over a wide range of viscosity from approximately 1 to 11 Poise (Figure 4.38 and Tables 4.20; 4.21). As discussed previously, viscosity modelling results demonstrate that at temperatures of ca. 1500°C all samples such as Camutue (CM=CW45); Catoca (CAT-67,CAT-50) Camatxia CAT60); Camagico (CMG17) and Caixepa (CX027) exhibit modelled

viscosities of  $1.5 \pm 1$  Poise and at lower temperature of ca.  $1200^{\circ}\text{C}$  all samples provide modelled viscosities of  $3 \pm 1$  Poise, which means that there is not a great difference in viscosity for a given temperature between samples, except Camatxia sample CMT02 which has a very different viscosity from the other samples. This is clearly due to the high content of silicon oxide ( $\text{SiO}_2 = 80.19\%$ ) and low magnesium oxide ( $\text{MgO} = 2.42$  wt%) observed in this sample (Table 4.20) compared with the others. Viscosity is determined mainly by  $\text{SiO}_2$ ,  $\text{Al}_2\text{O}_3$ ,  $\text{MgO}$  and  $\text{CaO}$  content in magmas. This is supported by Giordano *et al.* (2008) and Moussallam *et al.* (2016), who stated that these major chemical elements influence magma viscosity. When the temperature decreases from  $1450^{\circ}\text{C}$  to  $1250^{\circ}\text{C}$  the viscosity increases (see table 4.20 and 4.21). Higher levels of silica in magma cause higher viscosity due to the presence of strong Si-O bonds. When water is present in magma it has the ability to break Si-O bonds and therefore the viscosity decreases (Dingwell and Virgo, 1988; Giordano *et al.*, 2008; Petford, 2009).

Based on literature review (Wilson and Head 2007), it is suggested that in order for diamond to survive or be preserved, kimberlite magmas / melts would have lower viscosities and higher buoyancies (Sparks *et al.*, 2006) which enable rapid transport from the source mantle region to the surface. The work of Sparks *et al.* (2006) and Kamenetsky *et al.* (2011) reveals that kimberlite magma has a lower viscosity than other volcanic rocks such as basalt with high volatile mobility (Scott Smith, 1999b). The main implication is that rapid transport by magma will maximise the survival of diamonds as they pass through unstable and oxidising conditions of both lower pressures and temperatures. Although the range of sample compositions used to estimate the viscosities of the kimberlite magmas is small, the results can still be useful as it indicates lower viscosity, which means that diamonds may have been transported at higher speeds from the deep mantle to the surface, which helped them to survive. Because of the nature of the model used, and the limited analysed sample size, it is suggested that future work should investigate more samples in order to have a clearer picture regarding the viscosity of kimberlite magmas in Lunda provinces.

Viscosity results in Figure 4.38 (also see Appendix 4) show that the viscosity of pipes CM=CW45; CAT-67; CAT-50; CMG171; CMT 60 and CX027 are similar, whereas pipe CMT02 has a higher viscosity (Tables 4.20 and 4.21). According to Sato (2005), who also referenced aspects of the viscosity model of Bottinga and Weill (1972), changes in melt composition can be the result of crystallization or increases in crystallinity (Moussallam *et al.*, 2016). Silicate minerals which contain silicon dioxide ( $\text{SiO}_2$ ) are the most abundant compounds in the Earth's crust (Klein and Hurlbut, 1993). According to Philpotts and Ague (2011) and Deer *et al.* (1996), silicates are partially molten at temperatures of approximately  $1200^{\circ}\text{C}$  and become solid and cooled when temperature decrease to about  $600^{\circ}\text{C}$ . For example  $\text{SiO}_2$  (Quartz) become stable at temperature about  $600^{\circ}\text{C}$  (Deer *et al.*, 1996).

As stated above in Chapter 4, the viscosity model of Bottinga and Weill (1972) used in this project has a number of limitations. For example, a) the model does not take into consideration the effects of H<sub>2</sub>O, CO<sub>2</sub> and other volatiles. These two components have previously been reported to have a major influence on the viscosity of magma (Giordano *et al.*, 2008; Persikov, 2007; Persikov and Bukhtiyarov, 2013). The data in Figure 5.2 was taken from the work of Petford (2009) for basaltic andesite magma. The main reason for using this diagram (Figure 5.2) is intended to demonstrate how the how the volatile content (H<sub>2</sub>O) plays a major role in determining the viscosity of magma (Moussallam *et al.*, 2016). By using the work of Petford (2009) on the viscosity of basaltic andesite magma as an example (Figure 5.2), increasing the water content of magma from 1 to 5 wt. % results in a decrease of magma viscosity at a temperature of 1000<sup>0</sup>C from 3.4 to 2.3 Pa s. The viscosity of basalt magmas decreases as pressure or water content increases (Persikov *et al.* 2015). This reduction in viscosity caused by water dissolution is due to depolymerization of the silicate network (which means that there will be an increase in the melt basicity, normally resulting in a decrease in viscosity). On the contrary, in ultramafic kimberlite melts, the viscosity increases as pressure or water content increases (Persikov *et al.* 2015). The dissolution of H<sub>2</sub>O in kimberlite magma leads to the polymerization of the melt (decrease in its basicity). Kimberlite melts are rich in MgO, CaO (Persikov *et al.*, 2015), and the water occurs in the form of molecular H<sub>2</sub>O as opposed to -OH groups, consequently increasing the viscosity of kimberlite. Although the effect of pressure has not been considered in this project, it is useful to discuss here the effect of pressure as an important parameter in determining viscosity. The viscosity of both kimberlites and basalt magmas changes according to lithostatic pressure (Persikov and Bukhtiyarov, 2013). The interpretation from Figure 5.3 is that the viscosity of kimberlite magma increases with pressure, whereas the viscosity basaltic magmas will decrease as pressure increases under the given temperature and pressure conditions.

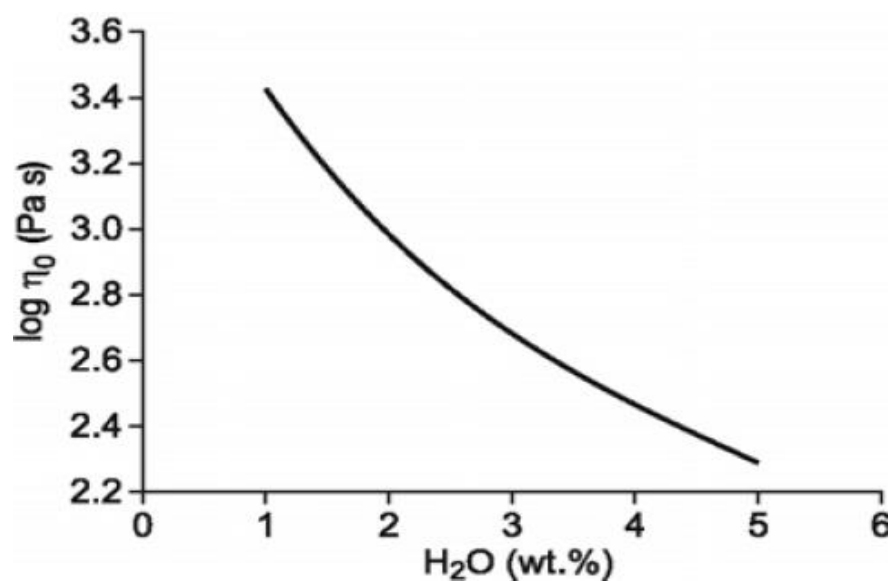


Figure 5.2. Plots showing the relationship between melt viscosity ( $\eta$ ), and H<sub>2</sub>O content at 1000°C from a basaltic andesite sill from MtTheron, Antarctica (Petford, 2009).

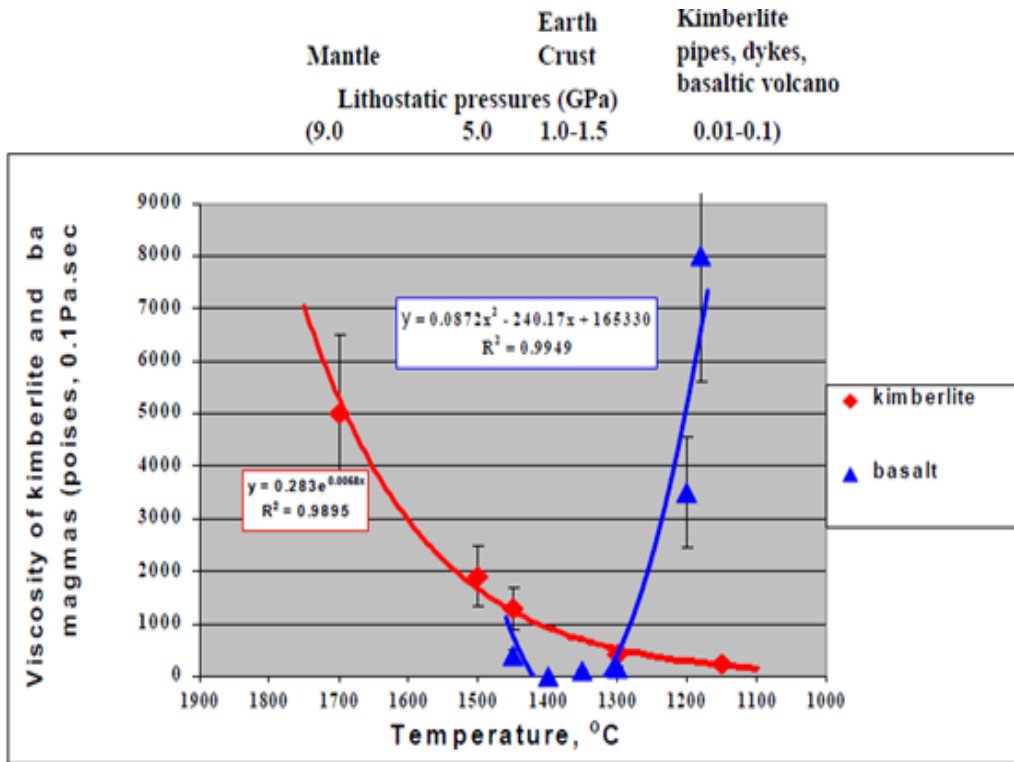


Figure 5.3. Dynamics of viscosity of kimberlite and basaltic magmas during their ascent from mantle to the Earth surface crust (Persikov and Bukhtiyarov, 2013).

Based on the work of Persikov and Bukhtiyarov (2013), it is believed that under the conditions of kimberlite origin (partial melting of carbonated peridotite) at depths ranging from 250 - 340 km and pressures ranging from 8 - 10 GPa (80 – 100 kbar) and temperatures of approximately 1700 °C, the volume content of crystals is approximately 10 % and consequently the viscosity of the melt tends to be high (approximately 35 Pa·s) (Persikov *et al.*, 2015), whereas at the near-surface during kimberlite formation, the viscosity of kimberlite melts is lower (about 10 Pa·s) with temperatures of about 1150°C and pressures ranging from 50 –100 MPa (Persikov and Bukhtiyarov, 2013). Although the effects of H<sub>2</sub>O and CO<sub>2</sub> have not been considered in this project, the trends in values of calculated viscosity are in general agreement with those previously published in literature (Figure 5.4 and Appendix 4).

Also it is important to state some important physical parameters that magma depends upon. When the temperatures increases, this cause the melt to expand and consequently the density of melt becomes lower, but in contrast at higher pressures, for example 9GPa (Persikov and Bukhtiyarov, 2013) the viscosity of kimberlite magma becomes higher and the melt becomes compressed and consequently this leads the density increasing (Persikov and Bukhtiyarov, 1999.). This means that that density is another important physical property of magma which is also influenced by both temperature and

pressure. Kimberlite melts follow the basic rules of magma physics (viscous silicate melt, crystals and volatiles or gases) (Kjarsgaard 2007).

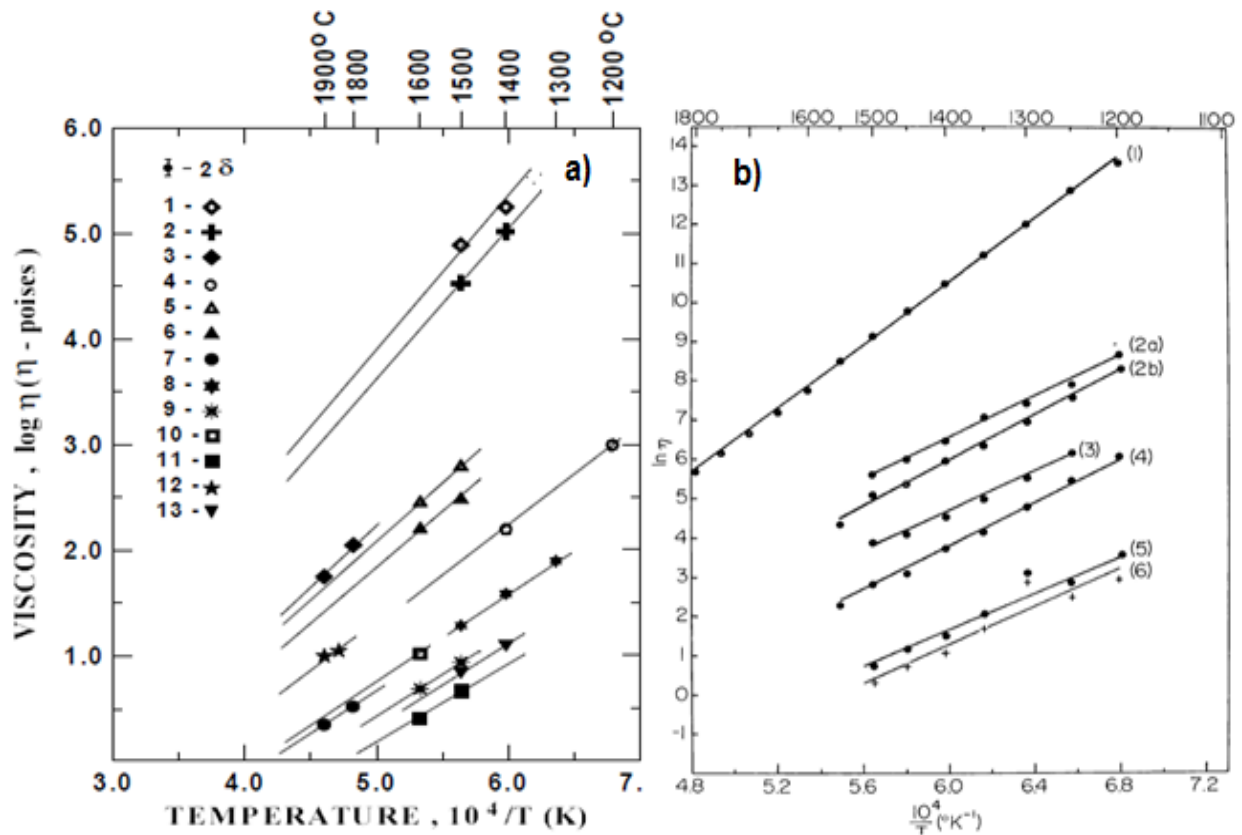


Figure 5.4. Temperature dependence of the viscosity, a) Persikov and Bukhtiyarov (1999) ,and b) Bottinga and Weill (1972)

### 5. 8. Resorption features of studied crystals of Angolan diamond (Catoca kimberlite)

Resorption and diamond deformation characteristics have been discussed widely in literature (Orlov, 1977; Robinson *et al.*, 1989; Bataleva *et al.*, 2012; Fedortchouk *et al.*, 2007; and Fedortchouk and Zhang 2011). After a detailed examination of some natural crystals of diamond from kimberlites of NE Angola (Figure 4.39), the optical results have provided strong evidence that the studied diamonds contain deformations which can be interpreted as showing resorption characteristics on their surfaces, such as trigonal etch-pits on faces, hillocks, and striation, and sharp steps along the edges (see Figure 4.39) and also the glossy surface features are observed on these crystals of diamond. The glossy surface features on diamonds have been also described by Zhang *et al.* (2015). These deformation characteristics on diamond are interpreted as products of interaction with their host magma during

ascent and the effects of increased oxygen fugacity (Robinson *et al.*, 1989). Diamonds found in eclogite and peridotite mantle xenoliths are well preserved compared to diamonds recovered from the host kimberlite (Stachel *et al.*, 2009; Stachel and Harris, 2007). The resorption of diamonds in kimberlite is related to higher oxygen fugacity during residence time in the transportation of kimberlite magma (Gurney and Zweistra, 1995). Further support for these resorption features being associated with kimberlite magma is because conductive geothermal or surface heat flow of  $38\text{mW/m}^2$  for the lithospheric mantle beneath the Lunda kimberlite province calculated by Castillo-Oliver *et al.* (2011) has been considered to be high enough for diamond formation (Stachel *et al.*, 2003).

The tetrahedral morphology/texture observed on these diamonds reflects a complex history of growth, and rounded shapes are due to dissolution. Similar diamond morphologies or kimberlite induced resorption features have been described by Fedortchouk *et al.* (2007) who stated that diamond impurities are high in kimberlite magma due to the higher nitrogen content (or aggregation of nitrogen defects) than those observed in mantle due to lower nitrogen content and high aggregation. Here, nitrogen is the main impurity in diamond and its concentration reflects conditions during diamond growth (Orlov, 1977), whereas the state of aggregation reflects the thermal history and duration of diamond residence in the mantle (Fedortchouk *et al.*, 2007). The crucial implication from the observed resorption conditions on the examined diamonds is that it may be linked with the metasomatic events described above during the origin of host diamond-bearing magmas, in the kimberlite reservoir. According to Fedortchouk and Zhang (2011), Fedortchouk *et al.* (2007), Robinson *et al.* (1989), dissolution of diamond in kimberlite occurs when fluid first attacks the edges and vertices of the diamond and leaves the interior of the faces almost intact. It can be assumed that this process may have taken place when the corrosive kimberlite melt causes a variety of dissolution features such as pits, etchings and striations to develop on the crystal faces Figure 4.39 (b) (Arima and Kozai, 2008; Fedortchouk *et al.*, 2005). Another important implication taken from these resorption processes on the deformed studied diamonds (Figure 4.39) is that it can help us to understand the mechanism of diamond oxidation in kimberlite magmas and to determine the main rate-controlling factors, for example  $f\text{O}_2$  changes during kimberlite ascent and emplacement (Fedortchouk and Zhang, 2011) and to be able to predict the degree of diamond preservation in a kimberlite reservoir (see 4.35).

As shown in Figure 4.39, the crystals of diamond show yellowish colours which are believed to be associated with the common impurity observed of nitrogen, in various states of aggregation. This is supported by Tappert and Tappert (2011) who described that normally the diamond in its pure form is colourless, but can become coloured due to imperfections, impurities of nitrogen and inclusions of

mantle xenolith minerals. Any of the diamond deformation elements can have major negative effects on market prices of diamonds.

A critical evaluation from the examined diamonds in this project (Figure 4.39) is that although their morphologies are complex, after a careful analysis, the inclusions are believed to be Epigenetic inclusions - (EI), which form probably after crystallization of diamond. This is supported by Stachel and Harris (2007), who explained that EI's are the result of penetration of fluids or melts into diamonds along cracks, and which may form in the Earth's mantle during kimberlite rising or after emplacement in the Earth's mantle. This study has confirmed that these inclusions are neither Protogenetic nor Syngenetic inclusions. This is because the morphology of Syngenetic inclusions contained in garnet cubo-octahedral on diamond materials these inclusions form simultaneously with the diamond by the same genetic process (Taylor *et al.*, 2003; Stachel and Harris, 2007) whereas protogenetic inclusions are formed before incorporation by the host diamond, and these inclusions show dodecahedral forms (Taylor *et al.*, 2003).

The potential rising questions regarding Catoca mantle diamond are following: Can the Catoca pipe be classified as a dodecahedral, with high diamond dissolution process? If so, why does the pipe contains more high percentage or volume of diamond content? If it becomes the truth that Catoca pipe is dodecahedral, therefore it may be assumed that the original mantle was good enough for possessing the high level of diamond content .

### **5. 9. Comparison of Lunda pipes and geochemistry with other kimberlite pipes**

Based on petrography, geochemical studies (see Chapters Three and Four), field work studies and observations of emplacement styles of sampled kimberlites facies, it is confirmed that kimberlites from Lunda provinces are similar to those from Brazil, Canada, Australia, South Africa and USA in terms of their geochemistry, morphology and diamonds (Scott Smith *et al.*, 2008; Field and Scott Smith, 1998; Musun and Scott Smith, 2006; Mitchell *et al.*, 2008; and Cas *et al.*, 2008). As discussed earlier in Sections 2.1, 2.2 and 3.1, Lunda kimberlites are referred to as Group I bodies: they are an ultramafic, potassic, volatile-rich igneous rock, where most show macrocrysts (larger grains) of minerals of garnet, phlogopite, olivine, pyroxene and oxide minerals (hematite, spinel and ilmenite), that are set in a finer matrix, which gives kimberlite rock a typical characteristic of inequigranular to porphyritic texture. Similar kimberlite textures have been found in Canadian kimberlites (Somerset Island) (Skinner, 2008; Mitchell *et al.*, 2008; and Donnelly *et al.*, 2010).

Diamond researchers (Nowicki *et al.*, 2007; Stachel and Harris, 1997) have described garnet harzburgites as potential indicators of the presence of diamond in kimberlite pipes. However, this research shows that the presence of garnet harzburgites in pipes is not always an accurate indication

that the pipe contains diamonds. For example, the Hanaus and Lauwrensia kimberlites from Namibia contain garnet harzburgites but the pipes have no diamond (Mitchell, 1991) compared with the diamondiferous kimberlites studied in this project (Catoca, Camatxia, Camagico, Caixepa and Camutue). This is because both Angolan pipes and South African pipes (Finsch; Frank Smith; Kimberley and Premier) and Botswanan kimberlites (Orapa, Tshabong and Jwaneng) and Zimbabwe (e.g. Colossus pipe) all are located with a cool thick old lithosphere zone (craton) whereas Namibian pipes are derived from off cratonic zones (see Chapter Two). In term of formation ages, most of the pipes described here and even those diamondiferous kimberlites from Brazil, Canada, D.R. Congo, China, Russia, Mali, Sierra Leone and Guinea are from the Mesozoic era (Gurney *et al.*, 2010; and Harggerty, 1999) in particular the Cretaceous age (Nixon, 1995).

Figure 5.5 shows the ideal occurrence model and petrogenesis of kimberlites from South Africa (Field and Scott Smith, 1998). The kimberlites from Lunda kimberlites and South Africa are similar and both are classified as Group I kimberlites (Field and Scott Smith, 1998 and Skinner, 2008). Therefore, Figure 5.5 can be taken as an approximation of the occurrence model and petrogenesis of Angolan kimberlites. As discussed in Section 3.1, kimberlite pipes from Lunda provinces are composed of rocks of different types. This differentiation is probably due to a powerful volcanic explosion that took place LP, but volcanoclastic kimberlite (VK), was classified as fragmental rocks, whereas the less explosive hypabyssal kimberlite (HK) was categorised as non-fragmental rocks. The observed and sampled pyroclastic kimberlites (PK), resedimented volcanoclastic kimberlite (RVK) and massive volcanoclastic kimberlite (MVK) are all variety of volcanoclastic kimberlite (Kjarsgaard, 2007).

As shown in Figure 5.5 the three main zones described here are crater, diatreme and root zone. All have different shapes and contrasting material filling in the zones, which clearly demonstrate that these zones were formed by varying processes within one overall emplacement event (Ringwood *et al.*, 1992; Keshav *et al.*, 2005). These three main zones of kimberlites and their filling material processes in the zones have also occurred elsewhere (Cas *et al.*, 2008; Mitchell, 1991; and Caro *et al.*, 2004). It has been explained by Scott Smith (1999) that the process of formation of the root zone may have occurred by stopping whereas diatreme occurred by fluidisation and crater occurred by explosive breakthrough (Cas *et al.*, 2008).

According to Mitchell (1991), who studied diamondiferous kimberlites of Premier mine in South Africa and Letseng diamond mine in Lesotho, diatreme formation processes which led to a uniform body of kimberlite pipes have a consistency of diamond grades in diatreme facies. The diamond consistency in diatreme zones have been also observed in NE Angolan pipes (information obtained as personal communications from local geologists and mineralogists at Catoca, Camagico and Camutue

mines). The kimberlite rocks studied in this research have been classified based on the conventional rock nomenclatures (Sparks *et al.*, 2006; Scott Smith *et al.*, 2008; and Cas *et al.*, 2008).

The geology of kimberlite pipes is complex. The kimberlites in different areas have distinct pipe shapes and internal geologies. For example the Attawapiskat kimberlites in Canada have dissimilar infill and emplacement from southern African kimberlite pipes (Webb *et al.*, 2004) and Angolan pipes. In addition, the hypothesis of derivation of kimberlites from depths greater than 400–650 km (Figure 2.4), which is greater than for any other igneous rock (Ringwood *et al.*, 1992), makes it important to investigate kimberlite petrogenesis of Angolan pipes, and understand the melting processes and composition of the mantle near the cratonic lithosphere and asthenosphere boundary. Another key aspect of kimberlite magma is that its composition has a relatively low content of SiO<sub>2</sub> and high volatile and trace element contents (Field and Scott Smith, 1998), and these chemical constituents influence the speed of kimberlite magma emplacement. An important implication in terms of diamond preservation is that kimberlite magmas with higher emplacement velocities provide better diamond survival conditions (Wilson and Head, 2007).

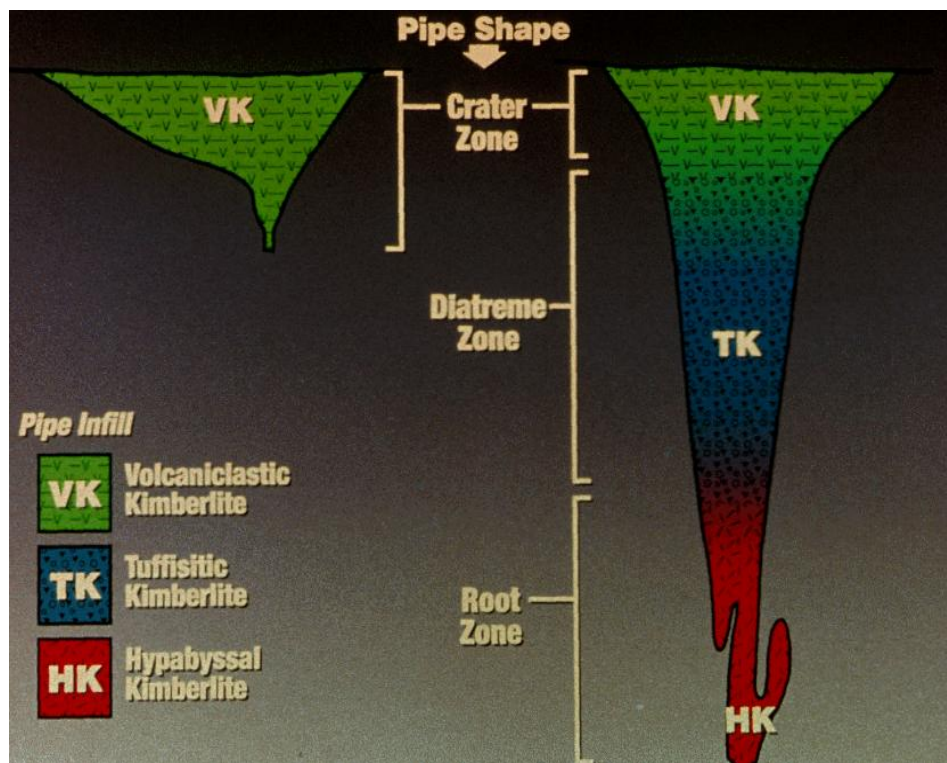


Figure 5.5. Illustration of kimberlite pipe and its terminology (Field and Scott Smith, 1998)

The occurrence model of crater facies of Angolan kimberlites is similar to those described by Skinner (2008). From Figure 5.6, it can be seen that the crater hole is infilled by side-wall collapse, crater extension and debris flow materials after first explosion of kimberlite magma. However, with longer periods of time, the rest of the crater hole is loaded with resedimented volcanoclastic kimberlite materials such as debris, conglomerates and sandstone originating from tuffisitic ring deposits (Skinner, 2008). It can be concluded, therefore, that the occurrence of crater facies is predominately with resedimented material, and with less pyroclastic kimberlite as well as with a few hypabyssal kimberlite materials (Sparks *et al.*, 2006; and Cas *et al.*, 2008). During sampling activity of the Lunda kimberlites studied here, it was noticed by the author that in many cases the graded beds and depositional features were absent, which led to the interpretation and conclusion that such tuffs are primarily airfall materials.

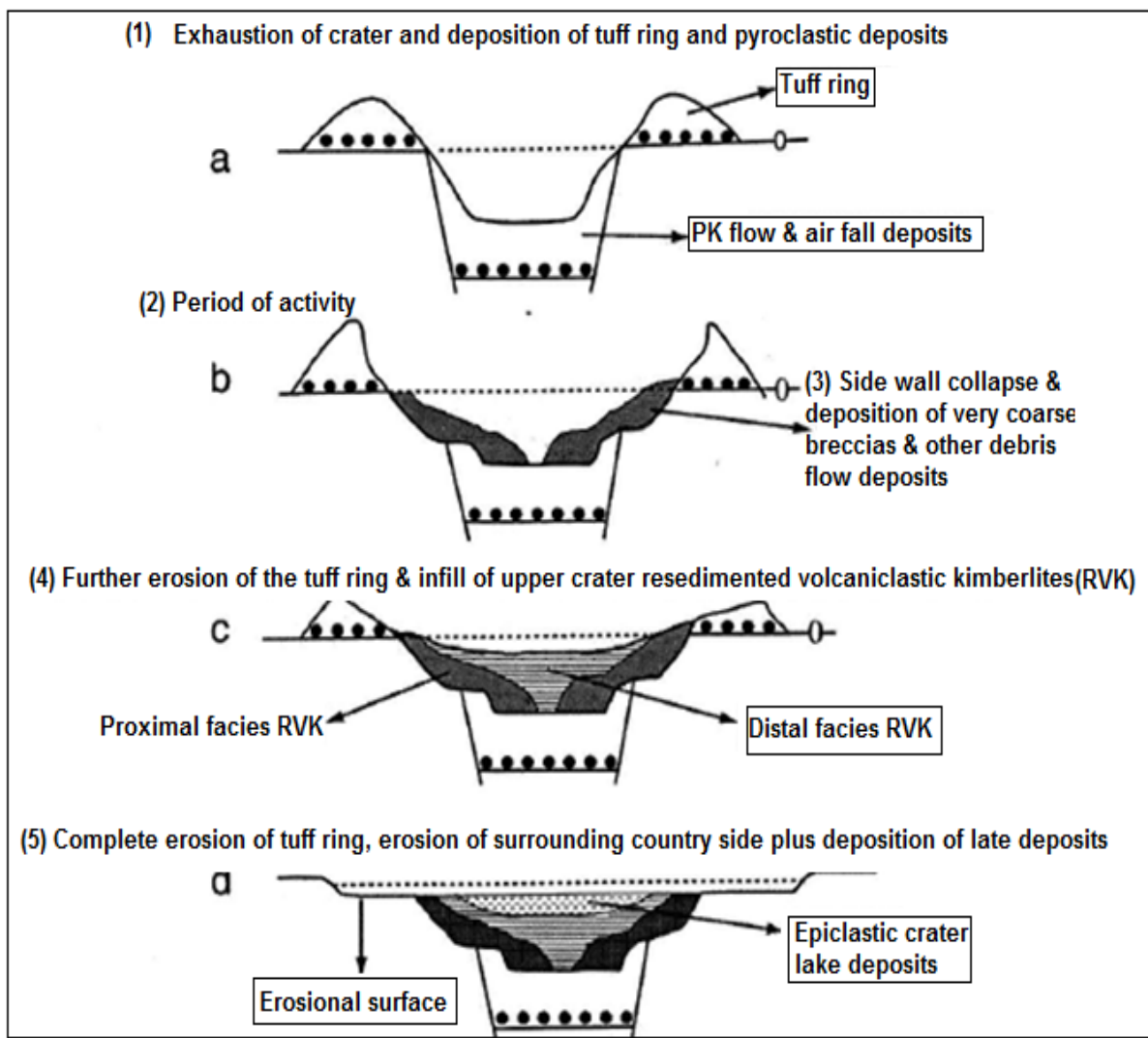


Figure 5.6. Demonstration model of class 1 crater formation (Skinner, 2008).

Based on findings and observed evidence from field work in Angola (Lunda provinces), the process of re-sedimentation of material on crater facies is extremely varied from the pyroclastic kimberlite (PK) material. For example, the major difference observed was that the re-sedimented volcanoclastic kimberlite (RVK) at Camutue, Catoca, Camatxia and Camagico mines was in some cases well bedded, whereas the PK is poorly bedded at these mines, and these kimberlites have features similar to those from Canada, South Africa and Australia (Scott Smith, 1998 and 1999).

## Chapter Six . Conclusions and suggestions for future work

Before this research was carried out, our understanding of the diamond variation grade, and diamond survival or preservation conditions of diamond within the Lucapa Graben, Angola (Western Africa) was poor. This project has presented answers to the question of the cause of problems linked to the diamond grade variation, quality, and size distributions observed between kimberlite pipes and diamond preservation condition in NE Angola. This is associated with variations in oxygen fugacity, metasomatoses events, poor preservation conditions, and the heterogeneous mantle. The interaction or infiltration of silicate-rich liquids and hydrothermal fluids are also the main sources of such oxidation processes in the Lunda diamond lithosphere

The geology of Angola has a complex history. The main reason for this complexity is due to a series of past tectonic events, which took place during the period of Archaean-Proterozoic transition. The Archean of the Angolan block suffered extension deformation during the Eburnean orogeny and consequently these tectonic events have dramatically modified the primary mantle petrology (evidenced in the thin section and rocks investigation sections of this research) and ultimately these events have contributed significant complexity to diamond exploration in Angola. This project has concluded that Angolan diamondiferous kimberlites are associated with extensional tectonic activity during rifting /opening of the south Atlantic, during the in Mesozoic era in particularly early Cretaceous. The Lucapa graben is the most prominent geological feature in Angola and this tectonic feature is zone of weakness that crosses the entire country, from NE, Lunda province (LP) to the SW that assisted the emplacement of kimberlites in NE Angola. This conclusion is supported by White *et al.* (1995) and Jelsma *et al.* (2004) who explained that kimberlite intrusions are favoured by extensional tectonic activity caused during time of a major oceanic or continental rifting. Concerning Lunda province (the studied region), however, the basement structures are the results of connection between regional structures (major mobile zones or faults, fracture corridors) and local structures (linear graben, rift valleys, internal fractures and deep faults within the Lucapa corridor, and consequently these structures have enabled kimberlite magma to reach the earth's surface (Helmstaedt and Gurney, 1997), and cool to form the kimberlite deposit which incorporates the diamond reservoir and facilitate its economical exploration (e.g. Camatxia, Caixepa Catoca, Camutue and Camagico mine).

Sampled kimberlite and mantle xenolith (peridotite and eclogite) rocks from Five different diamond mines (Camutue, Caixepa, Camatxia, Camagico and Catoca) have been analysed systematically. Petrography and both physical and chemical analyses have revealed the complex metasomatic history of the diamond-bearing mantle in the Lunda province, where the geochemistry result of primary

diamond indicator minerals garnet, ilmenite and pyroxenes proved that the Lunda diamondiferous mantle was subjected to significant metasomatism. The zoning, exsolution features and chemical changes from the studied minerals, also are clear evidences of metasomatism events of using tools such as the electron, proton and ion microprobes, but due to In addition, the petrography also provided evidence of later alteration or redox reactions. This leads to the conclusion with confidence, that the original Lunda lithosphere mantle or mantle rocks (P-type, E-type and kimberlite) were altered from the original minerals into secondary phases documented in this project, resulting of significant metasomatism generated probably by fluid agents (H<sub>2</sub>O, CO<sub>2</sub>). This result is also supported by the observed variations and diamond abundance and grade variation within Lunda province.

The evidence of petrographic and chemically analysed garnet mantle xenoliths from the Catoca kimberlite pipe has led to the conclusion that this peridotite and eclogite mantle have been subjected to significant metasomatism, leading to increasing contents of Ca and low Ti (e.g. sample Cat 18), which are indicative that resorption diamond may have taken place, probably in the host magma before kimberlite emplacement. This process may have been linked with significant increases in oxygen fugacity and this, in return, has increased the potential for diamond resorption in the Catoca kimberlites.

Concerning diamond preservation conditions, it can be concluded that the observed low diamond quality from the Catoca kimberlite pipe and its high measured redox ratios  $Fe^{3+}/\Sigma Fe$  of ilmenite indicator mineral is in agreement with the model of Gurney and Zweistra (1995) which supports the use of ilmenite redox ratios to measure diamond quality. By applying this model to the diamondiferous kimberlite pipes studied here, it indicates that diamond quality would be greater for Caixepa, Camatxia, and Camutue than for Catoca diamond kimberlite on the basis of lower measured iron redox ratios ( $Fe^{3+}/\Sigma Fe$ ) in the ilmenite indicator minerals from these pipes. The author of this thesis worked at Catoca mine as a diamond processor and mineralogist / geologist, and has personally observed the high volume of poor quality of diamonds obtained at the Catoca kimberlite mine.

The main conclusion taken from Figure 4.35 is that although the Catoca pipe is the richest among the primary diamond deposits within the Lucapa graben, the geochemical study of ilmenite carried out here has placed the Catoca pipe within the poor to no- preservation zone index according to the model (Figure 4.35). The most plausible explanation for Catoca having the high level percentage / volume (carats per 100 tonnes of mined rock) of observed diamond can be explained if its own mantle was particularly rich in diamonds prior to emplacement. This indicates that diamond concentration in the heterogeneous mantle was much greater at this point. Therefore, despite ilmenite being widely used as an indicator mineral for preservation conditions of diamonds, it is recommended that a precise

geochemical study of ilmenite and detailed regional geological investigation should be carried out before any conclusion is reached whether a particular kimberlite pipe is economically viable for diamond mining, or whether it is infertile. The absence of magnesium (Mg)-rich ilmenite in kimberlite ilmenite as an indicator mineral, in an exploration context, is not a reliable guide to estimate or conclude whether or not the host kimberlite pipe is economically viable.

One intention of the discussion and conclusions is to illustrate the promising nature of Mössbauer spectroscopy and EMPA in diamond research by studying ilmenite and other diamond indicator minerals. In addition, the geochemical results from EMPA data for analysed ilmenite, have led to the conclusion that Angolan pipes fall in the "kimberlite ilmenite" environment as illustrated in Figure 4.37. The present research has recommended that precise classification and identification of the ilmenite source lithology, especially in kimberlite deposits where ilmenite is used as indicator mineral, is fundamental from the perspective of economically-viable geological and mining exploration.

The Mössbauer determined iron redox ratio ( $\text{Fe}^{3+}/\sum\text{Fe}$ ) and fitted parameters (CS, QS, and LW) are consistent with Mössbauer data for natural ilmenites reported previously in the literature. Small variations observed between data sets may be associated with geological factors such as heterogeneity, pressure, temperature, environment and metasomatoses / alteration processes within sampled kimberlite pipes, all of which can impact upon iron oxidation state and environment within kimberlites. In addition, it is concluded that for some samples, for example CMT 58, CAT59HM1, CAT=MY001C and CAT 59 d, it was not possible to calculate the iron redox ratio of the ilmenite phases because these were multiphase materials with relatively low abundances of ilmenite and high abundances of amphibole. Separation of the respective ilmenite and amphibole  $\text{Fe}^{3+}$  components in Mössbauer spectra proved problematic as their hyperfine parameters (CS, QS and LW) are closely similar to each other. For these spectra, one  $\text{Fe}^{3+}$  doublet was fitted to the combined ilmenite and amphibole  $\text{Fe}^{3+}$  contributions. Consequently it was not possible to separately assess the  $\text{Fe}^{3+}$  content of the ilmenite phases from Mössbauer data. Multiple separation methods, such as Frantz magnetic and hand pick and separator, were applied in order to obtain the purest possible phases. It appears to be difficult to obtain clean single phase of ilmenite in some studied samples. This project has provided upper limits of the redox ratio in some ilmenites (see Table 5.1) by assuming that all  $\text{Fe}^{3+}$  in the relevant doublets arises from the ilmenite phase. This presents an "upper redox boundary" and does not necessarily quantify the iron redox ratio in these phases.

The high redox ratios,  $\text{Fe}^{3+}/\Sigma\text{Fe}$ , obtained from ilmenite minerals are associated with higher MgO contents. Based on the Mössbauer results from this project, it can be concluded that the analysed samples from the economical diamondiferous deposits at Caixepa, Camutue and Camatxia are believed to have crystallized under low  $f\text{O}_2$  conditions. Mössbauer spectra for analysed samples from Caixepa, Camutue and Camatxia kimberlite pipes are dominated by  $\text{Fe}^{2+}$  which is indicative of a more reducing, lower  $f\text{O}_2$  environment and consequently a higher chance for diamond survival because their ilmenites redox ratios  $\text{Fe}^{3+}/\Sigma\text{Fe}$ , are  $< 0.24$  whereas the samples from Catoca pipe with  $> 0.32$  of  $\text{Fe}^{3+}/\Sigma\text{Fe}$  are more oxidised with more ferric iron ( $\text{Fe}^{3+}$ ) (see Tables 4.3; and 4.2 and 5.1), indicating relatively poor diamond preservation conditions with higher levels of diamond resorption. The resorption evidence from the studied crystals of diamond in this project supports these observations. Even though Catoca mine produces more diamond than any other mine in the Lunda Province, the results of morphological studies of resorption features of Catoca diamond, combined with other results from Mössbauer, petrography and EMPA analyses, leads to the conclusion that more oxidizing environments existed in the Catoca diamondiferous kimberlite pipe compared with the others studied here.

Because of the analysed samples / minerals being altered and having undergone chemical changes during metasomatism, determination of the oxygen fugacity using chemical reactions is very challenging (see Chapter Four). It is suggested that in an economical diamond exploration environment, Mössbauer spectroscopy should be a key technique for analysis of iron redox in indicator minerals from sampled kimberlite rocks.

It can be concluded with confidence that the resorption of the collected and studied crystals of diamond from the Catoca mine may be related to higher oxygen fugacity during their residence in the deep mantle and transport to the surface, and that consequently they were exposed to more strongly oxidising conditions outside their stability field, leading to their corrosion and eventually to resorption. Characteristic deformation features on these diamonds are also caused by infiltration of silicate-rich melts and hydrothermal fluids during transportation by kimberlite magma. This is because the diamonds found in the enclosed eclogite and peridotite mantle xenolith rocks do not present such deformation features - they are well preserved compared to diamond recovered from the host kimberlite.

At temperatures of circa  $1500^\circ\text{C}$  the viscosity of sampled kimberlite magmas / melts for samples such as Camutue (CM=CW45); Catoca (CAT-67, CAT-60 and CAT 18); Camagico (CMG17), and Caixepa (CX027) all fall in a window of viscosity of  $1.5 \pm 1$  Poise and at lower temperatures of about  $1200^\circ\text{C}$  all samples falls in a window of viscosity of  $3 \pm 1$  Poise. This means that there is not a great

difference in viscosity for a given temperature between samples, except Camatxia sample CMT02 which has a very different viscosity from the other sample. This difference between CMT02 and other analysed samples is due to the high content of silicon oxide, ( $\text{SiO}_2 = 80.19 \text{ wt } \%$ ) and lower magnesium oxide ( $\text{MgO} = 2.42 \text{ wt } \%$ ) observed in this particular sample (see Tables 4.20; 4.21). It has been concluded that the viscosity modelling used in this research has given qualitative indications / suggestions that the studied kimberlites pipes probably have low viscosities and high fluidities that enabled rapid transport of diamond from the source mantle region to the surface and consequently maximise the survival of Lunda diamonds as they passed through unstable combinations, as occur at lower pressure and temperature conditions. Even with this new result, it is recommended that due to the limitations of the data used in this project it is not possible to reach a firm conclusion for the effects of kimberlite magma viscosity on the speed of transport to the surface, and the relationship between this and the quality and quantity of diamond observed. In order to reach a firmer conclusion, more samples are required to be studied systematically. The next viscosity study for kimberlite samples from Lunda province should be focused on this question. It is important to understand the viscosity processes of kimberlite magma and its implication in the economical geology.

The viscosity results obtained for the studied kimberlites pipes show low viscosity, nevertheless the high resorption and impurity of diamonds observed at the Catoca mine show tetrahedral morphology characteristics which are probably products of interaction with their host magma, higher nitrogen content or aggregation of nitrogen defects during ascent; and oxygen fugacity. Another limitation of the viscosity model used in this project is that it does not take into consideration the effects of  $\text{H}_2\text{O}$  and  $\text{CO}_2$  which are reported to have a major influence on the viscosity of magma. In addition, the modelling viscosity used in this research also did not considered the effect of pressure. The effect of pressure on kimberlite magma is important because it provide information about the behaviour of kimberlite magma at depths below the Earth's surface. For example, Figure 5.3 demonstrates that at the pressure ranging to 8-10 GPa (80 – 100 kbar), temperature approximately 1700 °C, the viscosity of kimberlite melt tends to be approximately 34 Pa·s whereas at pressures ranging from 50 –100 MPa, close to surface, during kimberlite formation, the viscosity of kimberlite melts can be estimated to be lower approximately 10 Pa·s with temperature about 1150 °C. n Therefore it is crucial for this project to recommends again tha next viscosity study for kimberlite samples from Lunda province should include the effects of  $\text{H}_2\text{O}$ ,  $\text{CO}_2$  and pressure in this modelling, because it is necessary in order to understand more quantitatively how the kimberlite magma behaved during its ascent to the Earth`s surface and consequently how diamond may have been affected.

Based on all evidences finding in this project, it can be concluded and summarised that the observed diamond grade variations and abundances within the Lucapa graben are associated with factors including metasomatism events, variable preservation conditions, dilution of ore with country rock,

and the heterogeneous mantle (which means that each kimberlite pipe has sampled and transported different amounts of diamond in the mantle to the surface) and oxygen fugacity (which was successfully measured by using redox ratio  $\text{Fe}^{3+}/\Sigma\text{Fe}$  of ilmenites inclusions in the host kimberlite rock, through combining the following advanced methods in diamond research:  $^{57}\text{Fe}$  Mössbauer spectroscopy, EMPA, XRD, XRF and petrography.

This project has concluded that the origin of megacryst minerals used in this research are from primitive or pro-tokimberlite magmas that separated from sub-lithospheric convecting mantle at several hundreds of kilometres depth.

**(Words count 75.180)**



**Appendix 1. Summary of the main thin sections and microscopic features of the textural types of kimberlite present at Lunda Province.**

<b>Sample number 1. Reference Cat-18. Rock name; Eclogite (mantle xenolith). Locality - Catoca Kimberlite.</b>										
	Minerals	Modal %	Occurrence	Grain size	Grain fabric	Cleavage	Colour in pp	Alteration features	Zonation	Overall rock texture
1	Clinopyroxene	30–50 vol. %	Phenocryst	>4mm	Subhedral Anhedral	2 nearly at 90°	Light-green	Deformation, growth and serpentinisation	None	inequigranular texture
2	Garnet	30–45 vol. %	Phenocryst	>3mm	Anhedral	None	Grey	Kelyphite texture (oxydation process)	None	
3	Rutile	≤4 vol. %,	Phenocryst	0.7–4 mm	Anhedral	None	Black-red	Growth	None	
4	Spinel/ Ilmenite	≤2 vol. %	Phenocryst	1 -3mm	Anhedral	None	Black	Rims	Possible?	
<b>Sample number 2. Reference CAT- 61. Rock name; pyroclastic kimberlite. Locality - Catoca Kimberlite.</b>										
	Minerals	Modal%	Occurrence	Grain size	Grain fabric	Cleavage	Colour in pp	Alteration features	Zonation	Overall texture
1	Carbonate	10–25 vol. %	Phenocryst/ Groundmass	0.5- 2mm	subhedral anhedral	None	Colourless	Reaction/ rims	Yes	porphyroblastic to inequigranular texture
2	Olivine	20-35 vol. %	Phenocryst	>3mm	Anhedral	None	Colourless	Fracture, rims and reactions	None	
3	Garnet	≤ 9 vol. %,	Phenocryst	>2mm	Subhedral	None	Grey	Fractures and rims	None	
4	Orthopyroxene	5-10 vol. %,	Phenocryst	0.7-1	Anhedral	1 perfect	Colourless	-	None	
5	Spinel/ilmenite	≤ 2 vol. %,	Phenocryst	>1mm	Anhedral	None	Black	Fractures	None	
6	Clinopyroxene	≤ 5 vol. %),	Phenocryst	0.7mm	Anhedral	2 at 90°	Light green	Fluid reaction/ fracture -	None	
7	Phlogopite	≤ 6 vol. %,	Phenocryst	1-4mm	Subhedral	1 perfect	Colourless	Reaction/fractures	Yes?	
8	Serpentine	15-20 vol. %,	Groundmass / Phenocryst	0.5-1mm	Anhedral	None	Colourless	Reaction/ rims	Yes	
<b>Sample number 3. Reference CAT-22. Rock name; eclogite (mantle xenolith). Locality - Catoca Kimberlite.</b>										
	Minerals	Modal %	Occurrence	Grain size	Grain fabric	Cleavage	Colour in pp	Alteration features	Zonation	Overall rock texture
1	Clinopyroxene	10-25 vol. %	Phenocryst	0.4-3mm	Anhedral	1 Good cleavage	Light green	Rim reaction and, fractures filled by Kpht		

Appendix 1. Continue. CAT-22, mantle xenolith.										
2	garnet	18-20 vol.%,	Phenocryst	1.5mm	subhedra l anhedral	None	Grey	Cracks filled with Kelyphite and calcite		porphyroblastic
3	Ilmenite	1-3 vol. %)	Phenocryst	0.7mm	Anhedral	None	Black	None		
4	Kelyphite	> 30 vol.%,	Groundmass	Very fine	-		Dark-brown			
5	Phlogopite	≤ 10 vol.%,	Groundmass	Very fine	-	1 perfect cleavage	Colourless	Fractures		
6	Calcite	10-15 vol.%,	Phenocryst	1-2mm	Subhedra l	Perfect cleavage	Colourless	Minors reactions along cleavage with Opx	Twining	
<b>Sample number 4. Reference CMT-02. Rock name; Peridotite Locality - Camatxia Kimberlite.</b>										
	Minerals	Modal %	Occurrence	Grain size	Grain fabric	cleavage	Colour in pp	Alteration features	Zonation /twining	Overall rock texture
1	Kelyphite	30–40 vol.%,	Complex structure, fine grained	Very fine grained materials	No visible	None	Brown-red	-	None	Inequigranular texture
2	Garnet	10–5 vol.%,	Phenocryst	> 3mm	Anhedral	None	Grey	Kelyphite texture	None	
3	Carbonate (calcite)	20-35 vol. %,,	Groundmass /Phenocryst	0.01– 0.51mm	Anhedral	None	Colourless	Growth	Possible?	
4	Clinopyroxene	15-10 vol. %	Phenocryst	>9mm	Anhedral	1 perfect	green	Reaction/ rims and	None	
5	Ilmenite	≤1%	Phenocryst	≤1 vol. %	Anhedral	None	Black		None	
<b>Sample number 5 Reference CMT-05. Rock name; Peridotite Locality - Camatxia Kimberlite.</b>										
	Minerals	Modal %	Occurrence	Grain size	Grain fabric	cleavage	Colour in pp	Alteration features	Zonation /twining	Overall rock texture
1	Olivine	20- 30 vol. %)	Phenocryst/ groundmass		Anhedral	None	Colourless	Simplectite texture	None	
2	Clinopyroxene	30–35 vol.%,	Phenocryst	0.2-1mm	Anhedral	1 good cleavage	Light green	Reaction around grain	None	porphyroblastic to
3	Kelyphite	≤10 vol.%,	Groundmass	Very fine grains	-		Red- orange	Reaction Rims on garnet	None	
4	spinel/ilmenite	≤3vol. %,,	Phenocryst	06–1mm	Anhedral	None	Black	Growth features	Possible ?	Inequigranular texture
5	garnet	15-20 vol. %	Phenocryst	>9mm	Anhedral	None	Grey	Reaction/ rims and irregular fractures	None	

Appendix 1. Continue.										
6	Serpentine	≤15 vol.%.	Groundmass /phenocryst	Fine grains	Anhedral	-	Colourless	Reaction process	-	
<b>Sample number 6. Reference CMT-01. Rock name; eclogite. Locality - Camatxia Kimberlite.</b>										
	Minerals	Modal %	Occurrence	Grain size	Grain fabric	cleavage	Colour in pp	Alteration features	Zonati on/twi ning	Overall rock texture
1	Olivine	25- 32 vol.%	Phenocryst	1-4mm	Anhedral	None	Colourless	symplectite texture and fractures	None	porphyroblastic to Texture.
2	Clinopyroxene and Garnet	20–30 vol.%	Phenocryst	1-3mm	Anhedral	One cleavage	Light	Reaction, Kelyphite	None	
4	spinel/ilmenite	≤5vol. %,	Phenocryst	0.6–2mm	Anhedral	None	Black	Poikilitic teexture	-	
5	Kelyphite	10- 17 vol. %	Complex structure, fine grained	0.4-2 mm	-	-	Orange-red	Reaction/ rims on garnet	None	
6	phlogopite	≤ 1 vol.%.	Phenocryst	0.4-4 mm	sub anhedral	One perfect	Colourless		None	
7	Serpentine	10-20 vol.%.	Groundmass	Very fine Materials	-	-	Colourless		None	

**Appendix 2. Summary of hand specimen description of sampled and studied samples.**

Order	Sample Ref:	Pipe Name	Borehole/ Sample Ref:	Depth, M	Qt	Description of Rock (grain size, morphology, and texture) and nomenclature for kimberlite (petrographic Facies).
1	Cat-18	Catoca	Mina NE parte,	horiz. 930 m, KBM complex	1	<b>Mantle eclogitic (bimineralic eclogite).</b> Bimineralic eclogite consist solely of garnet and clinopyroxene (omphacite - exhibiting cleavage). The garnet textures show symmetric patterns across the entire eclogite zone; only in few cases slight asymmetries are observed on this hand specimen. The garnet pattern is characterized by an alignment. Grain fabric <i>euhedral and anhedral</i> textures are present (grains rounding and angular) - well sorted. Medium - coarse grained rock, closely packed- very dense rock and ground mass crystallinity is welded. <b>Green-brown coloured rock.</b> The garnet and clinopyroxenes grains are interlocking crystals. Garnet contains elongate/ parallel grain in shape within fine grain of pyroxene. This bimineralic eclogite rocks is similar to those from premier kimberlite and Kaalvallei kimberlite (South Africa, Dlodla <i>et al.</i> 2006, Viljoen <i>et al.</i> 2005), South Eastern Dharwar craton (South India, Babu <i>et al.</i> 2008) and also those described by Hanraha and Brey (2009)
2	Cat-22	Catoca	047/35-1	508.2	2	<b>Mantle Eclogitic included in kimberlite magma.</b> This rock has a mixture of minerals, but eclogite comprise mainly garnet and pyroxene (bimineralic eclogite) and kimberlite part composed by chrome diopside, phogopite, pyroxene and also with garnet. Grain fabric <i>both euhedral and anhedral texture are present</i> (grains rounding and angular) it is well sorted, medium- coarse grained rock.. Closely packed density, the groundmass crystallinity is welded. Green-brown coloured rock. Colour- dark (kimberlite) and brown (eclogite). Porphyritic texture and grains are well interlocking. The boundary between eclogite and kimberlite is irregular form and it is visible on naked eye. <b>Nomenclature Kimberlitic: Hypabyssal Facies (HF).</b>
3	Cat-23	Catoca	035/315	Horiz. 860.5	1	Mantle Eclogitic ( <b>bimineralic eclogite composed solely by garnet and omphacite</b> ) Note that it is possible that a few accessories minerals phase such as rutile, ilmenite sulphides and aluminous spinel may be present, so it require further investigation. Phaneritic or porphyritic texture. Grain fabric - <i>subhedral texture are present</i> - well sorted. Medium - coarse grained rock, grains angular and also interlocking texture, closely packed- very dense rock and ground mass crystallinity is welded. Green-brown coloured rock
4	Cat-24	Catoca	075/385	69.1	1	Gar-Cpx rock (Mantle Eclogitic). Mantle Eclogitic ( <b>bimineralic eclogite composed solely by garnet and omphacite</b> ). Phaneritic texture. Grain fabric - <i>both subhedral and anhedral texture are present</i> well sorted. Medium - coarse grained rock, grains angular and also interlocking texture, closely packed- very dense rock and ground mass crystallinity is welded. Green-brown coloured rock. Note that Clinopyroxene is slightly moderate. Clinopyroxene exhibiting a symplectite texture. With clinopyroxene clearly growing from the garnet that is breaking down. The symplectite texture may be due to a reaction between adjacent phases or to exsolution of a rapidly cooling solid solution.
5	Cat-29	Catoca	047/35-1	595.9	1	<b>Mantle peridotitic (Iherzolite).</b> Phaneritic and porphyritic texture. Grain fabric - <i>both subhedral and anhedral texture are present</i> - well sorted. Medium - coarse grained rock, grains angular and interlocking texture, closely packed - very dense rock and ground mass crystallinity is welded. Green-brown coloured rock. Note that Clinopyroxene is slightly moderate. <b>Minerals:</b> garnet, chrome diopside, phogopite, pyroxene, Olivine (serpentinise), Ilmenite, spinel? <b>Colour:</b> Dark coloured rock.

**Appendix 2. Continue. Summary of hand specimen description of sampled and studied samples.**

9	Cat-50	Catoca	033/35	506,3	1	<b>Coherent Kimberlitte (CK).Nomeclature Kimberlitic:</b> coherent is applied to rocks formed by the solidification of magma lacking evidence for magmatic fragmentation or disruption (pyroclastic features, Scott Smith <i>et al.</i> 2008). <b>Hypabyssal Facies (HF) from dyke.Texture:</b> Porphyritic (large phenocrysts-country rock within groundmass, well sorted, closely packed and groundmass crystallinity is welded texture. <b>Minerals:</b> garnet, chrome diopside, phogopite, pyroxene, Olivine (dominant mineral in the rock but mostly is serpentenise), Ilmenite, perovskite? spinel?. <b>Colour:</b> Dark coloured kimberlite
10	Cat-53 Cat -5	Catoca	050/37	483,0	1	<b>Coherent Kimberlitte (CK). Nomeclature Kimberlitic: Hypabyssal Facies (HF) from dyke.</b> Coherent is applied to rocks formed by the solidification of magma lacking evidence for magmatic fragmentation or disruption (pyroclastic features, Scott Smith <i>et al.</i> 2008). <b>Texture:</b> Porphyritic (large phenocrysts-country rock within groundmass, well sorted, closely packed and groundmass crystallinity is welded texture. <b>Minerals:</b> garnet, chrome diopside, phogopite, pyroxene, Olivine (dominant mineral in the rock but is serpentenise), Ilmenite, perovskite? spinel? <b>Colour:</b> Dark
11	Cat-58	Catoca	050/37	543,0	1	<b>Coherent Kimberlitte (CK).Nomeclature Kimberlitic: Hypabyssal Facies (HF) from dyke. Texture:</b> Porphyritic (large phenocrysts-country rock within groundmass, well sorted, closely packed and groundmass crystallinity is welded texture. <b>Minerals:</b> garnet, chrome diopside, phogopite, pyroxene, Olivine (dominant mineral in the rock but is serpentenise), Ilmenite, perovskite? spinel?. <b>Colour:</b> Dark coloured kimberlite
12	Cat-59	Catoca	033/35	344.4	2	<b>Tuffisititc kimberlite breccia (TKB).Nomeclature Kimberlitic: Diatreme Facies (DF). Texture:</b> Porphyritic (large phenocrysts-country rock within fine groundmass, closely packed and groundmass crystallinity is welded texture. Grain fabric is well sorted. <b>Minerals:</b> garnet, chrome diopside, phogopite, pyroxene, olivine (dominant mineral but is serpentenised), ilmenite and sedimentary minerals (biotite and quartz). <b>Colour:</b> light green coloured rock
	Cat-60	Catoca	Mine NW	horiz. 900 m	1	<b>Pyroclastic Kimberlite. (PK). Nomeclature Kimberlitic: Crater Facies (CF). Texture:</b> Inequigranular & porphyritic. groundmass crystallinity is holecrySTALLINE, loosely packed (density) and grain fabric is moredately sorted. <b>Minerals:</b> Ilmenite ,garnet, chrome diopside, phogopite, pyroxene, Olivine (dominant mineral in the rock but is serpentenise) and hamatite red colour ( due to oxidation process, garnet Fe <sup>2+</sup> react with fluid to ptoduce Fe <sup>3+</sup> <b>Colour:</b> Light brown coloured kimberlite
13	Cat-61	Catoca	Mine SW	horiz. 900 m	1	<b>Pyroclastic Kimberlite. (PK). Nomeclature Kimberlitic: Crater Facies (CF).Texture:</b> Inequigranular & porphyritic. groundmass crystallinity is holecrySTALLINE, loosely packed (density) and grain fabric is moredately sorted. <b>Minerals:</b> Ilmenite ,garnet, chrome diopside, phogopite, pyroxene, Olivine (dominant mineral in the rock but is serpentenise) and hamatite red colour ( due to oxidation process, garnet Fe <sup>2+</sup> react with fluid to ptoduce Fe <sup>3+</sup> . <b>Colour:</b> Light brown coloured kimberlite
14	Cat-62	Catoca	Mine SW	horiz. 900 m	1	<b>Pyroclastic Kimberlite. (PK). Nomeclature Kimberlitic: Crater Facies (CF). Texture:</b> Inequigranular & porphyritic. groundmass crystallinity is holecrySTALLINE, loosely packed (density) and grain fabric euhedral and anhedral are present it is moredately sorted. <b>Minerals:</b> Ilmenite ,garnet, chrome diopside, phogopite, pyroxene, Olivine (dominant mineral in the rock but is serpentenise)
15	Cat- 67	Catoca	037/34	612.8 m	1	<b>Coherent Kimberlitte (CK)Nomeclature Kimberlitic: Hypabyssal Facies (HF) from dyke. Texture:</b> Porphyritic (large phenocrysts-country rock within fine groundmass, closely packed and groundmass crystallinity is welded texture. grain fabric euhedral and anhedral are present- it is well sorted. <b>Minerals:</b> garnet, chrome diopside, phogopite, pyroxene, Olivine (dominant mineral in the rock but is serpentenise), Ilmenite, perovskite? spinel? <b>Colour:</b> Dark coloured kimberlite

**Appendix 2. Continue. Summary of hand specimen description of sampled and studied samples.**

Order	sample ref.	Pipe name	Depth m	Qt	Description of Rock (grain size, morphology, and texture) and nomenclature for kimberlite (petrographic Facies)
1	CX 012	Caixepa	60.84m	1	<b>Pyroclastic Kimberlite (PK). With inclusion of mantle xenolith (P-types) Nomenclature Kimberlitic: Crater Facies (CF)</b> <b>Texture:</b> Inequigranular or porphyritic (with large phonocrysts of ilmenite and garnet within fine grained materials . groundmass crystallinity is holocrystalline, loosely packed (density) and grain fabric is moredately sorted. <b>Minerals:</b> Olivine (but is serpentinite), Ilmenite ,garnet, chrome diopside, phogopite, pyroxene ( Clinopyroxene) and hamatite red colour ( due to oxidation process, garnet Fe <sup>2+</sup> react with fluid to ptoduce Fe <sup>3+</sup> (Hematite). <b>Colour:</b> Grey coloured kimberlite. This rock contains more visible green chrome diopside crystals Cr>40%
2	CX 022	Caixepa	30m	1	<b>Pyroclastic Kimberlite (PK) . With inclusion of mantle xenoliths (p-types).Nomenclature Kimberlitic: Crater Facies (CF)</b> <b>Texture:</b> Inequigranular or porphyritic. groundmass crystallinity is holocrystalline, loosely packed (density) and grain fabric is moredately sorted. <b>Minerals:</b> Ilmenite ,garnet, chrome diopside, phogopite, pyroxene ( Clinopyroxene) and hamatite in red colour ( due to oxidation process, garnet Fe <sup>2+</sup> react with fluid to ptoduce Fe <sup>3+</sup> (Hematite). <b>Colour:</b> Grey coloured kimberlite. This rock contains some visible white components, probably <u>calcite</u> ? Note that calcite may be a late generated mineral
3	CX12	Caixepa	54.90m	1	<b>Pyroclastic Kimberlite (PK) . Also this rock contains a inclusion of mantle xenolith (P-types). Nomenclature Kimberlitic: Crater Facies (CF).</b> <b>Texture:</b> porphyritic (large phocryst of chrome diopside with groundmass). groundmass crystallinity is holocrystalline, loosely packed (density) and grain fabric is moredately sorted. <b>Minerals:</b> Ilmenite ,garnet, chrome diopside, phogopite, and hamatite in red colour ( due to oxidation process, garnet Fe <sup>2+</sup> react with fluid to ptoduce Fe <sup>3+</sup> (Hematite). <b>Colour:</b> Grey coloured kimberlite. This rock contains some visible veins of white materials, probably carbonate?Note that carbonete may be a late generated mineral
4	CX009	Caixepa	57m	1	<b>Pyroclastic Kimberlite (PK) . With inclusion of mantle xenoliths (P-types). Nomenclature Kimberlitic: Crater Facies (CF).</b> <b>Texture:</b> Inequigranular porphyritic. groundmass crystallinity is holocrystalline, loosely packed (density) and grain fabric is moredately sorted. <b>Minerals: Pyroxene (cpx),</b> Ilmenite ,garnet, chrome diopside, phogopite, pyroxene ( Clinopyroxene) and hamatite in red colour ( due to oxidation process, garnet Fe <sup>2+</sup> react with fluid to ptoduce Fe <sup>3+</sup> (Hematite). <b>Colour:</b> Grey coloured kimberlite. This rock contains some visible white components, probably carbonate, the late generated mineral
5	CX030	Caixepa	76.7m	1	<b>This rock is the combination of tuffisititc and pyroclastic Kimberlite (PK) rock,</b> devrived at boundery between diatrem and Crater phase. dominantly by Inequigranular porphyritic resulting in magacryst of garnet, ilmenite and olivine are paced in the fine ground mass material of serpentne and carbonete.the grain fabric is moredately. The equilibrium between Olv and Grt is visible but it most of these minerals are altered by hydrothermal fuid.
6	CX027	Caixepa	>45m	1	Tuffisititc kimberlite breccia (TKB), derived from diatreme facies. This rock is composed by several minerals including Grt, Olv, Spl and pyroxene. The handspecime is well sorted/grain fabric is moredately and crystalline rock, with minor alteration. porphyritic is is the main texture, Grey to light green coloured kimberlite rock. Oxidation process may have taken place in this took, where the ilmenite grains contains some lamellae features

**Appendix 2. Continue. Summary of hand specimen description of sampled and studied samples**

Order	sample ref.	Pipe name	Depth M	Qt	Description of Rock (grain size, morphology, and texture) and nomenclature for kimberlite (petrographic Facies)
1	CW045	Camutue	140.55	2	<b>Pyroclastic kimberlite, Texture:</b> porphyritic (where phocryst of Ilmenite and garnet in fine groundmass). groundmass crystallinity is holecryalline, moderate packed (density) and grain fabric is moredately sorted <b>Minerals:</b> Ilmenite ,garnet, olivine, phogopite, (due to oxidation process, garnet Fe <sup>2+</sup> react with fluid to ptoduce Fe <sup>3+</sup> (Hematite). <b>Colour:</b> Grey coloured kimberlite. This rock contains some visible fractures filled carbonate of white materials.
2	SSCM	Camutue	149m	1	<b>Tuffisitc kimberlite breccia (TKB). Diatreme Facies ( DF). Texture:</b> Porphyritic (large phenocrysts of country rock (Gneises) within fine groundmass, closely packed and groundmass crystallinity is welded texture. grain fabric is well sorted. <b>Minerals:</b> garnet, pyroxene, and, Olivine (dominant mineral in the rock but is serpentenise), Ilmenite, biotite and quartz also are present). <b>Colour:</b> light green coloured kimberlite
3	CMK	Camutue	98m	3	<b>Pyroclastic Kimberlite. (PK). Texture:</b> Inequigranular & porphyritic. groundmass crystallinity is holecryalline, loosely packed (density) and grain fabric is moredately sorted. <b>Minerals:</b> , pyroxene, Ilmenite garnet and altered livine and hamatite red colour ( due to oxidation process, garnet Fe <sup>2+</sup> react with fluid to ptoduce Fe <sup>3+</sup> <b>Colour:</b> Light brown coloured kimberlite
3	CM917 1	Camutue	102m	3	<b>Pyroclastic Kimberlite. (PK), diatreme facies. Texture:</b> Inequigranular & porphyritic. groundmass crystallinity is holecryalline, loosely packed (density) and grain fabric is moredately sorted. <b>Minerals:</b> , pyroxene, Ilmenite garnet and altered livine and hamatite red colour ( due to oxidation process, garnet Fe <sup>2+</sup> react with fluid to ptoduce Fe <sup>3+</sup> <b>Colour:</b> Light green /brown
4	CW45 CM	Camutue	98m	2	<b>Pyroclastic Kimberlite. (PK). Crater, facies rock,</b> composed by several minerals including Grt, Olv, Px and minor oxides minerals probably Spl or Ilm. /grain fabric is slightly moredately, with minor alteration due to the fluid migration in crack mantle rock (oxidation process. Inequigranular is is the main texture on this rock, light green/brown coloured kimberlite rock.
5	CM003	Camutue	139m	2	<b>A mixture of PK rock with some inclusion of mantle xenolith (P-type), derived from diatreme</b> This is composed mainly by Olv, Gnt, Px, and minors oxides minerals (ilmenite and spinel). The grain fabric is poorly sorted, probably due to the alteration/oxidation process in this rock. The megacrysts minerals (Olv, Gnt) are supported by fine matrix of altered Olv/serpentine and carbonate. porphyritic is the main texure in this rock
6	CM N1 P-type	Camutue	~ 50m	1	<b>Pyroclastic kimberlite with some inclusion of P-tpe. This is crater facies rock,</b> with Grt, Olv and Ilm as main minerals. Inequigranular texture, the groundmass crystallinity is holecryalline (allcrystal are entirely crystalline, not glass), moderate packed (density). Most of P-type minerals are altered

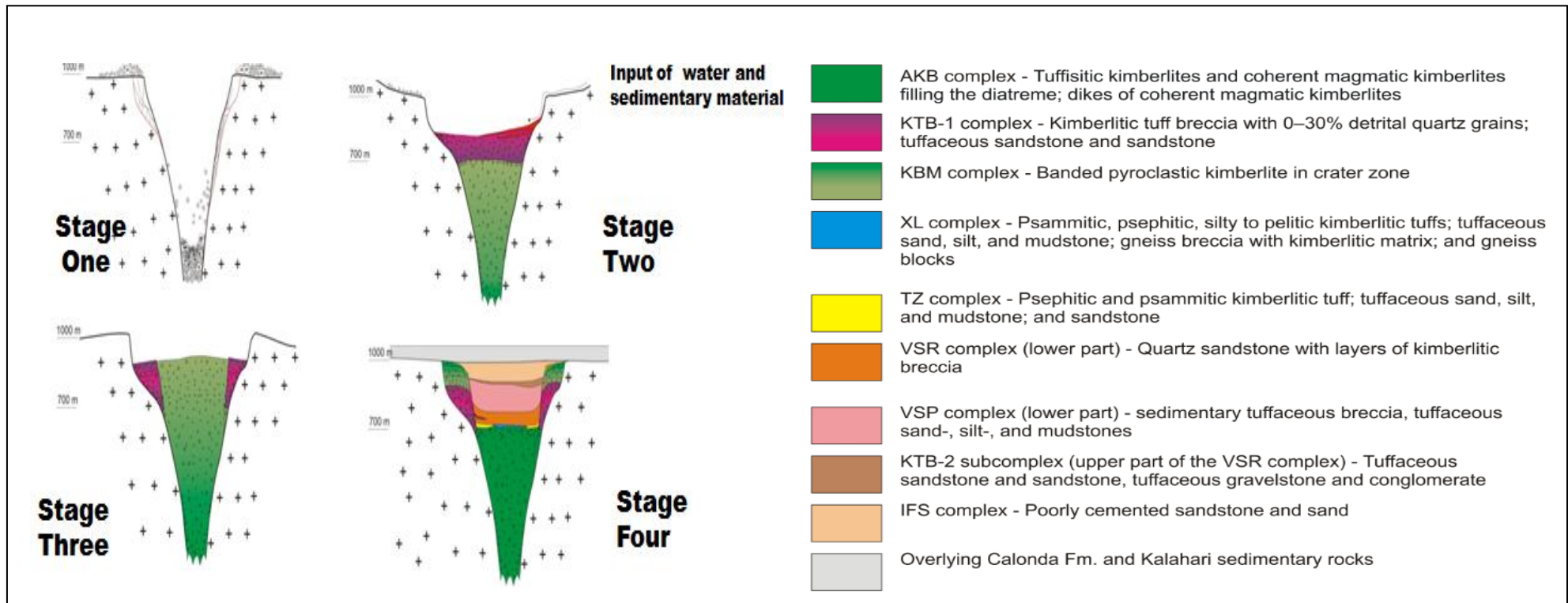
**Appendix 2. Continue. Summary of hand specimen description of sampled and studied samples from Camatxia kimberlite**

Order	Sample ref.	Pipe name	Depth m	Qt	Description of Rock (grain size, morphology, and texture) and nomenclature for kimberlite (petrographic Facies)
1	CMT0.1	Camatxia	45.84m	1	<b>Mantle eclogitic (bimineralic eclogite)</b> from crater facies, composed by garnet and clinopyroxene (exhibiting cleavage) with minor oxide minerals (rutile or spinel). Grain fabric euhedral and anhedral textures are present (grains rounding and angular) - poorly sorted. Medium - coarse grained rock, moderate packed and ground mass crystallinity is moderate welded (all crystals are entirely crystalline, not glass), inequigranular texture. <b>Green-brown coloured rock.</b> The garnet and clinopyroxene grains are interlocking crystals, but this rock is less dense than those E-type from Catoca.
2	CN and MZ	Camatxia	130m 110m	2	<b>Pyroclastic Kimberlite (PK)</b> , derived from diatreme facies. These rocks are composed by Ilm, Grt, Olv, Spl and pyroxene, but most of Olv from both rocks is altered. The rocks are moderately sorted and the grain fabric is moderately crystalline rocks, with minor alteration. porphyritic is the main texture, Dark, grey to light green coloured kimberlite rock. The mineral alteration is evidence of Oxidation process may have taken place in these rocks,
3	CMT 02	Camatxia	27m	1	<b>Mantle eclogitic (bimineralic eclogite) from Crater Facies (CF)</b> <b>Texture:</b> Inequigranular, groundmass crystallinity is holocrystalline, loosely packed (density) and grain fabric is moderately sorted. <b>Minerals:</b> garnet, pyroxene (Clinopyroxene) This rock is highly oxidised, due to oxidation process, where the garnet $Fe^{2+}$ reacted with fluid to produce $Fe^{3+}$ kelyphite materials. <b>Colour:</b> brown rock. This rock contains alteration process
4	CMT 003 and CMT04	Camatxia	35 m	2	<b>Pyroclastic Kimberlite (PK) with a inclusion of mantle xenolith. Nomenclature Kimberlitic: Crater Facies (CF)</b> <b>Texture:</b> porphyritic texture, where the large phenocryst garnet, pyroxene and olivine of with groundmass of carbonate serpentine. The groundmass crystallinity is holocrystalline, loosely packed (density) and grain fabric is poorly sorted. <b>The inclusion of P-type is composed by Ilmenite, garnet, pyroxene.</b> this rock is more oxidised, and it can be assumed that Hematite may be present in red colour (due to oxidation process, garnet $Fe^{2+}$ react with fluid to produce $Fe^{3+}$ in Hematite or kelyphite). <b>Colour:</b> brown coloured kimberlite and green on side of mantle xenolith inclusion
5	CMT05	Camatxia	55m	1	<b>Mantle eclogitic (bimineralic eclogite)</b> from crater diatreme facies, composed by garnet and clinopyroxene (exhibiting cleavage). Reaction kelyphite rims and irregular fractures on garnet are evidence of oxidation process in this rock. The grain fabric euhedral and anhedral textures are present (grains rounding and angular), also poorly sorted rock. Medium - coarse grained rock, moderate packed and ground mass crystallinity is poor/moderate welded (all crystals are entirely crystalline, not glass), inequigranular texture. <b>Green-brown coloured rock.</b> The garnet and clinopyroxene grains are interlocking crystals, but this rock is less dense than those E-type from Catoca. The visible reaction kelyphite rims on garnet is, probably the late generated mineral/product
6	CMT 60	Camatxia	77.m	1	<b>Tuffisitic Kimberlite (PK)</b> derived from diatreme facies. The main texture is porphyritic because the large phenocrysts - of fragmented country rock, and minerals (ilmenite, garnet, pyroxene, phlogopite, pyroxene) within fine groundmass of serpentine. This rock is well or closely packed and groundmass crystallinity is welded texture. The grain fabric euhedral and anhedral are present - it is well sorted. Similar grain texture observed at Catoca - sample Cat 67. Some visible alteration of minerals by hydrothermal fluid are present in this rock

**Appendix 2. Continue. Summary of hand specimen description of sampled and studied samples, from Camagico pipe**

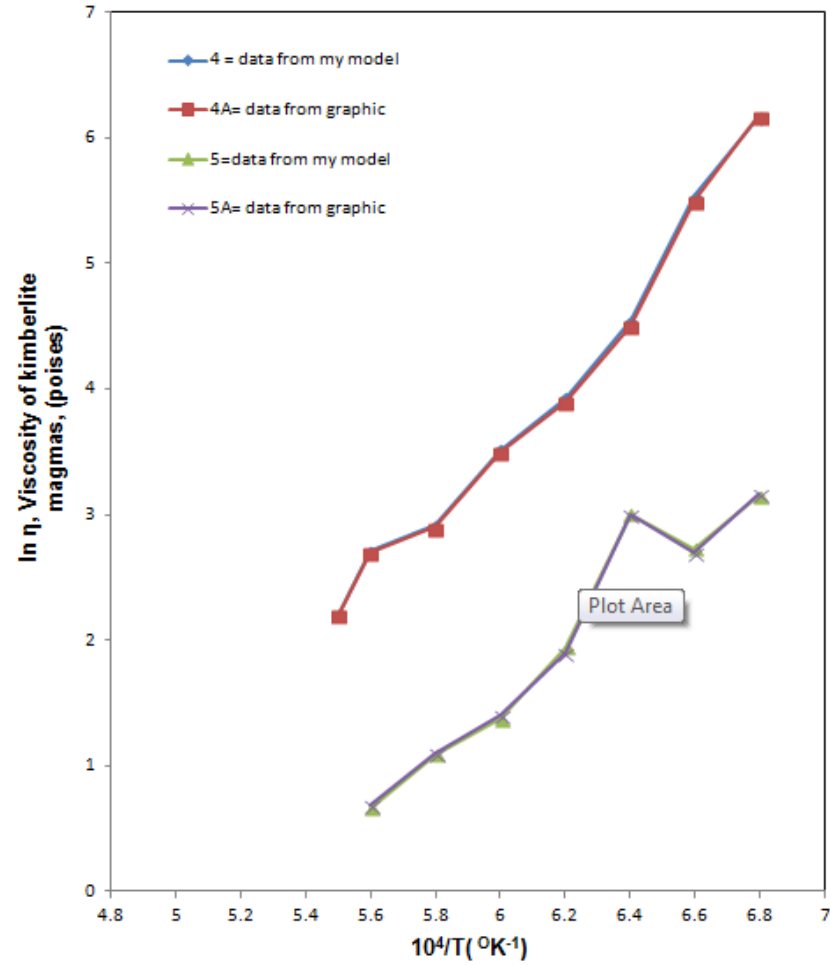
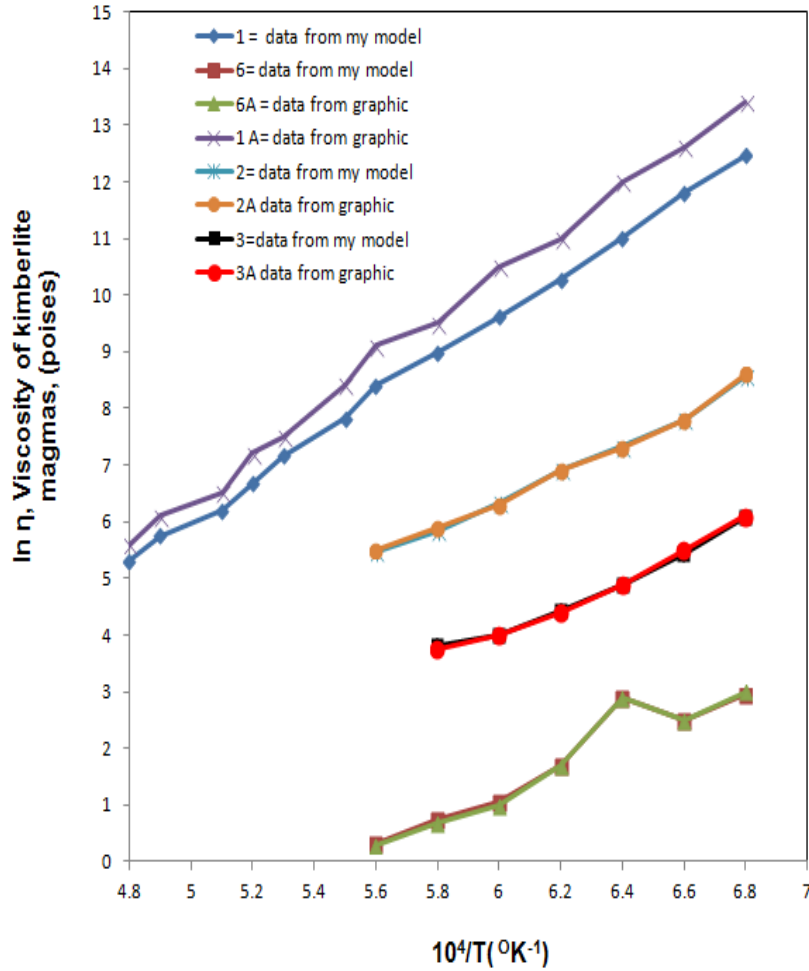
Order	sample ref.	Pipe name	Depth M	Qt	Description of Rock (grain size, morphology, and texture) and nomenclature for kimberlite (petrographic Facies)
1	CMG 002	Camagico	95m	1	<b>Pyroclastic kimberlite with inclusion of P-type, Texture, from crate facies.</b> Inequigranular & porphyritic is the main texture. the megacryst of garnet, olivine, and oxides minerals are all supported by groundmass of serpentine and very fine grained of carbonate. The grain fabric is moderately sorted but in some area (P-type) is poorly sorted. <b>The</b> groundmass crystallinity is holocrystalline, poor to moderately packed (density). The rims on garnet are evidence of oxidation process, the original garnet Fe <sup>2+</sup> may have reacted with fluid to produce Fe <sup>3+</sup> Hematite? and fine rich iron kelyphite material. Colour: dark-grey coloured kimberlite.
2	CMG 006	Camagico	87m	2	<b>Pyroclastic kimberlite with inclusion from Crater facies. Texture:</b> Porphyritic where large phenocrysts of Garnet and olivine are within fine groundmass of serpentine. groundmass crystallinity rock is moderately packed. The grain fabric is moderate to well sorted texture. <b>Minerals:</b> garnet, pyroxene, and, Olivine are dominant mineral in the rock but serpentine is present in this rock, Ilmenite, light green to brown coloured kimberlite.

**Appendix 3. The occurrence model of Angolan pipes (example of Catoca kimberlite pipe).**



Reference. This diagram was given by a geologist colleague called Pervov at Catoca mine, during filed trip in Angola, in 2012. It was modified from original

**Appendix 4. Illustration of validation of the viscosity model and comparison of the research model (data from this project) with those published viscosity data. The result shows satisfactory agreement over a wide range of viscosities. Note that data labeled as data from my graphic are from this project and those data from graphic are those published by Bottinga and Weill (1972).**



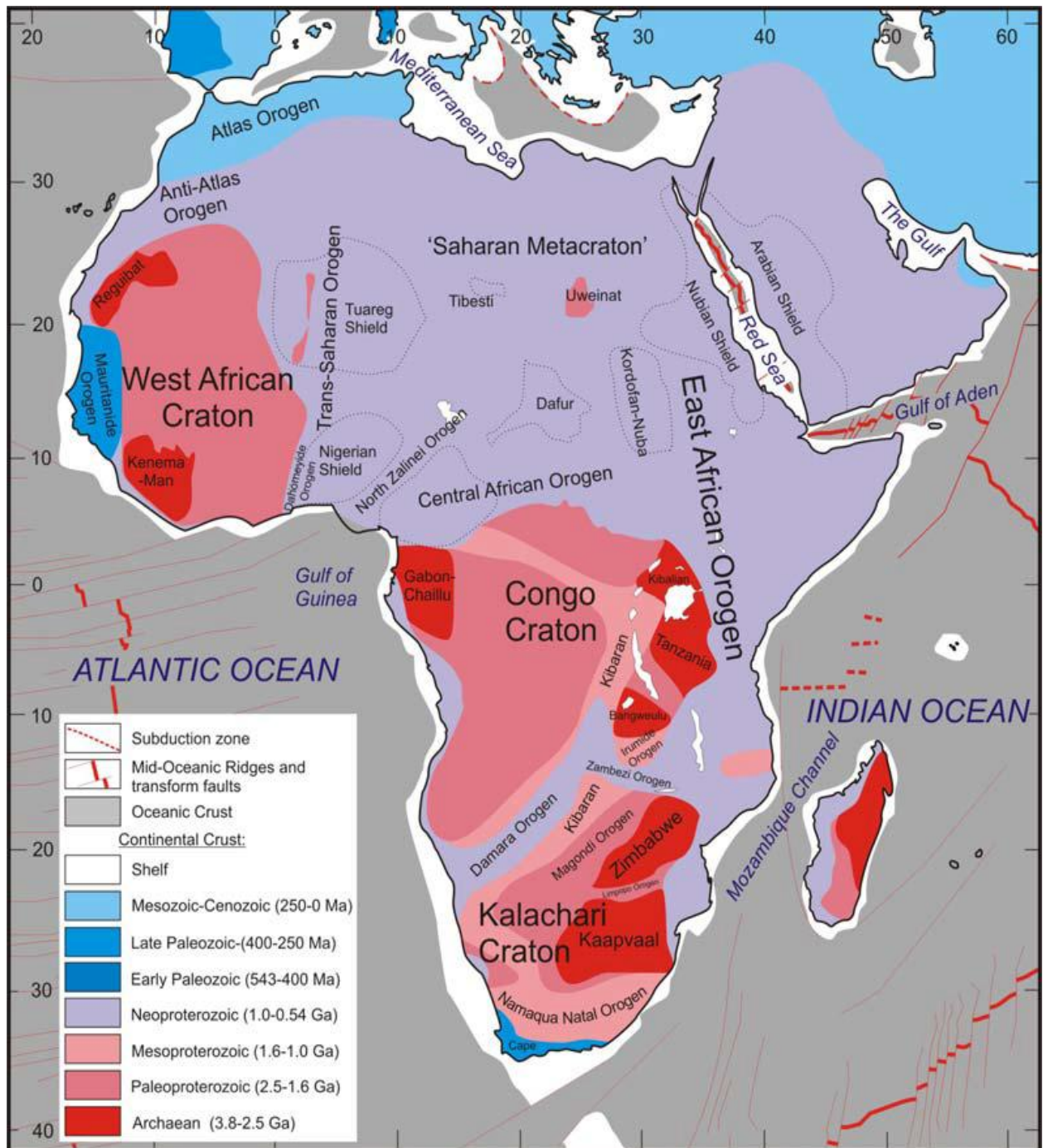
Appendix 5. Summary of hand specimen samples (photos) used this project.



Appendix 5. Continue of hand specimen samples (photos) used this projec



**Appendix 6. Age of African crustal basement.** These ages are for the time of crustal formation or the time of thermal or tectonic crustal reworking (Van Hinsbergen, et al., 2011)



## Chapter Seven: References.

Agee, J. J., Garrison, J. R and Taylor, L. A., (1982). Petrogenesis of Oxide Minerals in Kimberlite, Elliott County, Kentucky (USA). *American Mineralogist*. Vol.67, pp. 28–42.

Allsopp, H. L., Burger, A. J., Van Zyl, C., (1967). A minimum age for the premier kimberlite pipe yielded by biotite Rb-Sr measurements, with related galena isotopic data. *Earth and Planetary Science Letters*. Vol. 3, pp.161-166

Alymova, N., (2012). Picroilmenite xenoliths and xenocrysts in Yakutian kimberlites. *Geophysical Research Abstracts*, Vol. 14, EGU2012-3691-2.

Arima, M., and Kozai, Y., (2008). Diamond dissolution rates in kimberlitic melts at 1300–1500°C in the graphite stability field. *European Journal of Mineralogy*, Vol. 20, Issue 3, pp.357-364.

Arima, M., (1998). Experimental study of growth and resorption of diamond in kimberlitic melts at high pressures and temperatures. *Proceedings of the 7<sup>th</sup> International, Kimberlite Conference*, pp. 32–34.

Ashchepkov I.V., Rotman A.Y., Somov S.V., Afanasiev, V. P., Downes H, Logvinova A.M., Nossyko S., Shimupi J., Palessky, S.V, Khmelnikova O.S., Vladykin N.V., (2012). Composition and thermal structure of the lithospheric mantle beneath kimberlite pipes from the Catoca cluster, Angola *Tectonophysics*, Vol. 530–531, pp. 128–151.

Bancroft, G., (1979). Mössbauer spectroscopic studies of the chemical state of iron in silicate minerals. *Journal de Physique Colloques*, Vol. 40, pp.C2-464-C2471.

Basseka, C. A., Shandini, Y., and Tadjou, J.M., (2011).Subsurface structural mapping using gravity data of the northern edge of the Congo Craton. *South Cameroon, Geofizika*, Vol. 28, No. 2, pp. 229–245.

Bataleva, Y.V., Palyanov, Y. N., Sokol, A. G., Borzdov, Y.M., and Palyanova, G. A., (2012). Conditions for the origin of oxidized carbonate-silicate melts: Implications for mantle metasomatism and diamond formation. *Lithos*, Vol. 128–131, pp. 113-125.

Batumike, J. M., Griffin, W. L., O'Reilly, S.Y., Belousova, E. A., Pawlitschek, M., (2009). Crustal evolution in the central Congo-Kasai Craton, Luebo, D.R. Congo: Insights from zircon U–Pb ages, Hf-isotope and trace-element data. *Precambrian Research*, Vol. 170, Issue 1-3, pp. 107–115.

Bell, D. R., Gregoire, M., Grove, T. L., Chatterjee, N., Carlson, R.W and Buseck, P. R., (2005.). Silica and volatile-element metasomatism of Archean mantle: a xenoliths-scale example from the Kaapvaal Craton. *Contributions to Mineralogy and Petrology*. Vol. 150, pp. 251- 267

Blatt, H and Tracy, R. J., (1995). *Petrology: Igneous, Sedimentary and Metamorphic*. 2<sup>nd</sup> Edition. Published by W. H. Freeman ISBN 10: 0716724383 ISBN 13: 9780716724384.

Bottinga, Y. and Weill, D., (1972). The viscosity of magmatic silicate liquids: a model for calculation. *American Journal of Science*, Vol. 272, pp. 438-475.

Boyd, F. R., and Danchin, R. V., (1980). Lherzolites, eclogites and megacrysts from some kimberlites of Angola. *American Journal of Science*, Vol. 280, pp. 528-5491.

Boyd, F. R., and Gurney, J.J., (1986). Diamonds and the African Lithosphere. *Science*, Vol. 232, pp. 472-477.

Bragg diffraction.svg. (2015).

[https://commons.wikimedia.org/wiki/File:Bragg\\_diffraction.svg](https://commons.wikimedia.org/wiki/File:Bragg_diffraction.svg). (Visited on 05/03/2015)

Brouwer, P., (2010). *Theory of XRF*. PANalytical, 3<sup>rd</sup> edition, pp. 4-59.

Bull, J. N., Tennant, W.C., Ballaran, T. B., Nestola and McCammon, C. A., (2012). Anisotropic mean-squared-displacement tensor in cubic almandine garnet: a single crystal <sup>57</sup>Fe Mössbauer study. *Physics and Chemistry of Minerals*, Vol. 39, Issue 7, pp. 561–575.

Canil, D., and O'Neill, H. St. C., (1996). Distribution of ferric iron in some upper mantle assemblages. *Journal of Petrology*, Vol. 37, pp. 609-635.

Canil, D., and O'Neill, H. St. C., (1996). Distribution of ferric iron in some upper mantle assemblages. *Journal of Petrology*, Vol. 37, pp. 609-635.

Carmichael, I. S. E., and Nicholls, J., (1967). Iron-titanium oxides and oxygen fugacities in volcanic rocks. *Journal of Geophysical Research*, Vol. 72. Issue, 18, pp. 4665–4687.

Caro, G., Kopylova, M. G., and Creaser, R., (2004). The hypabyssal 5034 kimberlite of Gahcho Kue cluster, SouthEastern Slave craton, NorthWest territories, Canada: Agranite-contaminated group-I kimberlite. *The Canadian Mineralogist*, Vol. 42, pp. 183-20.

Cas, R., Porritt, L., Pittari, A., and Hayman, P., (2008). A New Approach to Kimberlite Facies Terminology Using a Revised General Approach to the Nomenclature of all Volcanic Rocks and Deposits: Descriptive to Genetic. *Journal of Volcanology and Geothermal Research*, Vol. 174, Issue 1-3, pp. 226–240.

Cas, R.A.F., Hayman, P., Pittari, A., Porritt, L., (2008). Some major problems with existing models and terminology associated with kimberlite pipes from a volcanological perspective, and some suggestions. *Journal of Volcanology and Geothermal Research*, Vol. 174, Issue 1-3, pp. 209–225.

Castillo-Oliver, M., Melgarejo, J. G., and Goncalves, A. O., (2011). Use of Indicator Minerals in Diamond Exploration: a Comparison between Barren and Fertile Kimberlites in Angola. *Macla n° 15. Revista de la Sociedad Española de Mineralogía*, pp. 59-60.

Chatterjee, N. (2012). Electron Microprobe Analysis. Course 12.14. Notes. ([https://ocw.mit.edu/courses/earth-atmospheric-and-planetary-sciences/12-141-electron-microprobe-analysis-january-iap-2012/lecture-notes/MIT12\\_141IAP12\\_coursenotes.pdf](https://ocw.mit.edu/courses/earth-atmospheric-and-planetary-sciences/12-141-electron-microprobe-analysis-january-iap-2012/lecture-notes/MIT12_141IAP12_coursenotes.pdf)). Visited on 10/03/2017

Clifford, T.N., (1966).Tectono-metallogenic units and metallogenic provinces of Africa. *Earth and Planetary Science Letters*, Vol. 1, Issue 6, pp. 421–434.

Cookenboo, H., and Grütter, H., (2010) Mantle-derived indicator mineral compositions as applied to diamond exploration. *Geochemistry: Exploration, Environment, Analysis*, Vol. 10, No. 1, pp. 81–95,

Correia, E. A., and Laiginas, F. A. T. P., (2006). Garnets from the Camafuca-Camazambo kimberlite (Angola) *Annals of the Brazilian Academy of Sciences*, Vol. 78 No.2, pp. 309-315.

Craig, R. J., (2001). Ore-mineral texture and the tales they tell. *The Canadian Mineralogist*, Vol. 39, pp. 937-956.

Creighton, S., Harvey, S., and Read, G., (2011). Diamond exploration on the Sask craton: A challenge for current Paradigms. *Saskatchewan Geological Survey. Abstract Volume*.

Creighton, S., Stachel, T., Matveev, S., Hofer, H., McCammon, C.A., Luth, R. W., (2009). Oxidation of the Kaapvaal lithospheric mantle driven by metasomatism. *Contributions to Mineralogy and Petrology*, Vol. 157, pp. 491–504.

Czyzycki, M., Bielewski. M., Lankosz , M., (2009). Quantitative elemental analysis of individual particles with the use of micro-beam X ray fluorescence method and Monte Carlo simulation. *X-Ray Spectrometry*, Vol. 38, pp, 487–491.

Das, B. D. S. S., Sudarsham, M., Reddy, V. R., Chintalapudi, S. N.,and Majumdar, C. K., (1996). <sup>57</sup>Fe Mössbauer studies on natural ilmenite. *Indian Journal of Pure and Applied Physics*, Vol.34, pp. 474-479.

Dasgupta, R., (2013). Ingassing, Storage, and Outgassing of Terrestrial Carbon through Geologic Time, *Reviews in Mineralogy and Geochemistry*, Vol. 75 pp. 183-229.

De Boorder, H.,(1982). Deep-reaching fracture zones in the crystalline basement surrounding the West Congo System and their control of mineralization in Angola and Gabon. *Geoexploration*, Vol. 20, Issue 3-4, pp. 259-273.

De Grave, E., and Van Alboom. A., (1991). Evaluation of Ferrous and Ferric Mössbauer Fraction. *Physics and Chemistry of Minerals*, Vol. 18, pp. 337-342.

Deer W. A. F. R. S., Howie, R. A. and Zussman, J. (1992). *An Introduction to the Rock-Forming Minerals*. London: Longmans Publishing Company.

Deysel, K (2007). Leucoxene study: a mineral liberation analysis (MLA) investigation The 6<sup>th</sup> International Heavy Minerals Conference "Back to Basics". The Southern African Institute of Mining and Metallurgy, pp. 167-172.

Dickson, D P. E and Berry. F, J. (2005) *Mössbauer Spectroscopy*. Cambridge University. Press: Cambridge.

Dingwell, B. D and Virgo. D, (1988).Viscosities of melts in the NaO<sub>2</sub>-FeO-Fe<sub>2</sub>O<sub>3</sub>-SiO<sub>2</sub> system and factors controlling relative viscosities of fully polymerized silicate melts. *Geochimica et Cosmochimica Acta*, vol.52, pp. 395 -403.

Dirks, P.H.G. M., Blenkinsop, T. G., Jelsma., H.A., (2003). The geological evolution of Africa, Geology, Vol. IV. In: Stuwe K, Grasemann de Vivo (eds) Encyclopedia of life support systems. UNESCO Publishing, EOLSS Publishers Co Ltd. Oxford, UK.

Dobosi.G., and Kurat. G., (2010). On the origin of silicate -bearing diamondites. Mineralogy and Petrology, Vol. 99, pp. 29-42.

Dollase, W. A., and Newman, W. I., (1984). Statistically most probable stoichiometric formulae. American Mineralogist, Vol. 69, pp. 553-556.

Donnelly, C. L., Griffin , W. L., O'Reilly, S.Y., Norman, J., Pearson, N., and Shee, S.R., (2010).The Kimberlites and related rocks of the Kuruman Kimberlite Province, Kaapvaal Craton, South Africa. Contributions to Mineralogy and Petrology, Vol. 161, pp. 351–371.

Duarte, J. M. G., and Campbell, S. L., (2009). Mössbauer Spectroscopy. Massachusetts Institute of technology, USA

Droop, G.T. R., (1987). A general equation for estimating Fe<sup>3+</sup> concentrations in ferromagnesian silicates and oxides from microprobe analyses, using stoichiometric criteria, Mineralogical Magazine, Vol. 51, pp. 431-43.

Dyar, M. D., Agresti, D. G., Schaefer, M. W., Grant, C. A., and Sklute, E.C., (2006). Mössbauer Spectroscopy of Earth and Planetary Materials. The Annual Review of Earth and Planetary Science, Vol. 34 pp. 83–125.

Dyar, M. D., (1984). Precision and inter-laboratory reproducibility of measurements of the Mössbauer effect in minerals. American Mineralogist, Vol. 69, pp. 1127-1144.

Eeckhout, S.G. and De Grave, E. (2003). Evaluation of Ferrous and Ferric Mössbauer Fraction. Part II. Physics and Chemistry of Minerals, Vol. 30, pp. 142-146

El-Shazly, A. K., (2004). Textures of Ore Deposits and associated features. Geology, Vol 481. Earth Resources, pp. 1-4.

Emery, D and Marshall, J. D., (1989). Zoned calcite cements: has analysis outpaced interpretation? Sedimentary Geology Vol. 65, Issues 3–4, pp. 205-210.

Erazo, F. J., (1999). Mössbauer Spectroscopy of Iron Porphyrins

<http://faculty.knox.edu/cschulz/M%C3%B6ssbauer/index.html> (visited on 30/11/2016).

Fedortchouk, Y., and Canil, D., (2009). Diamond oxidation at atmospheric pressure: development of surface features and the effect of oxygen fugacity *European Journal of Mineralogy*, Vol. 21. No 3, pp. 623-635.

Fedortchouk, Y., Canil, D., and Semenet, E., (2007). Mechanisms of diamond oxidation and their bearing on the fluid composition in kimberlite magmas. *American Mineralogist*, Vol. 92, pp. 1200–1212.

Fedortchouk, Y., and Canil, D., (2004). Intensive Variables in Kimberlite Magmas, Lac de Gras, Canada and Implications for Diamond Survival. *Journal of Petrology*, Vol. 45, No 9, pp. 1725–1745.

Fedortchouk, Y., and Zhang, Z., (2011). Diamond resorption: link to metasomatic events in the mantle or record of magmatic fluid in kimberlitic magma? *The Canadian Mineralogist*. Vol. 49, pp. 707-719.

Fewster, P. F., (2014). A new theory for X-ray diffraction. *Acta Crystallographica A*, Vol. 70, pp. 257-282.

Field, M., Stiefenhofer, J., Robey, J., Kurszlaukis, S., (2008). Kimberlite-hosted diamond deposits of southern Africa: A review. *Ore Geology Reviews*, Vol.34, pp33–75

Field, M., and Scott Smith, B.H., (1999). Contrasting Geology and Near-Surface Emplacement of Kimberlite Pipes in Southern Africa and Canada. *Proceedings of the Seventh International Kimberlite Conference*, Vol. 1, pp. 214-237.

Finger, L.W., (1972). The uncertainty in the calculated ferric iron content of a microprobe analysis. *Year Book, Carnegie Institution of Washington*, Vol.71, pp.600–603.

Forder, S. D., (2004), *The Use of Mössbauer Spectroscopy in Metallurgy*, ISIAME, Madrid, Newsletter Vol. 24, No. 8

Francis, D., and Patterson, M., (2009). Kimberlites and aillikites as probes of the continental lithospheric mantle, *Lithos*, Vol. 109, Issues 1–2, pp. 72–80.

Frank Press and Raymond Siever., (1986). *Earth*. Fourth Edition. Hardcover. Published by W. H. Freeman.

Ganga J., Rotman, A. Y. and Nosiko, S., (2003). Pipe Catoca, an example of the weakly eroded kimberlites from North-East of Angola, 8<sup>th</sup> International Kimberlite Conference Long Abstract”.

Gibb, T. C, and Greenwood, N. N., and Twist, W.,(1969). The Mössbauer spectra of natural ilmenites. *Journal of Inorganic and Nuclear Chemistry*, Vol.31, Issue 4, pp. 947-954.

Gibb, T. C., (1977). *Principles of Mössbauer Spectroscopy*, (Chapman and Hall: London).

Giles, H. L., Hurley, P. W., and Webster, H. W. M., (1995). Simple approach to the analysis of oxides, silicates and carbonates using x-ray fluorescence spectrometry. *X-ray spectrometry*, Vol. 24, Issue 4, pp. 205–218.

Giordano, D., Russell. J, K and Dingwell, D. B., (2008). Viscosity of magmatic liquids: a model. *Earth and Planetary Science Letters*, Vol. 271, pp. 123–134.

Giuliani, A., Kamenetsky, V. S., Kendrick. M. A., Phillips, D., Wyatt. B.A., Maas., R. (2013). Oxide, sulphide and carbonate minerals in a mantle polymict breccia: Metasomatism by proto-kimberlite magmas, and relationship to the kimberlite megacrystic suite. *Chemical Geology*, Vol, 353 pp.4–18

Greenwood, N. N and Gibb, T. C, (1971). *Mössbauer Spectroscopy*. Chapman and Hall: London.

Griffin W. L., Moore R. O., Ryan C. G., Gurney J. J., and Win T. T. (1997) Geochemistry of magnesian ilmenite megacrysts from southern African kimberlites. *Russian Geology. and Geophysic*. Vol.38:2, pp.421– 443

Griffin, W. L and Ryan, C. G., (1995). Trace elements in indicator minerals: area selection and target evaluation in diamond exploration. *Journal of Geochemical Exploration*. Vol. 53, Issues 1–3, pp. 311–337.

Grütter, H. S., Gurney, J. J., Menzies. A., H., Winter, F., (2004). An updated classification scheme for mantle-derived garnet, for use by diamond explorers. *Lithos*, Vol. 77, pp. 841– 857.

Guiraud, R., Bosworth, W., Thierry, J., Delplanque, A., (2005). Phanerozoic geological evolution of Northern and Central Africa: An overview. *Journal of African Earth Sciences*, Vol. 43, pp. 83–143.

Guo, W. Q., Malus, S., Ryan, D. H and., Altounian, Z.(1999). Crystal structure and cation distributions in the  $\text{FeTi}_2\text{O}_5$ – $\text{Fe}_2\text{TiO}_5$  solid solution series. *Journal of Physics: Condensed Matter*, Vol. 11, No 3, pp. 6337–6346.

Gunter M. E., Dyar, M. D., Twamley. B., Foit Jr, F. F., and Cornelius S,(2003). Composition,  $\text{Fe}^{3+}/\sum\text{Fe}$ , and crystal structure of non-asbestiform and asbestiform amphiboles from Libby, Montana, U.S.A. *American Mineralogist*, Vol. 88, pp 1970–1978.

Gurney, J. J., Helmstaedt, H and Moore, R. O., (1993). A review of the use and application of mantle mineral geochemistry in diamond exploration. *Pure and Applied Chemistry*, Vol. 65, No. 12, pp. 2423-2442.

Gurney J. J., Helmstaedt, H. H. Richardson, S. H. and Shirey S. B (2010). *Diamonds through Time*. *Economic Geology*, Vol. 105, pp, 689-712.

Gurney, J. J., and Switzer, G. S., (1973). The discovery of garnets closely related to diamonds in the Finsch Pipe, South Africa. *Contributions to Mineralogy and Petrology*, Vol 39: pp. 103-116.

Gurney, J. J., and Zweistra, P., (1995). The interpretation of the major element compositions of mantle minerals in diamond exploration. *Journal of Geochemical Exploration* Vol. 53, Issue 1–3, pp. 293–309.

Gütlich. P., (2005). *Mössbauer Spectroscopy –Principles and Applications*

[http://www.ak-guetlich.chemie.uni-mainz.de/Dateien/Moessbauer\\_Lectures.pdf](http://www.ak-guetlich.chemie.uni-mainz.de/Dateien/Moessbauer_Lectures.pdf) (Visted, 18/05/2015)

Haggerty, S. E., (1999). A Diamond Trilogy: Superplumes, Supercontinents, and Supernovae. *Science*, Vol. 285, pp. 851-860.

Harlow, G. E and Levinson, A. A., (2008). A World of Diamonds. 9<sup>th</sup> International Kimberlite Conference Extended Abstract No. 9IKC-A-00000. pp. 1-3

Harte, B., Gurney, J. J., (1981). The mood of formation of the Cr poor megacrystic suites from kimberlites. *Journal of Geology* Vol. 89, pp.749–753.

Harte, B., (2010). Diamond formation in the deep mantle; the record of mineral inclusions and their distribution in relation to mantle dehydration zones. *Mineralogical Magazine*, Vol. 74, pp. 189–215.

Harvey, S.E., Kjarsgaard, B. A., and Kelley, L. I., (2001). Kimberlites of Central Saskatchewan: Compilation and Significance of Indicator Mineral Geochemistry with Respect to Diamond Potential. Saskatchewan Geological Survey, Summary of Investigations, Vol. 2, pp.147-161.

Haschke, M., (2014). Laboratory Micro-X-Ray Fluorescence Spectroscopy, Springer Series in Surface Sciences, Vol. 55, Springer International Publishing Switzerland (Chapter 1, XRF-Basics).

Hatton. C., (2009). Geotherms, Lithosphere Thickness and Sedimentary Basins. 11<sup>th</sup> .SAGA Biennial Technical Meeting and Exhibition Swaziland, pp.217 -220.

Heaman, L. M., Kjarsgaard, B.A., Creaser, R. A, (2003). The timing of kimberlite magmatism and implications for diamond exploration: A global perspective. *Lithos*, Vol. 71, pp.153–184.

Helmstaedt , H. H and Gurney. J. J., (1997). Geodynamic controls of kimberlites - What are the roles of hotspot and plate tectonics? *Russian geology and geophysics*, Vol.38. No 2, pp. 492-508

Helmstaedt, H. H, Gurney. J. J. and Richardson S. H., (2010). .Ages of Cratonic Diamond and Lithosphere Evolution: Constraints on Precambrian Tectonics and Diamond. *Exploration Mineralogical Association of Canada*, Vol. 48, No. 6, pp.1385-1408.

Horiba., (2016). <http://www.horiba.com/uk/scientific/products/x-ray-fluorescence-analysis/tutorial/x-ray-fluorescence-the-basic-process/>, (visited on 04/10/2016).

Hutchinson, M. T., (2005). Diamondiferous kimberlites from the Garnet Lake area, west Greenland: exploration methodologies and petrochemistry. Workshop on Greenland's diamond potential, Danmarks og Grønlands Geologiske Undersøgelse Rapport Vol. 68, Issue 7-9, Copenhagen.

Hutchinson, M.T. and Heaman, L.M., (2008). Chemical and physical characteristics of diamond crystals from Garnet Lake, Sarfartoq, West Greenland: an association with carbonatitic magmatism. *Canadian Mineralogist*, Vol. 46, pp.1063-1078.

Jacob, D. E, (2004). Nature and origin of eclogite xenoliths from Kimberlites. *Lithos* Vol. 77, pp. 295-316

Jancik, D and Mashlan, M., (2002). Fast Determination of  $Fe^{2+}/Fe^{3+}$  Ratio in Ilmenite. *Hyperfine Interactions*, Volume 139/140, pp.715–719

Janney, P. E., Shirey, S. B., Carlson, R.W., Pearson, D. G., Bell, D. R., Le Roex., A. P., Ishikawa, A., Nixon, P. H., and Boyd, F. R.,(2010). Age, Composition and Thermal Characteristics of South African Off-Craton Mantle Lithosphere: Evidence for a Multi-Stage History. *Journal of Petrology*, Vol. 51, No 9, pp. 1849-1890.

Jelsma, H. A., de Wit, M.J., Thiart, C., Dirks, P. H. G. M., Viola, G., Basson, I. J., Anckar, E.,( 2004). Preferential distribution along transcontinental corridors of kimberlites and related rocks of southern Africa. *South African Journal of Geology*, Vol. 107, pp. 301–324.

Jelsma, H. A., Barnett., W. Richards. S., Lister. G., (2009). Tectonic setting of kimberlites. *Lithos*, Vol. 112. pp. 155–165.

Jelsma, H. A., Krishnan, U., Perritt, S., Preston, R., Winter, F., Lemotlo, L., van der Linde G., Armstrong, R., Phillips, D., Joy, S., Costa, J., Facatino, M., Posser, A., Kumar, M., Wallace, C., Chinn, I., Henning, A., (2013) Kimberlites from Central Angola: A Case Study of Exploration Findings. Extended Abstract. Proceedings of 10th International Kimberlite Conference.

Kamenetsky, V.S., and Kamenetsky, M. B and Maas, R., (2011). New identity of the kimberlite melt: Constraints from unaltered diamondiferous Udachnaya-East pipe kimberlite, Russia. In: *Advances in Data, Methods, Models and Their Applications in Geoscience*. InTech Open Access Publisher, pp. 181-214.

Kamenetsky, V.S., Kamenetsky, M. B., Weiss, Y., Navon, O., Nielsen, T. F. D and Mernagh, T. P. (2009). How unique is the Udachnaya-East kimberlite? Comparison with kimberlites from the Slave Craton (Canada) and SW Greenland. *Lithos* Vol. 112, pp. 334-346

Kaminsky, F.V., Sablukov, S. M., Sablukova., L. I., Shchukin, V. S., and Canil, D, ( 2002). Kimberlites from the Wawa area, Ontario. *Canadian Journal of Earth Sciences*, Vol. 39, No 12, pp. 1819-1838

Kerr, D. E., Dredge, L.A. Kjarsgaard, I. M., Knight, R. D., and Ward, B. C., (1997). Kimberlite Indicator Minerals in Till, Central Slave Province, N.W.T., Canada. Paper 44. *Exploration Geochemistry. Proceedings of Exploration Vol 97: Fourth Decennial International Conference on Mineral Exploration*. pp. 359–362

Keshav, S., Corgne, A., Gudmundur, H., Gudfinnsson, G. H., Bizimis, M., McDonough, W. F., and Fei Y., (2005). Kimberlite petrogenesis: Insights from clinopyroxene-melt partitioning experiments at 6 GPa in the CaO-MgO-Al<sub>2</sub>O<sub>3</sub>-SiO<sub>2</sub>-CO<sub>2</sub> system, Vol. 69, No. 11, pp. 2829–2845.

Keulen, N., Hutchison, M. T., and Frei, D., (2009). Computer-controlled scanning electron microscopy: A fast and reliable tool for diamond prospecting. *Journal of Geochemical Exploration* Vol, 103, pp. 1–5.

Kjarsgaard, B. A., (2007). Kimberlite Pipe Models: Significance for Exploration. *Ore Deposits and Exploration Technology*. Geological Survey of Canada, Paper 46, pp. 667-677.

Klein, C and Hurlbut, C., (1993). *Manual of Mineralogy* (after James D. Dana), 21<sup>st</sup> Edition. Published by John Wiley & Sons.

Kornprobst J., (1984). Kimberlites I : Kimberlites and Related Rocks.: Proceedings of the “Third international kimberlite conference” Vol. 1 ; 465pp

Kozai, Y., and Arima, M., (2005). Experimental study on diamond dissolution in kimberlitic and lamproitic melts at 1300– 1420 °C and 1 GPa with controlled oxygen partial pressure. *American Mineralogist*, Vol. 90, pp. 1759–1766.

Kröner, A., and Stern, R. J., (2004.). Pan-African Orogeny. *Encyclopedia of Geology*, Vol. 1, Elsevier, Amsterdam, pp.1-12.

Kusky, T. M., Abdelsalam, M., Stern, R. J., and Tucker, R. D., (2003). Evolution of the East African and related orogens and the assembly of Gondwana. *Precambrian Research*. Vol. 123: Issue 2-4, pp. 81-85.

Latfard, D., (1995). Experimental evidence for the exsolution of ilmenite from titaniferous spinel. *American Mineralogist*, Vol. 80, pp. 968-981.

Lewis, H. C., (1887). On diamantiferous peridotite and the genesis of diamond. *Geological Magazine* Vol. 4, pp. 22–24.

Lewis, H. C., (1888). The matrix of diamond. *Geological Magazine* Vol.5, pp.129–131.

Luth. R. W, Virgo, D., Boyd. F. R., Wood. B. J., (1990). Ferric iron in mantle-derived garnets. Implications for thermobarometry and for the oxidation state of the mantle. *Contributions to Mineralogy and Petrology*, Vol. 104, pp. 56-72.

Maddock, A. G., (1997) *Mossbauer Spectroscopy: Principles and Applications of techniques*  
Hoorwood Chemical Science Series.

Mahotkin L. L, Gibson, S. A. Thompson, R. N, Zhuravlev, D. Z and. Zherdev, P. U. (2000). Late Devonian Diamondiferous Kimberlite and Alkaline Picrite (Proto-kimberlite?) Magmatism in the Arkhangelsk Region, NW Russia. *Journal of Petrology*. Vol. 41 No 2, pp. 201–227

Maruoka, T., Kurat, G., Dobosi., G., and Koeberl, C., (2004). Isotopic composition of carbon in diamonds of diamondites: Record of mass fractionation in the upper mantle. *Geochimica et Cosmochimica Acta*, Vol. 68, No. 7, pp. 1635–1644.

McClenaghan, M. B. (2005). Indicator mineral methods in mineral exploration. *The Geological Society of London*. Vol. 5 No. 3, pp. 233-245.

McCandless, T. E., (1990). Kimberlite xenoliths wear in high energy- fluvial system: experimental studies. *Journal of Geochemical Exploration*, Vol. 37, pp. 323-331.

McCammon, C. A., (2005). Mantle oxidation state and oxygen fugacity: Constraints on mantle chemistry, structure, and dynamics, in *Earth`s Deep Mantle: Structure, Composition, and Evolution*, Geophysical Monograph. Series, Vol. 160, pp. 221–242.

McCammon, C. A., (1994). A Mössbauer milliprobe: Practical considerations. *Hyperfine Interactions*, 92, 1235–1239.

McCammon, C. A., Chinn, I. L., Gurney, J. J., and McCallum, M. E., (1998). Ferric iron content of mineral inclusions in diamonds from George Creek, USA determined using Mössbauer spectroscopy: Implications for oxygen fugacity. *Contribution to Mineralogy and Petrology*, Vol.133, pp. 30-37.

McCammon, C. A., Griffin, W. L., Shee, S. R., and O'Neill, H. S. C., (2001). Oxidation during metasomatism in ultramafic xenoliths from the Wesselton kimberlite, South Africa: implications for the survival of diamond. *Contributions to Mineralogy and Petrology*, Vol. 141, Issue 3, pp. 287-296.

Meyer, H. O., (1968). Chrome Pyrope: An Inclusion in Natural Diamond. *Science* (New York, N.Y) Vol.160. Issue 3853, pp.1446-1447.

Meyer, H. O. A., (1985). Genesis of diamond: a mantle saga. *American Mineralogist*, Vol. 70, pp. 344-355.

Meyer, H. O. A., Waldman. M. A., and Garwood. B., (1994). Mantle xenoliths from kimberlie near Kirkland lake, Ontario. *The Canadian Mineralogist*, Vol.32, pp.295-306.

Ministry of Mines and Mineral Development Zambia (2016). <http://www.zambia-mining.com/cratons.html>. (Last visited 14/12/2014).

Mitchell, R. S and Giardini, A. A., (1977). Some minerals inclusions from African and Brazilian diamonds: their nature and significance. *American Mineralogist*, Vol. 62, pp. 756-762.

Mitchell, R. H., (1977). Geochemistry of magnesian ilmenites from kimberlites in South Africa and Lesotho. *Lithos*. Vol. 10, Issue 1, pp. 29-37

Mitchell, R.H., (2006). Potassic magmas derived from metasomatized lithospheric mantle: nomenclature and relevance to exploration for diamond-bearing rocks. *Journal of the Geological Society of India*, Vol. 67, pp. 317–327.

Mitchell, R. H., (1979). Magnesian Ilmenite and Its Role in Kimberlite Petrogenesis. *The Journal of Geology*, Vol. 81, No. 3, pp. 301-311.

Mitchell, R. H., Skinner, E. M. W., and Scott Smith B. H., (2008). Tuffisitic Kimberlites: Mineralogical Characteristics Relevant to their Formation. 9<sup>th</sup> International Kimberlite Conference Extended. Abstract No. 9IKC-A-00054.

Mitchell, R. H., (1984) .Garnet Iherzolites from the Hanaus-I and Louwrensia kimberlites of Namibia. *Contributions to Mineralogy and Petrology*, Vol. 86, Issue 2, pp. 178-188.

Mitchell, R. H., (1995). Kimberlites, orangeites, and related rocks. Plenum Press, New York.

Mitchell, R. H., (1991). Kimberlites and Lamproites: Primary source of diamond. *Geoscience Canada*, Vol.18. No. 1, pp. 1-16.

Moecher, P., (2004). Characterization and Identification of Mineral Unknowns: A Mineralogy Term Project *Journal of Geoscience Education*, Vol. 52, No. 1, pp. 5-9.

Moore, A. E., and Lock, N. P., (2001). The origin of mantle-derived megacrysts and sheared peridotites evidence from kimberlites in northern Lesotho - Orange Free State (South Africa) and Botswana pipe clusters. *South African Journal of Geology* 104.

Moore., A and Belousova, E, (2005). Crystallization of Cr-poor and Cr-rich megacryst suites from the host kimberlite magma: implications for mantle structure and the generation of kimberlite magmas. *Contribution Mineralogy Petrology*, Vol. 149, pp. 462–481.

Morris, T. F., Crabtree, D., Sage, R. P, and Averill, S. A., (1998). Types, abundances and distribution of kimberlite indicator minerals in alluvial sediments, Wawa–Kinniwabi Lake area, Northeastern Ontario: implications for the presence of diamond-bearing kimberlite. *Journal of Geochemical Exploration* 63, pp, 217–235.

Mössbauer, R. L., (2000). The discovery of the Mössbauer effect. *Hyperfine Interactions*, Vol. 126, pp. 1-12.

Moussallam, Y., Morizet, Y., Gaillard, F., (2016). H<sub>2</sub>O–CO<sub>2</sub> solubility in low SiO<sub>2</sub>-melts and the unique mode of kimberlite degassing and emplacement. *Earth and Planetary Science Letters*, Vol. 447 pp. 151–160.

Musun, K., and Scott Smith, B, H., (2006). The Pimenta Bueno Kimberlite Field, Rondonia, Brazil: evidence for tuffisitic kimberlite. 8<sup>th</sup> International Kimberlite conference, long abstract.

Nixon, P. H., (1995). The morphology and nature of primary diamondiferous occurrences. *Diamond Exploration: Into the 21<sup>st</sup> Century*. *Journal of Geochemical Exploration*. Vol, 53, Issues 1–3, pp. 41–71.

Nixon, P. H., and Boyd, F. R., (2010). Age, Composition and Thermal Characteristics of South African Off-Craton Mantle Lithosphere: Evidence for a Multi-Stage History. *Journal of Petrology*, Vol.51. No. 9, pp. 1849-1890.

Nowicki, T., Galloway, M., le Roex, A., Gurney, J., Smith, C., and Canil, D., (2008). Iron-in-perovskite oxygen barometry and diamond resorption in kimberlites and lamproites from southern Africa, Russia and Australia. 9th International Kimberlite Conference Extended Abstract No. 9IKC-A-00124, pp. 1-3.

Nowicki, T. E., Moore, R. O., Gurney, J. J., and Baumgartner, M. C., (2007). Diamonds and associated heavy minerals in kimberlite. Review of key concepts and applications. *Developments in Sedimentology*, Vol. 58, pp. 1235–1267.

Orlov, Y. L., (1977). *The Mineralogy of the Diamond*. Published by John Wiley, New York, ISBN 10: 0471018694 ISBN 13: 9780471018698.

Patterson, M., Francis, D., and McCandless, T., (2009). Kimberlites: Magma or mixture. *Lithos*, Vol. 112, Supplement 1, pp.191-200.

Pasteris, J. D., (1984). Kimberlite Complex mantle melts. *Annual Reviews in Earth and Planetary Science*, Vol. 12, pp. 133-153.

Pax, R. A., and Stewart, G. A., (2012). Quantitative Determination of Phases Using Mössbauer Spectroscopy and X-ray Diffraction: A Case Study of the Fe-Ti-O System. *Proceedings, 36<sup>th</sup> Annual condensed matter and materials meeting*.

Pereira, E., Rodrigues, J., and Reis, B., (2003). Synopsis of Lunda geology, NE Angola: Implications for diamond exploration. *Comunicações do Instituto Geológico e Mineiro*, Tomo 90, pp. 189-212.

Pereira, E., Tassinari, C. C. G., Rodrigues, J. F., Van-Dúnem, M. V., (2011). New data on the deposition age of the volcano-sedimentary Chela Group and its Eburnean basement: implications to post- Eburnean crustal evolution of the SW of Angola. *Comunicações Geológicas*, Vol. 98, pp.29-40.

Persikov, E. S., Bukhtiyarov, P. G., and Sokol, A. G., (2015). Change in the viscosity of kimberlite and basaltic magmas during their origin and evolution (prediction). *Russian Geology and Geophysics*, Vol. 56, pp 885–892.

- Persikov, E. S., and Bukhtiyarov, P. G., (2013). Viscosity of kimberlite and basaltic magmas during their ascent from mantle to the crust. Non-reviewed online article.  
[https://www.researchgate.net/profile/E\\_Persikov/publication/284027855\\_Relationship\\_between\\_diffusivity\\_of/links/564b144c08ae9cd9c8281bb5](https://www.researchgate.net/profile/E_Persikov/publication/284027855_Relationship_between_diffusivity_of/links/564b144c08ae9cd9c8281bb5) (last accessed 10 / 01 / 2017).
- Persikov, E. S., (2007). Structural chemical model to calculate and predict the viscosity of magmatic melts in full range of compositions and conditions. General Assembly EGU-2007. Vienna. Geophysical Research. Abstracts, Vol.9, A-02262, SRef-ID: 1607-7962/gra/EGU2007-A-02262C. European Geosciences Union.
- Pervov, V. A., Somov, S. V., Korshunov, A. V., Dulapchii, E. V., and Félix, J. T., (2011). The Catoca Kimberlite Pipe, Republic of Angola: A Paleovolcanological Model. *Geology of Ore Deposits*. Vol. 53, No. 4, pp. 295–308.
- Persikov, E. S., and Bukhtiyarov, P. G., (1999). The effect of temperature and pressure on the viscosity of model magmatic melts in the range acid-ultrabasic. *Geokhimiya*, No.12, pp. 1256-1267.
- Petford, N., (2009). Which effective viscosity? *The Mineralogical Society*. Vol.73, Issue 2, pp. 167-19.
- Philpotts, A. R., and Ague, J. J. (2011). *Principles of Igneous and Metamorphic Petrology* Cambridge University Press 2nd Revised edition.
- Powell, R., and Powell, M., (1977). Geothermometry and oxygen barometry using coexisting iron-titanium oxides: a reappraisal. *Mineralogical Magazine*, Vol. 41, pp. 257-263.
- Press, F., and Siever, R.,(1986). *Earth*. W. H. Freeman; 4th edition edition.
- Quintiliani, M., (2005).  $^{57}\text{Fe}$  Mössbauer spectroscopy analysis of spinels:  $\text{Fe}^{3+}/\text{Fe}_{\text{tot}}$  quantification accuracy and consequences on  $f\text{O}_2$  estimate. *Periodico di Mineralogia*, Vol. 74, pp.139-146.
- Rao, N. K., and Rao, G. V. U., (1965). Intergrowths in ilmenite of the beach sands of Kerala, *Mineralogical Magazine*, Vol 35, No. 269, pp. 118-130.
- Richard, S. M., (1977). Some mineral inclusions from African and Brazilian diamonds: their nature and significance. *American Mineralogist*, Vol. 62, pp. 756-762.

Richardson, S. H., and Harris, J. W., (1997). Antiquity of peridotitic diamonds from the Siberian craton: *Earth and Planetary Science Letters*, Vol. 151, Issue 3-4, pp. 271-277.

Ringwood, A. E., Kesson, S. E., Hibberson, W., and Ware, N., (1992). Origin of kimberlites and related magma. *Earth and Planetary Science Letters*, Vol. 113, Issue 4, pp. 521–538.

Robinson, D. N., Scott, J. A., Van Niekerk, A., and Anderson, G., (1989). The sequence of events reflected in the diamonds of some southern African kimberlites. In: Ross, J. (Ed.), *Kimberlites and Related Rocks*, Vol. 2. Geological Society of Australia, Special Publication. Blackwell Scientific Publications, Perth 14: 980–990.

Rollinson, H. R., Adetunji, J., and Yousif, A. A., Gismelseed, A. M., (2012). New Mössbauer measurements of  $\text{Fe}^{3+}/\Sigma\text{Fe}$  in chromites from the mantle section of the Oman ophiolite: evidence for the oxidation of the sub-oceanic mantle. *Mineralogical Magazine*, Vol. 76, Vol.3, pp. 579–596.

Roberts, E., Jelsma, H. A., and Hegna, T., (2015). Mesozoic Sedimentary Cover Sequences of the Congo Basin in the Kasai Region, Democratic Republic of Congo, pp. 163-191.

Roble-Cruz, S., Lomba, A., Melgarejo, J. C., Gali, S., and Goncalves, A.O., (2009). The Cucumbi Kimberlite, NE Angola Problems to Discriminate Fertile and Barren Kimberlites, *Revista de la Sociedad Española de Mineralogía*, Vol. 11, pp. 159-160..

Robles-Cruz, S. E., Watangua, M., Isidoro, L., Melgarejo, J.C., Galí, S., and Olimpio, A. (2009): Contrasting compositions and textures of ilmenite in the Catoca kimberlite, Angola, and implications in exploration for diamond. *Lithos*, Vol. 112, Supplement 2, Special Issue 9IK., pp. 966-975.

Robles-Cruz, S. E., Watangua, M., Melgarejo, J.C., Galí, S., (2008). New Insights into the Concept of Ilmenite as an Indicator for Diamond Exploration, Based on Kimberlite Petrographic Analysis. *Revista de la Sociedad Española de Mineralogía*, Vol. 9, pp. 205-206

Royal Society of Chemistry, (2016)

<http://www.rsc.org/Membership/Networking/InterestGroups/MossbauerSpect/Intropart1.asp> (visited on 23/02/2016).

Ruebenbauer, K. and Sepioł, B. H., (1985). Goldanskii-Karyagin effect and external magnetic field method as tools to measure anisotropy of the recoilless fraction in amorphous materials, Vol. 23, Issue 3, pp 351–374.

Ruskov, T., Spirov, I., Georgieva M., Yamamoto, S., Green, H. W., McAmmon, C. A., and Dobrzhinetskaya, L. F., (2010). Mössbauer spectroscopy studies of the valence state of iron in chromite from the Luobusa massif of Tibet: implications for a highly reduced deep mantle. *Journal of Metamorphic Geology*, Vol. 28, pp 551–560.

Russell, J. K., Porritt, L. A., Yan Lavalleye, Dingwell. B., (2012). Kimberlite ascent by assimilation-fuelled buoyancy. *Letters to Nature*, 481,352–356.

Santana, G. P., Fabris, J. D., Goulart, A. T. and Santana, D. P., (2001). Magnetite and its transformation to Hematite in a soil derived from steatite. *Revista Brasileira de Ciência do Solo*, Vol. 25, pp. 33-42.

Sato. H., (2005). Viscosity measurement of subliquidus magmas: 1707 basalt of Fuji volcano. *Journal of Mineralogical and Petrological Sciences*, Vol. 100. No. 4, pp 133-142.

Seda, T., and Hearne, G. R., (2004). Pressure induced  $\text{Fe}^{2+} + \text{Ti}^{4+} \rightarrow \text{Fe}^{3+} + \text{Ti}^{3+}$  intervalence charge transfer and the  $\text{Fe}^{3+}/\text{Fe}^{2+}$  ratio in natural ilmenite ( $\text{FeTiO}_3$ ) minerals. *Journal of Physics: Condensed Matter*, Vol. 16, pp. 2707-2718.

Seda, T., (2003). Basic theory of the Mössbauer effect. pp. 1-27.  
<http://www.physics.wvu.edu/sedat/moss.pdf> (Visited on 20/08/2015).

Scott Smith, B. H., Nowicki, T. E., Russell, J. K., Webb, K. J., Hetman C. M., Harder M., and Mitchell, R. H., (2008). Kimberlites: Descriptive Geological Nomenclature and Classification, in *Extended Abstracts of the 9<sup>th</sup> International Kimberlite Conference*. Frankfurt, Abstract, No. 9IKC\_A\_00124.

Scott Smith, B. H., (2006). Canadian kimberlites: geological characteristics relevant to emplacement. Long Abstract for Kimberlite Emplacement Workshop.

[http://www.scottsmithpetrology.com/publications/files/canadian\\_kimberlites\\_geological\\_characteristics.pdf](http://www.scottsmithpetrology.com/publications/files/canadian_kimberlites_geological_characteristics.pdf) (Visited on 06/23/2014).

Scott Smith, B. H., (2008). Canadian kimberlites: Geological characteristics relevant to emplacement *Journal of Volcanology and Geothermal Research*, Vol. 174, Issues 1–3, pp 9–19.

Scott Smith B. H., (1999). Near-surface emplacement of kimberlites by magmatic processes. <http://www.scottsmithpetrology.com/publications/files/60-SCOTT-SMITH,.pdf> (Visited on 24/05/2014).

Schiano, P., Clocchiatti, R., Shimizu, N., Weis, D., Mattielli, N., (1994). Cogenetic silica-rich and carbonate-rich melts trapped in mantle minerals in Kerguelen ultramafic xenoliths: implications for metasomatism in the oceanic upper mantle. *Earth and Planetary Science Letters* 123, pp. 167–178

Schulze, D. J., (1997). The Significance of Eclogite and Cr-poor Megacryst Garnets in Diamond Exploration. Canadian Institute of Mining, Metallurgy and Petroleum. *Exploration, Mining and Geology*, Vol. 6, No. 4, pp. 349-366

Shaw, H. R., (1972). Viscosities of magmatic silicate liquids: An empirical model of prediction. *American Journal of Science*, Vol. 272, pp. 438-475.

Shirey, S. B., Cartigny, P., Frost, D. J., Keshav, S., Nestola, F., Nimis, P., Pearson, D. G., Sobolev N. V., Walter, M. J., (2013). Diamonds and the geology of mantle carbon. *Reviews in Mineralogy and Geochemistry*, Vol. 75, No. 1, pp. 355–421.

Shirey, S. B. and Shigley, J. E, (2013). Recent Advances in Understanding the Geology of Diamonds. *Gems & Gemology*. Vol. 49, No. 4.

<http://www.gia.edu/gems-gemology/WN13-advances-diamond-geology-shirey> (visited on 04/10/2016).

Shore, M., and Fowler, A. D., (1996). Oscillatory zoning in minerals: A common phenomenon. *The Canadian Mineralogist* Vol. 34, pp. 1111-1126.

Shchukina, E. V., Agashev A. M and Pokhilenko N. P., (2016). Metasomatic origin of garnet xenocrysts from the V. Grib kimberlite pipe, Arkhangelsk region, NW Russia. *Geoscience Frontiers*. pp. 1-11

Simakov, S. K., (2006). Redox state of eclogites and peridotites from sub-cratonic upper mantle and a connection with diamond genesis. *Contributions to Mineralogy and Petrology*, Vol. 151, No 3, pp. 282-296.

Singhvi, A. K., Gupta, D. K., Gokhale, K. V. G. K. and Rao, G. N., (1974). Mössbauer spectra of ilmenites from primary and secondary sources. *Physica Status Solidi A*, Vol. 23, Issue 1, pp. 321–324.

Skinner, E. M. W., Clement, C. R., (1979). Mineralogical classification of Southern African kimberlites. Second International Kimberlite Conference, Santa Fe. American Geophysical Union, pp. 129–139.

Skinner, E. M. W., Marsh, J. S., (2004). Distinct kimberlite pipe classes with contrasting eruption processes. *Lithos*, Vol. 76, pp 183–200.

Skinner, E. M. W., (2008). The emplacement of class 1 kimberlites. *Journal of Volcanology and Geothermal Research*, vol. 174, pp. 40–48.

Skinner, C. P., (1989). The petrology of peridotite xenoliths from Finsch kimberlite, South Africa. *South African Journal of Geology* Vol. 92, pp 197–206.

Skinner, E. M. W., (1989). Contrasting Group 1 and Group 2 kimberlite petrology: towards a genetic model for kimberlites. In: Ross, J., Jacques, A.L., Ferguson, J., Green, D.H., O'Reilly, S.Y., Danchin, R.V., Janse, A.J.A. (Eds.), *Kimberlites and Related Rocks, Volume 1. Proceedings of the Fourth International Kimberlite Conference, Geological Society of Australia Special Publication 14, Perth*, A pp. 528–544.

Skinner, E. M. W., Smith, C. B., Bristow, J. W., Scott-Smith, B. H. and Dawson, J. B. (1985). Proterozoic kimberlites and lamproites and preliminary age for the Argyle pipe, Western Australia. *Transactions of the Geological Society of South Africa*, Vol.88, pp 335--340.

Smith, C.B., (1983). Pb, Sr, and Nd isotopic evidence for sources of African kimberlite. *Nature*, Vol. 304, pp. 51–54.

Smith, C. B., (1983). Rubidium–Strontium, Uranium–Lead and Samarium–Neodymium isotopic studies of kimberlite and selected mantle-derived xenoliths. Unpublished Ph.D. thesis, University of the Witwatersrand, Johannesburg, South Africa.

Smith, C. B., Allsopp, H. L., Kramers, J. D., Hutchinson, G., Roddick, J. C., (1985). Emplacement ages of Jurassic–Cretaceous South African kimberlites by the Rb–Sr method on phlogopite and whole-rock samples. *Transactions of the Geological Society of South Africa*, Vol. 88, pp 249–266.

Smith, C. B., Gurney, J. J., Harris, J. W., Otter, M.L., Kirkley, M.B., Jagoutz, E., (1991). Neodymium and strontium isotope systematics of eclogite and websterite paragenesis inclusions from single diamonds, Finsch and Kimberley Pool, RSA. *Geochimica et Cosmochimica Acta*, Vol. 55, pp. 2579–2590.

Smith, C. B., Sims, K. M., Chimuka, L., Beard, A. D., Townend, R., (2003). Kimberlite metasomatism at Murowa and Sese pipes, Zimbabwe. Eighth International Kimberlite Conference. Extended Abstracts, Victoria, BC, Canada.

Smith, C. B., (2004). Geodynamic Setting of Kimberlites. American Geophysical Union, Spring Meeting, abstract.

Sobolev, V. N., McCammon, C. A., Taylor, L. A., Snyder, G. A. and Sobolev, N. V., (1999). Precise Mössbauer milliprobe determination of ferric iron in rock-forming minerals and limitations of electron microprobe analysis, *American Mineralogist*, Vol. 84, pp.78–85.

Sobolev, N. V. (1977). Deep-seated Inclusions in Kimberlites and the Problem of the Composition of the Upper Mantle. American Geophysical Union, Washington, DC.

Sobolev, N. V., Lavrentiev, Y. G., Pospelova, L. N., Sobolev, E. V., (1969). Chrome pyropes from Yakutian diamonds. *Doklady Akademii Nauk SSSR*. Vol.189, pp.162-165

Sparks, R. S. J., (2013). Kimberlite volcanism. *Annual. Review. Earth Planet. Science*. Vol. 41, pp.497- 528.

Sparks, R. S. J., Brooker, R. A., Field, M., Kavanagh, J., Schumacher, J. C., Walter, M. J., and White, J., (2009). The nature of erupting kimberlite melts. *Proceedings of the 9<sup>th</sup> International Kimberlite Conference*. *Lithos* Vol. 112, pp. 429-438.

Sparks, R. S. J., Baker, L., Brown, R.J., Field, M., Schumacher, J., Stripp, G., Walters. A., (2006). Dynamical constraints on kimberlite volcanism, *Journal of Volcanology and Geothermal Research* Vol, 155. pp. 18–48.

Spetsius Z. V., Taylor, L. A., Valley, J. W., Deangelis, M.T., Spicuzza, M., Ivanov, A. S., Banzeruk, V. I., (2008) Diamondiferous xenoliths from crustal subduction: garnet oxygen isotopes from the Nyurbinskaya pipe, Yakutia. *European Journal of Mineralogy*, Vol. 20 Number 3, pp. 375 - 385.

Stagno, V., Ojwang, D. O., McCammon, C.A, and Frost, D.J., (2013). The oxidation state of the mantle and the extraction of carbon from Earth's interior, *Letters to Nature*, Vol. 493, pp.84–88.

Stachel, T., (2003). Peridotitic and eclogitic diamond source and the origins of cratonic roots, University of Alberta, Canada.

Stachel, T. and Harris, J. W., (2008). The origin of cratonic diamonds constraints from mineral inclusions, *Ore Geology Reviews*, Vol. 34, Issues 1–2, pp.5–32.

Stachel, T., Harris, J. W., Tappert, R and Brey, G. P., (2003). Peridotitic diamonds from the Slave and the Kaapvaal cratons similarities and differences based on a preliminary data set. *Lithos*, Vol. 71. pp. 489– 503.

Stachel, T., Viljoen, K. S., Brey, G., Harris, J. W., (1998). Metasomatic processes in lherzolitic and harzburgitic domains of diamondiferous lithospheric mantle. *Earth and Planetary Science Letters* 159, pp. 1-12.

Stachel, T., Aulbach, S., Brey, G. P., Harris, J. W., Leost, I., Tapper, R., Viljoen, K.S., (2004). The trace element composition of silicate inclusions in diamonds: a review. *Lithos*, Vol. 77. Issues 1–4, pp. 1–19

Stachel. T., Brey, G. P., Harris J. W., (2005). Inclusions in sublithospheric diamonds: glimpses of deep mantle. *Elements*, Vol. 1, pp. 73-78.

Stern, R. J., (2007). Neoproterozoic crustal growth: The solid Earth system during a critical episode of Earth history, *Gondwana Research*, Vol. 14, Issues 1-2, pp. 1-18.

Swanson, H. E, and, Tatge, E (1951). Standard X-Ray Diffraction Patterns. *Journal of Research of the National Bureau of Standards* Vol. 46, No. 4, research paper 2202.

Tack, L., Wingate, M. T. D., De Waele, B., Meert, J., Belousova, E., Griffin, B., Tahon, A., and Fernandez-Alonso, M., (2010). The 1375 Ma "Kibaran Event" in Central Africa: prominent

emplacement of bimodal magmatism under extensional regime Precambrian Research. Precambrian Research, Vol. 180, No. 1-2, pp.63-84.

Tappert, R., and Tappert, M. C., (2011). Diamonds in Nature: A Guide to Rough Diamonds. Book Review /Crystallography Reviews, pp. 304-308. Heidelberg, Dordrecht, London, New York, Springer.

Taylor, L. A., Anand, M., and Promprated, P., (2003). Diamonds and their inclusions: Are the criteria for syngeneis valid? 8<sup>th</sup> International Kimberlite Conference, Long Abstract  
<http://citeseerx.ist.psu.edu/viewdoc/download;jsessionid=0CCE71DE04260D0D3C4BBF7A84F2C61F?doi=10.1.1.617.9109&rep=rep1&type=pdf> (Visited on 30/09/2013 and 08/06/2014)

Taylor, L. A., Keller, R. A., Snyder, G.A., Wang, W., Carlson, W. D., Hauri, E. H., McCandless, T., Kim, K. R., Sobolev, N. V., and Bezborodov, S. M., (2000). Diamonds and their mineral inclusions and what they tell us?: a detailed “Pull-Apart” of a diamondiferous eclogite. International Geological Reviews. Vol. 42, pp. 959 – 983.

Taylor, L. A., Spetsius, Z. V, Wiesli R., Anand, M., Promprated, P., and Valley, J. W., (2003). The origin of mantle peridotite: Crustal signature from Yakutian Kimberlites. 8<sup>th</sup> International Kimberlite Conference Long Abstract, pp 1-5.  
<http://www.unalmed.edu.co/~rrodriguez/MODELOS/peridotites%20kimberlites.pdf> (Visited on 24/12/2015)

Thomassot, E., Cartigny, P., Harris, J.W., Viljoen, (Fanus), K. S., (2007). Methane-related diamond crystallization in the Earth's mantle: Stable isotope evidences from a single diamond-bearing xenoliths, Earth and Planetary Science Letters 257, pp. 362–371.

Torro, L., Villanova, C., Castillo, M., Campeny, M., Goncalves, A.O., Melgarejo, J.C., (2012). Niobium and rare earth minerals from the Virulundo carbonatite, Namibe (Angola). Mineralogical Magazine, Vol. 76 (2), pp. 393–409.

Tronche, E. J., Van Kan Parker, M., de Vries, J., Wang, Y., Sanehira, T., Li, J., Chen, B., Gao, L., Klemme, S., McCammon, C.A., and van Westrenen, W., (2010) The thermal equation of state of FeTiO<sub>3</sub> ilmenite based on in situ X-ray diffraction at high pressures and temperatures. American Mineralogist, Vol 95, pp, 1708–1716.

Van Hinsbergen, D. J. J., Buiter, S. J. H., Torsvik, T. H., Gaina, C. and Webb, S. J., (2011). The Formation and Evolution of Africa: A Synopsis of 3.8 Ga of Earth History. Geological Society, London, Special Publications, Vol. 357, pp. 1–8.

Vearncombe, S., Vearncombe, J. R., (2002). Tectonic controls on kimberlite location, southern Africa. *Journal of Structural Geology*. Volume 24, Issue 10, Pages 1619–1625.

Vieira, V. W. A., Knudsen, J. M., Roy-Poulsen, N. O., and Campsie, J. (1983). Mössbauer Spectroscopy of Pyroxenes from Two Meteorites (Achondrites). *Physica Scripta*. Vol. 27, pp. 437–444.

Virgo, D., Luth, R. W., Moats, M. A., Ulmer, G. C., (1988). Constraints on the oxidation state of the mantle: an electrochemical and  $^{57}\text{Fe}$  Mössbauer study of mantle-derived ilmenites. *Geochimica et Cosmochimica Acta*, Vol. 52, pp. 1781–1794.

Wagner, P.A., (1914): *The Diamond Fields of Southern Africa*. Published by the Transvaal Leader. Johannesburg South Africa. 347pp.

Waerenborgh, J. C., Figueiras, J., Mateus, A., and Gonçalves, M., (2002). Nature and mechanism of ilmenite alteration: a Mössbauer and X-ray diffraction study of oxidized ilmenite from the Beja-Acebuches Ophiolite Complex (SE Portugal). *Mineralogical Magazine*, Vol. 66 (3), pp. 421–430

Wallace, M. E., Green, D. H., (1988). An experimental determination of primary carbonatite magma composition. *Nature*, Vol. 335, 343–346

Webb, K. J., Scott Smith, B. H., Paul, J. L. and Hetman, C. M., (2004). Geology of the Victor Kimberlite, Attawapiskat, Northern Ontario, Canada: cross-cutting and nested craters. *Lithos*, Vol. 76, pp. 29–50.

White, J. L., Sparks, R. S. J., Bailey, K., Barnett, W.P., Field, M., Windsor, L., (2012). Kimberlite sills and dykes associated with the Wesselton kimberlite pipe, Kimberley, South Africa. *Journal of the South African Geological Society*, Vol. 115.1 pp. 1–32.

White, S. H., de Booder and Smith, C. B., (1995). Structural controls of kimberlites and lamproite emplacement, *Journal of Geochemical Exploration*, Vol. 53, pp. 245–264.

Wilson, L. and Head, J. W., (2007). Kimberlite ascent and eruption, *Nature*, Vol. 447, pp. 53–57

Wyatt, B. A., Baumgartner, M., Anckar, E., Grutter, H., (2004). Compositional classification of kimberlitic and non-kimberlitic ilmenite. *Lithos* Vol. 77 pp. 819– 840.

Wyatt, B. A., (1979). Mangoan ilmenite from the Premier kimberlite. *Geological Society of South Africa, Geokongres*, pp. 456-460.

Wyatt, B. A., (1977). The melting and crystallization behaviour of a natural clinopyroxene-ilmenite intergrowth. *Contributions to Mineralogy and Petrology*, Vol.61, pp. 1-9.

Yambissa. M. T., Bingham. P, A and Forder, S. D. (2014). Mantle conditions and geochemical environment as controls of diamond survival and grade variation in kimberlite diamond deposits: Lunda Province, NE Angola, *Proceedings of the 30<sup>th</sup> International Conference on Ore Potential of Alkaline, Kimberlite and Carbonatite Magmatism*, Vol. 1, pp. 237-239.

Zhang, Z., Fedortchouk, Y., and Hanley. J, J., (2015). Evolution of diamond resorption in a silicic aqueous fluid at 1–3 GPa: Application to kimberlite emplacement and mantle metasomatism. *Lithos* Vol. 227, pp 179–193.

Zhang, C., and Duan, Z., (2009). A model for C–O–H fluid in the Earth's mantle. *Cosmochimica Acta*, Vol.73, Issue 7, pp. 2089-2102

Zhao, D., Essene, E. J., Zhang, Y., (1999). An oxygen barometer for rutile–ilmenite assemblages: oxidation state of metasomatic agents in the mantle Earth and *Planetary Science Letters*, Vol. 166, pp. 127–137.